COLLISION TECTONICS : METAMORPHIC AND GEOCHRONOLOGICAL CONSTRAINTS FROM PARTS OF HIMACHAL PRADESH, NW-HIMALAYA

A THESIS

submitted in fulfilment of the
requirements for the award of the degree
of
DOCTOR OF PHILOSOPHY
in
APPLIED GEOLOGY

By

SANDEEP SINGH

Ak Jain
26/11/93
Professor and Head
Department of Earth Sciences
University of Roorkee
ROORKEE

DEPARTMENT OF EARTH SCIENCES
UNIVERSITY OF ROORKEE
ROORKEE-247 667 (INDIA)

NOVEMBER, 1993

Gratis

Dedicated
to
Friends,
Understanding
&
LOVE

Candidate's Declaration

I hereby certify that the work, which is being presented in this thesis entitled **"COLLISION TECTONICS : METAMORPHIC AND GEOCHRONOLOGICAL CONSTRAINTS FROM PARTS OF HIMACHAL PRADESH, NW-HIMALAYA"** in fulfilment of the requirement for the award of the Degree of **Doctor of Philosophy**, submitted in the **Department of Earth Sciences** of the University, is an authentic record of my own work carried out during a period from February, 1988 to October, 1993 under the supervision of **Prof. A. K. JAIN** and **Dr. RM. Manickavasagam.**

The matter embodied in this thesis has not been submitted by me for the award of any other Degree.

Sandeep Singh
26th Nov. '93

(SANDEEP SINGH)

Candidate's Signature

This is to certify that the above statement made by the candidate is correct to the best of our knowledge.

Signature of Supervisors

AKJain
26/11/93

(A. K. JAIN)

Professor
Department of Earth Sciences
University Of Roorkee
ROORKEE - 247 667, INDIA

26/11/93

(RM. MANICKAVASAGAM)

Reader
Department of Earth Sciences
University Of Roorkee
ROORKEE - 247 667, INDIA

The Ph. D. viva-voce examination of **Mr. SANDEEP SINGH**, Research Scholar was held on 01-11-1994.

AKJain

Signature of Guides

V.C. 4/11/94

Signature of External Examiner

ACKNOWLEDGEMENTS

I abhor acknowledgements, but my conscience will not rest till I fully acknowledge all the helps and care extended to me during the thesis. First of all I would like to dwell upon this opportunity to express the immense gratitude I feel towards **Prof. A. K. Jain**, Department of Earth Sciences, University of Roorkee, Roorkee, whose guidance and support have always not only initiated me towards endeavors but also helped me reach their successful completion. I donot find enough words to thank him for the excellent and incomparable guidance he provided me not only during the thesis work but also throughout my course work and my stay in Roorkee and also for keeping patience with me whenever things were not working out as expected.

I also express my deep sense of gratitude to **Dr. RM. Manickavasagam**, Reader, for his perpetual guidence at every juncture of field and laboratory work and invaluable suggestions.

I owe, with regards, my unfeigned gratefulness to **Prof. D. G. Gee**, Department of Minerology and Petrology, Institute of Geology, University of Lund, Lund, SWEDEN, for the precious suggestions during my stay at SWEDEN as well as during later part of the thesis work. **Prof. Gee** and **Dr. P. G. Andreasson**, from University of Lund, Lund, have extended financial support during my stay in Sweden. Geochronological work was carried out at Laboratory for Isotope Geology, Swedish Museum of Natural History, Stockholm, SWEDEN, under the guidance of **Prof. S. Claesson** for his guidance and teaching for which I am grateful.

My sincere thanks are to **Mrs. Paula Allart** for introducing me to sample preparation, to **Mrs. Ann-Marie Khr** for chemical preparation of the sample, and to **Dr. Hans Schoberg** for his guidance and helpful discussions during

geochronological work on mass-spectrometer. I thank **Dr. Bengt Lindquist, Lars Gerschman, Magnus Hedberg, Leif Jansson, Marie Svensson, Knut Christiansson,** and **Dan Holtstam** for their help for making my stay pleasent and memorable. Thanks are also due to **Dr. Oke Johansson, Dr. Torbjorn Skiold** and **Dr. Kjell Billstrom** for useful suggestions on the inital draft of Chapter 6.

I am very much obliged to **Mrs. Vesleymoy Heintz Gee** for her guidance and moral support during my whole stay in SWEDEN. My thanks also goes to **Ms. Leena Paulin** who helped me a lot during my stay in laboratory of Isotope Geology in Stockholm, SWEDEN.

Encouragement and help receieved from **Dr. Pulok K. Mukherjee,** Scientist, Wadia Institute of Himalayan Geology is thankfully aknowledged. I also aknowledge his discussion with me, which was useful in elucidating certain aspect of geochemistry of granite. The help rendered by **Dr. V. C. Thakur,** Director, for arranging the geochemical analysis is thankfully acknowledge. Thanks also goes to **Dr. N. K. Saini, Dr. P. P. Khanna** and other scientists from Wadia Institue of Himalayan Geology are highly appreciated for providing facilities for geochemical analysis.

I am also very much thankful to **Prof. B. B. S. Singhal,** and **Late Prof. R. K. Goel,** ex-heads, Department of Earth Sciences, University of Roorkee, Roorkee, INDIA, for extending all the possible facilities during the tenure of research work.

The thesis forms a part of the major project sanctioned to **Prof. V. K. S. Dave,** Principal Investigator of the Department of Science and Technology (DST) programme on "Evolution of Metamorphic Belts of Himalaya" (Grant No. 1760-14-61). I owe my gratitude to **Prof. Dave** for financial support from this programme and providing guidance in the due course of work. Part of the field work was funded by the University of Roorkee (Grant No. 106-14-99) for which I am thankful to Dean, Research and Industrial Liaison.

For the most friendly, excellent and unflappable companionship, my heart-felt thanks to dears **Dr. R. C. Patel, Manoj Dangwal, Dr. Kush Garg, Dr. Sulekha, Dr. A. Asokan, Dr. Rajeev Sinha, Alok Sahai, R. K. Singh, L. P. Singh, Dr. Rajeev Gautam, Dinesh Tiwari, Manoj Pant, Dr. Pankaj Srivastava, Anurag Khanna, Pradeep Vishunawat, Manas Mohanti, Jay Ram Sahoo, Akshya Pradhan, Dr. Ashok Solanki, Devesh Tiwari, Sanjaya Agarwal** and **Subodh Rajput.**

I am also very much indebted to **Dr. Kamlesh Jain, Prof. R. P. Mathur, Neena Mathur, Shikha Sinha, Kumkum Tiwari, V. K. Tiwari, Sakhshi, Ankur Tiwari, Ajaya Gairola** and **Shipra Gairola** for their moral support and constant encouragement during my stay in Roorkee.

Thanks are due to **Ranjan, Roma, Neena, Shikha Sharma, Sapna Sharma, Margret, Chandra Mohan, Kuki, Achal Mittal, Rajneesh Garg, Pikoo** and **Montu** for making my stay pleasent, cheerful and memorable.

I am also very thankful to **Shri. S. P. Negi**, Executive Engineer and all his staff members of HPPWD, Rampur Bushahar, for providing the accomadation and other logistic support during the field work. How can I forget to acknowledege **Ramesh Chand** and **D. K. Singh** for their expert driving in the Himalayan terrain during field works as well as **Ramkaran** for making the field work successful, without whose help I am not able to think what would have happened in the field.

The help extended in computer application from **Dr. A. K. Saraf** and **Dr. Rajiv Sinha** is highly appreciated. I am also indebted to **Mr. Tarun K. Raghuvansi, Sanjeev Sharma, Atanu Roy Choudhary** and **Anirban Basak** for taking pain in the finalisation of Chapters.

I am thankful to **Kamesh Gupta** for neat drafting. Help extended by **R. C. Punj, Ram Dal** and **Amar Singh** in preparation of thin sections and polished sections,

Puran Sharma in the reproduction of photograph.

Special thanks to faculty for their perceptive guidance and tutorship which helped me strengthen my convictions on intended academic pursuits.

My sincere and affectionate gratitude is due to **Mummy, Papa, Dada, Bhabhi** and my neice **Shreya** for strengthening my moral to reach the goal.

Last but not least my thanks goes to all near and dear ones who helped me directly or indirectly during this work.

Sandeep Singh
26th Nov. '97

(SANDEEP SINGH)

Abstract

The Himalaya is located on the seismically-active northern margin of the Indian Plate, and provides an unique opportunity to investigate collision-related geodynamic processes of a young orogenic belt during the Cenozoic-Quaternary. Collision of the northerly-moving Indian Plate with the Eurasian Plate has considerably remobilised the Precambrian basement and cover sediments of the Indian Plate since 50 Ma.

The basic objective of the present work is to provide better tectonometamorphic and geochronological constraints on the collision tectonics of various metamorphic nappes along the Sutlej Valley and Chor Mountains in Himachal Pradesh.

Detailed geological work along the Sutlej valley and Chor Mountain has revealed the following major tectonic units:

(a) The Lesser Himalayan Proterozoic sedimentary foreland of quartzite-volcanic association, now exposed in many windows.

(b) The Bajura/Kulu Nappe of the Middle Proterozoic mylonitised augen gneiss, bounded by the Kulu Thrust at its base and the Main Central Thrust (MCT) / Jutogh Thrust (JT) at the top.

(c) The Higher Himalayan Crystalline (HHC) belt in the north is thrust southwestward over the Proterozoic Lesser Himalayan foreland of the Kulu-Rampur Window and Bajura/Kulu Nappe along the folded MCT/JT. Atleast two Proterozoic concordant to discordant magmatic events have been identified in the HHC, which lacks any Tertiary leucogranite bodies in the basal part.

(d) The Jutogh Nappe in parts of Chor Mountain and Luhri-Anni-Dalash region is separated from the Bajura/Kulu Nappe and less metamorphosed Chail Nappe by the Jutogh Thrust. The contact of the Chor granitoid, occurring at the top of the Jutogh metamorphics is characterised by intensely mylonitised porphyritic granite gneiss due to presence of the Chor thrust.

Between Jakhri and Wangtu, the HHC belt has undergone four distinct deformational phases. The earliest isolated tightly appressed `flame type' F_1 fold hinges are developed on lithological/metamorphic banding S_0 having axial plane foliation S_1, which appears to be the earliest recognisable penetrative planar fabric. The most pervasive second deformational phase develops an intense planar fabric S_2, which is axial planar to the N-NE/S-SW plunging F_2 folds. Being the main foliation, it is a composite planar fabric with S- surface being consistently rotated SW due to C-shear fabric. It possesses a strong down-the-dip N to NNE plunging stretching/mineral lineation L_2, that is coaxial to the F_2 isoclinal reclined folds. Asymmetric megacrysts, pressure fringes and rotational garnet etc. reveal a consistent southwestward verging broad ductile shear zone during the Himalayan Orogeny.

The third deformational D_3 phase is characterised by two distinct early D_{3a} and late D_{3b} phases. In the D_{3a} phase, F_{3a} folds are mainly isoclinal, inclined-type with gentle to moderately-dipping axial surfaces (S_{3a}). F_{3a} folds plunge either N 100° or N 300° at low angles. In the later D_{3b} phase of the same deformational event, coaxial asymmetric, SW-verging F_{3b} folds are mostly crenulation-type, whose hinges form a prominent lineation. Earlier L_2 lineation is folded around many F_{3b} hinges. The axial plane foliation S_{3b} of these folds in metapelite and granite gneiss strike N100° with very steep dips of about 60°-80° towards N or S.

The effects of late deformational phase D_4 are weak and sporadic during brittle-ductile and brittle regime. Thrust-faults, shear bands and quartz-filled

tension gashes are developed during this late stage deformation.

The deformational pattern of the HHC contrasts with the Jutogh Nappe in its frontal parts of the Simla Hills and Chor Mountains. In the frontal Jutogh Nappe, earliest D_{C1} deformation phase produces an E or W plunging tight to isoclinal, recumbent to moderately inclined folds on lithological layering of the sedimentary origin S_0 and is of Himalayan in age. This corresponds to the D_2 deformational phase of the HHC.

The HHC and Jutogh metamorphic nappe have undergone a polyphase Barrovian-type metamorphism under upper greenschist to amphibolite facies condition. Two sections have been investigated for detailed metamorphic evolution along (a) the Nauhra-Shamra treverse in southern parts of the Chor Mountain within the Jutogh Nappe and (b) Jakhri-Wangtu section along the Sutlej valley in the lower parts of the HHC. Mineral assembleges reveal the presence of two metamorphic grades in the HHC: (i) garnet and staurolite grade transition zone and (ii) staurolite-kyanite grade, while garnet grade rocks are present in basal Jutogh Nappe of the Chor Mountain. These assemblages appear to grow during the main deformational event, predating the mylonitic textures of the nappe translation.

Suitable assamblages were probed to evaluate the pressure and temperature conditions of metamorphism, by using the garnet-biotite (GB) thermometer and garnet-plagioclase-sillimanite/kyanite-quartz (GPAQ) and garnet-plagioclase-biotite-muscovite (GPBM) barometers. Along the Nauhra-Shamra section, syntectonic garnet core of M_{C1} indicate a variation of about 130° C from 520° C to 650° C, while post-tectonic garnet rim reveals a cooling path of the metamorphic pile with temperature falling between 480° C and 550° C at 5.4 to 7.8 kbar from its base towards higher structural levels. This variation seems to be real rather than apparent, hence is indicative of the metamorphic inversion in the Jutogh Nappe. In addition the Sutlej valley section of the HHC, garnet

records a temperature of about 520° C at the base along the MCT during the M_2 metamorphism and attains a maximum of 650° C towards higher structural levels. The pressure could not be estimated due to lack of suitable assemblage in this section. On the basis of the temperature data, this section also provides evidences of possible inversion in HHC.

Major and trace elemental analyses of 15 samples from important granitoid bodies reveal their peraluminous S-type character within the granite, quartz-monzonite and monzonitic field on quartz-orthoclase- plagioclase normative plot. The Rb vs Y + Nb discrimination plot indicate that these bodies are of Within Plate Granite (WPG). The Spidergram plotting of compatible and incompatible elements as well as REE normalised plots indicate similar chemical characters for porphyroclastic granite, the Wangtu granite and the Chor granite, like the Hunza granite of North Pakistan. However, these bodies are geochemically different from the Tertiary Gangotri (Garhwal) and Manaslu (Nepal) leucogranites.

Four granitoid samples from the hanging wall of the MCT/JT in the HHC and Jutogh Nappe have been dated by U-Pb systematics on zircons using isotopic dilution technique. The U-Pb zircon ages are of about 2.0 Ga, 1.8 Ga and 0.9 Ga, indicating the presence of the Proterozoic elements in the NW-Himalaya. The Chor granitoid in frontal parts of the Jutogh Nappe presents a complex history in the deformed and undeformed components; the latter yields an upper intercept of primary crystallisation age of 910 ± 23 Ma (2σ) from 7-point regression line, though better age of 912 ± 6 Ma (2σ) is estimated from 5-point regression line. Although the deformed Chor granitoid is not the best sample for this analysis, it also confirms the 900 Ma age for the granitoid. Basal parts of the HHC contain discordant aplitic granite bodies, whose U-Pb zircon age of 2068 ± 5 Ma (2σ) from 5-fraction regression line indicates an Early Proterozoic period of granite crystallisation. Another Early Proterozoic period of 1866 ± 10 Ma (2σ) for crystallisation event is indicated from U-Pb zircon age from the Wangtu

granitoid from a 5-fraction regression line. $^{87}Sr/^{86}Sr$ ratios from all these samples ranges between 0.706 to 0.716 and indicate their protolith to be the Archean-Proterozoic continental crust of the Indian Plate.

Deformational patterns in this part of the Himalayan metamorphic belt indicate that the Main Central Thrust and Jutogh Thrust *sensu stricto* were formed during or after late D_3 deformational event, and transported the ductily deformed metamorphic pile. These thrusts post-date the main progressive metamorphic events. P-T estimation, textural relationship and localised inverted metamorphic isograds can be explained in terms of ductile shearing, which caused the S-C fabric and, in turn, the inverted metamorphism in the HHC.

The HHC and Jutogh Nappe contain numerous Proterozoic granitoid bodies, emplaced during an early to syn-D_1 deformational event, and are now deformed into gneisses due to the Himalayan Orogeny. Although various bodies were emplaced atleast during three Proterozoic magmatic events having identical crustal protoliths, their geographical distribution may possibly be controlled by involvement of distinct tectonostratigraphic units within the Proterozoic basement.

It, therefore, appears that collision tectonics in parts of NW-Himalaya has caused, not only intense imbrication of remobilised Proterozoic basement in various metamorphic nappes, but also the Lesser Himalayan Foreland in window zone. Tectonometamorphic data from these nappes clearly reveal that main metamorphic evolution is synchronous with ductile shearing in a thick intracontinental ductile shear zone and predates the brittle-ductlile to brittle emplacement of metamorphic nappes along the Main Central Thrust and Jutogh Thrust.

CONTENTS

CHAPTERS

CHAPTER 1 : INTRODUCTION

1.1 PREAMBLE

The Himalaya defines the seismologically-active northern margin of the Indian Plate and displays evidences of orogenic processes due to collision of the Indian indenter with the Eurasian Plate during the Cenozoic (Dewey and Bird, 1970; Molnar and Tapponier, 1975). It provides an unique opportunity to study the collision-related geological processes viz., sedimentation, deformation, magmatism and metamorphism at different crustal levels.

The Himalaya records the Late Mesozoic history of the closure of the Tethyan Ocean by subduction of the oceanic crust of the Indian Plate beneath the Eurasian Plate and the development of an Andean-type continental margin (Fig. 1.1; Brookfield and Reynold, 1981; Honegger *et al.*, 1982; Coward *et al.*, 1986; Searle *et al.*, 1987; Pecher and Le Fort, 1986; Thakur, 1987, 1993; Sharma, 1991).

Collision Tectonics has considerably deformed the Higher Himalayan Basement metamorphics since 50 Ma. This deformation takes place within a major intracontinental ductile shear zone (Jain and Anand, 1988; Le Fort, 1988) and its subsequent southward thrusting, initially along the Main Central Thrust (MCT) zone and later along the Main Boundary Fault (MBF) and Main Frontal Thrust (MFT).

The Higher Himalayan Crystalline (HHC), presently exposed along the Great Himalayan Range (Fig. 1.1), constituted the `Precambrian basement' for the Phanerozoic Tethyan sedimentary pile (Bagati, 1990; Bhargava *et al.*, 1991). This is also evidenced from the recent high resolution U-Pb zircon ages from the Pakistan sector of the metamorphic belt, wherein the Indian continental crust having granitoids / gneisses of 400 - 500 Ma, 1800 - 2000 Ma and 2500 Ma were found

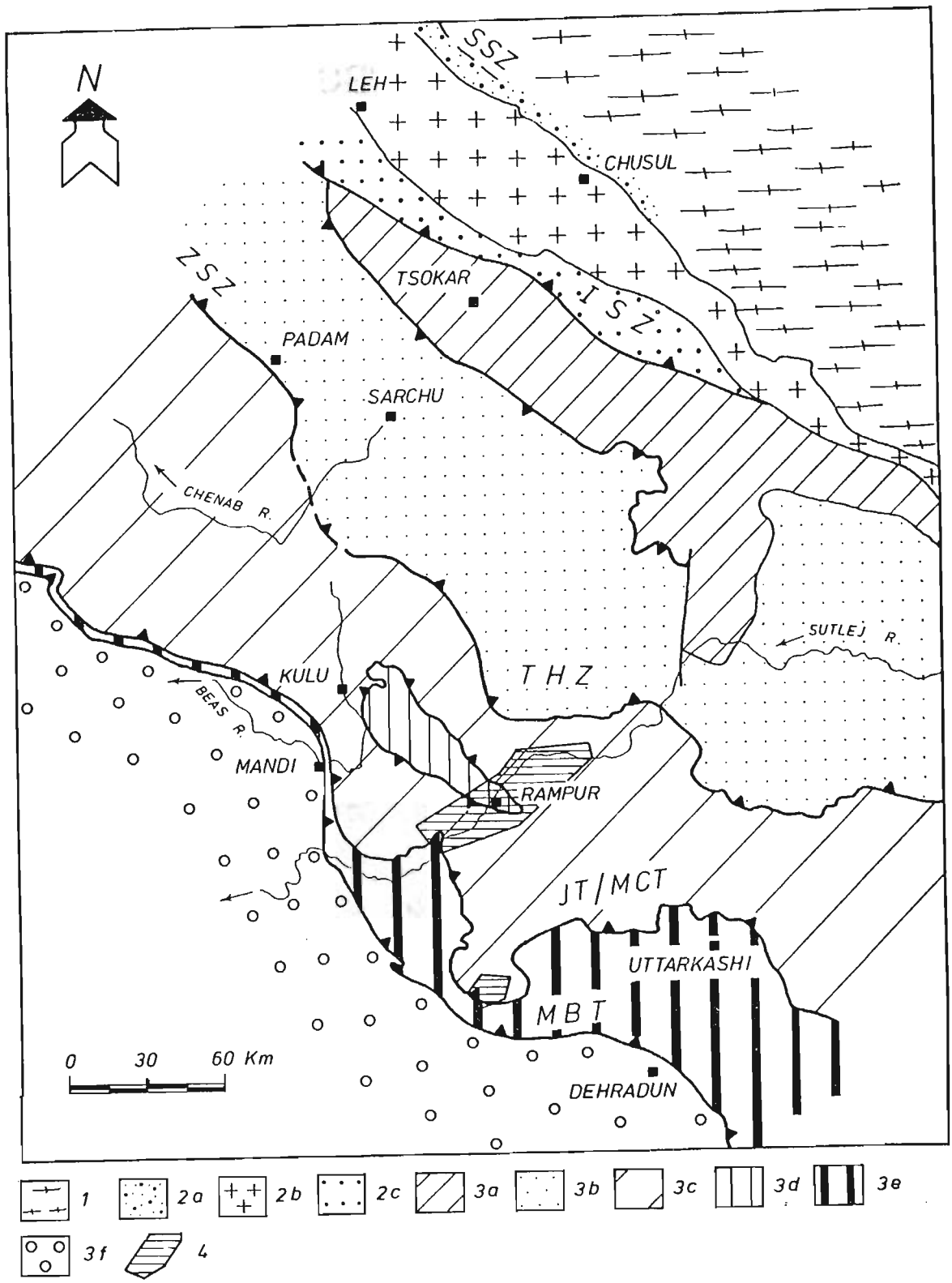

Figure 1.1 : Simplified tectonic map of the NW-Himalaya showing main units on northern margin of the Indian Plate. 1 : Eurasian Plate margin - (a) Karakoram batholith complex (KBC). 2 : Indian Plate Subduction Zone - (a) Shyok Suture Zone (SSZ), (b) Ladakh Batholith Complex, (c) Indus Suture Zone (ISZ). 3 : Himalayan Collision Zone - (a) Tso-Morari Crystalline, (b) Tethyan Sedimentary Zone, (c) Himalayan Metamorphic Belt, (d-e) Lesser Himalayan Proterozoic Foreland, (f) Sub-Himalayan Collision sedimentary Zone. 4 : Area of investigations. MBT - Main Boundary Thrust, JT/MCT - Jutogh Thrust/Main Central Thrust, ZSZ - Zanskar Shear Zone, THS - Trans-Himadri Shear.

reworked during the Himalayan orogeny (Zeitler *et al.*, 1989; Treloar *et al.*, 1989; Pognante *et al.*, 1990; Searle *et al.*, 1992).

Geochronological data have considerably constrained the subduction-related phenomenon along the Indus Tangpo Suture Zone (ITSZ) in Pakistan, Ladakh and southern Tibet (Honegger *et al.*, 1982; Scharer *et al.*, 1984). Detailed tectonometamorphic and geochronological coverage over the Higher Himalayan Crystalline (HHC) have only been available by Rb-Sr whole rock isochron ages and a few mineral ages by Rb-Sr, K-Ar, ^{39}Ar-^{40}Ar and fission track techniques in the NW-Himalaya and Nepal (Mehta, 1977; Debon *et al.*, 1981, 1986, 1987; Trivedi *et al.*, 1984; Honegger *et al.*, 1982; Searle, 1986; Le Fort, 1986; Deniel *et al.*, 1987). Table 1.1 summarises the available Rb-Sr whole rock isochron ages from the metamorphic belts of the NW-Lesser and Higher Himalayas.

1.2 OBJECTIVES

The basic objective of the present investigations are to provide tectonometamorphic and geochronological constraints on the Collision Tectonics of various metamorphic nappes in the NW-Himalaya, Himachal Pradesh along the Sutlej Valley and Chor Mountains.

Some of the detailed objectives are as follows :

* Comparison of deformational and strain patterns from the different metamorphic nappe units

* Tectonometamorphic evolution and P-T determination using suitable geothermobarometry

Table 1.1: Rb-Sr Whole rock ages from Himachal, Garhwal and Kumaoun Himalaya

LOCATION	ROCK TYPE/LITHOLOGICAL UNIT	AGE	$(^{86}Sr/^{87}Sr)_i$	SOURCE	REMARK
1.DALHOUSIE					
a.Around Dalhousi	Granite,granite gneiss/Jutogh Nappe	472±50	0.709	Bhanot et al., 1974, 1975	3 point isochron
b. -do-	Pegmatite/JN	362±50	0.709	- do -	- do -
2.MANDI					
a.Around Mandi	Granite/JN	500±100	0.8608 ± 0.9322	Jager et al., 1971	4 point isochron
b. -do-	- do -	545±12	0.7019 ±0.0015	Mehta, 1977	3 point isochron
c. -do-	Leucocratic granite/JN	311±6	0.8110 ±0.0007	- do -	- do -
d. -do-	Metabasic xenolith in granite/JN	640±20	0.7001 ±0.0005	- do -	- do -
3.KULU-MANALI					
a.Mandi-Rohtang Pass	Gneiss/Higher Himalayan Metamorpics (HHM)	581±9	0.7113 ±0.0007	- do -	5 point isochron
b.Kulu area	Migmatitic gneiss/HHM	500±8	0.7109 ±0.0007	- do -	4 point isochron
c.S-Lahul	Intrusive granite/HHM	495±16	0.7200 ±0.002	Frank et al., 1977	10 point isochron
4.RAMPUR-LARGI WINDOW					
a.Bandal-Largi	Meta-rhyolite & Granite gneiss	1840±70 ±0.0027	0.7083	- do -	4 point isochron
b.Bandal	Biotite granite gneiss/Window Zone	1220±100	0.748 ±0.100	Bhanot et al., 1976, 1979	3 point isochron
c.Manikaran	Uranite from quartzite/Window Zone	1232±120		Bhalla & Gupta, 1979	U-Pb 6 point concodia plot
4A.NIRATH-BARAGAON	Mylonite/Base of JN and HHC	1430±150	0.746	Bhanot et al., 1978	6 point isochron

Table 1.1 continued...

4B.WANGTU-JEORI	Gneiss/HHC	2025±86	0.7074 ±0.01	Kwatra et al., 1986	6 point isochron
5.NAITWAR, TONS VALLEY	Gneiss/Naitwar Crystalline Unit	1811±133	0.707 ±0.017	Singh et al., 1986	4 point isochron
6.HANUMAN CHATTI, YAMUNA VALLEY	Gneiss/HHM	1972±102	0.703 ±0.010	Singh et al., 1986	4 point isochron
7.BHATWARI BHAGIRATHI VALLEY	Gneiss/HHM	2047±119	0.706 ±0.007	- do -	- do -
8.HARSIL BHAGIRATHI VALLEY	Gneiss/HHM	521±39	0.713 ±0.009	- do -	5 point isochron
9.BHILGANGA VALLEY					
a.Rihee-Gangi	Gneiss/HHM	1841±86	0.710 ±0.010	- do -	4 point isochron
b.Brijrani Gad	Mylonitised granite gneiss/HHM	1276±12	0.82	Bhattacharya et al.,1981	3 point isochron
c.Ignedi nala	- do -	1139±46	1.10	- do -	9 point isochron
d.Chailli	Granite gneiss/HHM	2121±60	0.710 ±0.20	Raju et al., 1982	4 point isochron
e.Ghuttu	- do -	1763±116	0.727 ±0.029	Singh et al., 1985	5 point isochron
f.Chirpatiya khal	- do -	1708±131	0.732 ±0.147	- do -	4 point isochron
10.LANSDOWN	Granite gneiss/Almora Unit	334±24	0.791 ±0.009	- do -	5 point isochron
10A.DUDATOLI	Gneiss/Almora Unit	501±38	0.732 ±0.005	- do -	6 point isochron
11.AMRITPUR					
a.Amritpur	Gray granite/Ramgarh Nappe	1110±131	0.741	- do -	5 point isocron
	White Granite/Ramgarh Nappe	1585±192	0.947	- do -	4 point isochron
12.RAMGARH					
a.Ramgarh	Porphyritic & mylonitic granite gneiss/Ramgarh Nappe	1765±60	0.7235 ±0.0046	Trivedi etal., 1984	11 point isochron
b.Kiodal	Gneiss/Ramgarh Nappe	731±120	0.765	Singh, 1982	4 point isochron

Table 1.1 continued...

c.Rampur-Padampuri	- do -	1238±128	0.768	- do -	5 point isochron
13.ALMORA-CHAMPAWAT					
a.Rameshwar	Augen gneiss/Almora Nappe(Basal part)	1820±130	0.7144 ±0.0118	Trivedi etal., 1984	6 point isochron
b.Almora-Champawat	Granodiorite/Almora Nappe(Upper part)	560±20	0.7109 ±0.0013	- do -	15 samples
14.BAIJNATH-GWALDAM					
a.Gwaldam	Granite/Baijnath Klippe	1700±70	0.7375 ±0.0127	Trivedi etal., 1984	6 point isochron
b. - do -	- do -	1300±80	0.793	Pandey et al., 1981	5 point isochron
c.Baijnath	- do -	1130±110	0.736	- do -	4 point isochron
		1320±370	0.755	- do -	- do -
15.ASKOT-DHARAMGARH					
a.Askot-Dharamgarh	Augen gneiss/Askot Klippe	1795±30	0.7090 ±0.0015	Trivedi etal., 1984	9 point isochron
16.MUNSIARI					
a.Naurik	Gneiss/HHM	1910±88	0.724	Singh et al., 1985	5 point isochron
b.Tawaghat	- do -	1906±220	0.724	- do -	9 point isochron

* Relationships between deformational episodes and granitoid emplacement

* Geochemical characters and genesis of various granitoids

* U-Pb zircon dating of granitoids

* Modelling of collision tectonics

1.3 TECTONIC FRAMEWORK : A REVIEW

The Lesser and Higher Himalayan morphotectonic domains in the northwestern region comprises large-scale extensive allochthonous metamorphic nappes, which are thrust over the Lesser Himalayan Proterozoic sedimentary foreland, exposed in various windows. Some of the major tectonic units in Himachal Pradesh are reviewed below.

1.3.1 Jutogh Nappe

The name Jutogh was coined by Oldham (1887) and formalised by Pilgrim and West (1928) for medium grade pelitic and semipelitic rocks constituting an important allochthonous folded nappe in the Lesser and Higher Himalayas in parts of the Sutlej-Ravi valleys, Himachal Pradesh (also Sharma, 1977; Bhargava, 1980). The frontal parts of this nappe has been transported much to the south along the Jutogh Thrust over the Lesser Himalayan Proterozoic foreland of quartzite-volcanics and granitoids, now exposed in the Kulu-Rampur Window (Fig. 1.2; Frank *et al.*, 1977; Sharma, 1977; Bhargava *et al.*, 1991). Subthrust parts of the Jutogh nappe expose the Chail metamorphics in the front. A middle Proterozoic (1430 ± 150 Ma - Bhanot *et al.*, 1978) Nirath-Baragaon porphyroclastic mylonitised augen gneiss is intermittantly sandwitched between the Jutogh nappe and the

sedimentary foreland, probably as a much extensive distinct Bajura/Kulu nappe (Fig. 1.2; Frank *et al.*, 1977; Gururajan and Virdi, 1984; Bhargava *et al.*, 1991).

The Jutogh Nappe is one of the most important tectonic unit in Himachal Pradesh and can be traced into two main outcrops :

(i) the pear-shaped klippe around Shimla, and
(ii) the almost-continuous metamorphic belt from Chor Hills to Kinnaur-Garhwal above the Main Central Thrust (MCT) as the Higher Himalayan Crystalline (HHC) in upper reaches of Sutlej-Chenab valleys.

These metamorphics are either unconformably overlain by the Tethyan sedimentary zone towards northwest in Chamba-Bharmaur region or seperated from the latter by the Zanskar Shear Zone/Trans-Himadri zone in the north (Srikantia *et al.*, 1978; Honegger *et al.*, 1982; Herren, 1987; Valdiya, 1989; Staubli, 1989; Jain *et al.*, 1991; Patel *et al.*, 1993).

1.3.2 Kulu-Rampur Window

The existence of a tectonic "window" around Rampur was first indicated by Berthelsen (1951), where deeply eroded Proterozoic quartzite-volcanics association was discovered beneath the enormous pile of the metamorphics and gneisses, exposed along the Sutlej river and its tributaries (Sharma, 1977; Frank *et al.*, 1973, 1977; Mehta, 1976, 1977; Sharma, 1976; Bhargava *et al.*, 1972)

The Kulu-Rampur Window zone exposes stromatolite-bearing dolomitic limestone, slate and metavolcanic-quartzite association. A belt of deformed Proterozoic Bandal Granite, having a strike-length of about 50 km and width of about 12 km, occurs as a concordant intrusive sheet within the window. The granite contains numerous xenoliths of the country rocks and intrudes the

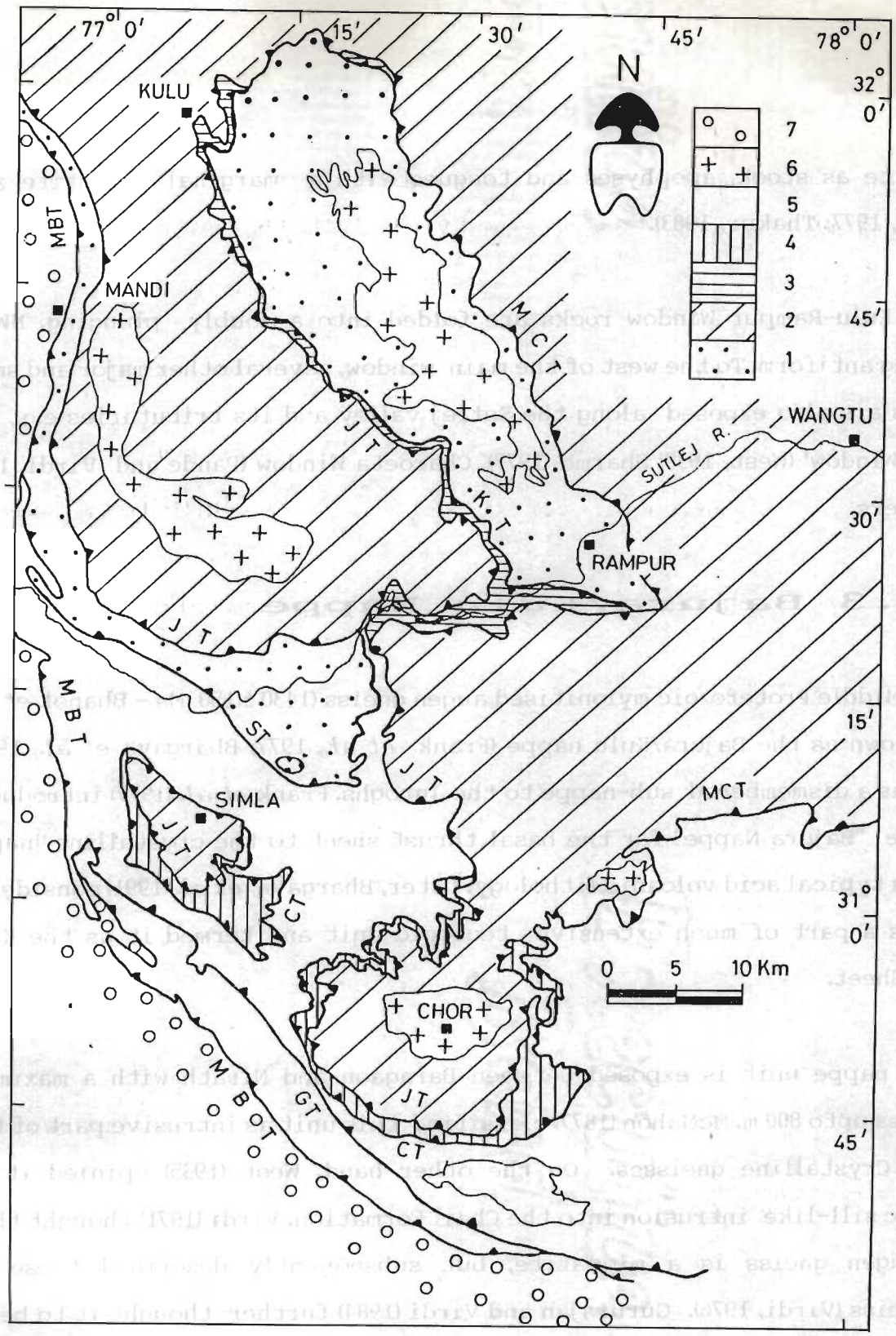

Figure 1.2 : Geological map of the Himachal Pradesh, India. (1) Rampur - Kulu - Shali Window (2) Jutogh Thrust Sheet (3) Chail Thrust Sheet (4) Bajura-Kulu Thrust Sheet (6) Granite/Granite Gneiss (5) Simla-Deoban-Garhwal Group (7) Sub-Himalayan Tertiary Belt. MCT-Main Central Thrust, JT-Jutogh Thrust, CT-Chail Thrust, MBT-Main Boundary Thrust, KT-Krol Thrust, GT-Giri Thrust, ST-Suketi Thrust.

quartzite as stock, apophyses and tongues with a marginal migmatite zone (Sharma, 1977; Thakur, 1983).

The Kulu-Rampur Window rocks are folded into a doubly plunging, NW-SE trending antiform. To the west of the main window, several other major and small windows are also exposed along the Sutlej valley and its tributaries e.g., the Shali `Window' (West, 1939; Sharma, 1977), Charoeta Window (Pande and Virdi, 1970) and others.

1.3.3 Bajura/Kulu Nappe

The Middle Proterozoic mylonitised augen gneiss (1430 ± 150 Ma - Bhanot *et al.*, 1978), known as the Bajura/Kulu nappe (Frank *et al.*, 1977; Bhargava *et al.*, 1991), occurs as a dismembered sub-nappe to the Jutoghs. Frank *et al.* (1977) introduced the name "Bajura Nappe" for the basal thrust sheet to the crystalline nappe having a typical acid volcanic lithology. Later, Bhargava *et al.* (1991) considered these as a part of much extensive tectonic unit and termed it as the Kulu Thrust Sheet.

This nappe unit is exposed between Baragaon and Nirath with a maximum thickness upto 800 m. McMahon (1877) classified this unit as intrusive part of the Central Crystalline gneisses. On the other hand, West (1935) opinied it as magmatic sill-like intrusion into the Chail Formation. Virdi (1971) thought that the augen gneiss is a migmatite, but subsequently described these as orthogneiss (Virdi, 1976). Gururajan and Virdi (1984) further thought it to be of intrusive character and deformed during the Himalayan thrusting event. However, Sharma (1977) believed that the augen gneiss is of metasomatic in character.

1.4 SELECTION OF THE AREA

Segments of the various tectonic units cited above have been investigated in parts of Himachal Pradesh along the Sutlej Valley and Chor Mountains between latitudes 30°45'N to 31°35'20"N and longitudes 77°15'E to 78°0'10"E during several field visits (Fig. 1.1).

1.5 SCOPE OF THE WORK

The scope of the thesis in terms of inputs to the Collision Tectonics is confined to geological and structural relationships of various units, tectonometamorphic evolution of the metamorphic nappes and geochemical-geochronological constriants on the various granitoids. These inputs are detailed below:

* Geological set-up, structure and tectonic relationships of the Jutogh Nappe, Kulu-Rampur Window and Bajura/Kulu Nappe

* Identification and mutual relationships between various deformational episodes
  - Structural analysis of mesoscopic structures and their relation to regional tectonics
  - Deformational and fold interference pattern
  - Relationship between deformational episodes and granitoid emplacement
  - Determination of finite strain in metamorphic nappes

* Tectonometamorphic history and P-T determination using different geothermobarometry

* Geochemistry of different granitoids

* U-Pb zircon dating of various granitoid bodies

* Tectonic modelling of the Collision zone.

1.6 METHODOLOGY

* Systematic geological mapping on 1:50,000 scale using Survey of India toposheet nos. 53 E /7, 10, 11, 14; 53 F /5, 9, 53 I /2 and sampling of different lithotectonic units

* Detailed study of various structural elements viz. folds, faults, foliation and lineation of different generations and their mutual relationships

* Data collection and structural analysis in different sub areas, using standard techniques

* Finite strain analysis using Rf/ϕ technique

* Textural and petrological studies on different mineral assembles from metamorphic nappes

* Electron Probe Micro Analyser (EPMA) analysis of metamorphic rocks for P-T determination

* Major, trace and REE elemental analyses of different granitoid samples for genetic relationships using X-ray fluroscentmeter (XRF) and Induced Coupled Plasma Analyser (ICPA)

* Age determination by U-Pb zircon isotopic dilution techniques using mass spectrometer

* Determination of initial $^{87}Sr / ^{86}Sr$ ratio using U-Pb modal age of zircon by massspectrometer.

CHAPTER 2: GEOLOGICAL FRAMEWORK

2.1 INTRODUCTION

The earliest knowledge of the geology of the Himalaya came from the pioneers like Medlicott (1864), Stoliczka (1866), Oldham (1883), Griesbach (1893), Hayden (1904) and others. Among the next generation of workers, Wadia (1928, 1957), Pilgrim and West (1928), Auden (1934, 1935, 1937) and Heim and Gansser (1939) produced classical works on the Himalaya. Within the last thirty years, the Himalayan Geology got much impetus and concerted attention from the geologists and geophysicsists.

The present state of knowledge of the regional geology, structure and tectonics of the Himalaya does not provide sufficient data and clear understanding, to evolve a valid and unanimously acceptable model for the evolution of this orogenic belt (Thakur, 1980; 1993). Much of these veiw points arise through divided opinions on stratigraphic nomenclature, unfossiliferous character of rocks and lack of sufficient manpower in comparison to the investigators, engaged in other orogenic belts.

The regions along the Sutlej Valley in Himachal Pradesh between Baragaon-Nirath-Jeori-Wangtu and the Chor area (Fig. 1.2) are important in understanding tectonometamorphic evolution of parts of the NW-Himalaya. The present chapter encompasses detailed geological framework of the region with brief description, distribution and mutual relationships of various tectonostratigraphic units. Figure 2.1 provides a wider geological cross-section through the area.

Figure 2.1 : Geological cross-section through the Himalaya in Himachal Pradesh 1 : Sub-Himalayan Collision sedimentary belt. 2 : Lesser Himalayan Proterozoic Foreland - (a) Krols and Infra Krols (b) Simla Group, (c) quartzite, (d) volcanics and (e) carbonaceous phyllite/slates. 3 : Chail Nappe. 4 : Jutogh metamorphics. 5 : Proterozoic granitoid bodies. 6 : Bajura/Kulu Nappe, 7 - Higher Himalayan Crystalline -(a) Jeori Formation and (b) Wangtu Granite Complex. MBT - Main Boundary Thrust, GT - Giri Thrust, CT - Chail Thrust, JT - Jutogh Thrust, CRT - Chor Thrust, KT - Kulu Thrust, MCT - Main Central Thrust, CHT - Chaura Thrust, GR - Giri River, AR - Asan River and SR - Sutlej River.

2.2 TECTONOSTRATIGRAPHY

Detailed geological mapping along the Sutlej valley and Chor area has revealed the following major tectonostratigraphic units (Figs. 2.2, 2.3; Table 2.1):

(a) Lesser Himalayan Proterozoic sedimentary foreland, exposed in the Kulu-Rampur Window and numerous other small windows.

(b) Bajura/Kulu Nappe of the Middle Proterozoic mylonitised augen gneiss.

(c) Higher Himalayan Crystalline (HHC) belt constituting the hanging wall of the Main Central Thrust (MCT) between Jakhri and Wangtu.

(d) Jutogh Nappe in parts of the Chor Mountain and Luhri-Dalash region.

2.3 LESSER HIMALAYAN PROTEROZOIC SEDIMENTARY FORELAND

The Lesser Himalaya is made up of Proterozoic and partly Early Paleozoic volcano-sedimentary sequences, deposited over a long span of time through a number of sedimentary cycles (Srikantia, 1976; Valdiya, 1980; Virdi, 1988). This foreland is exposed in the outer and inner Lesser Himalayan belts (Srikantia and Bhargava, 1974). The outer belt is exposed as the continuous belt in the frontal parts, while the inner belt constitutes several tectonic windows due to erosion of the overlying allochthonous metamorphic nappes.

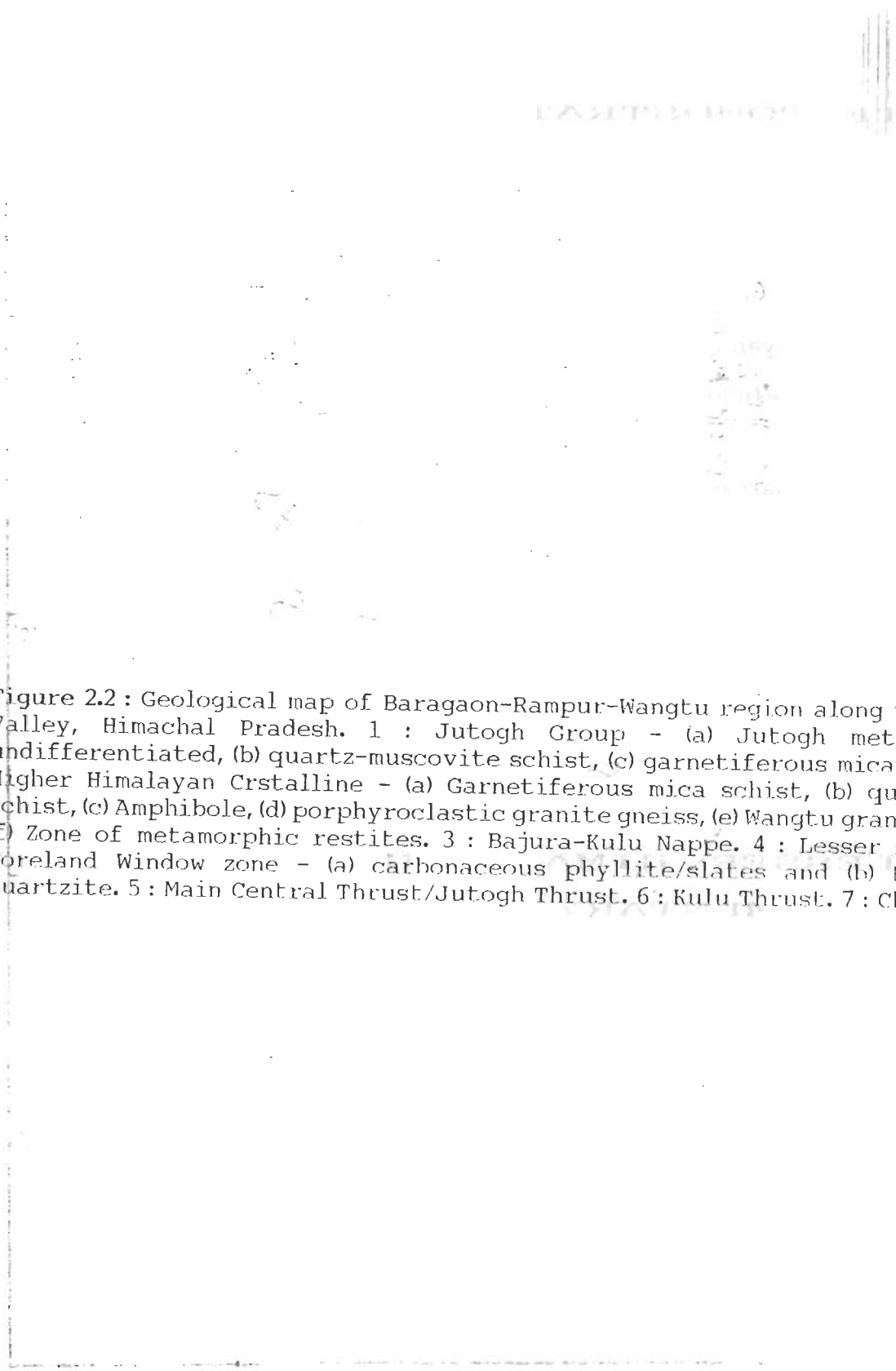

Figure 2.2 : Geological map of Baragaon-Rampur-Wangtu region along the Sutlej Valley, Himachal Pradesh. 1 : Jutogh Group - (a) Jutogh metamorphics undifferentiated, (b) quartz-muscovite schist, (c) garnetiferous mica schist. (2) Higher Himalayan Crstalline - (a) Garnetiferous mica schist, (b) quartz-mica schist, (c) Amphibole, (d) porphyroclastic granite gneiss, (e) Wangtu granitoid, and (f) Zone of metamorphic restites. 3 : Bajura-Kulu Nappe. 4 : Lesser Himalayan Foreland Window zone - (a) carbonaceous phyllite/slates and (b) Manikaran Quartzite. 5 : Main Central Thrust/Jutogh Thrust. 6 : Kulu Thrust. 7 : Chaura

Table 2.1 Lithotectonic setting of the Himalayan metamorphic belt along Sutlej Valley and Chor Mountain, Himachal Pradesh

SUTLEJ VALLEY				CHOR AREA			
Tectonic Unit	Lithological Unit		Lithology	Tectonic Unit	Lithological Unit		Lithology
HIGHER HIMALAYAN CRYSTALLINE (HHC)	Wangtu granite gneiss		Porphyroclastic granite gneiss, fine grained gneiss, schist and amphibolite	JUTOGH NAPPE	Chor Granitoid		Non-foliated homogeneous granite
							Porphyritic granite gneiss
							Biotite granite gneiss
	------ Chaura Thrust----------				-----Tectonic Contact----------		
			Fine-grained grey gneiss and pegmatitic gneiss				Dolerite dykes
	Jeori Formation		Amphibolite				Hornblende schist and amphibolite
			Quartz-muscovite schist		Jutogh Group		Mica schist and associated white marble
			Gernetiferous mica schist and gneiss				Upper quartzite
							Carbonaceous schist and associated black marble
							Lower quartzite
---------- Jutogh Thrust ----------							
BAJURA/KULU NAPPE			Mylonitised augen gneiss		----------Jutogh Thrust----------		
				CHAIL NAPPE	Chail Formation		
---------- Kulu Thrust ----------							
KULU-RAMPUR WINDOW (Lesser Himalayan Sedimentary Zone)	Rampur Group	Carbonaceous slate/ phyllite	Quartzite, quartz schist, chlorite schist, metavolcanics				
		Mainkaran Quartzite					
		Rampur Volcanics					

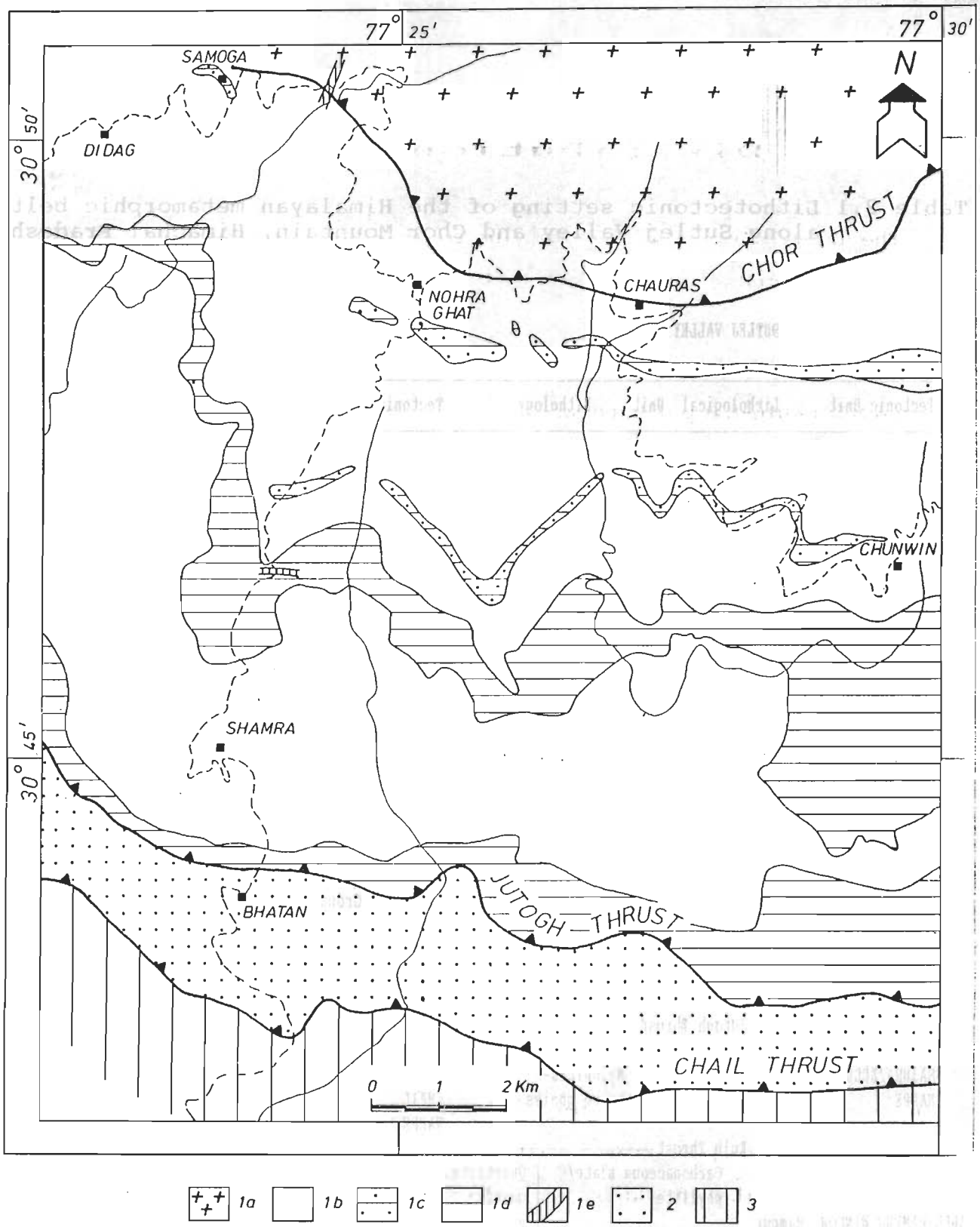

Figure 2.3 : Geological map of the Chor Mountain region, Himachal Pradesh. 1 : Jutogh Group - (a) Chor granitoid, (b) mica schsist/gneiss, (c) marble with carbonaceous phyllite, (d) quatzite and (e) dolerite dyke. 2 : Chail Group and 3 : Lesser Himalayan sedimentary sequence.

2.3.1 Distribution

The Lesser Himalayan Proterozoic foreland is exposed in the following antiformal windows along the Sutlej Valley beneath the allochthonous metamorphic nappes in this area:

(a) Main Kulu-Rampur Window,

(b) Charoeta Window to the west of the Kulu-Rampur Window

(c) Luhri-I and Luhri-II windows further downstream along the Sutlej river, and

(d) Shali belt as a long linear belt in the westernmost part of the area.

The Kulu-Rampur Window is approximately 100 km long NW-SE trending linear belt in parts of the inner Lesser Himalaya. McMahon (1881) described the window rocks around Rampur as the Infra-Krols. Auden (1934) indicated that the Larji series of dolomite, limestone, slate and quartzite also occurs as "window", similar to the "Shali Window", as described by West (1939). Subsequently, Berthelsen (1951) and Jhingran *et al.* (1950) indicated the probable presence of a tectonic window at Rampur.

In Kulu-Rampur Window, quartzite-volcanic-carbonaceous phyllite/slate sequence has been classified as the Rampur Group. While no fossils have been discovered so far, its original stratigraphic sequence has been locally imbricated, thus producing localised tectonic lenses of the Rampur Volcanics within the Manikaran Quartzite. Within the main window, the Early to Middle Proterozoic sedimentary sequence is regionally comprised of the Rampur Volcanics (Sm-Nd whole rock age - 2509 ± 94 Ma; Bhat and Le Fort, 1992) and the overlying thick Manikaran Quartzite and carbonaceous phyllite. A concordant Bandal granitoid of batholithic dimension (Rb-Sr whole rock age - 1840 ± 70 Ma; Frank *et al.*, 1977) intrudes the Proterozoic sedimentary succession in the core

of the Kulu-Rampur Window (Sharma, 1977; Frank *et al.*, 1977; Bhanot *et al.*, 1976).

2.3.2 Lithology

The Rampur Group has been subdivided into the following units.

a. Rampur Volcanics: The Rampur Volcanics is mainly exposed on the western flank of the Kulu-Rampur Window along the Sutlej valley below quartzite and carbonaceous phyllite. This formation comprises greenish phyllite and schist between Nogli gad to Rampur with thick quartzite and phyllite intercalations. At Rampur, the formation contains deformed amygdolidal volcanic flows within greenish chlorite schist and phyllite. Most of the amygdules are filled in with secondary minerals like chlorite, calcite, quartz etc. and have undergone very high flattening strain, forming a consistently N to NE or S to SW plunging lineation. At places, these volcanics are highly sheared and crenulated with boudinaged quartz veins parallel to the foliation. Further upstream, these metavolcanics occur as the tectonic lenses within the massive Manikaran Quartzite. The age of this volcanic has been assigned as 2509 ± 94 Ma by Bhat and Le Fort (1992) by Sm-Nd whole rock isochron. These volcanics constitute the Green Bed Member of Sharma (1977) and representing Early Proterozoic volcanism in the inner Lesser Himalaya.

The Rampur Volcanics is low grade metamorphosed basic volcanic-volcanoclastic association and probably coeval with other Proterozoic Mandi-Darla Volcanics, exposed in near vicinity within the Shali belt. It also has equivalents in Dharagad, Damtha and Berinag as rift-related volcanics of spilitic character (Pareek, 1973; Patwardhan and Bhandari, 1974). This volcanic activity appears to have started during the late stage deposition of metasediments with subordinate metabasites (Bhat and Le Fort, 1992).

b. Manikaran Quartzite: The quartzite of the Rampur Group is exposed beneath the Jutogh Thrust (JT)/ Main Central Thrust (MCT) from Jakhri to Rampur within the Kulu-Rampur Window as a thick lithostratigraphic unit. It is thrust over by the Bajura/Kulu Nappe on the western side and the HHC on the eastern side of the window. Thick quartzite sequence overlies the Rampur Volcanics. It is mainly composed of white massive thickly bedded quartzite, but light greenish, grey and banded quartzite is also locally seen. Within the massive quartzite, a few ductile shear zones have also been observed (Fig. 2.4 a) due to which the quartzite grades into the quart-mica schist within the shear zone. However, presence of cross-beds and ripple cross-beds indicate normal stratigraphic succession within the Manikaran Quartzite. Towards southeast around Kasa and Pat villages, quartzite reveals uranite mineralisation as veins and disseminated ores. Uranium mineralisation is estimated to be around 1232 ± 120 Ma by U-Pb age in this quartzite unit near Kulu (Bhalla and Gupta, 1979).

c. Carbonaceous slate/phyllite: The carbonaceous slate and phyllite are mainly exposed on western parts of the main Kulu- Rampur Window and also in other small windows, where it is thrust over by overlying mylonite augen gneiss along the Kulu Thrust (Fig. 2.2). Dark grey to blackish and brown coloured thinly laminated carbonaceous slate and phyllite are highly contorted and friable. The carbonaceous phyllite is also characterised by S- and C- shear fabric indicating that upper block has moved towards SW. Carbonaceous phyllite and interbedded thin dark grey and massive quartzite indicate a gradational stratigraphic contact with the underlying Manikaran Quartzite. Development of quartz fabric in pressure shadow zone around pyrite crystal define locally developed stretching lineation. Upon weathering, pyrite imparts a reddish and yellowish colouration to the rocks. Carbonaceous phyllite is sporadically phosphatic and also rarely contain calcareous intercalations.

d. Dolomitic limestone: In the western parts of the area, the dolomitic limestone

Figure 2.4 a : Massive Manikaran Quartzite with a few NE-dipping ductile shear zones cutting across the lithological bedding. Loc. : About 4 km from Rampur town in the Sutlej valley on the National highway 22.

Figure 2.4 b : Conglomerate within the Chareota Window having well rounded elongated pebbles and boulders of quartzite and orthoquartzite composition with closely-packed pitted boundaries due to pressure soloution. Loc. : On the left bank of the Sutlej river near Chareota village.

Figure 2.4 c : Cliff-forming Nirath-Baragaon mylonitic augen gneiss of the Bajura/Kulu Nappe. Photograph looking east from bridge of Luhri village.

Figure 2.4 d : Porphyroclastic granite gneiss of the Wangtu granite complex showing elongated and deformed megacrysts of alkali feldspar, quartz and plagioclase, embedded in extremely fine-grained greasy-looking foliated groundmass of quartz, feldspar and mica. Loc. : Near Nugalsari.

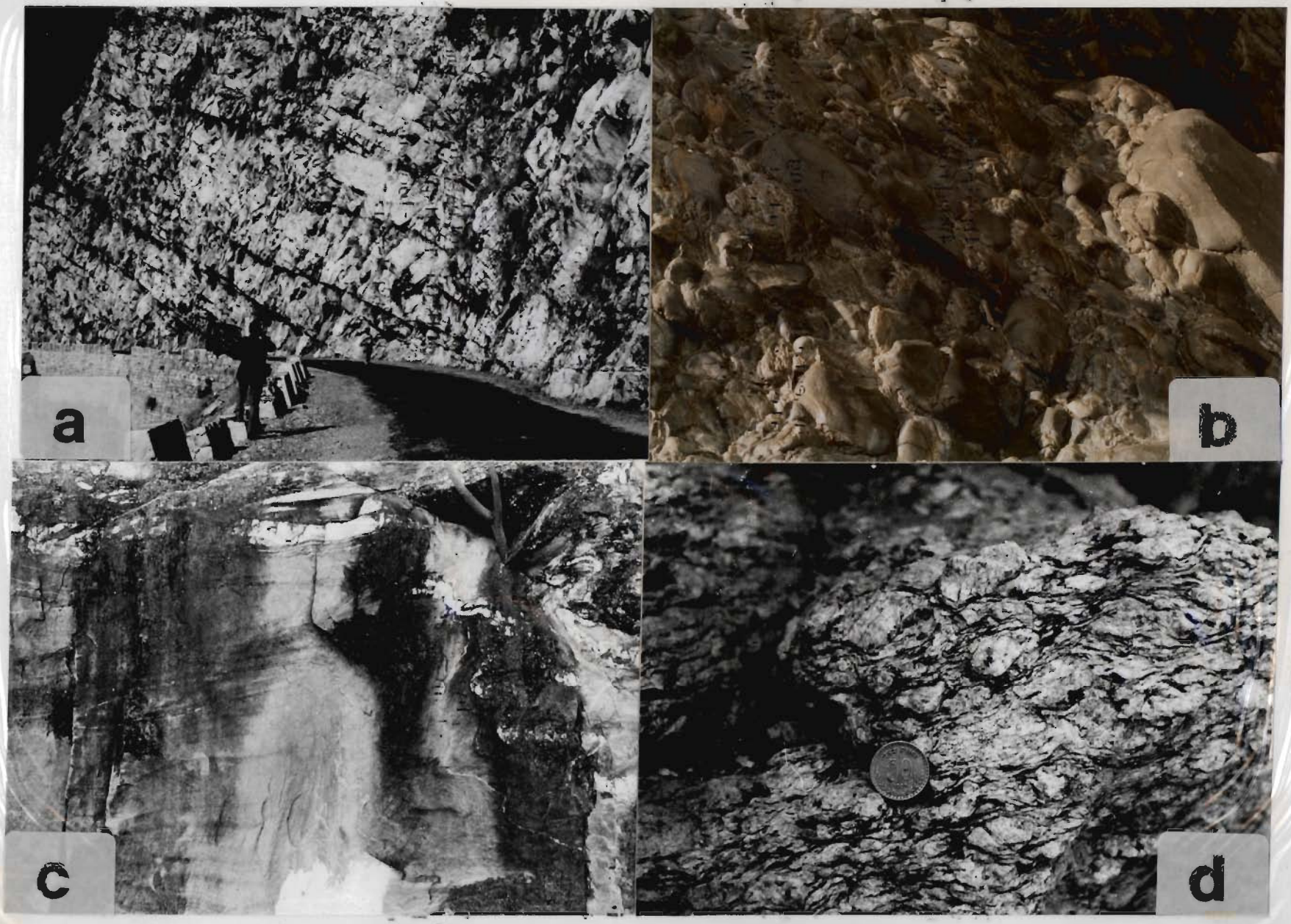

FIGURE 2.4

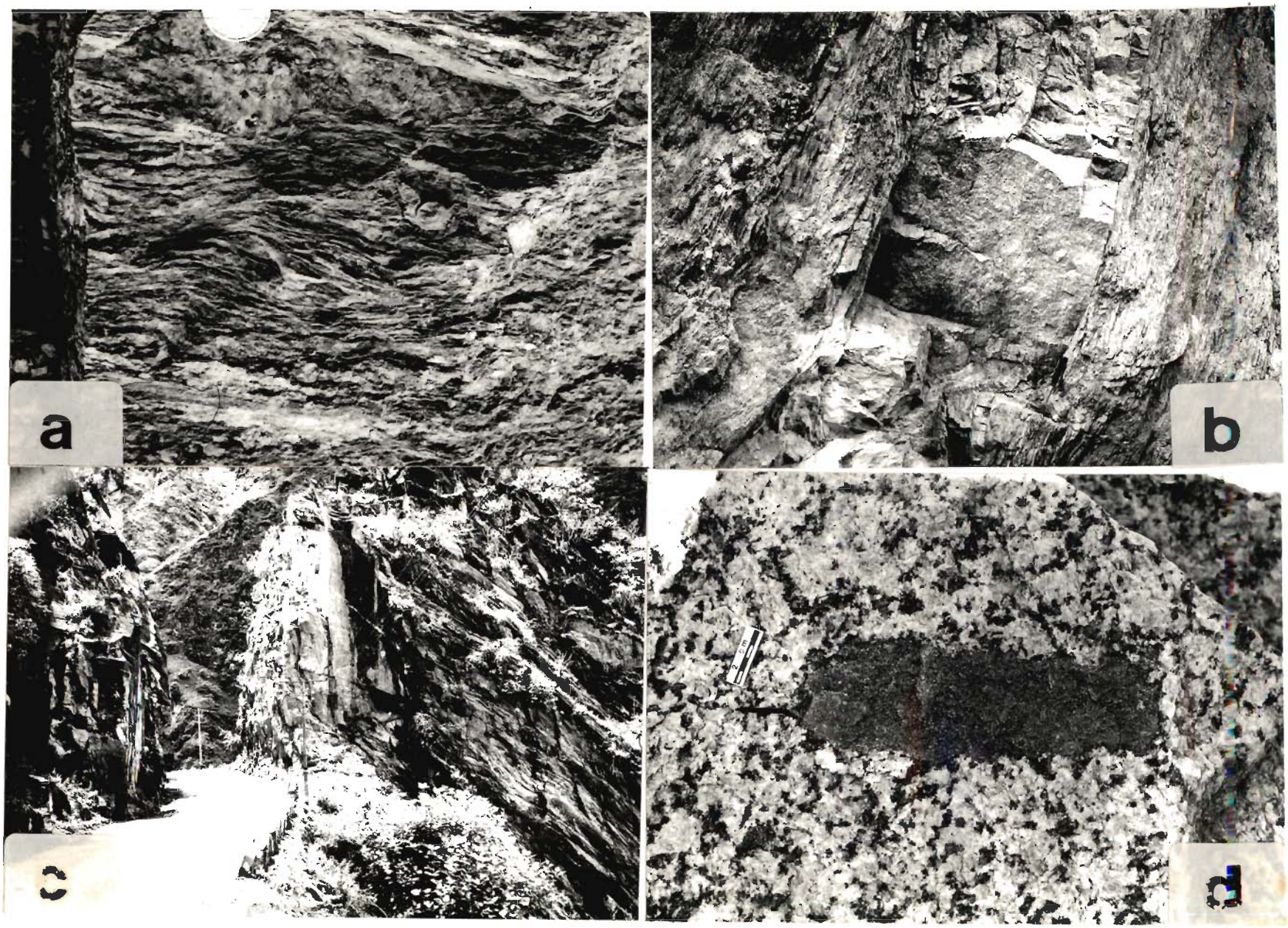

FIGURE 2.5

is exposed within the Shali Window along its easternmost margin. Greyish, reddish and yellowish dolomitic limestone reveals layering with beds ranging in thickness from 5 to 30 cm. Massive, hard and compact limestone beds have characteristic elephant-skin weathering. Greyish calcareous phyllite and phyllite intercalation are common and impart strong foliation. A mineral lineation of sericite and muscovite is distinctly seen on many foliation plane. Thin bands of greyish chert, lenticles of black chert, lenses of quartzite impart the rock a bedded character. The limestone is deformed into lenses with argillaceous beds wrapping around the lenses due to intense shearing.

e. Conglomerate and slate: The Cheroata Window contains localised outcrop of quartzitic and orthoquartzitic conglomerate, having well rounded elongated pebbles and boulders embeded in sandy matrix (Fig. 2.4 b). Most of the boulders range in size from 10 to 30 cm and possess closely packed pitted boundaries, characterised by pressure solution phenomenon (Fig. 2.4 b). These fragments are well elongated on a poorly developed foliation, which trends ENE-WNW and dips 60x/NE. Prominent pebble lineation plunges down-the-dip towards NE at steep angle. At places, the quartzite conglomerate are embedded in graphitic or carbonaceous phyllitic matrix. Greyish graded siltstone and shale alteration are highly contorted and deformed within the window zone, hence it is often difficult to workout detailed stratigraphic relationships within the window zone, in which argillaceous rocks are mainly exposed.

2.4 BAJURA/KULU NAPPE

Frank *et al.* (1977) introduced the term "Bajura Nappe" for a typical lithological association of highly mylonitised augen gneiss having typical acid volcanic affinity for a basal thrust sheet to the "Crystalline Nappe". Later, Bhargava *et al.* (1991) considered this unit as a part of much extensive nappe

Figure 2.5 a : Nirath-Baragaon mylonitised augen gneiss containing well-developed mylonitic foliation with stretched quartz-feldspar rich bands near Nirath village. Also seen are δ-shaped asymmetrical feldspar augen and an extensional foliation band in the left. Scale : photograph 22 cm long.

Figure 2.5 b : Metapelite sequence of garnetiferous mica schist/gneiss of the Jeori Formation having psammite band of 1.30 m thickness. Loc. : 3 km upstream from Jeori.

Figure 2.5 c : Almost vertically diping fine-grained grey granite gneiss (light coloured), emplaced within garnetiferous mica schist (dark shades) of the Jeori Formation as concordant igneous bodies along the metamorphic banding. Loc. : 7 km milestone towards Jakhri near road bend of the Maglad Khad on National highway 22.

Figure 2.5 d : Undeformed Wangtu granitoid showing equigranular randomly oriented dark coloured biotite with quartz and feldspar having xenolith of biotite schist. Loc. : Wangtu bridge on left bank of the Sutlej river.

(Fig. 1.2) and termed it as the Kulu Thrust Sheet. In the present work, this tectonic unit has been designated as the Bajura/Kulu Nappe, a sub-nappe to the Higher Himalayan Crystalline/Jutogh Nappe. Earlier, Frank *et al.* (1977) incorporated the underlying carbonaceous phyllite/slate within this nappe along with the mylonitised augen gneiss, while Sharma (1977) mapped these units as part of the Kulu-Rampur Window. Virdi (1971) and Gururajan and Virdi (1982) believed that the mylonitised augen gneiss as part of the Chail Group. Considering the occurrence of highly mylonitised augen gneiss with a well developed L-S fabric, a probable acid volcanic affinity and its tectonised lower and upper sharp contacts, only this lithology has been incorporated in the Bajura/Kulu Nappe. On the basis of their gradational contacts, the underlying carbonaceous phyllite/slate and the Manikaran quartzite have been classified as parts of the Kulu-Rampur Window zone.

2.4.1 Distribution

Highly mylonitised augen gneiss with large quartz and feldspar megacrysts is intermittently exposed between Ravi and Sutlej Valleys. Low-grade metamorphosed quartzite-volcanic- phyllite association of the Rampur Group is abruptly overlain by a 800 m thick dismembered mylonite and is bounded by the Kulu Thrust at its base and MCT/Jutogh Thrust at its top.

The age of the augen gneis belt has been assigned as 1430 ± 150 Ma, based on six-point Rb-Sr whole-rock isochron with an initial high $^{87}Sr/^{86}Sr$ ratio of 0.746 indicating its derivation from the remobilised crustal material (Bhanot *et al.*, 1978).

2.4.2 Lithology

a. Mylonitised augen gneiss: Massive grey to dark grey, hard, compact, highly sheared and mylonitised augen gneiss is characterised by cliff-forming lithounit along the Sutlej valley (Fig. 2.4 c). It contains elongated and deformed alkali feldspar, quartz and plagioclase megacrysts, embeded in extremely fine grained greenish greasy-looking and foliated groundmass of quartz, feldspar and mica (Fig. 2.4 d). Due to intense deformation along the margins, megacrysts have undergone grain-size reduction, recrystallisation and development of blastomylonite and ultramylonite. The megacrysts show flattened mantles and elongated tails of either dynamically recrystallised or reaction-softened minerals. Megacryst's tails are derived from originally larger grains by grain-size reduction. At times, extremely thinned tails of intensely strained megacrysts are folded, when these taper off away from the megacryst. In such cases, ribbon structures parallel the preferred mica orientation.

The mylonitised augen gneiss contains a well-developed mylonitic foliation due to preferred orientation and alternations of stretched quartz-feldspar-rich bands with muscovite-biotite-chlorite bands (Fig. 2.5 a). On all scale, chlorite and mica are seen anastomosing quartz and feldspar megacrysts along S- and C- planes, wherever shearing is prominent. The general trend of the mylonitic foliation is nearly ENE-WSW with low to moderate dips towards NNE or SSW. The most prominent character of augen mylonite is the presence of a very strong stretching/mineral lineation on main foliation giving it a L-S tectonite character. This lineation is marked by strong preferred orientation of mica and streaked alkali feldspar, quartz and plagioclase augen. Both lineation and foliation are folded due to later deformations, which have produced doubly plunging antiformal windows along the Sutlej valley, indicating that large-scale open folding has been superposed upon the mylonitisation.

Compositional banding due to alternation of quartz-feldspar and mica-rich bands parallels the main foliation. Further, aplitic veinlets of 10 to 20 cm thickness are deformed into layered fine grained gneiss.

Numerous ductile shear zones affect the augen mylonite and reveal discordant relationships to the main mylonitic foliation. Contacts of these shear zones are gradational, wherein coarse augen-rich bands are progressively reduced in size from the shear zone walls towards the centre of the shear zone (also see Chapter 3).

A prominent discrete brittle fracture pattern transect the main mylonitic foliation orthogonally and is rarely marked by syntaxial quartz fabric perpendicular to the wall of the fracture zones.

2.5 HIGHER HIMALAYAN CRYSTALLINE

The Higher Himalaya Crystalline (HHC) of the NW-Himalaya is exposed along the Great Himalayan Range and constitutes the "Precambrian Basement" for the Phanerozoic Tehtyan sedimentary pile (Bagati, 1990; Bhargava *et al.*, 1991). The HHC predominantly incorporates pelitic and psammitic metamorphosed sequences having deformed granitoid bodies and gneiss of 400-500 Ma, 1800- 2000 Ma and 2500 Ma, which have been reworked during the Himalayan orogeny (Zeitler *et al.*, 1989; Treloar *et al.*, 1989; Pognante *et al.*, 1990; Searle *et al.*, 1992). The Tethyan sediments are infolded or separated from the HHC along its northern margin by the Zanskar Shear Zone (ZSZ)/ Trans-Himadri Thrust (Searle, 1986; Herren ,1987; Valdiya, 1989; Patel *et al.*, 1993). The HHC is regionally thrust southwestward over the Proterozoic Lesser Himalayan quartzite-volcanic association and intrusive Bandal granitoids of the Kulu-Larji-Rampur Window along the folded Main Central Thrust (MCT)/Jutogh Thrust (JT) and associated splays.

2.5.1 Distribution

The Jakhri-Wangtu region along the Sutlej Valley provides a good cross-section of the Higher Himalayan Crystalline (HHC). A thick stack of about 15 to 20 km of the HHC is exposed along the NE flank of the Kulu-Rampur window beyond Jakhri. The HHC is comprised of the following mappable lithounits in the southern parts of the Sutlej valley section.

2.5.2 Lithology

a. Jeori Formation: The HHC belt includes the Jeori Formation near its base. It lies between MCT and the newly recognised Chaura thrust, which has been delineated on the basis of deformation and strain patterns (see Chapter 3). Earlier, this formation has been designated as the Sarahan series or as a part of the Wangtu gneiss (Jhingran *et al.*, 1950). The base of the HHC consists of garnetiferous mica schist, quartz-muscovite schist, amphibolite and different varieties of gneiss. The whole unit has undergone four deformational phases out of which the second deformation is the most prominent.

(i) Garnetiferous mica schist/gneiss: It is the most abundant lithology in the basal parts of the HHC in immediate vicinity of the MCT between Jakhri and Jeori. Metapelitic sequence with a few psammite bands is made up of light to dark grey, garnetiferous mica schist with very thin alternating bands of quartzo-feldspar and mica-rich gneiss on cm scale (Fig. 2.5 b). These are extremely well foliated, medium grained schist and gneiss. The main foliation is characterised by strong preferred orientation of biotite and muscovite with interspersed quartz. Along the Maglad Khad near Jeori, discordant fine grained grey granite gneiss, aplite and pegmetite intrude the metapelite as concordant to discordant igneous bodies along the metamorphic banding (Fig. 2.5 c).

A prominent lineation characterises the basal part of the HHC and is marked by linear preferred orientation of chloritised biotite, muscovite and elongated quartz and feldspar megacryst in gneiss. It plunges consistently down-the-dip of the main foliation towards N/NE. Abundant quartz veinlets are boudinaged along the foliation. Development of shear zones within this unit is noteworthy with S- and C- fabric development indicating top-to-SW transport direction.

(ii) Quartz-muscovite schist: A small outcrop of quartz-muscovite schist is exposed along the upper reaches of Maglad Khad, a tributary to Sutlej river. It is a light grey, quartz-rich schist and contains quartz, muscovite and chlorite.

(iii) Amphibolite: Fine to medium grained dark coloured and highly foliated amphibolite bodies are occasionally exposed within the Jeori Formation. These are mostly 1 to 10 m thick, except for a mappable band of about 300 m thickness near Jeori along the National highway 22 A.

b. Wangtu granite gneiss: In the northeastern parts of the area, monotonous medium to coarse, porphyroclastic granitic gneiss is well exposed having a tectonised contact with the underlying Jeori Formation along the Chaura thrust. It imperceptibly grades into the undeformed granitoid near Wangtu, where it contains numerous xenoliths and restites of highly foliated metamorphics (Fig. 2.5 d). The whole complex is predominant gneissic in character and has been classified into the Wangtu granite gneiss.

The porphyroclastic gneissic component is light to dark grey due to biotite variation in the gneiss. The megacrysts are made up of quartz, K-feldspar and plagioclase, which are wrapped around by biotite-muscovite flakes (Fig. 2.6 a). Feldspar megacrysts are buff, elongated and slightly weathered, whereas quartz

Figure 2.6 a : Porphyroclastic granite gneiss of the NHC having elongated metric augen along S-C shear fabric. Note gradation of augen gneiss into a zone and development of banded gneiss. Loc. : Near Chaura.

Figure 2.6 b : Undeformed and mylonitised Chor granitoid showing alternating and parallel ac... mylonite and ultramylonite bands near contact with the Jutogh metamorp... along the Chor Thrust. Loc. : About 3 km NW of Nauhra, Chor Mountains.

Figure 2.6 c : Porphyritic granite of the Chor granitoid with very coarse grained quartz and feldspar phynocrysts of varying shapes and size embedded in fine-grained mica-rich groundmass. Loc. : Nala section about 4 km NE of Nauhra, Chor mountain area.

Figure 2.6 d : Undeformed, dark coloured, massive olivine dolerite dykes occurring as thin intrusives along joints in the Chor granitoid. Loc. : About 6 km NW of the Nauhra village about 500 m above the main road.

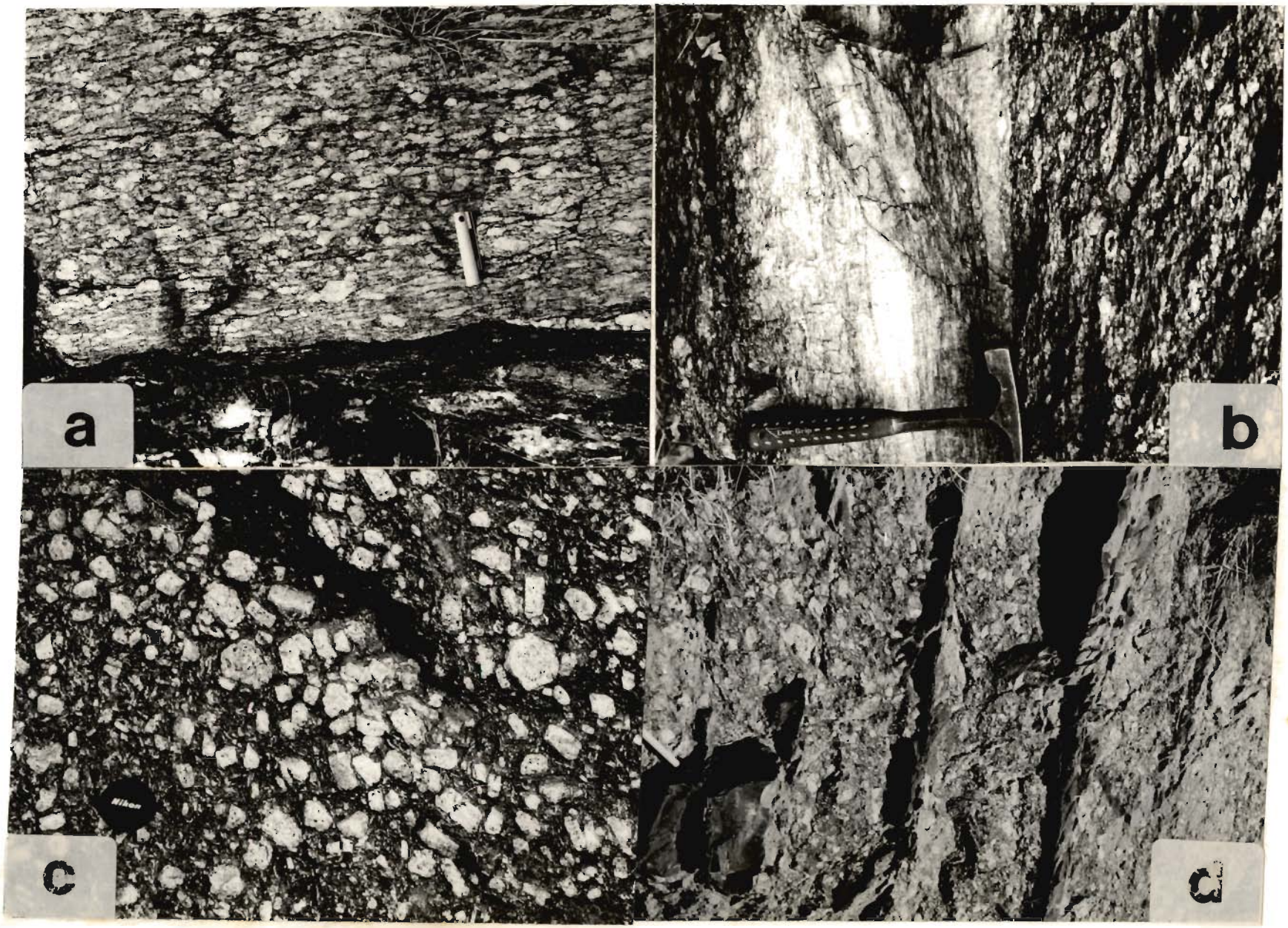

FIG. 2.6

is greyish, vitreous and fresh in character. S-C shear fabric and augen having asymmtric tails within the granite gneiss indicate top-to-SW sense of movement. Porphyroclastic granite gneiss misperceptibly merges into coarse grained undeformed granite exposed, around Wangtu bridge.

Numerous metapelitic bands of biotite-rich schist and amphibolite occur as restites within the Wangtu granite gneiss about 2 km to the NW of Wangtu bridge, indicating a distinct intrusive relationship of the granite gneiss within the metamorphics.

It may be noteworthy that three distinct gneissic components constitute the HHC along the Sutlej valley (Singh, 1987):

(i) Dark coloured biotite-rich paragneiss alteration with mica schist and garnetiferous mica schist of the Jeori Formation.

(ii) Discordant fine grained, grey granite gneiss and its associated pegmetite and aplite phase, intruding the Jeori metamorphics as discordant to concordant igneous bodies along the lithological/metamorphic banding.

(iii) The monotonous Wangtu granite gneiss of mostly porphyroclastic character.

2.6 JUTOGH NAPPE

The term Jutogh was introduced by Oldham (1887) for a sequence of limestone, schist and quartzite, exposed around Jutogh and Shimla. It was subsequently formalised by Pilgrim and West (1928). The base of the Jutogh sequence was regarded as the Jutogh Thrust, along which the metamorphics are thrust over the less metamorphosed Chail Series (Pilgrim and West, 1928).

The Jutogh Group metamorphics of Himachal Pradesh constitutes a major

allochthonous nappe of low to high grade pelitic and semipelitic metamorphosed rocks in the frontal parts within the Lesser Himalaya (Fig. 1.2; Pilgrim and West, 1928; Sharma, 1977; Srikantia and Sharma 1977; Srikantia and Bhargava, 1984).

2.6.1 Distribution

The Jutogh Nappe can be traced into two main outcrops in Himachal Pradesh as one of the most important tectonic unit (Fig. 1.2):

(i) Chor mountain in the frontal parts, from where the Jutogh extends as a folded succession towards north around Narkanda and Luhri-Dalash area (Virdi, 1971; Sharma, 1977; Bhargava *et al.*, 1991).

(ii) Isolated pear-shaped klippe of the Shimla Hills.

Towards south, the Jutogh Group also contains the Chor granite massif as an almost circular outcroping body, lying structurally above the metamorphics. The Jutogh Nappe rests tectonically over the less metamorphosed Chails. The Jutoghs are comprised of lower quartzite, carbonaceous schist and black marble, upper quartzite, mica schist and white marble. These metasediments have been emplaced by basic bodies, now metamorphosed to hornblende schist and amphibolite and a few undeformed and unmetamorphosed dolerite dykes. As has been observed by earlier workers (McMahon, 1886,1887; Pilgrim and West, 1928; Bisaria and Saxena, 1968), hornblend schist and amphibolite are confined only to the Jutogh rocks and do not occur in the Chor granite, whereas dolerite cuts across granite-metamorphic contact and post-date the emplacement of the Chor granite.

2.6.2 Lithology

a. Jutogh Group: The frontal parts of the Jutogh Nappe reveal the following mappable units:

(i) Lower quartzite: Tecono-stratigraphically, the lowermost unit of the Jutogh Group is exposed around Shamra and is seperated from the carbonaceous schist of the Chail Group by the well known Chail Thrust. The quartzite is grey to yellow, fine grained, massive to poorly foliated. It contains poorly preserved ripple marks indicating normal stratigraphic sequence at least locally. The quartzite predominantaly consists of quartz with chlorite, biotite, muscovite and iron-oxides as accessories. With the increasing mica percentage, the rock grades into quartz-mica schist and phyllite. The mica mineral lineation plunges either towards east or west on the bedding foliation planes dipping gently towards NE.

(ii) Carbonaceous schist and black marble: The quartzite is bounded by carbonaceous schist having intercalated black marble bands on either sides. Dark grey to black thin marble bands within the carbonaceous schist contain coarse calcite and dolomite with garnet, epidote and zoisite. Carbonaceous schist is highly friable and weathered with yellowish brown stains due to iron leaching. It comprises of biotite, graphite, garnet and quartz. A Lower Cambrian age has been assigned to the carbonaceous schist on the basis of acritarch remains (Sah *et al.*, 1977).

(iii) Upper quartzite: Schistose quartzite and mica schist intercalation overlie the carbonaceous phyllite. Buff to greyish white quartzite contains quartz, sericite, iron-oxide with small amount of biotite and zircon. The quartzite also preserves locally developed cross-bedding indicating normal stratigraphy.

(iv) Mica schist/gneiss: Different variations of schist and gneiss are exposed overlying the upper quartzite units till the main exposure of the Chor granite at the top is exposed. Medium grained reddish brown to dark grey, biotite-muscovite schist contains numerous segregated quartz-rich schistose bands. Foliated layers are intensely folded and locally sheared. Mica- rich schist imperceptibly grades into greyish-yellowish-brown, medium to coarse grained garnetiferous mica schist consisting of garnet, biotite, muscovite, feldspar and quartz. Chlorite and iron-oxides also occur as the alteration product of biotite and garnet.

(v) Amphibolite: Dark green amphibolite bodies are associated with the Jutogh metapelite and marble as concordant to discordant bodies of varying thickness upto 10 m. The amphibolite is well foliated, and contains a distinct mineral lineation of actinolite, chlorite and biotite. At places, the amphibolite also contains a few garnet grains.

b. Chor Granitoid: The Chor granitoid consists of biotite granite gneiss, porphyroclastic granite gneiss and non-foliated homogeneous granite, which are intruded by dolerite dykes. Pilgrim and West (1928) opined that the Chor granite is a laccolith, which intruded into a `syncline' of the Jutoghs. The granitoid is well exposed and occupy the high altitude. This body contains granitoid rocks having buff to grey, fine to coarse grained and foliated to non-foliated character. Three main granitoid types have been identified in the Chor granitoid on the basis of their appearances.

(i) Biotite granite gneiss: The biotite granite gneiss forms the outer margin of the Chor massif and is seen always along the tectonised contact with the Jutogh metamorphics. Along the margin, the Chor granitoid is foliated with preferred oriented mica, feldspar and quartz along the main gneissosity and lineation. Marginally the granite gneiss contains many xenolith of the low grade

metamorphic rocks. The foliations within the granite gneiss and Jutogh metamorphics is almost parallel and is mylonitic in character (Fig. 2.6 b). A few ultramylonite bands mark the contact indicating the presence of a tectonised contact along the margin of the granitoid body.

(ii) Porphyroclastic granite gneiss: The porphyroclastic granite gneiss is grey, very coarse grained and composed of quartz, feldspar, biotite and mica of varying shapes and size (Fig. 2.6 c). The porphyroclasts are fractured and deformed. The plagioclase feldspar occurs in subordinate amount to K-feldspar. The latter registers gradual increase in size towards the interior due to which the rock attains a porphyroclastic appearence (Fig. 2.6 c). Feldspar megacrysts are mostly undeformed with beautiful subhedral boundaries and zoned mica inclusions. With increasing deformation towards the contact with the Jutogh metamorphics, megacrysts attain augen shapes with elongated tails in fine granied foliated grounmass (see Fig. 3.33 a).

(iii) Non-foliated homogeneous granite: Towards north, the Chor granitoid body grades into light-coloured, non-foliated homogeneous granite in the interior of massif, having small amount of biotite and muscovite in comparision to its margins. The large part of the Chor granitoid lacks perceptible foliation and lineation, hence appears to be least deformed. It is therefore ideal for U-Pb dating (see Chapter 6).

c. Dolerite: Two types of dolerite dykes are present in the area. Deformed and foliated metadolerite bodies are encountered at 8 km milestone on the Nohra-Shamra road having hard, massive, less foliated metadolerite lenses, which are wrapped around by strongly foliated and weathered actinolite schist within the Jutogh metamorphics. Undeformed, dark coloured, massive olivine dolerite cuts across the contact of Jutogh metamorphics with the Chor granitoid and occurs as thin intrusives along joints with chilled margin (Fig. 2.6 d).

CHAPTER 3: DEFORMATIONAL HISTORY

3.1 INTRODUCTION

The concept of deformational phases yields a framework of successive movements and deformational events by observing the geometric features in rocks. Deformation leads to extension and contraction in different directions in a body, and generally to shear displacement between layers. Structures thus formed in the rocks due to the relative ductility contrast and orientation of layers with respect to principal strain axes are related to rock rheology under specific stress and strain rate conditions of deformation (Huber *et al.*, 1980). The following standard structural criteria are useful in identification of deformational phases and successive movements:

(i) Structural forms showing characteristic geometric style reflects the rock rheology. The structures, formed in successive phases, often show different geometric style because each deformational phase takes place in a particular pressure-temperature-strain rate condition.

(ii) Successive deformational phases produce small-scale structures, which are supposed to give characteristic geometric interference pattern. That is why events of different phases are distinguished at outcrop level with their overprinting relationships.

The above concepts of deformational phases have been applied to the HHC and Jutogh Nappe units of the Sutlej Valley and Chor Mountain to decipher the deformational history and in understanding the tectonometamorphic evolution of parts of the NW-Himalaya.

The present chapter deals with detailed deformational phases of the region with a brief description, distribution and mutual relationships of different structures and granitoid emplacement in various tectonostratigraphic units.

3.2 DEFORMATION PATTERN OF THE HIGHER HIMALAYAN CRYSTALLINE (HHC)

3.2.1 Deformational phases

The Higher Himalayan Crystalline (HHC) belt of the hanging wall of the Main Central Thrust (MCT) along the Sutlej Valley section between Jakhri and Wangtu is thrust over the Rampur Group along an antiformally folded thrust and characterised by four distinct deformation phases. Of these, the second phase D_2 is marked by prominent S_2 axial-plane foliation, related to reclined N- to NNE-plunging F_2 folds and a coaxial stretching/mineral lineation L_2. These structures were developed by southwesterly verging ductile shear during the Himalayan Orogeny.

a. First deformation phase (D_1): The first deformational phase D_1 in the HHC is nearly obscured. However, a few isolated occurrences indicate the presence of earliest, extremely appressed tight to isoclinal F_1 folds with very long-drawn stretched, hinges and limbs of the 'flame type'. These folds are developed on lithological/metamorphic banding (S_0) (Fig. 3.1 a).

The development of F_1 folds is also found on quartz veins and fine-grained grey granitic bodies and associated pegmatite, which cut across the lithological/metamorphic banding S_0 (Figs. 3.1 b-d). In such cases, the foliation S_1, parallels the axial surfaces of the F_1 folds and is at an angle to

dithological/metamorphic banding S_0 on the limbs. In the grey fine-grained granitoid veinlets, this foliation is not well developed and characterised by poorly-oriented quartzo-feldspathic minerals but becomes prominent due to strong preferred mica orientation (Figs. 3.1 c, d). In such cases, only one foliation is seen in the veinlets. When traced into the pelites, this foliation crenulates the metamorphic banding S_0 around the hinge zone of F_1 folds (Fig. 3.1 c). This foliation is oriented at high angle to S_0 layering in tightly appressed hinge zone (Figs. 3.1 b, c). The intrusive fine grained grey granitic bodies and associated pegmatite bodies are emplaced either early during the D_1 deformation or syntectonic to this important, though poorly recorded, event.

Despite the presence of a few F_1 folds, earliest linear structures L_1 are generally not observed. Most F_1 folds exhibit oblique profile sections and lack of suitable exposure of rock faces for measurements. L_1 lineation appears to be obliterated due to subsequent intense penetrative D_2 deformation.

b. Second deformation phase (D_2): The structures, associated with the second phase of deformation D_2, are profusely developed in the HHC. The associated F_2 folds are mostly close to isoclinal and reclined in character with relative thickening of fold hinges (Figs. 3.2 a, b; 3.3 a). The F_2 folds are developed either on the pre-existing metamorphic banding (S_0) or S_1 gneissosity/foliation, which predates this most prominent deformation (Fig. 3.3 b). These folds mostly plunge either N or S at moderate to steep angles almost in the dip direction of their axial plane foliation S_2 (Figs. 3.2 a, 3.3 a). However, it is discordant to S_0/S_1 along hinge zones. S_2 foliation can be seen developed at an angle to the former on the limb or in hinge zones of the F_2 folds developed on gneissic bands (Fig. 3.2 a). Otherwise, it parallels the S_0/S_1 planar surface and is indistinguishable from these earlier foliation. In the present work, it is, therefore, shown as the main foliation Sm, wherever this foliation has been measured without associated F_2

Figure 3.1 a : Earliest, extremely appressed tight to isoclinal F_1 folds with very long-drawn limb of `flame type`. Also seen are Type-3 interference pattern due to presence of F_2 folds at low angles to F_1. Loc. : Near Kinnu along Sarahan-Kinnu road section.

Figure 3.1 b : Isolated hinges of F_1 folds developed on fine-grained grey granite, which cuts across the lithological/ metamorphic banding S_0. Loc. : About 7 km from Sarahan along Sarahan-Kinnu road.

Figure 3.1 c : F_1 folds developed on fine-grained grey granite gneiss having axial-plane foliation S_1 across the vein. Loc. : About 10 km from Jeori upstream along the National highway 22.

Figure 3.1 d : F_1 folds on fine grained grey granite gneiss with long-drawn limbs. Loc. : As in figure 3.1 c.

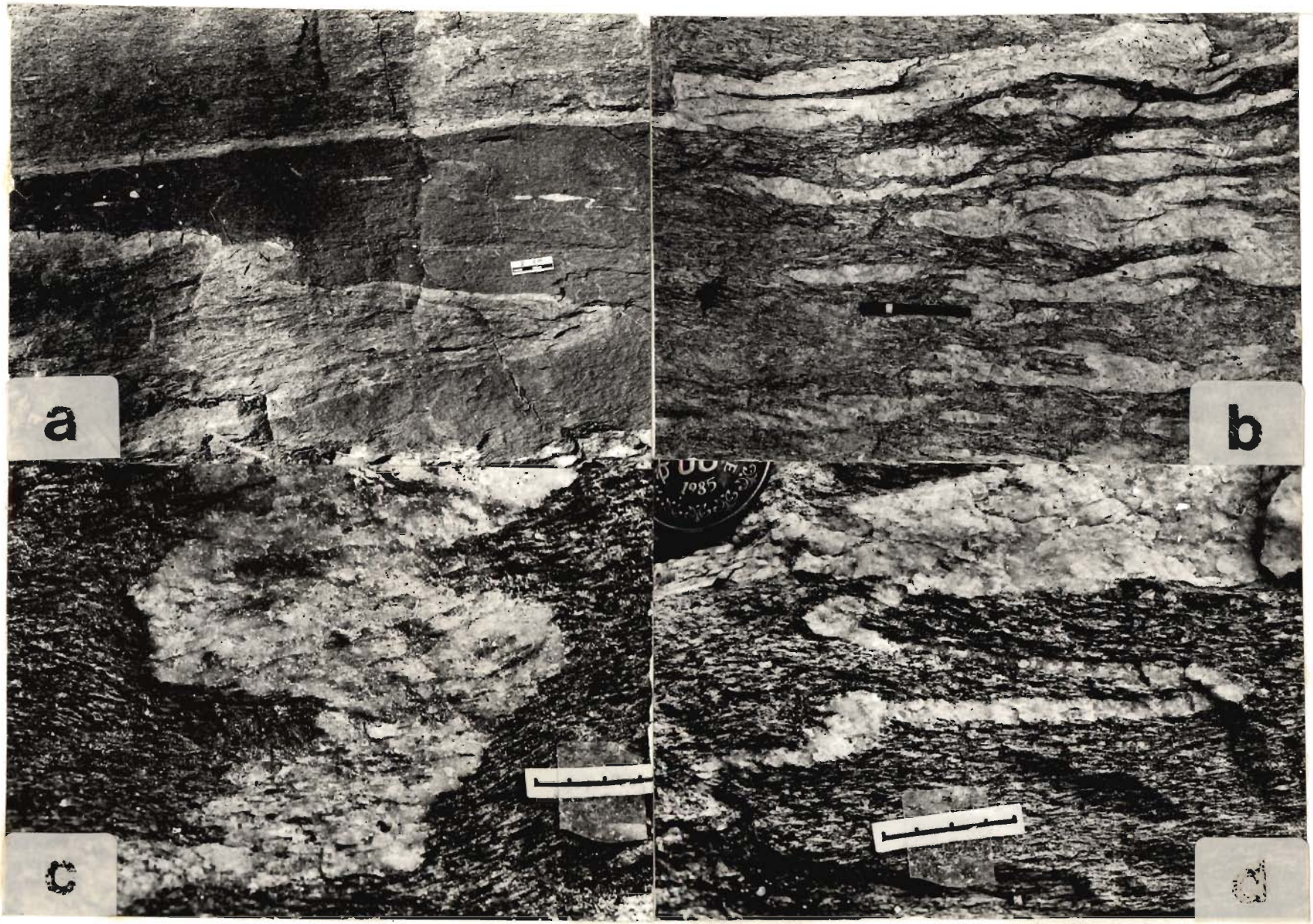

FIG. 3.1

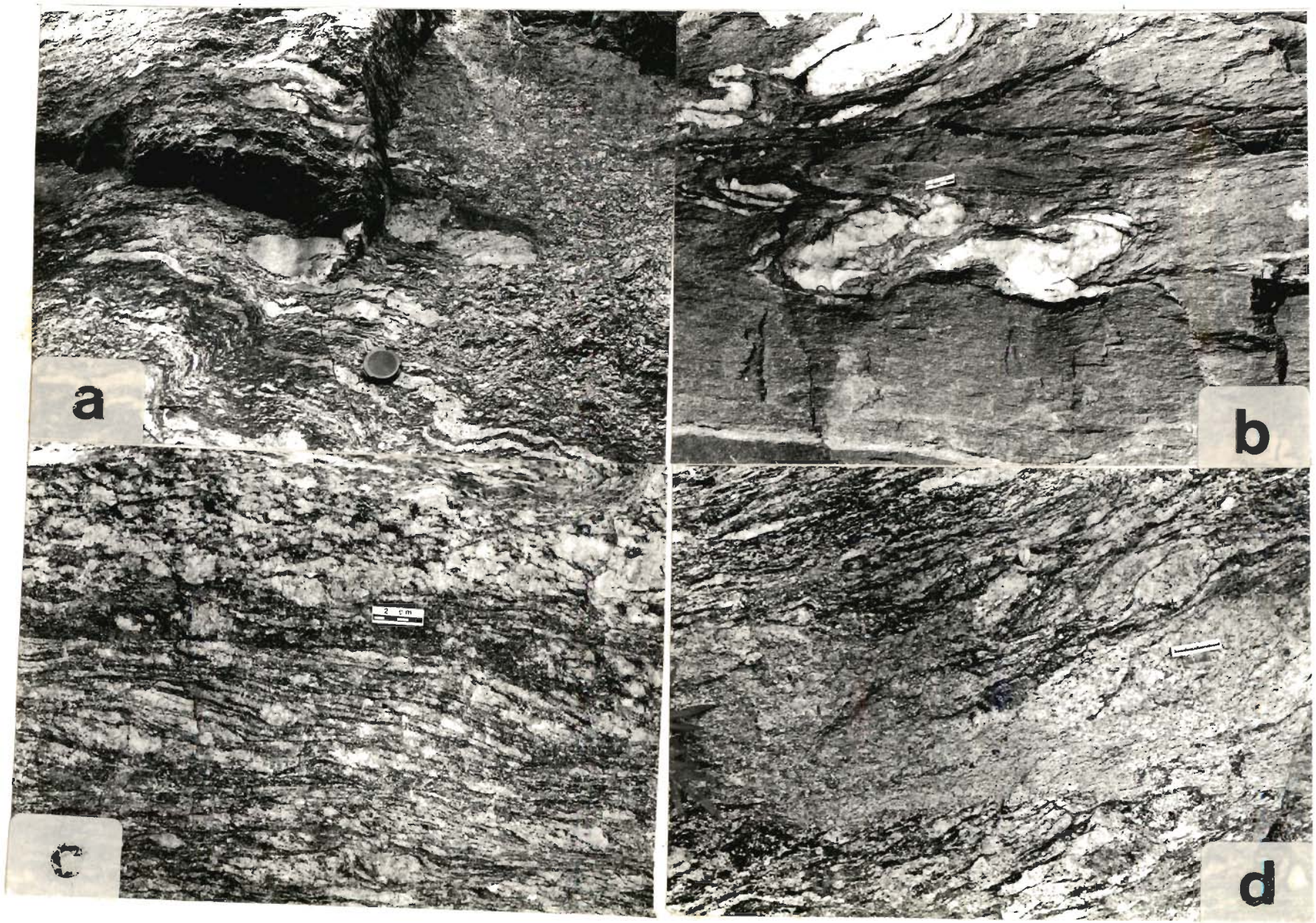

FIG. 3.2

Figure 3.2 a : Isoclinal reclined F_2 folds with relative thickening of fold hinges and shearing of limbs in porphyroclastic granite gneiss. Loc. : Near Nugalsari village.

Figure 3.2 b : F_{3a} folds having sheared limbs and moderately thickened hinges of competent gneissic layers in garnetiferous mica schist. Loc. : Near Sarahan.

Figure 3.2 c : S-C shear fabric in porphyroclastic granite gneiss having sigmoidal bending of S- foliation due to C- shear zones. Also seen are asymmtrical feldspar augen having σ tails. Loc. : Near Bhabhanagar, about 4 km upstream of the Sutlej river.

Figure 3.2 d : S- and C- shear fabric with asymmetrical disposition of quartzo-feldspathic augen in XZ section showing SW-vergence of the upper block. Loc. : About 4 km from Nugalsari towards Jeori.

Figure 3.3 a : Isoclinal reclined F_2 folds developed on the pre-existing S_1 foliation/gneissosity with relative thickening of their hinges and crenulation of earlier foliation. Loc. :

Figure 3.3 b : Sketch of development of F_2 folds on the preexisting metamorphic banding S_0 or S_1 foliation/ gneissosity from the photograph taken near.

Figure 3.3 c : Sketch of developmant of F_2 folds and S_2 axial plane foliation on preexisting S_1 foliation.

Figure 3.3 d : Sketch of development of F_{3a} isoclinal inclined folds and S_{3a} axial plane foliation near Chaura village.

Figure 3.3 e : Sketch of the development of crenulation F_{3b} folds and related S_{3a} axial plane foliation within the quartz vein and pelitic rocks along the Maglad gad near Jeori village.

Figure 3.3 f : Development of crenulation F_{3b} folds and related S_{3a} axial plane foliation on the main foliation Sm about 6 km upstream of the Sutlej river from Jeori village.

ALL SKETCHES ARE DAWN FROM FIELD PHOTOGRAPH

folds. The main foliation strikes approximately N110° and dips either N or S at moderate to steep angles upto 70°. Steepening of the main foliation towards NE is noteworthy nearer to the contact with the Wangtu granite gneiss.

In the pelitic and psammitic sequences, S_2 foliation as well as the main foliation S_m are defined by preferred orientation of the phyllosilicate and quartz (Fig. 3.3 c), while a few amphibolite bands reveal preferred orientation of actinolite. In the northeast and elsewhere, granitic gneiss is characterised by the porphyroclastic growth of both K-feldspar, plagioclase and quartz, which are wrapped around by mica. Long axes of megacrysts in porphyroclastic granite gneiss generally lie in S_2 planes with development of S- and C-planar surfaces (cf., Berthe *et al.*, 1979). S-surfaces sweep around the megacrysts with their asymmetric tails defining newly-developed C-shear surfaces (Figs. 3.2 c,d). Angular relationship between S- and C-surfaces shows presence of ductile shear zones (Fig. 3.2 c; Berthe *et al.*, 1979).

The prominent lineation L_2 is developed as stretching/mineral lineation, either on S_2 foliation or main foliation S_M. L_2 is characterised by preferred orientation of prismatic, flaky or inequidimensional minerals in all the lithotectonic units. It is generally coaxial to the F_2 folds and plunges moderately due N to NE or S to SW in the whole area. According to Escher and Waterson (1974), stretching lineations is indicative of direction of tectonic transport in orogenic belts and widely considered to have originated during crustal shortening in ductile shear zones.

c. Third deformational phase (D_3) : The third deformational phase D_3 is characterised by two distinct phases, which are classified here as early D_{3a} and late D_{3b} deformational phases.

In the D_{3a} phase, F_{3a} folds are mostly isoclinal to tight, inclined-type with

gentle to moderately inclined axial surfaces and marked by moderate thickening of competent layers in hinge zones (Figs. 3.3 d, 3.4 a). The F_{3a} folds plunge either ENE or WNW at low angles. The axial plane foliation S_{3a}, associated with F_{3a} folds, reveals recrystallised phyllosilicate and quartz (Fig. 3.3 d).

In the later D_{3b} phase, probably of the same deformational event, F_{3b} folds are mostly crenulation-type having angular to rounded hinges (Figs. 3.3 e, f; 3.4 b), whose axes form a prominent lineation. These folds are coaxial to F_{3a} folds and plunge gently either ENE or WNW. These folds show variable interlimb angles ranging from 30° to more than 100° and wavelength-amplitude relationship depending upon lithological contrast (Fig. 3.4 b). The F_{3b} folds are mostly asymmetric in character and southwestward-verging (cf., Butler, 1982). In hinge zones of the F_{3b} fold, earlier L_2 lineation plunges gently on either side due to folding. The axial planar foliation S_{3b} of these folds in metapelites and granite gneiss strikes N 100° with dips varying between 45° to 80° towards N or S.

d. Fourth deformational phase (D_4) : The effects of late deformational phase D_4 are weak and sporadic during specific brittle-ductile and brittle-type local conditions. Thrust-faults, shear bands and quartz-filled tension gashes are developed during this late stage of deformational history. Further, very gently northerly plunging open cross-folds are also depicted from synoptic diagrams of S_2 foliation and folding structures of D_3 phase. These folds are mostly culmination and depressions.

Thrust faults cut across the crenulation foliation S_{3b} at gentle to moderate angles (Figs. 3.4 c, d), indicating post-D_3 deformational structures of discrete-type with northerly dipping planar to undulatory surfaces. These faults contain cm-thick fault gauge having distinct shear-controlled subparallel foliated character and reveal south-verging movements of the hanging wall (Fig. 3.4 c). Roof and floor thrusts are very distinctly observed, at

places, to generate duplex geometry of these thrust zones (cf., Butler, 1982). It appear that numerous such thrust faults are indicative of the overall MCT geometry in the brittle zone and have evolved during thrust movements. Within the fault zones, discrete surfaces are developed in orientation of displacement shears (D-shear), Riedel shears (R-shears), conjugate shears (R-shears) and P-shears to produce shear lenses.

3.2.2. Superposed fold patterns

Interference fold patterns, produced by superposition of folds of different generations are common in the HHC and useful in deciphering the age relationships and deformational patterns. However, no large-scale mappable interference pattern controlling the distribution of various lithotectonic units within the HHC has been recorded in this region probably due to lack of useful widespread marker lithounits and steep rugged terrain. The interference patterns of Type-2 and Type-3, described by Ramsay (1967), have been observed due to overprinting of the following folds of different generations.

Fold systems		Type of fold interference patterns
F_1	F_2	Type-3
F_2	F_{3a}	Type-2
F_2	F_{3b}	Type-2
F_{3a}	F_{3b}	Type-3

a. Type-2 fold interference pattern: This patterns is noted due to overprinting of gently plunging F_{3a} and F_{3b} folds on reclined F_2 folds (Figs. 3.5 a, b; 3.6 a, c). F_{3a} and F_{3b} folds have westerly striking and steeply dipping axial surfaces with NW-plunging hinges; while F_2 folds have NE-plunging hinge zones (Figs. 3.5 a, b; 3.6 a,

Figure 3.4 a : Isoclinal to tight F_{3a} folds having gently plunging hinges and stteply dipping axial surfaces. These folds are marked by moderate thickening of competent layers in hinge zones near Chaura.

Figure 3.4 b : F_{3b} crenulation folds showing variable interlimb angles between 30° and 100° and slight movement along prominent axial plane foliation S_{3b} along Maglad gad.

Figure 3.4 c : Small-scale thrust surfaces cutting across the F_{3b} crenulation folds and showing movement of the upper block towards right hand. Also note presence of lensoid shape duplex due to roof and floor thrust. Loc. : About 4 km upstream from the Jakhri.

Figure 3.4 d : Sketch of the same thrust surfaces marked by the layers of brittle fault gouge.

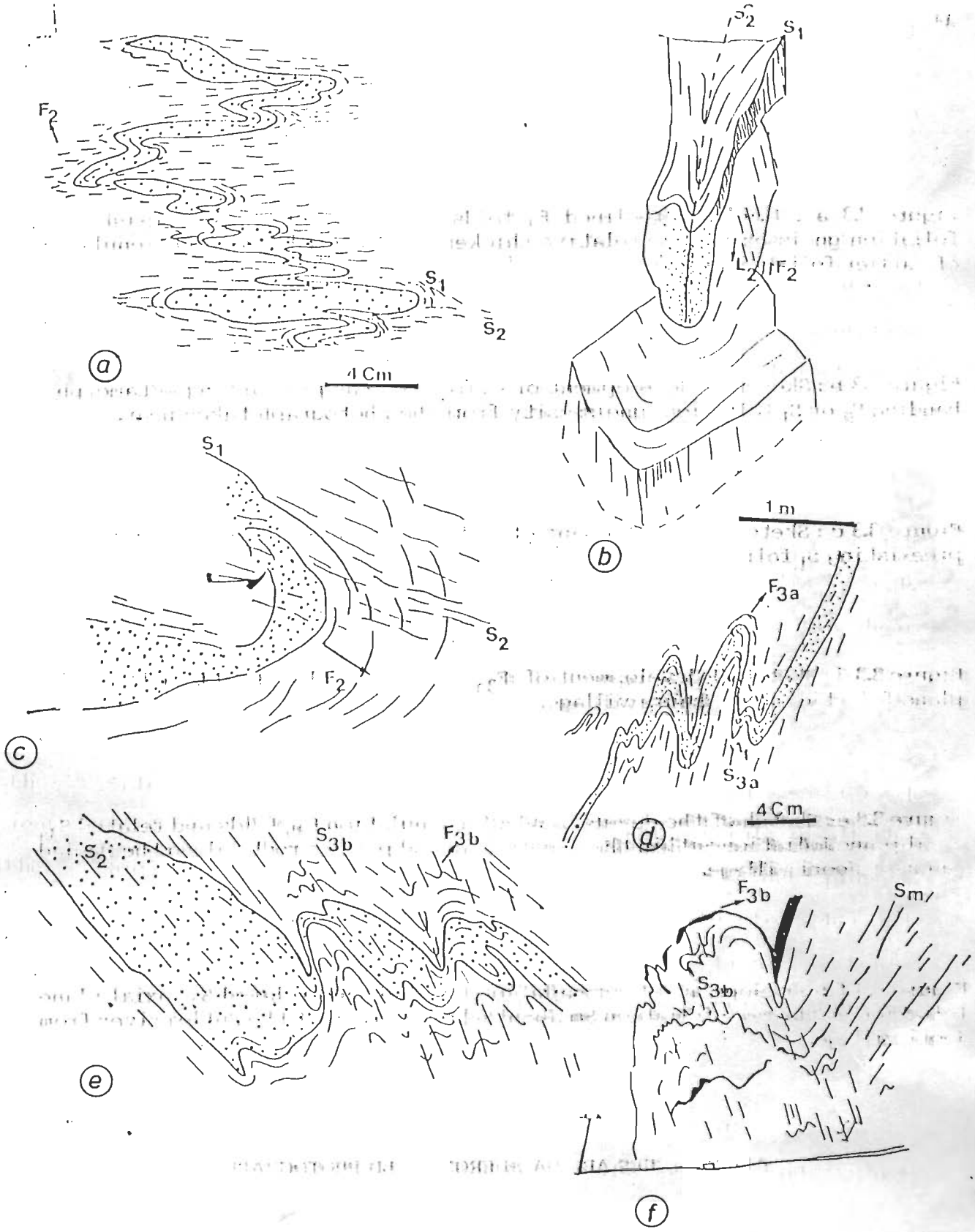
F2
S1
S2
4 Cm
a
S2
S1
L2
F2
b
S1
S2
F2
c
1 m
F3a
S3a
d
4 Cm
S2
S3b
F3b
e
F3b
Sm
S3b
f

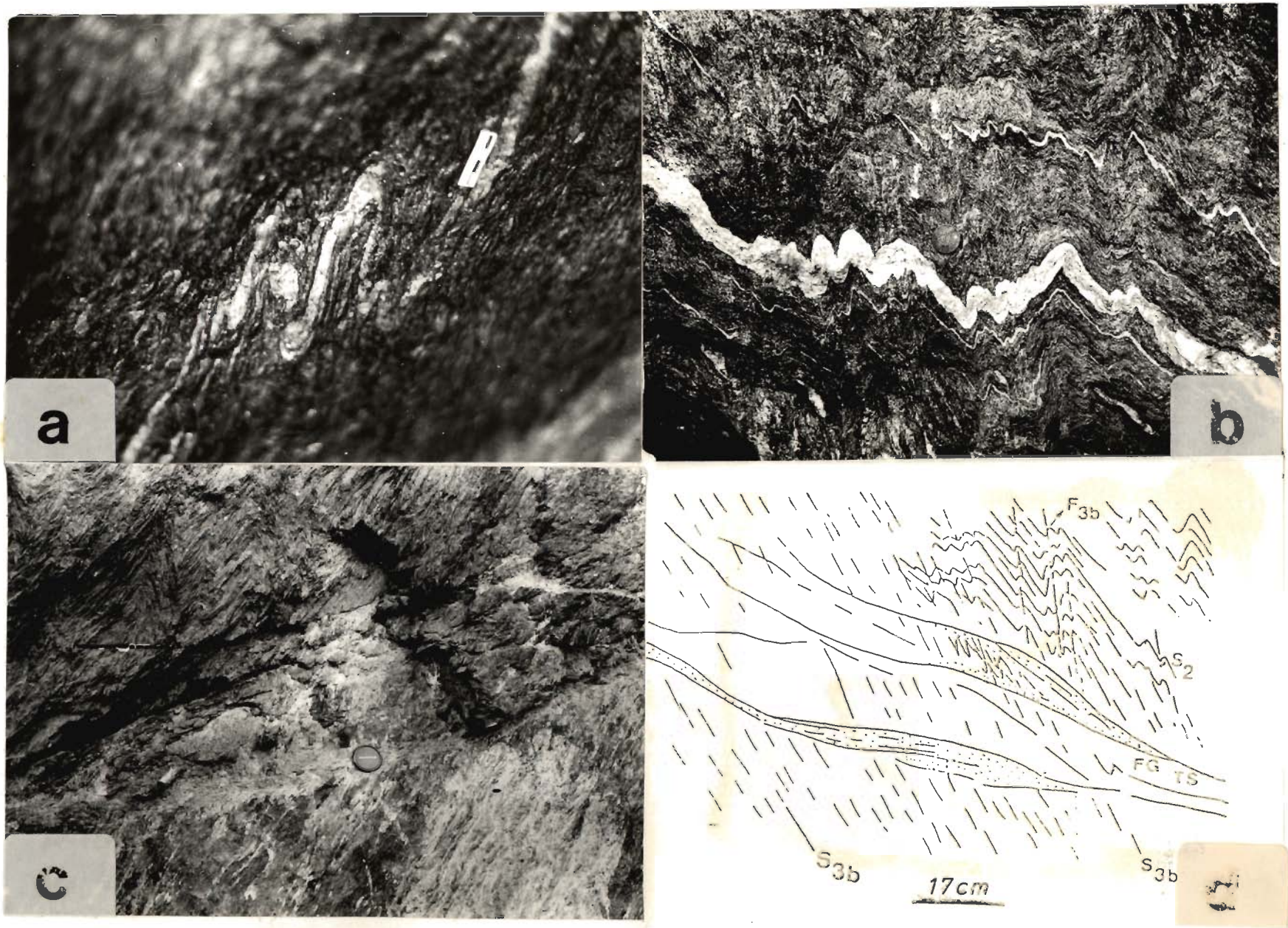

FIG. 3. 4

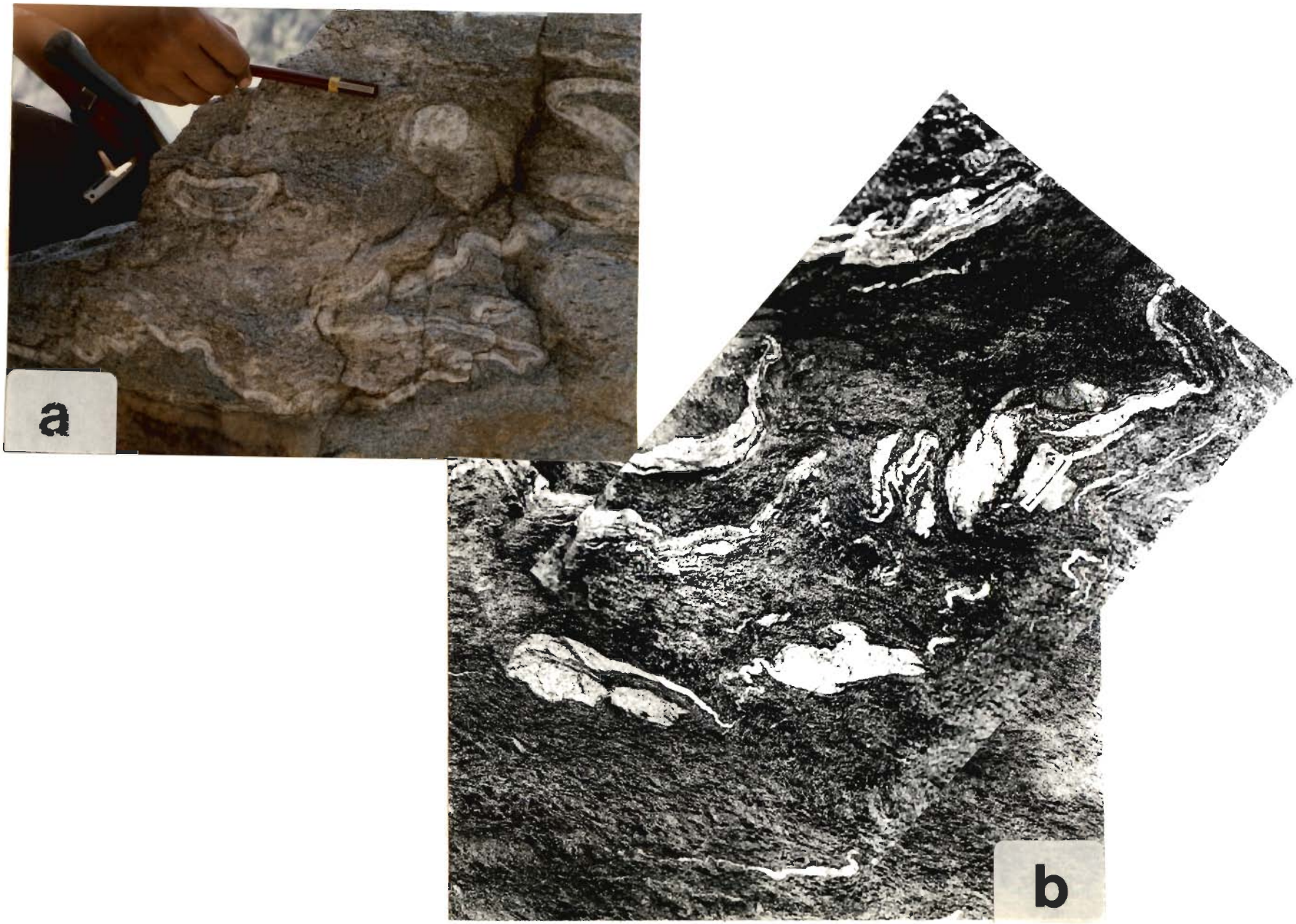

FIG. 3 .5

Figure 3.5 a : Boomrang shaped Type-2 and hook-shaped Type-3 interference fold pattern produced due to overprinting of F_{3b} and F_{3a} folds on F_2 and of F_{3a} on F_{3b} folds respectively. Also note that recumbant F_{3a} folds and crenulation F_{3b} folds are developed during D_3 deformation. Loc. : Near temple after Nugalsari.

Figure 3.5 b : Hook-shaped Type-3 interference fold pattern produced by superposition of F_{3b} fold on F_2 fold about 3 km downstream from the Chaura along the national highway 22.

Figure 3.6 a : Sketch of figure 3.5 a showing boomrang-shaped Type-2 and hook shaped Type-3 interference fold pattern.

Figure 3.6 b : Sketch of hook-shaped Type-3 interference fold pattern produced by superposition of F_{3b} fold on F_2 fold near Jeori.

Figure 3.6 c : Sketch of figure 3.5 b hook-shaped Type-3 interference fold pattern produced by superposition of F_{3b} fold on F_2 fold.

Figure 3.6 d : Hook-shaped Type-3 interference fold pattern, produced by superposition of F_{3b} fold on F_2 fold near Nugalsari village.

Figure 3.6 e and 3.6 f : Sketch of hook-shaped Type-3 interference fold pattern produced by superpositioning of F_{3b} fold on F_{3a} fold about 4 km downstream from the Nugalsari village.

ALL SKETCHES ARE DAWN FROM FIELD PHOTOGRAPH

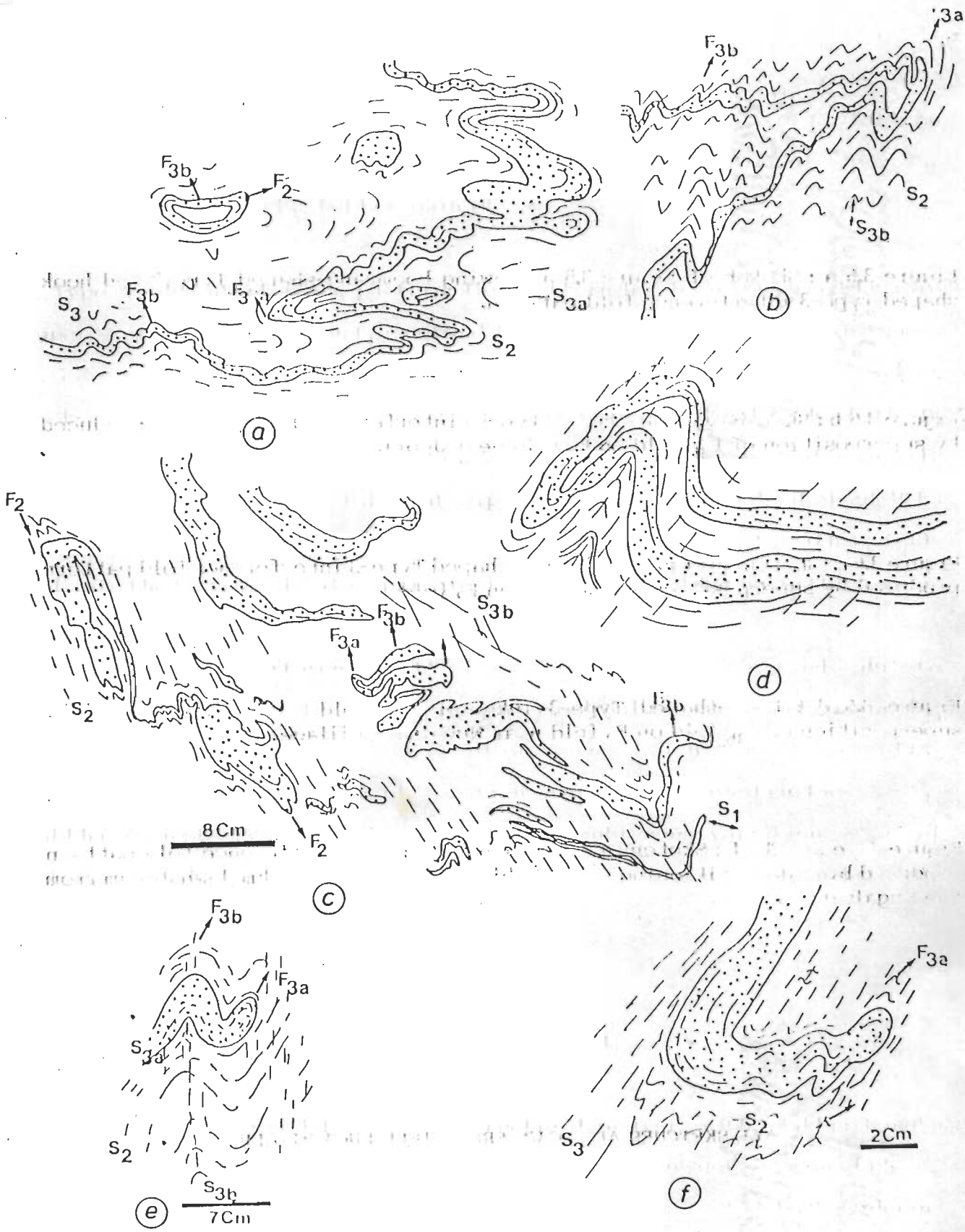
F3b
F2
S3
F3b
F3
S3a
S2
a
3a
F3b
S2
S3b
b
F2
S2
F3b
S3b
F3a
8Cm
F2
c
F3b
S1
d
F3b
F3a
S3a
S2
e
S3b
7Cm
F3a
S2
S3
2Cm
f

c). Type-2 mushroom-shaped interference pattern gives rise to mirror image pattern (Figs. 3.5 a; 3.6 a), which has resulted from superposition of F_{3b} folds on F_2 folds. In such cases, F_2 folds become nonplanar-noncylinderical, while S_{3b} axial surfaces of the F_{3b} folds remain planar.

b. Type-3 fold interference pattern: This pattern has been observed by rare superposition of F_2 folds on F_1 isoclinal folds (Fig. 3.1 a) and in other instances by more common superposition of F_{3b} on F_{3a} folds (Figs. 3.5 b; 3.6 c-f; 3.7 a-c). Hooked- shaped interference pattern involves the F_1 isoclinal folds of the D_1 phase with the superposed F_2 folds (Fig. 3.1 a) with axial surfaces striking nearly parallel to those earlier F_1 folds but dipping steeper at an angle of about 10 to 20x to the S_1 foliation (Fig. 3.1 a). Near coaxial relation of F_2 with F_1 folds indicate the latter to be also approximately northerly-plunging in this region.

Type-3 fold interference pattern is more commonly observed due to superposition of F_{3b} folds on NW-plunging isoclinal to close and coaxial F_{3a} folds (Figs. 3.5 b; 3.6 c-e; 3.7 a). As a result of superposition of nearly coaxial F_{3a} and F_{3b} fold systems, considerable rotation in attitude of axial surfaces of F_{3a} fold has been observed. In such cases, a nearly continuous variation in dips of sub-horizontal S_{3a} axial plane foliation can be seen to moderately and steeply dipping (Figs. 3.7 b, c).

3.2.3 Structural analysis

a. Analysis of individual domains: For structural analysis of the Jakhri-Wangtu area, data on various structural elements from different deformational phases were collected along certain traverses and plotted on 1:50,000 scale. Considering the overall set-up and structural homogeneity, eleven domains have been delineated (Fig. 3.8). The fabric data of each domains were then plotted on lower

Figure 3.7 a : Hook-shaped Type-3 interference fold pattern produced by superposition of F_{3b} fold on F_{3a} fold along the Maglad gad near Jeori village.

Figure 3.7 b : Hook-shaped Type-3 interference fold pattern produced by superposition of F_{3b} fold on F_{3a} fold near Chaura along the national highway 22.

Figure 3.7 c : Hook-shaped Type-3 interference fold pattern produced by superposition of F_{3b} fold on F_{3a} fold about 4 km upstream from Nugalsari on the national highway 22.

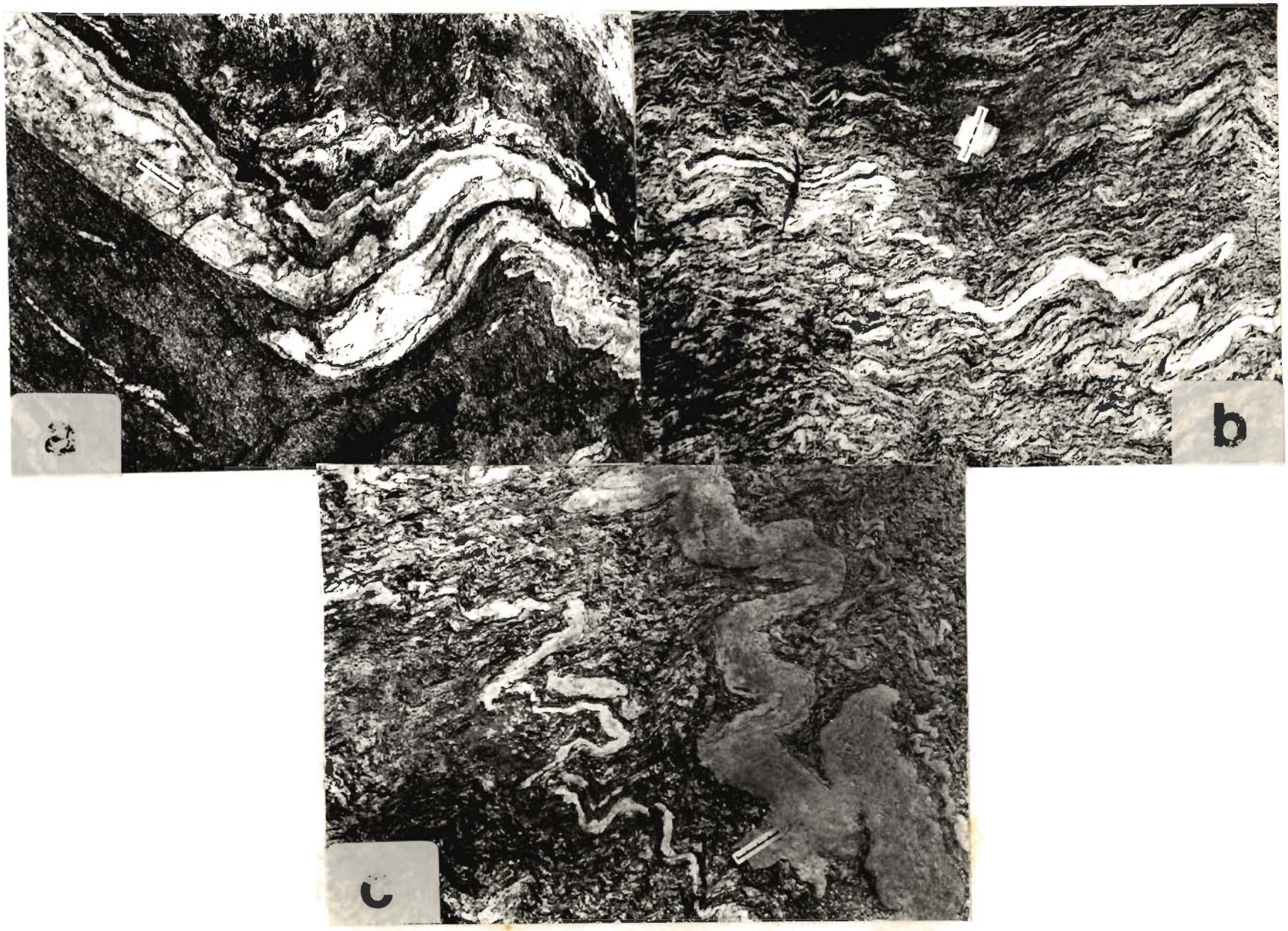

FIG. 3.7

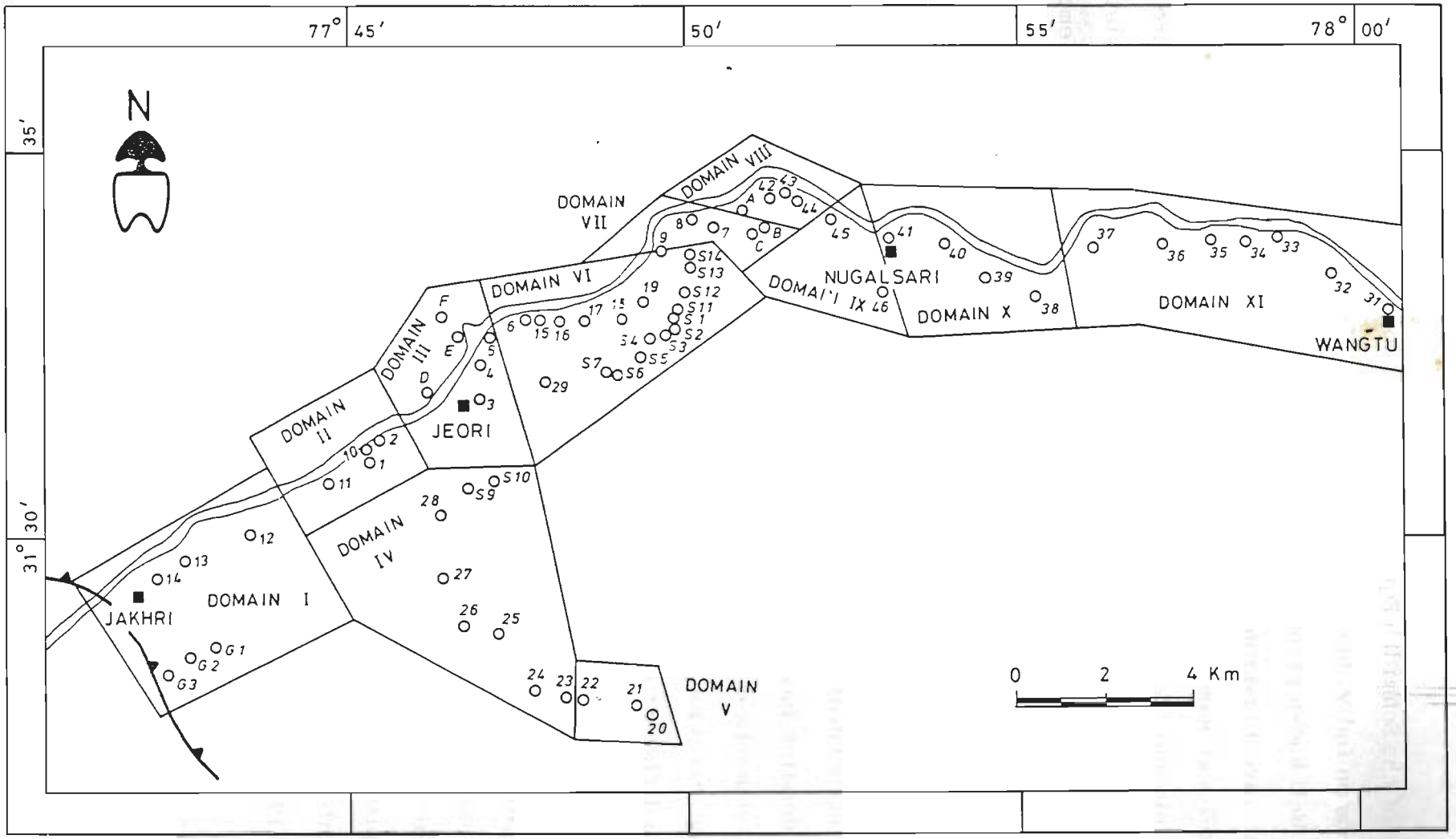

Figure 3.8 : Distribution of domains/subareas for structural analysis of the Higher Himalayan Crystalline (HHC) along the Sutlej valley between Jakhri and Wangtu.

hemisphere of the Schmidth Equal Area Net and contoured, wherever sufficient observations on individual structural elements in each domains are available (Table 3.1). Well known principles of structural analysis have been adopted in the present investigation, as has been described by Turner and Weiss (1963), Ramsay (1967) and Ramsay and Huber (1983). Spatial variation of different structural elements ahve been shown in Figures 3.9 and 3.10, while Figure 3.11 shows the trajectories of main foliation and lineation. Due to consistent structural homogeneity, and to avoid repetitions various structural elements have been shown on Schmidt plots from each domain (Figs. 3.12 to 3.19) with their synoptic pattern described below.

b.Synoptic structural pattern : Investigations on the mesoscopic scale in individual domains have demonstrated a complex orientation of the most of the structural elements due to distinct superposed deformation phases. In the Jakhri-Wangtu section, the HHC unit has been macroscopically analysed for deciphering different distinctive characters.

(i) S_1 foliation and F_1 folds: Evidence of earliest deformation D_1 are rarely observed along the Jakhri-Wangtu section. Flame-type F_1 folds are exposed in such a manner that it has not been posible to measure their hinges. These folds happen to produce type-3 interference pattern with F_2 folds (Fig. 3.1 a), hence it can be inferred that the F_1 folds are NE-plunging at low to moderate angles. Their axial plane foliation S_1 strikes nearly E-W and dips 30-50°/N-NE.

(ii) F_2 folds: The F_2 folds are developed on the earlier foliation and most prominent in metapelites and metapsammites of the Jeori Formation. These are very sparsely developed in the Wangtu Granite Complex. F_2 folds regionally plunge 37°/N 14° (Fig. 3.20 a).

Table 3.1 : Structural data of different domains from Jhakri-Wangtu region along the Sutlej valley, Himachal Pradesh.

DOMAIN	ROCK TYPE	AREA	STRUCTURAL FABRIC	ORIENTATION	FIGURE
I	Garnetiferous mica schist and banded gneiss	Around Jakhri and west of Gaura village	⨯ S_2	Due south	3.12 a
			F_2	Due north	3.12 b
			L_2	N 12°/38°	3.12 c
			⨯ S_M	N 105°/40°/N	3.12 d
			⨯ S_{3b}	N 135°/72°/NE N 135°/84°/SW	3.12 e
			F_{3b}	Due east	3.12 f
II	Garnetiferous mica schist, banded gneiss and amphibolite	Confluence of Maglad Khad with Sutlej River	⨯ S_2	Due south	3.13 a
			F_2	Due north	3.13 b
			L_2	N 6°/38°	3.13 c
			⨯ S_M	N 74°/45°/N	3.13 d
			⨯ S_{3b}	N 140°/16°/NE	3.13 e
			F_{3b}	Due E and W	3.13 f
III	Garnetiferous mica schist, banded gneiss and a thick amphibolite band	Along the National Highway 22	⨯ S_2	Due south	3.14 a
			F_2	Due north	3.14 b
			L_2	N 12°/45°	3.14 c
			⨯ S_M	N 96°/44°/N	3.14 d
			⨯ S_{3b}	N 96°/82°/N N 105°/80°/S	3.14 e
			F_{3b}	Due E and W	3.14 f
IV	Garnetiferous mica schist and qartz-mica schist	Around Kinnu village in the upper reachs of Maglad Khad along the right bank	⨯ S_2	Due south	3.15 a
			F_2	Due north	3.15 b
			L_2	N 13°/38° N 188°/1°	3.15 c
			⨯ S_M	N 121°/22°/N	3.15 d
			⨯ S_{3b}	N 89°/62°/N N 93°/72/S	3.15 e
			F_{3b}	Due E and W	3.15 f
V	Garnetiferous mica schist and banded gneiss	Around Bannaya village on the right bank of Maglad Khad	⨯ S_M	N 175°/30°/N	3.16 a
			L_2	Due north	3.16 b
			⨯ S_{3b}	N 109°/45°/N N 109°/88°/S	3.16 c
			F_{3b}	Due east	3.16 d

Table 3.2 continued...

DOMAIN	ROCK TYPE	AREA	STRUCTURAL FABRIC	ORIENTATION	FIGURE
VI	Garnetiferous mica schist and banded gneiss	Along National Highway 22 and Old Hindustan-Tibet road	⨯ S_2	Due south	3.17 a
			F_2	Due north	3.17 b
			L_2	N 14°/57°	3.17 c
			⨯ S_M	N 101°/57°/N N 101°/89°/S	3.17 d
			⨯ S_{3b}	N 105°/83°/S N 106°/88°/N	3.17 e
			F_{3b}	Due ESE and WNW	3.17 f
VII	Porphyroclastic Wangtu Granite Gneiss	Around Chaura village	⨯ S_M	N 102°/70°/N N 102°/89°/S	3.18 a
			L_2	N 337°/60°	3.18 b
VIII	Porphyroclastic Wangtu Granite Gneiss	NE of Chaura village	⨯ S_M	N 107°/65°/N N 107°/87°/S	3.18 c
			L_2	N 305°/55°	3.18 d
IX	Porphyroclastic Wangtu Granite Gneiss	Along National Highway 22	⨯ S_M	N 134°/88°/N N 134°/43°/S	3.18 e
			L_2	N 254°/54°	3.18 f
X	Porphyroclastic Wangtu Granite Gneiss	Along National Highway 22	⨯ S_M	N 155°/31°/W	3.19 a
			L_2	Due SW	3.19 b
XI	Porphyroclastic Wangtu Granite Gneiss	Around Wangtu village	⨯ S_M	N 85°/62°/N	3.19 c
			L_2	N 334°/58°	3.19 d

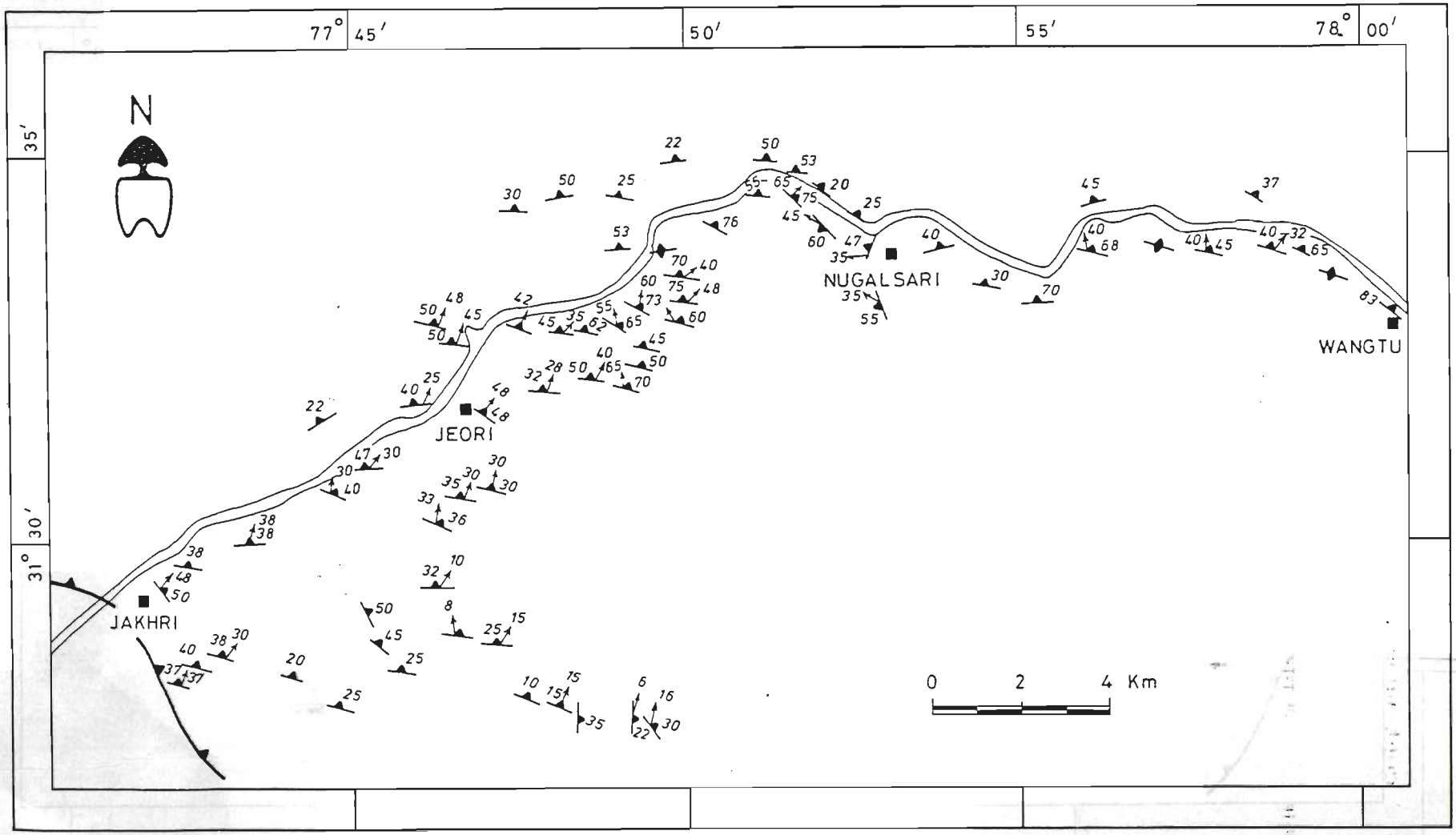

Figure 3.9 : Structural map showing orientation of main foliation (S_m) and lineation L_2 within the Higher Himalayan Crystalline (HHC) along the Sutlej valley between Jakhri and Wangtu.

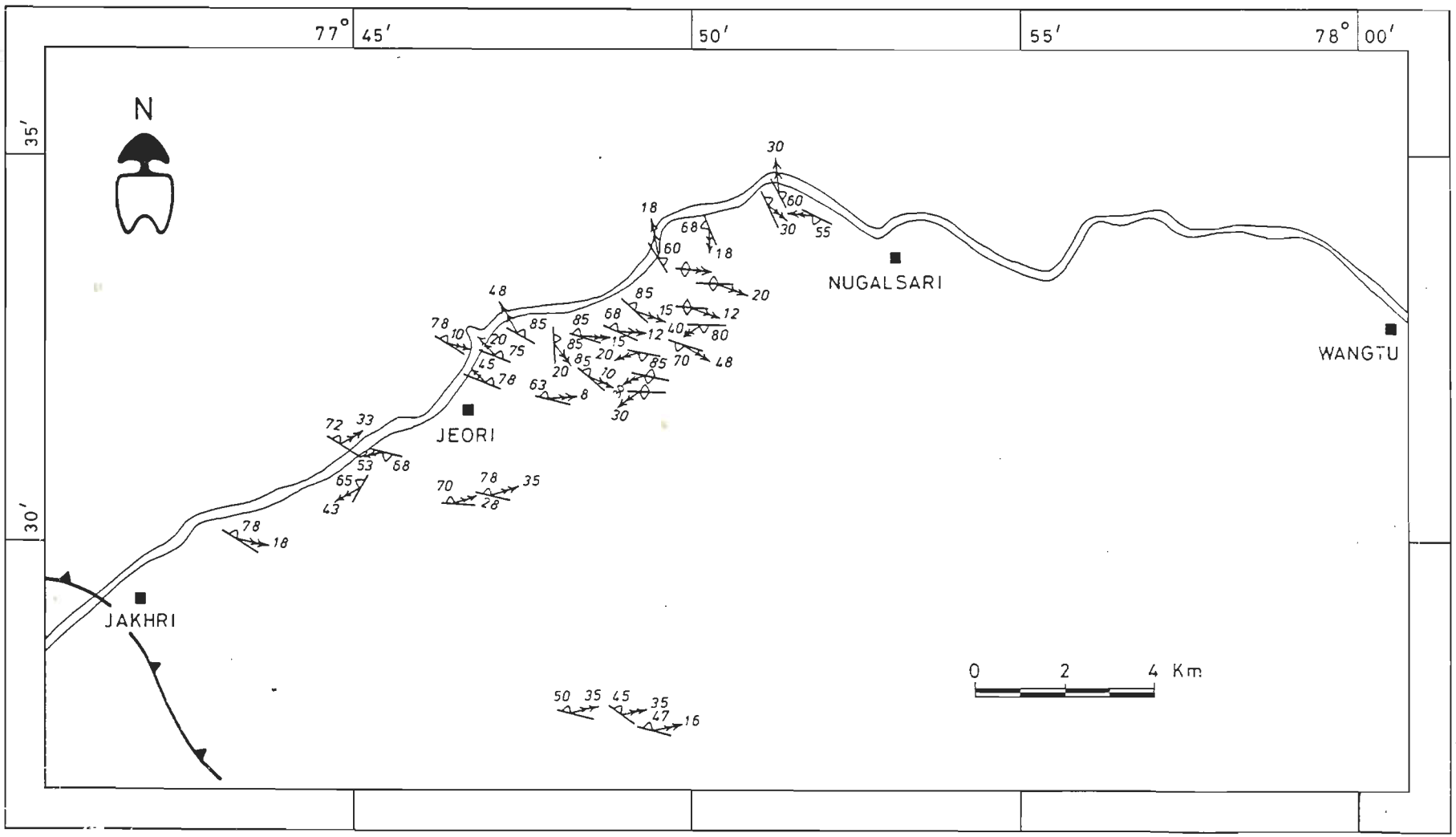

Figure 3.10 : Structural map showing distribution of S_{3b} and F_{3b} folds within the Higher Himalayan Crystalline (HHC) along the Sutlej valley between Jakhri and Wangtu.

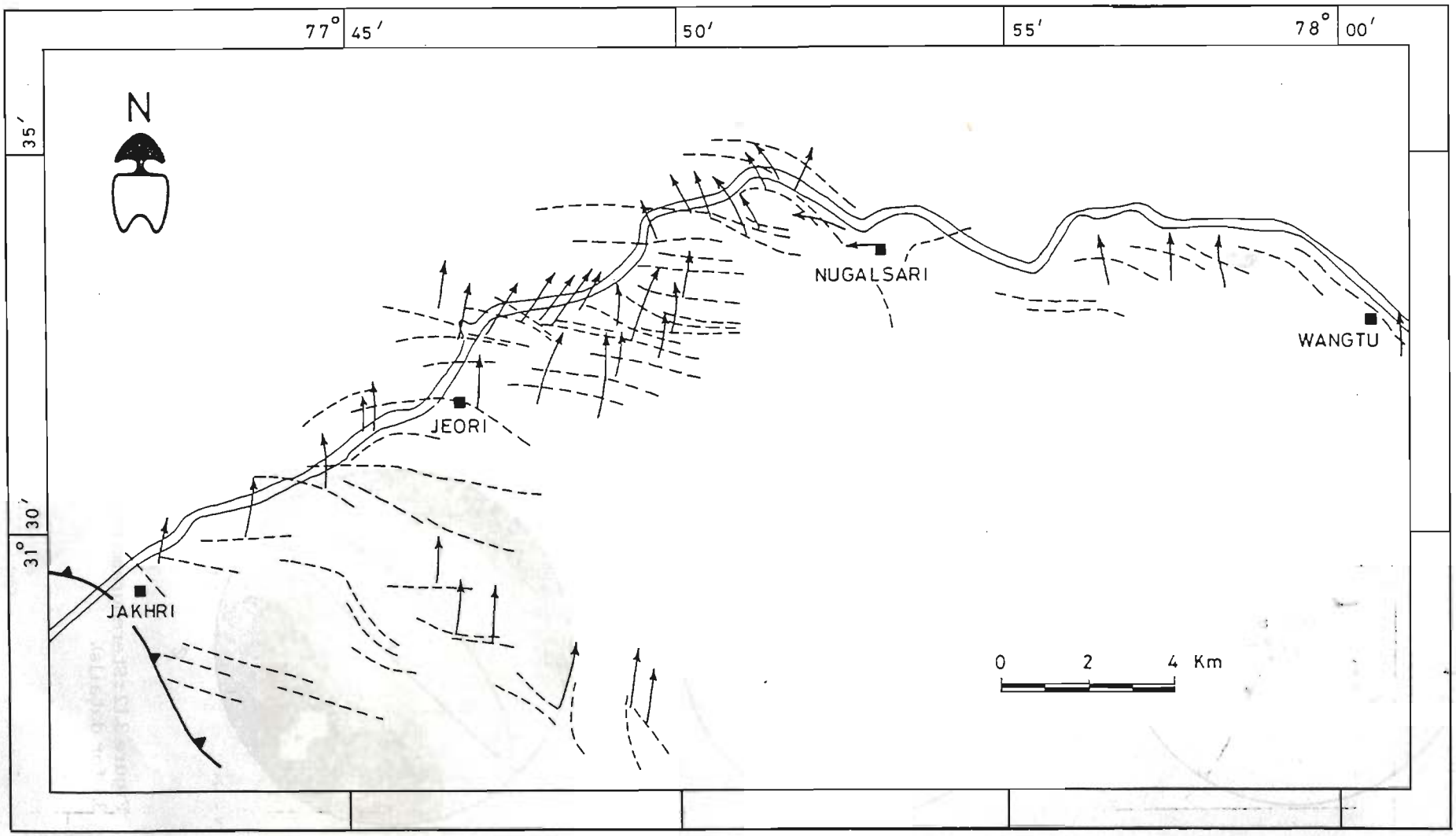

Figure 3.11 : Trajectory map of main foliation S_m and lineation L_2 of the Higher Himalayan Crystalline (HHC) along the Sutlej valley between Jakhri and Wangtu.

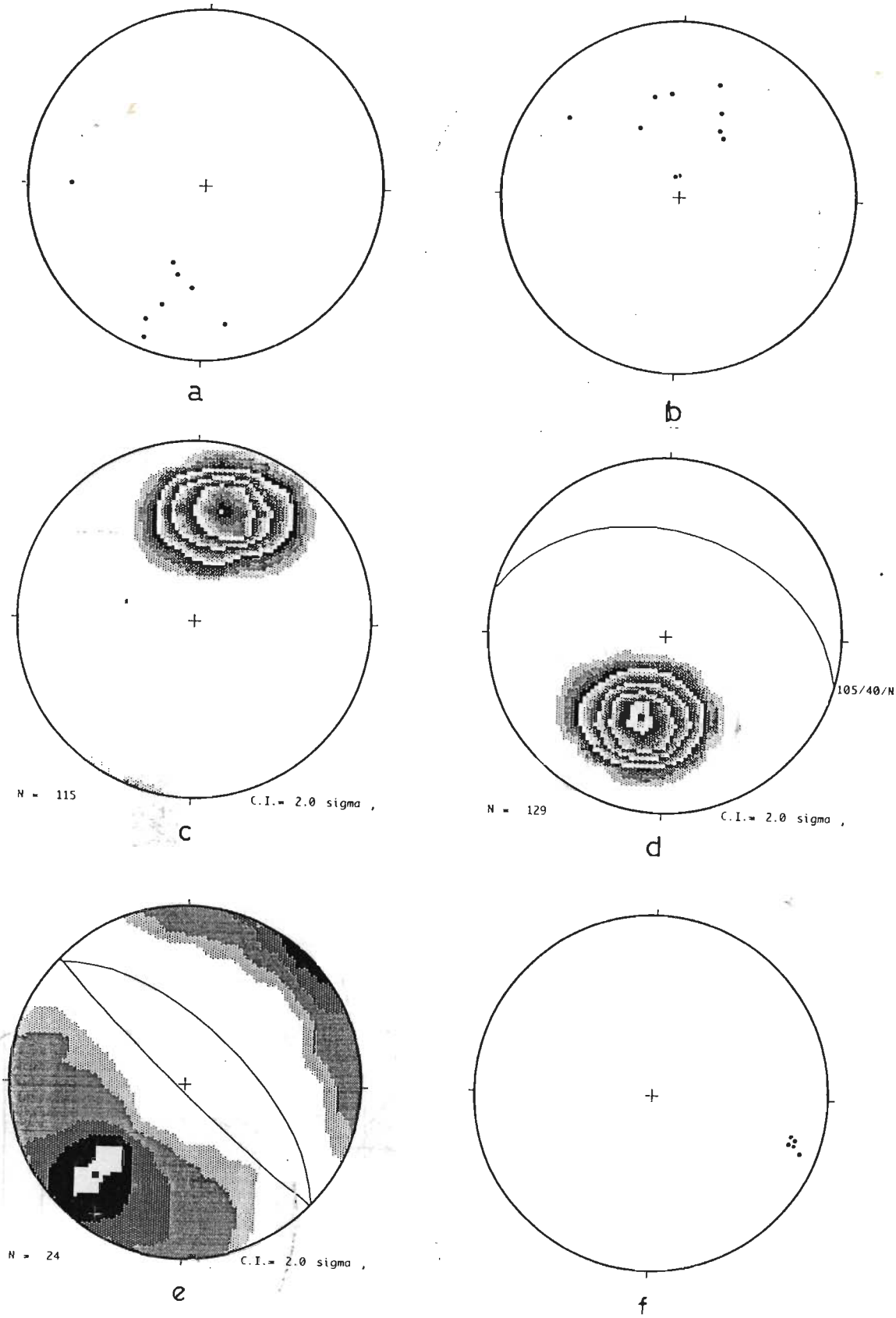

Figure 3.12 : Stereograms of different structural elements of Domain I (see Table 3.1 for datails).

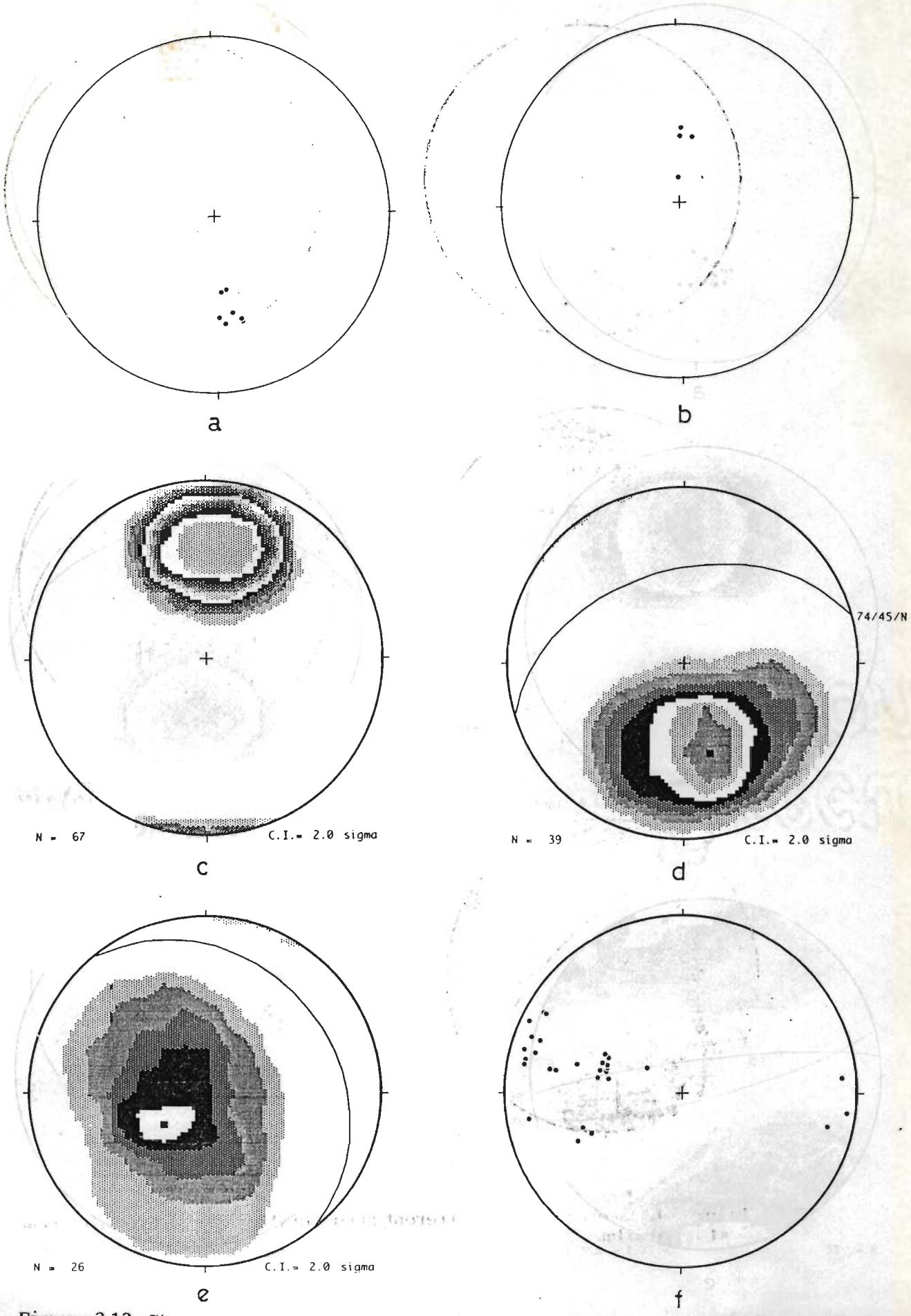

Figure 3.13: Stereograms of different structural elements of Domain II (see Table 3.1 for datails).

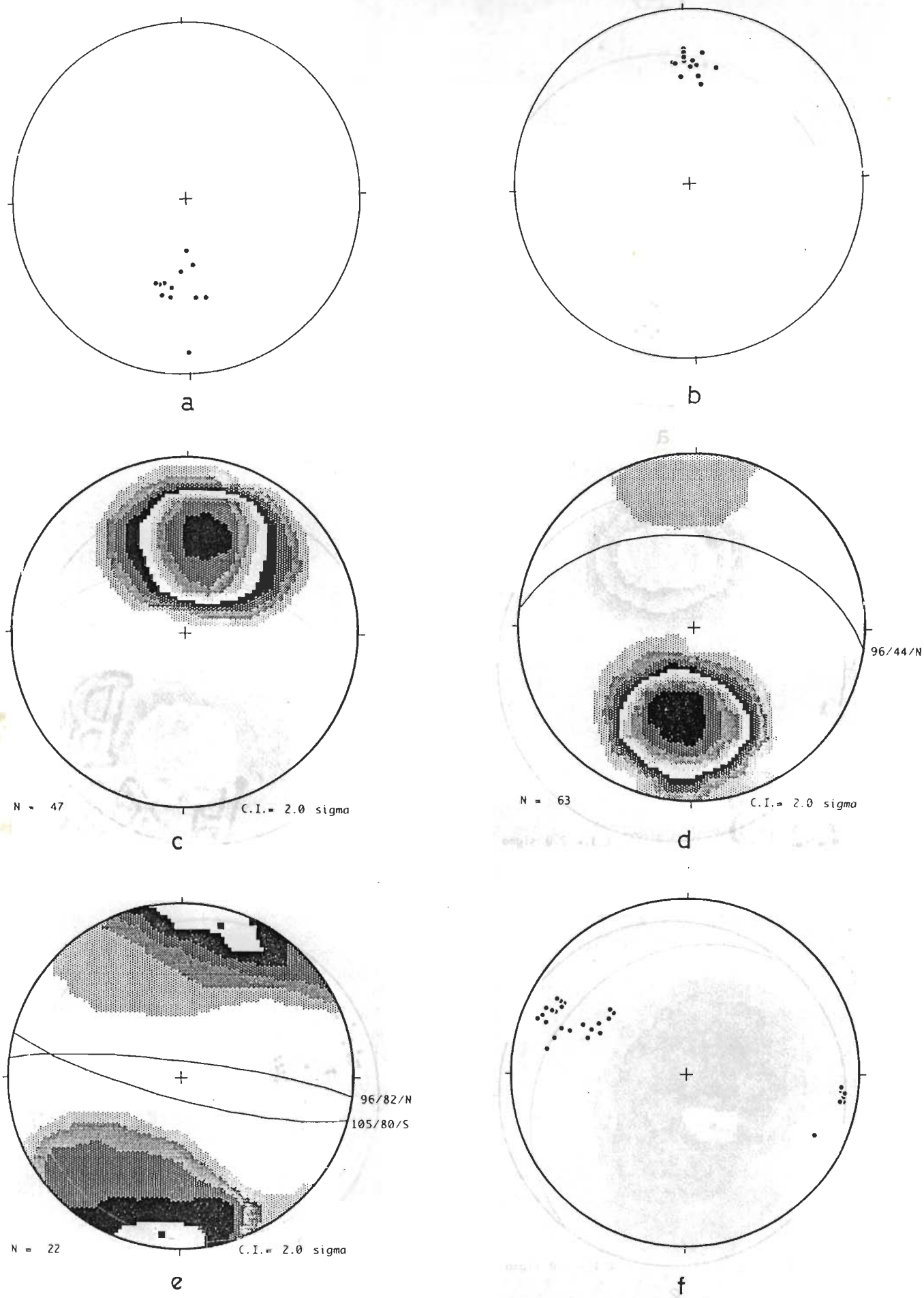

Figure 3.14 : Stereograms of different structural elements of Domain III (see Table 3.1 for datails).

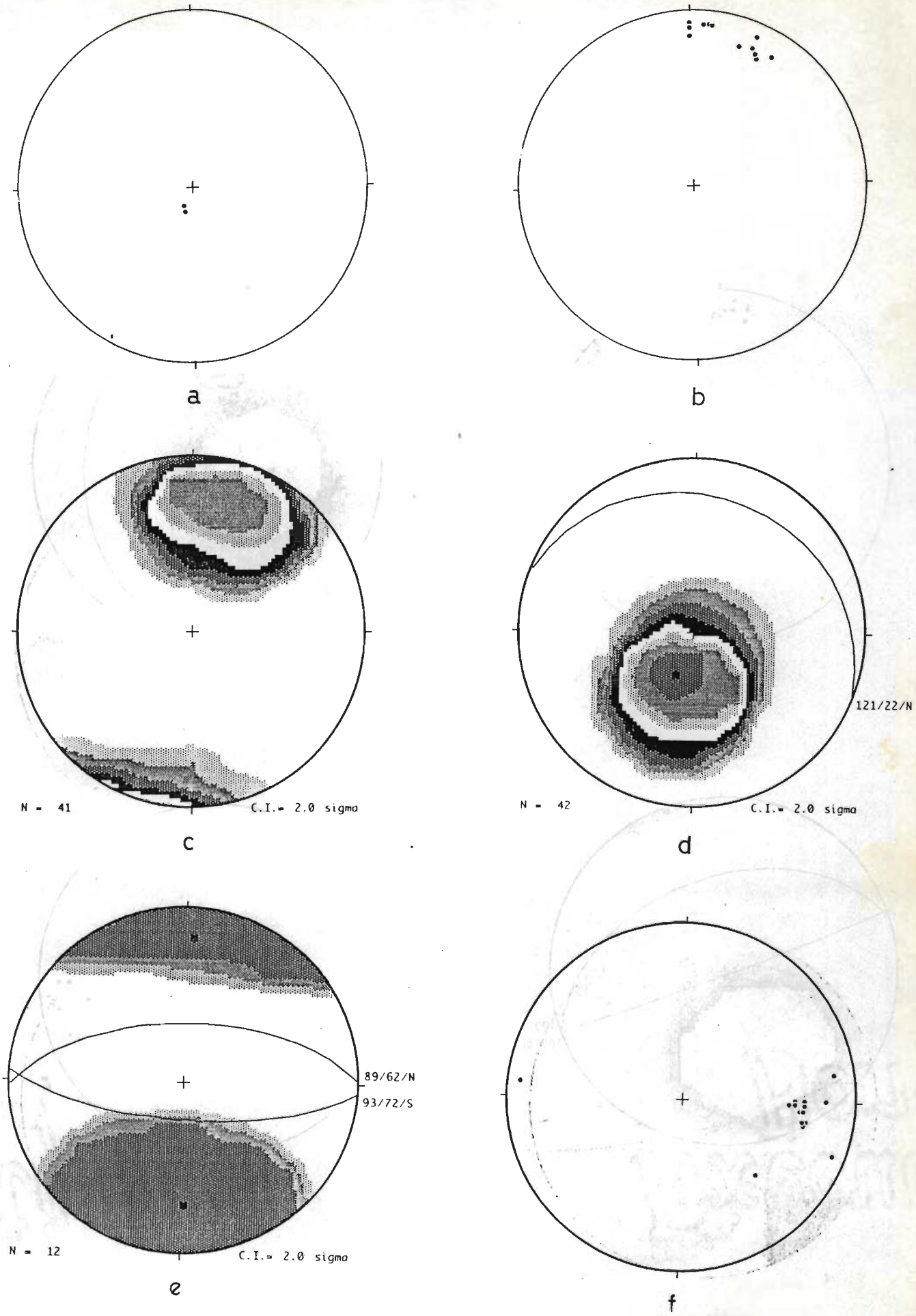

Figure 3.15 : Stereograms of different structural elements of Domain IV (see Table 3.1 for datails).

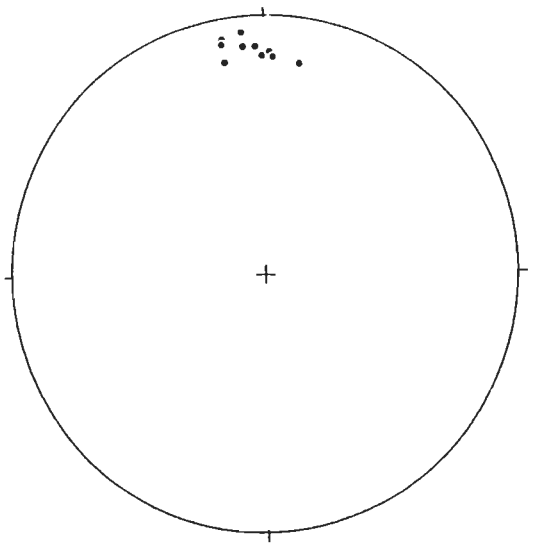

a

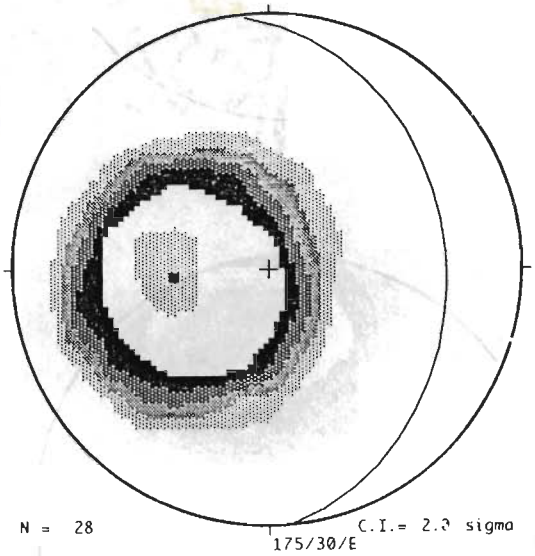

b

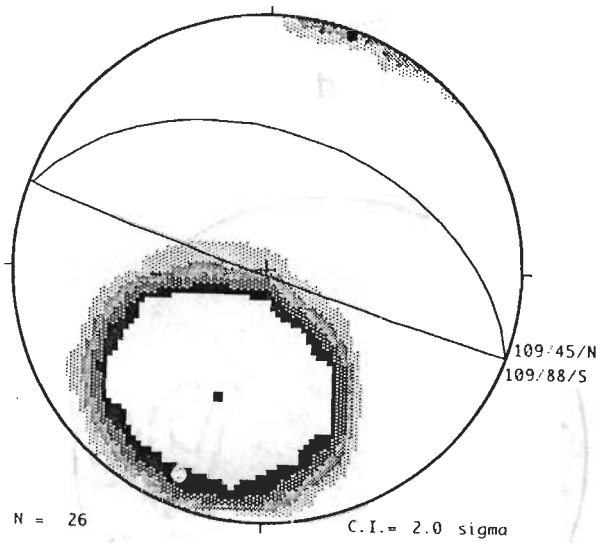

c

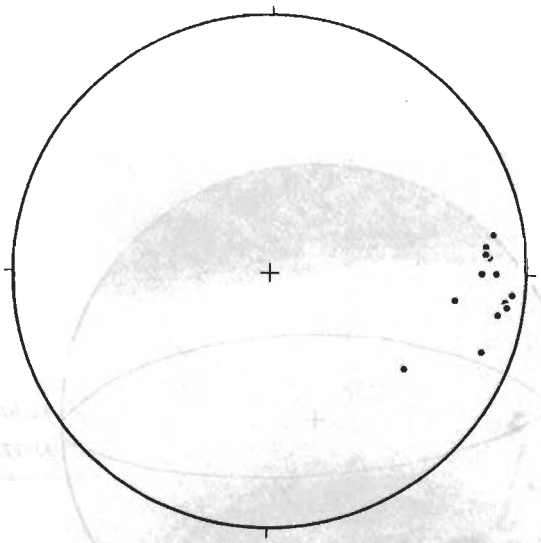

d

Figure 3.16 : Stereograms of different structural elements of Domain V (see Table 3.1 for datails).

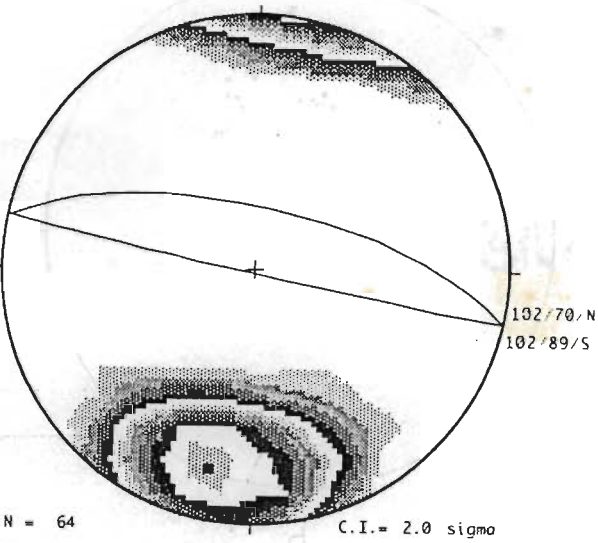

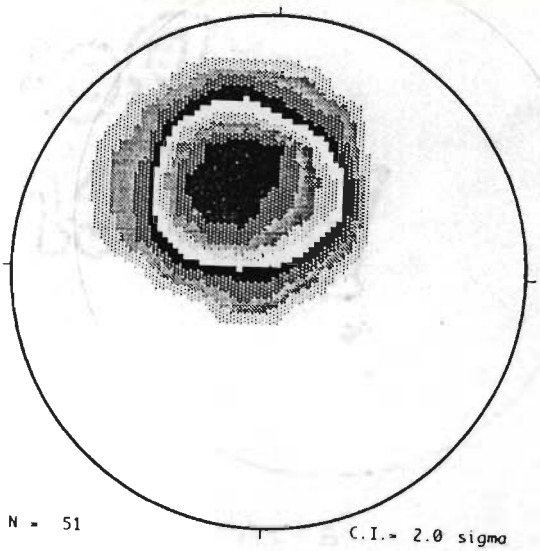

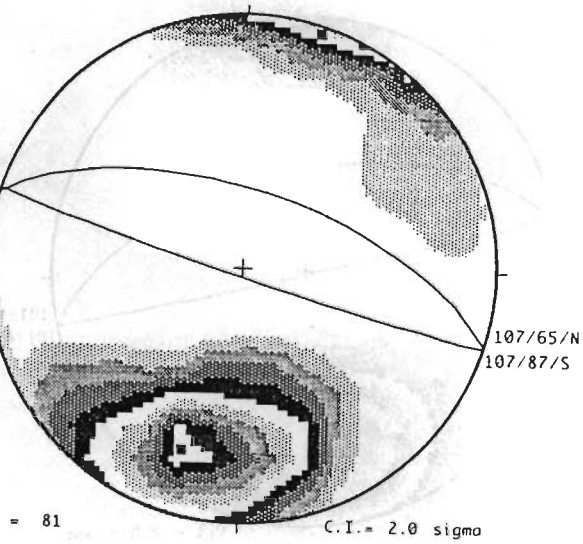

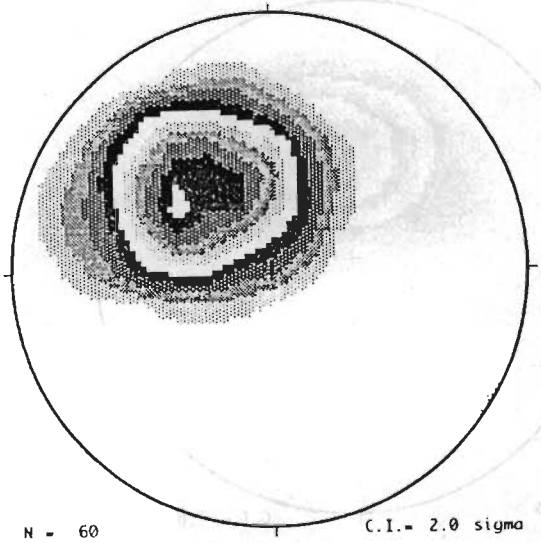

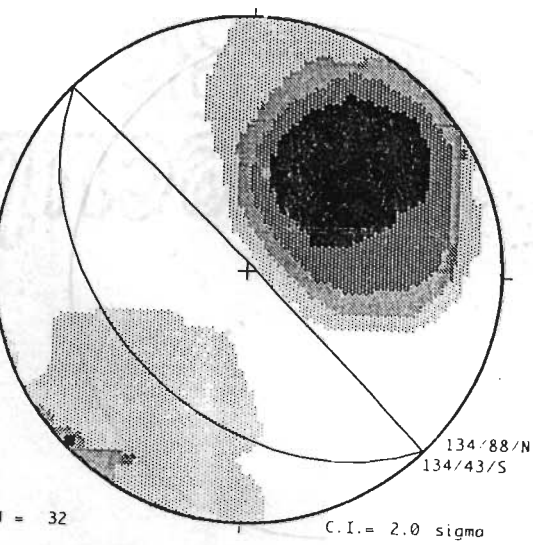

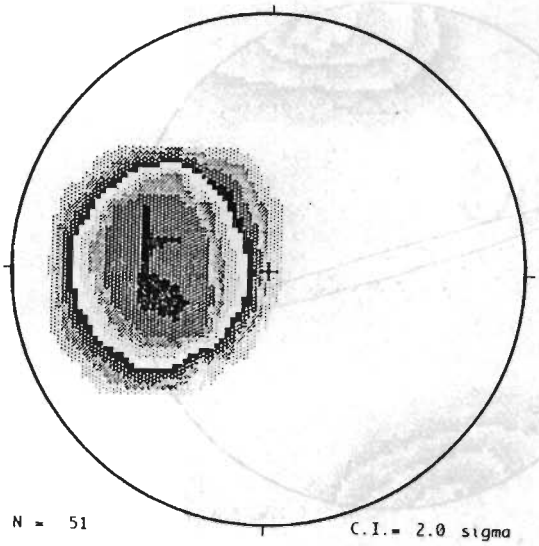

Figure 3.18 : Stereograms of different structural elements of Domain VII, VIII and IX (see Table 3.1 for datails).

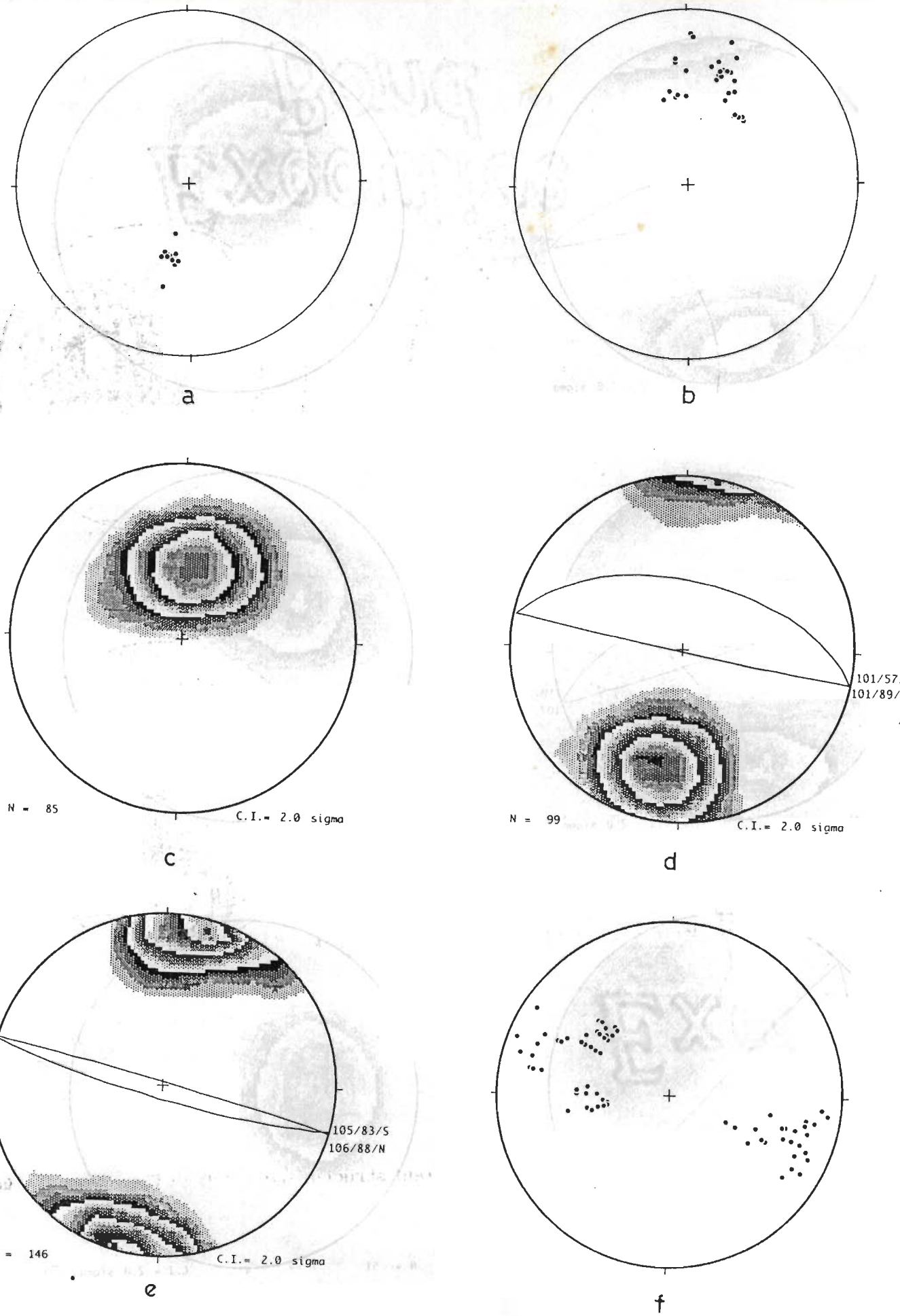

Figure 3.17 : Stereograms of different structural elements of Domain VI (see Table 3.1 for datails).

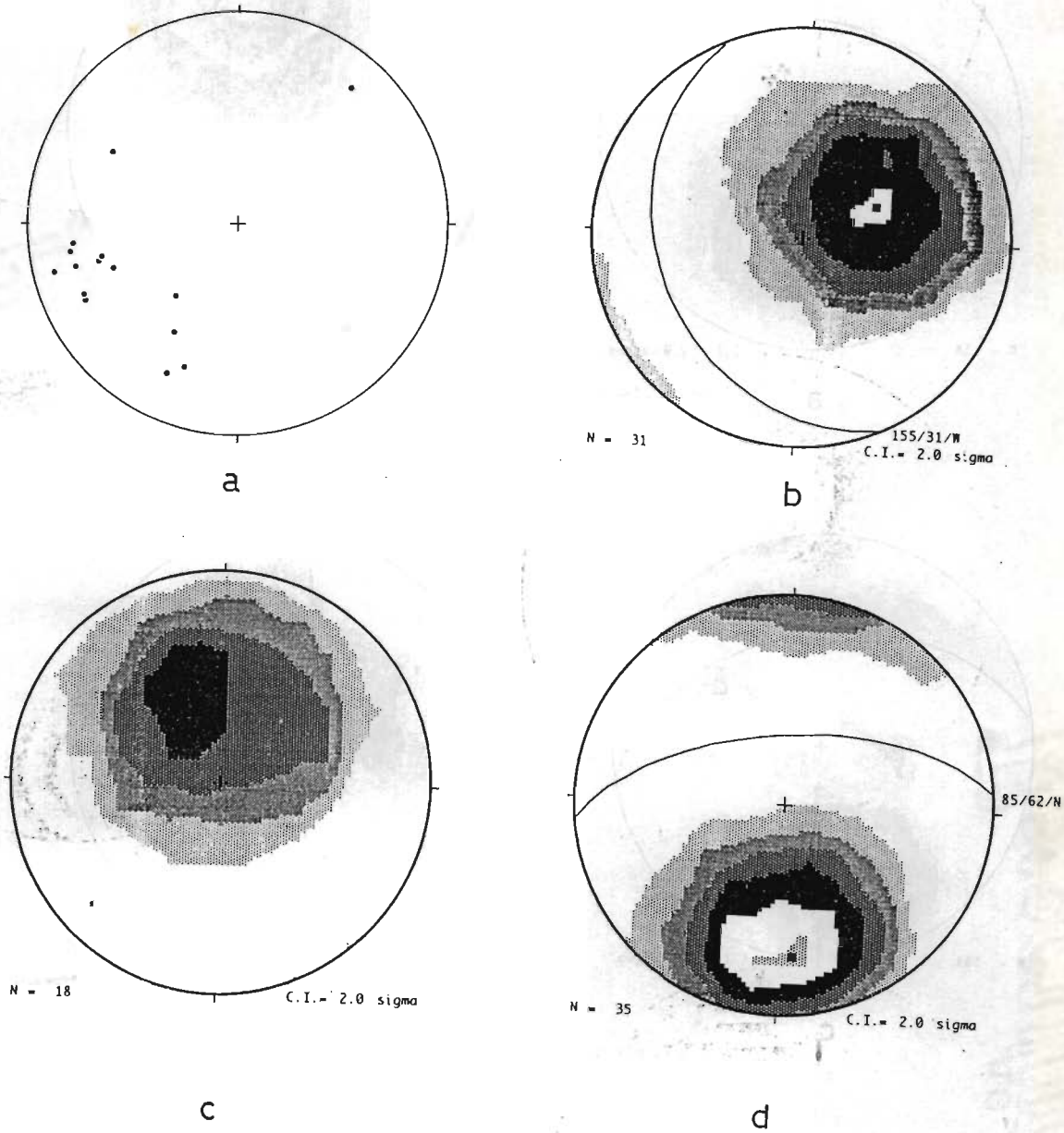

Figure 3.19: Stereograms of different structural elements of Domain X and XI (see Table 3.1 for datails).

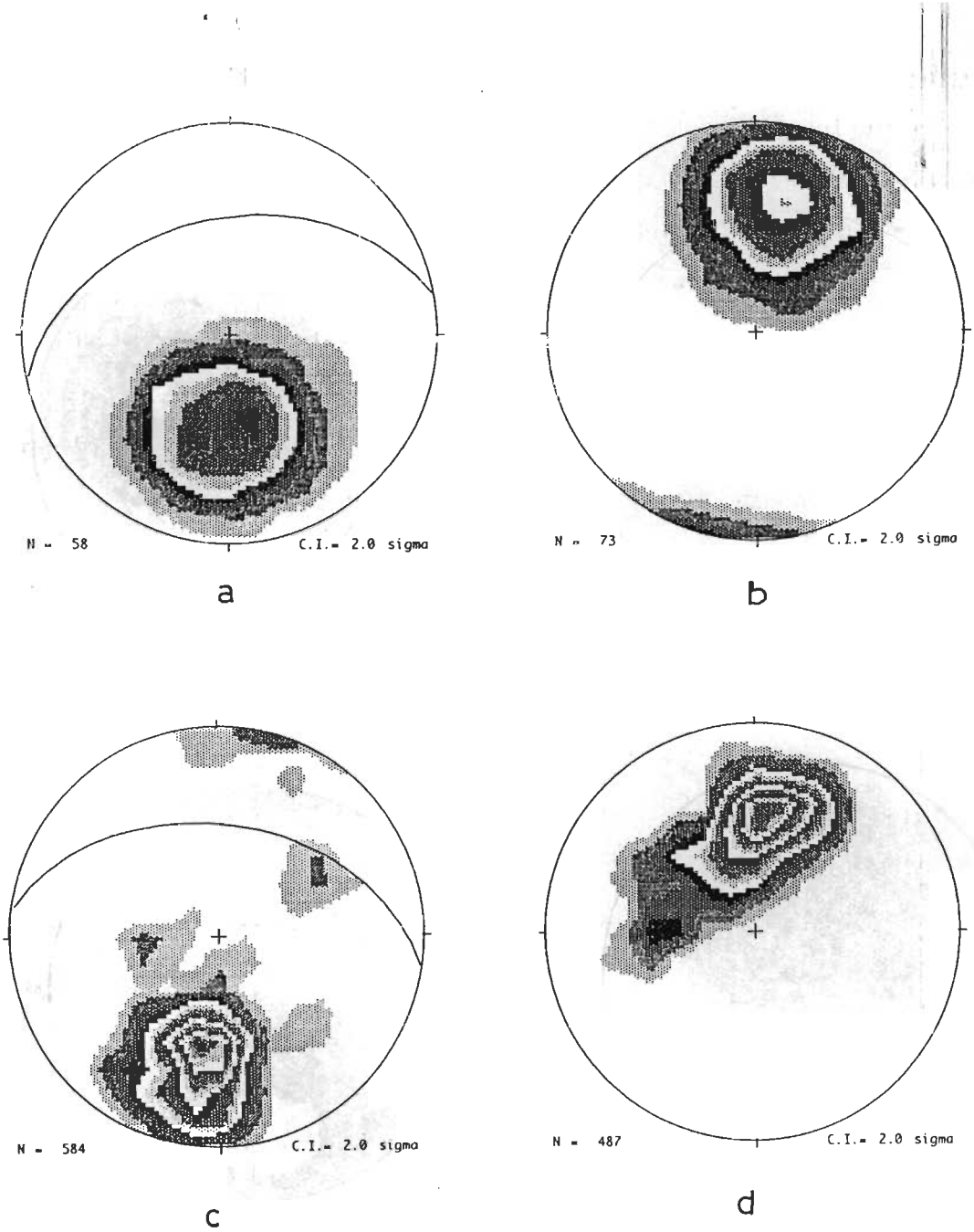

Figure 3.20 : Synoptic stereograms of the D_2 deformational event from the HHC.

(iii) S_2 foliation: The axial plane foliation S_2, associated with the F_2 folds is slightly oblique by about 20° to the main foliation S_M strikes N 79° with a dip of 44° towards N (Fig. 3.20 b). These foliations are defined by preferred orientation of feldspar, quartz and phyllosilicates.

(iv) L_2 lineation: The most remarkable structural feature of this region is the considerable homogeneous mineral/stretching lineation L_2 in its amount and orientation (Fig. 3.20 c). On macroscopic scale, this lineation plunges 38° towards N 4°. However, a few domains reveal steeper plunge and variable orientation due to presence of the latter macroscopic scale folds near the root zone (domain VII, VIII, IX and X).

(v) S_M foliation: Due to intense penetrative repeated D_1 and D_2 deformations, earliest metamorphic banding/lithological layering S_0 and S_1 foliation have transposed into a consistent most prominent main foliation S_M. This foliation strikes N 109° and dips 45° N (Fig. 3.20 d). It may be noteworthy that S_M and S_2 foliation dip at the same angles, while these have slightly discordent strikes. Only in the hinge zones of F_2 folds, it has been possible to distinguish and seperate S_2 foliation from the main foliation S_M. It is also been observed that S_M foliation is subsequently affected by folds during the D_3 deformational phase.

It has also been noteworthy that a gradual steepening of the main foliation S_M takes place from the MCT towards the Wangtu Granite Complex, which also contains numerous almost vertical dipping metamorphic enclaves.

(vi) S_{3a} foliation: Synoptic diagram of poles to S_{3a} foliation, an axial plane foliation of recumbent to gently inclined F_{3a} folds, shows near complete girdle (Fig. 3.21 a) striking N 140° with a π-axis plunging 16° N 50°, thus indicating effects of later cross-folds in this part of the Higher Himalaya.

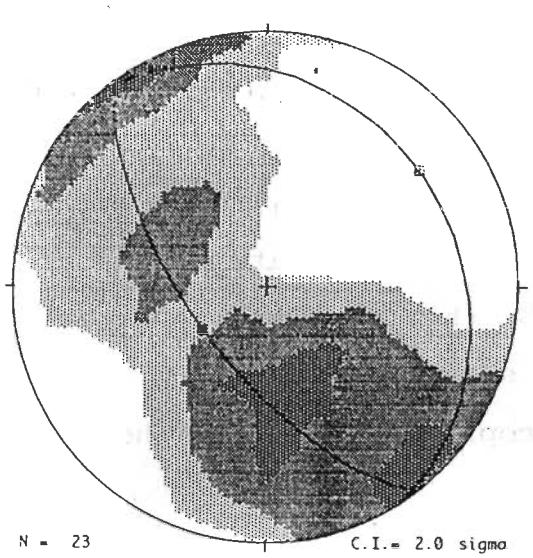

a

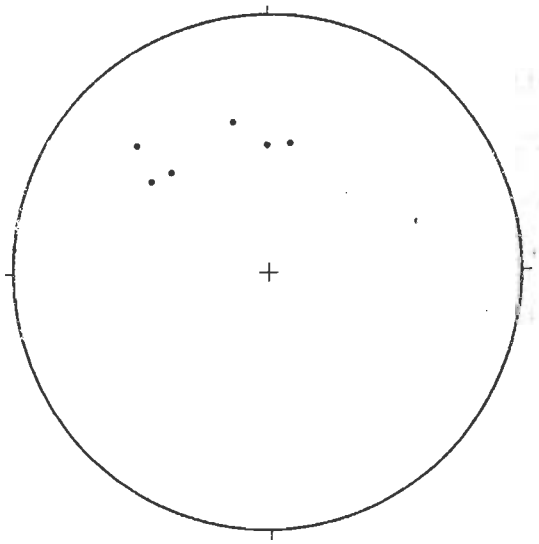

b

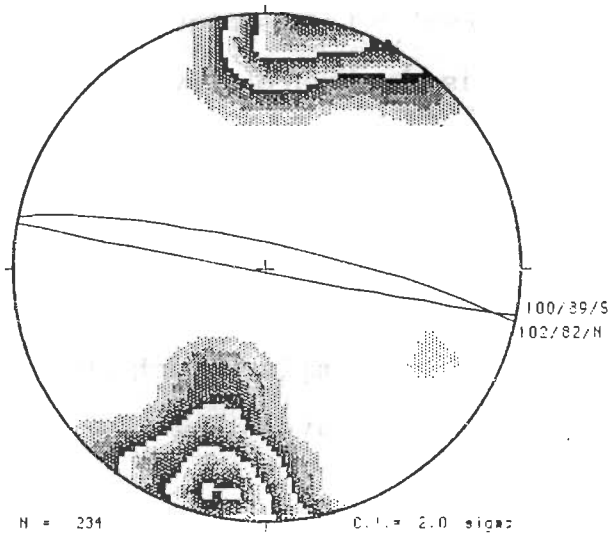

c

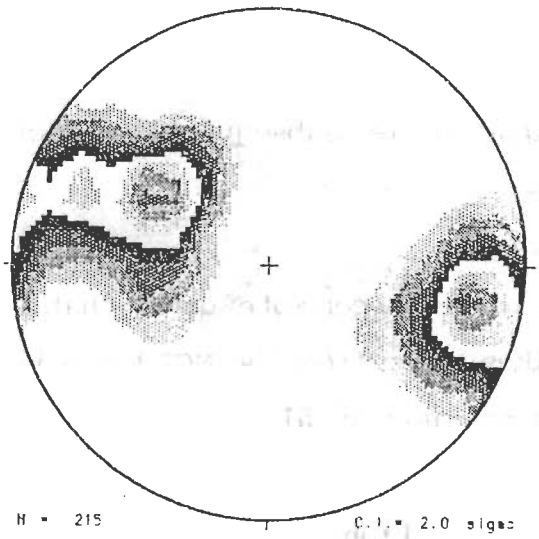

d

Figure 3.21 : Synoptic stereograms of the D_3 deformational event from the HHC.

(vii) **F_{3a} fold hinge:** A few F_{3a} fold hinges clearly depict a spread in their orientation and amount of plunge towards N and NW (Fig. 3.21 b).

(viii) **S_{3b} foliation:** Synoptic diagram of the S_{3b} crenulation foliation show that the S_{3b} foliation strikes N 100° and N 102° with a dip towards 89°/S and 82°/N respectively (Fig. 3.21 c). The corresponding πS_{3b} girdle reveals its axis plunging gently towards E, which apparently coincides with the F_{3b} folds indicating the fanning of the S_{3b} foliation.

(ix) **F_{3b} fold hinge:** Synoptic diagram of F_{3b} fold hinges indicate a considerable spread of plunge along a partial girdle with two point maxima corresponding to 48°/ N 298° and 22°/ N 101° (Fig. 3.21 d). The formation of this girdle is due to the development of late D_4 culmination and depression.

3.2.4 Strain analysis

a. **Choice of strain markers:** The Wangtu granite gneiss abounds in porphyroclastic feldspar grains with distinct grain boundaries. These are enhanced by dark coloured phyllosilicates and transluscent quartz. Feldspar grains appear to have syntectonically stretched and elongated during the D_2 deformation and attained distinct measurable grain boundaries. Strain analysis of the Wangtu granite gneiss was undertaken to delineate strain patterns of the D_2 deformation, because the Wangtu granite gneiss appears to have been emplaced after the HHC had undergone the D_1 deformation.

b. **Methodology:** The break-up of material used for strain analysis is as follows (Fig. 3.22): 9 samples, photographs of XZ and YZ planes from one locality and 6 tracings of the XZ planes from different localities. Approximately 50 to 120

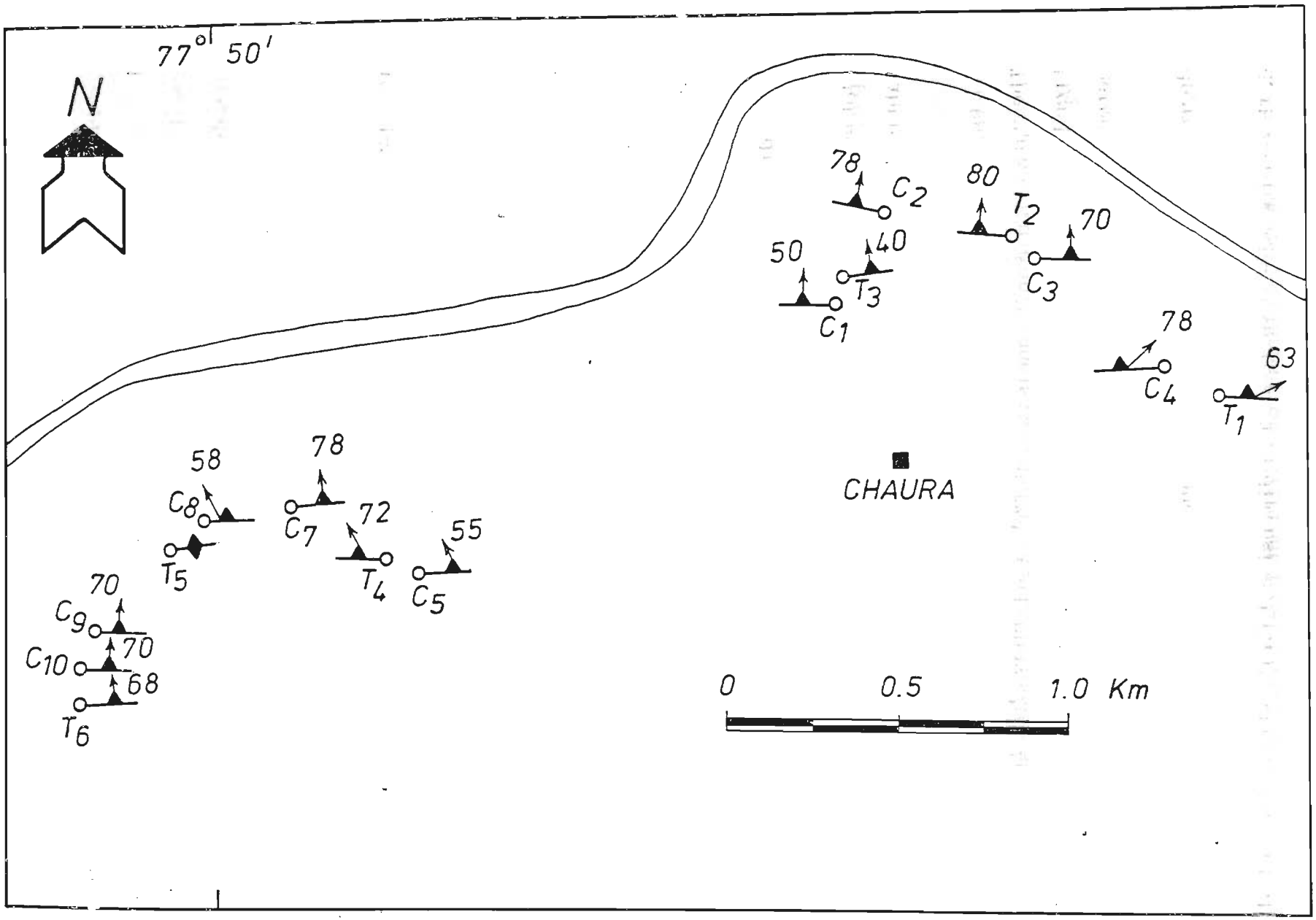

Figure 3.22 : Structural map of the main foliation and lineation showing location of samples from porphyroclastic granite gneiss of the Wangtu granite complex of the HHC, used for strain analysis along the Sutlej valley.

feldspar megacrysts were measured on each of the XZ and YZ sections. Rock samples were polished and treated with lacquer to enhance visual contrast between grain outlines. These were then traced on a cellophane transparent sheet so as to simplify measurement of long and short axes of grains. The angle m, subscribed by X-axis of individual grains with a reference line parallel to the trace of the foliation S_m, has also been measured.

Comparative strain analysis by Rf/ϕ method (Ramsay, 1967; Dunnet, 1969; Lisle, 1977, 1985), long/short axis method (Ramsay, 1967), centre-to-centre method (Ramsay, 1967), and 'nearest neighbour' centre-to-centre method have been attempted by many workers. It has been repeatedly emphasised that Rf/ϕ method, though somewhat time-consuming, provides most reliable and reproducible results, hence the Rf/ϕ method has been adopted in the present work. Onion curves of Dunnet (1969) and Lisle (1985) were used in the determination of Rs values. Three dimensional strain data were plotted on Flinn, logarithmic and Hsu graphs (cf., Ramsay and Huber, 1983) and given in Table 3.2.

c. Two dimensional analysis: Rf/m data from the selected samples and photographs were plotted and matched with the onion curves (Fig. 3.23 - 3.27). Most of the data plot symmetrically in Rf/ϕ graph indicating a general lack of initial preferred fabric before the main deformation.

Rs values in XZ section of the Wangtu granite gneiss varies from 4.0 to 8.5. The variation in the R_{XZ} values is not continuous but follows a particular trend. As one moves from the contact of porphyroclastic granite gneiss with garnetiferous mica schist and gneiss of the Jeori Formation, R_{XZ} values attain a maximum of 8.50 in the centre of atleast three ENE-trending zone. R_{XZ} decreases on either side of these zone to almost 4.0.

d. Three dimensional analysis: Two-dimensional finite strain data of all

TABLE-3.2 : Two dimensional strain values of Porphyroclastic Wangtu granite gneiss from the Sutlej Valley, Himachal Pradesh.

SN	Sample no.	Section	Rfmax	Rfmin	Rs(calc)	Rs(grap.)
1.	C1	XZ	11.27	3.05	5.86	5.75
		YZ	5.85	2.30	3.668	3.60
2.	C2	XZ	7.814	3.502	5.23	5.25
		YZ	4.8266	2.196	3.25	3.2
3.	C3	XZ	6.82	3.067	4.575	4.4
		YZ	66.428	2.65	4.127	4.2
4.	C4	XZ	14.583	4.8	8.366	8.5
		YZ	7.56	2.53	4.37	4.0
5.	C5	XZ	8.48	2.77	4.84	4.8
		YZ	3.09	1.724	2.308	2.3
6.	C7	XZ	6.21	2.836	4.1966	4.0
		YZ	3.88	2.105	2.857	2.85
7.	C8	XZ	7.475	2.98	4.719	4.8
		YZ	6.475	2.5433	4.058	4.0
8.	C9	XZ	10.375	2.295	4.879	5.0
		YZ	3.718	2.384	2.97	2.85
9.	C10	XZ	7.606	4.560	5.88	5.75
		YZ	4.611	2.074	3.09	3.0
10.	PL7	XZ	7.42	2.8417	4.59	4.6
		YZ	5.1038	2.5888	3.63	3.6
11.	T1	XZ	8.5714	2.808	4.90	5.0
12.	T2	XZ	10.18	2.692	5.40	5.5
13.	T3	XZ	11.42	2.941	5.79	5.75
14.	T4	XZ	10.7	3.372	6.00	6.0
15.	T5	XZ	9.35	3.00	5.29	5.25
16.	T6	XZ	18.566	4.06	8.68	8.5

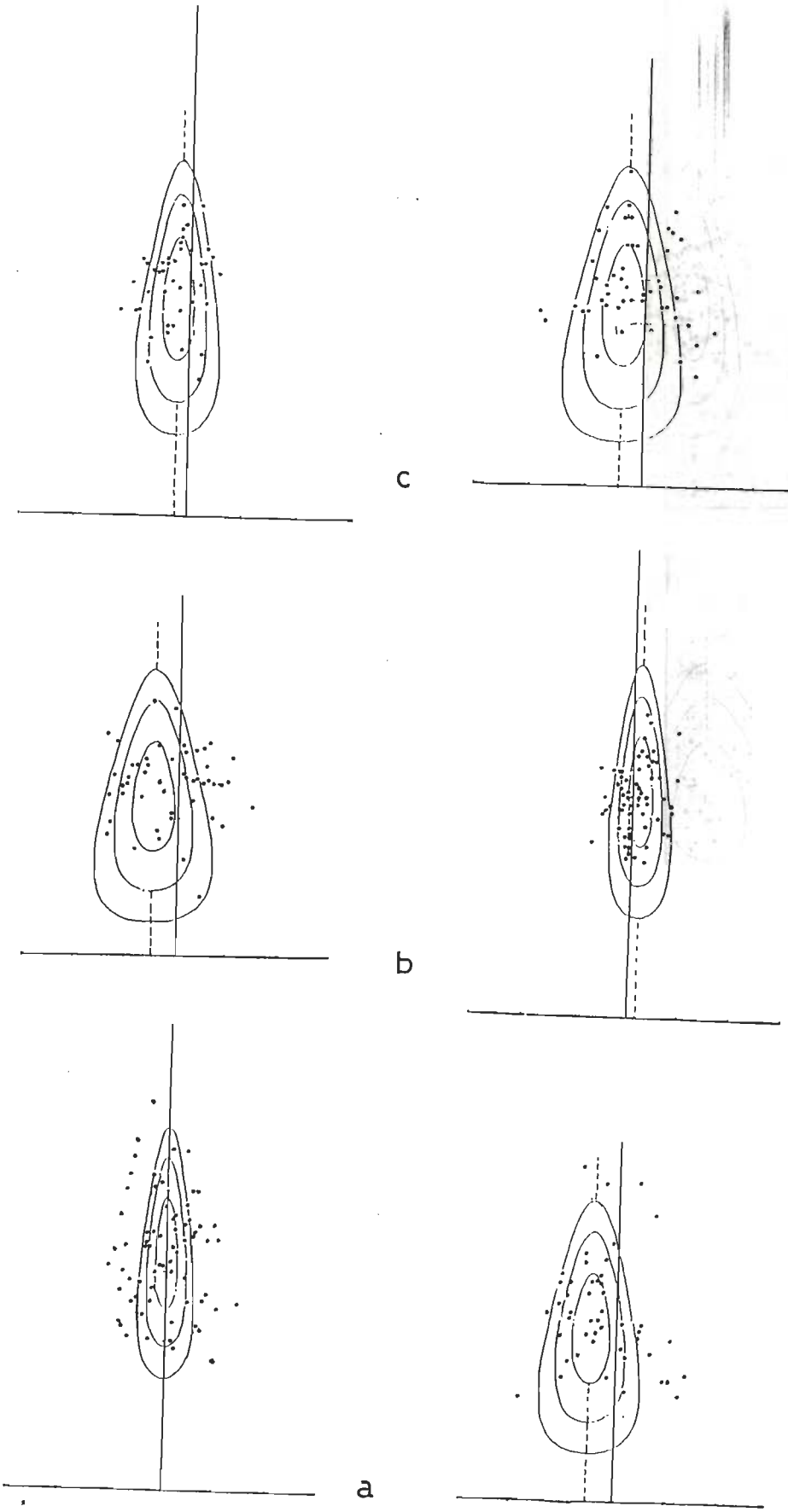

Figure 3.23 : Rf/ϕ plots of XZ and YZ planes of samples (a) C_1 (b) C_2 and (c) C_3.

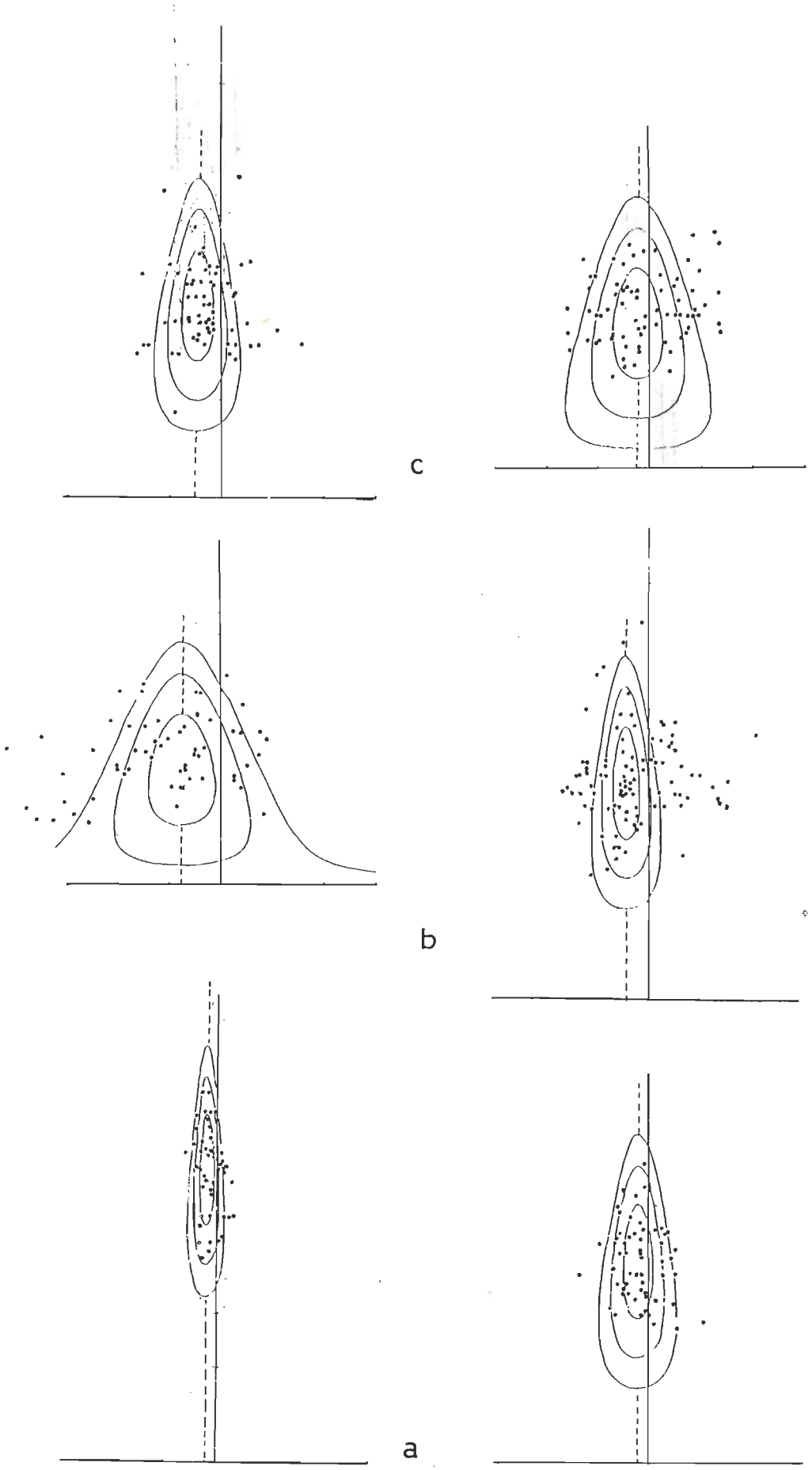

Figure 3.24 : Rf/ϕ plots of XZ and YZ planes of samples (a) C_4 (b) C_5 and (c) C_7.

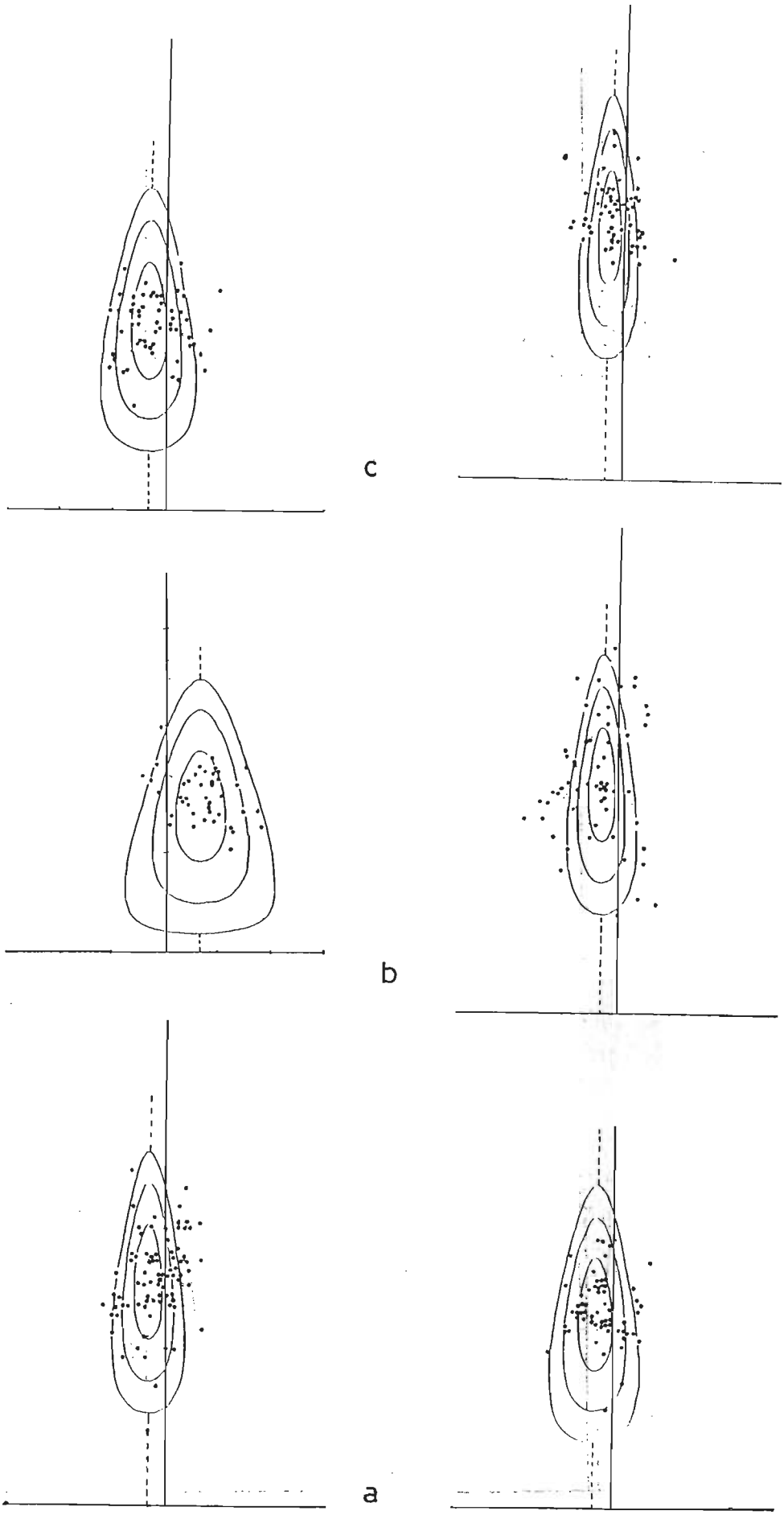

Figure 3.25 : Rf/ϕ plots of XZ and YZ planes of samples (a) C_8 (b) C_9 and (c) C_{10}.

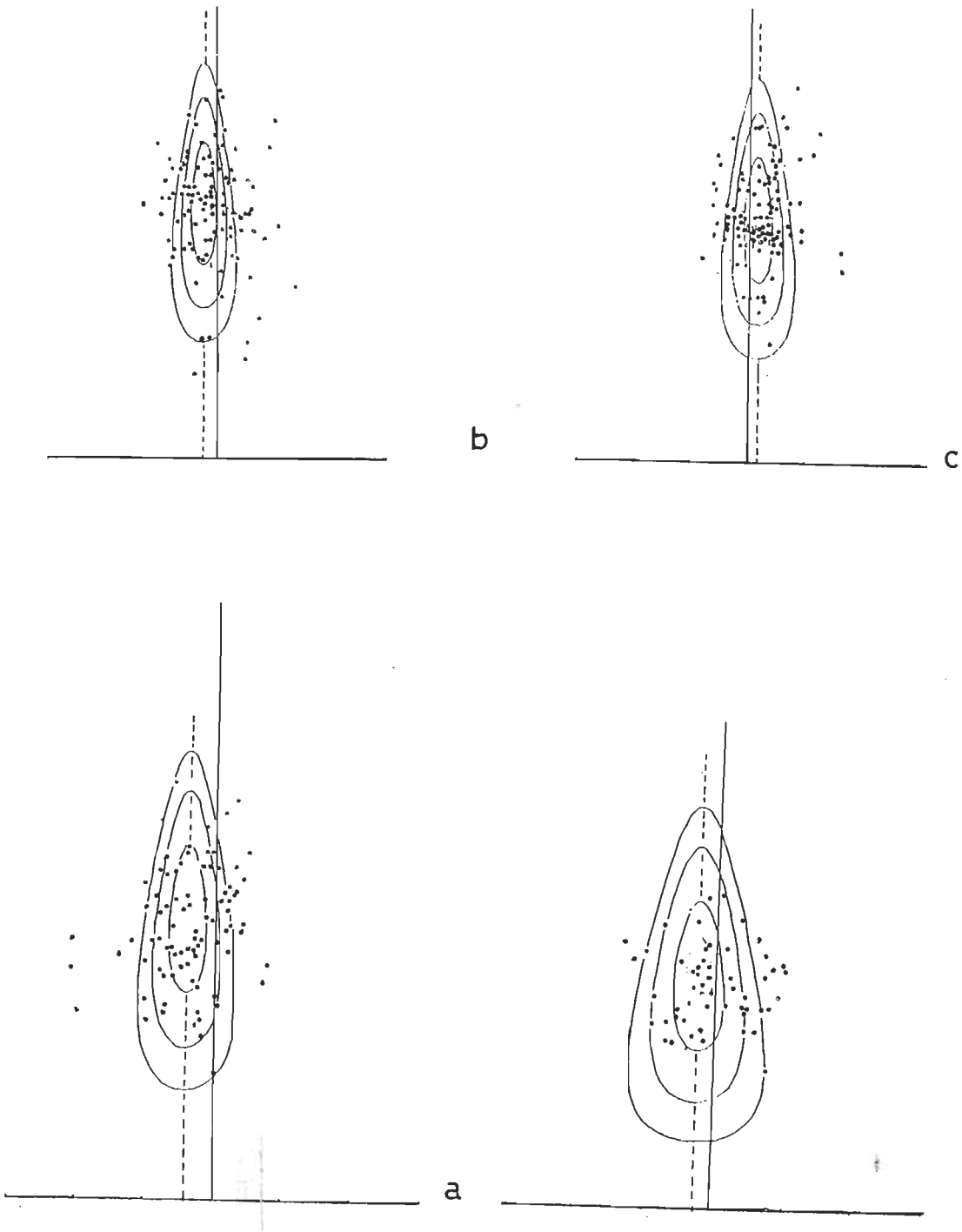

Figure 3.26 : Rf/ϕ plots of XZ and YZ planes of sample (a) PL_7 and YZ plane of samples (b) T_1 and (c) T_2.

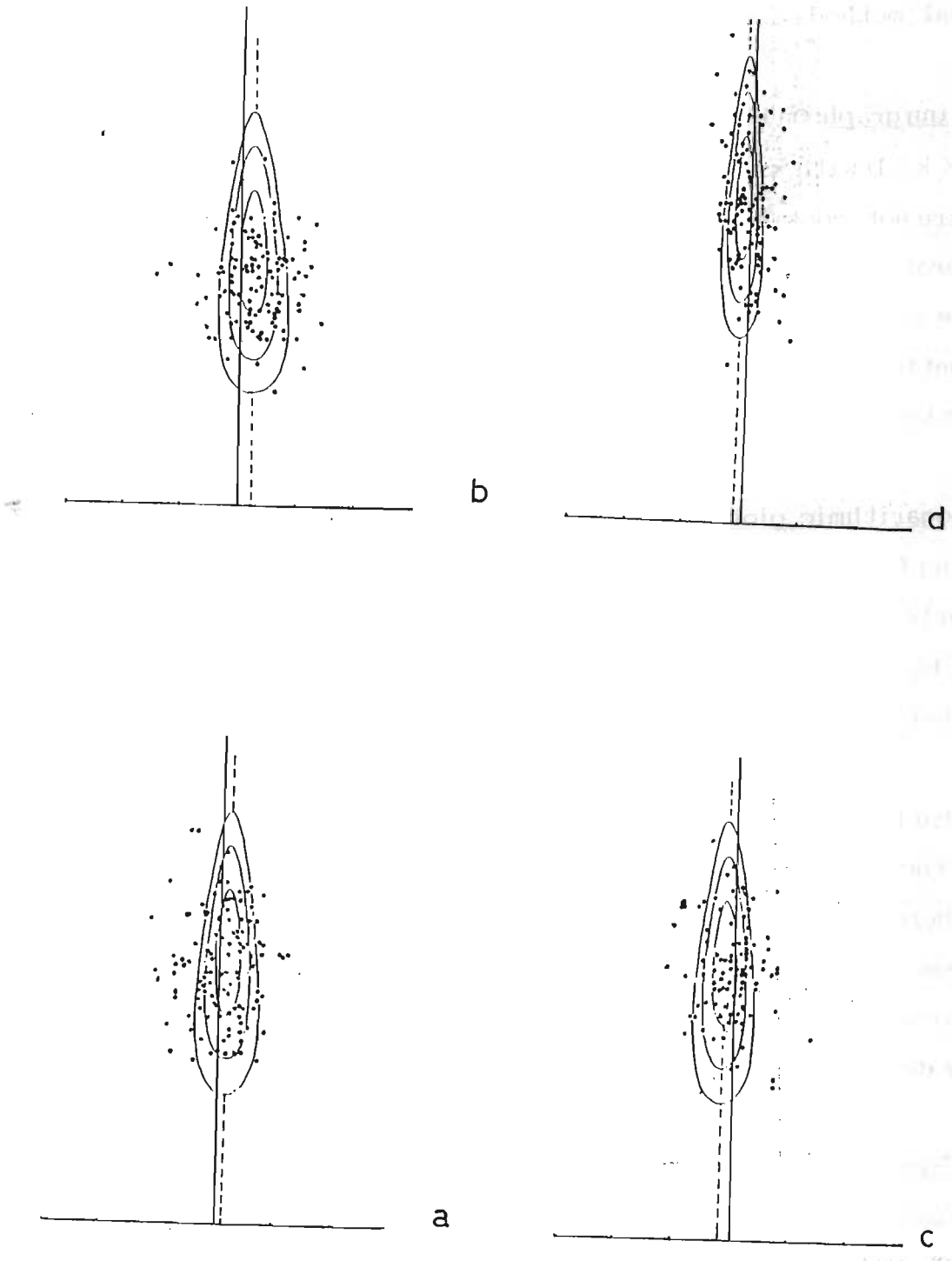

Figure 3.27 : Rf/ϕ plots of YZ planes of samples (a) T_3 (b) T_4 (c) T_5 and (d) T_6.

feldspathic-porphyroclasts by Rf/ϕ techniques are integrated for three dimensional strain analysis to determine the shape of strain ellipsoid and values of different strain parameters viz., k, K, τ and ε_s (Table 3.3). Different graphical methods are used for shape analysis of the strain ellipsoid.

(i) **Flinn graph:** On the Flinn graph, all data points are lying in the flattening field ($0 < k < 1$) with k values varying from 0.0125 to 0.832. The variation in the k values are not continuous and ranges from nearly uniaxial prolate ellipsoid to nearly prolate-oblate and thus approaching the field of plane strain (Fig. 3.28 a). As one moves away from the contact of porphyroclastic granite gneiss with the garnetiferous mica schist, k values are maximum (0.831) near the contact and decrease to 0.066 away from the contact towards higher tectonic levels.

(ii) **Logarithmic plot:** On the logarithmic plot, all data points lie in the flattening field ($0 < K < 1$). The values of K varies from 0.027 to 0.879 and range from nearly uniaxial prolate strain ellipsoid to nearly prolate-oblate field (Fig. 3.28 b). Type of strain is mostly finite flattening strain, except in one sample where strain is nearly plane strain.

(iii) **Hsu plot:** In the case of the polar graph, all the data points are lying again in the flattening field ($0 < \tau < +1$). The values of τ varies from +0.0643 to +0.9474, whereas the values of ε_s varies from 1.02 to 1.53 (Fig. 3.29). As one moves away from the contact of porphyroclastic granite gneiss with the garnetiferous mica schist, ε_s values are maximum (1.25) near the contact and gradually decreases to 1.02 in the western part into higher tectonic levels.

(iv) **Strain variation in profile section:** The trend of regional foliation and orientation of strain ellipsoid in parts of porphyroclastic Wangtu gneiss indicate that this zone probably is made up of atleast three subsidiary ductile shear zones with bulk strain field of flattening-type throughout the

TABLE - 3.3 : Three dimensional strain values of Porphyroclastic Wangtu granite gneiss along with different parameters viz. k, K, and ϵs from the Sutlej Valley, Himachal Pradesh.

SN	Sample No.	R_{xz}	R_{yz}	R_{xy}	X:Y:Z:	ln R_{yz}	ln R_{xy}	ln R_{xz}	k	K		ϵs
1.	C_1	5.75	3.6	1.59	5.75:3.6:1	1.28	0.46	1.749	0.226	0.362	0.4684	1.28
2.	C_2	5.25	3.2	1.64	5.25:3.2:1	1.16	0.49	1.658	0.291	0.425	0.4035	1.20
3.	C_3	4.4	4.2	1.04	4.40:4.2:1	1.43	0.039	1.48	0.0125	0.027	0.9474	1.19
4.	C_4	8.5	4.0	2.125	8.50:4.0:1	1.38	0.753	2.14	0.375	0.543	0.2961	1.53
5.	C_5	4.8	2.3	2.08	4.80:2.3:1	0.83	0.73	1.56	0.831	0.879	0.0643	1.10
6.	C_7	4.0	2.85	1.40	4.0:2.85:1	1.04	0.33	1.38	0.216	0.32	0.5151	1.02
7.	C_8	4.8	4.0	1.20	4.80:4.0:1	1.38	0.18	1.56	0.066	0.13	0.7699	1.21
8.	C_9	5.0	2.85	1.75	5.0:2.85:1	1.04	0.55	1.60	0.405	0.534	0.30378	1.15
9.	C_{10}	5.75	3.0	1.92	5.75:3.0:1	1.09	0.65	1.749	0.460	0.594	0.2547	1.25
10.	PL_7	4.60	3.6	1.28	4.60:3.6:1	1.28	0.247	1.526	0.356	0.193	0.676	1.16

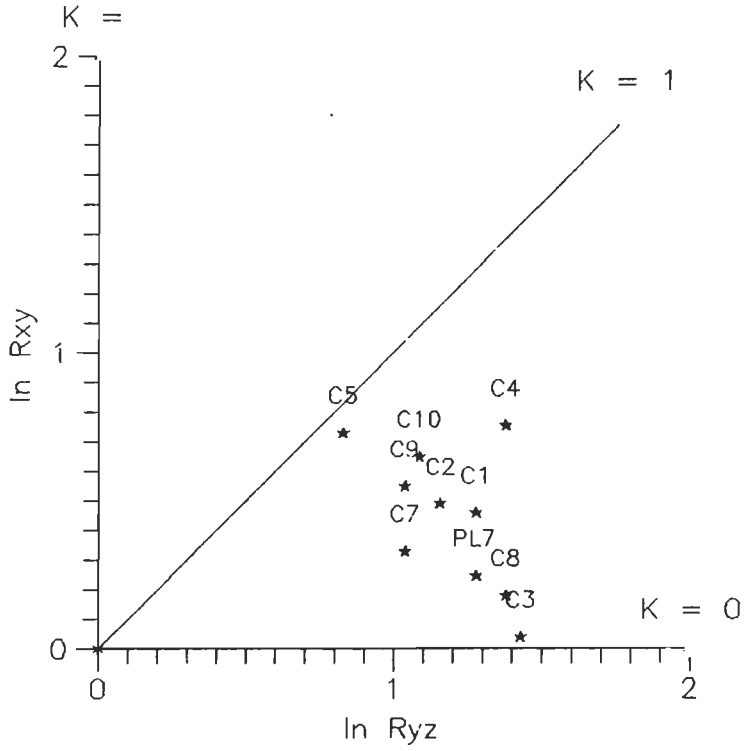

Figure 3.28 b : Logrithmic plot showing strain data of samples lying in flattening field.

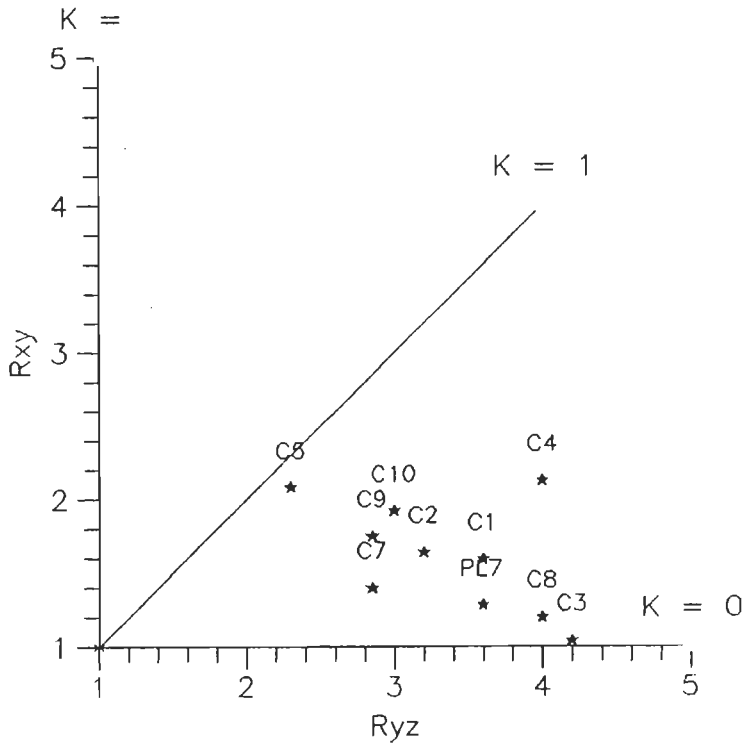

Figure 3.28 a : Flinn graph showing strain data of samples lying in flattening field.

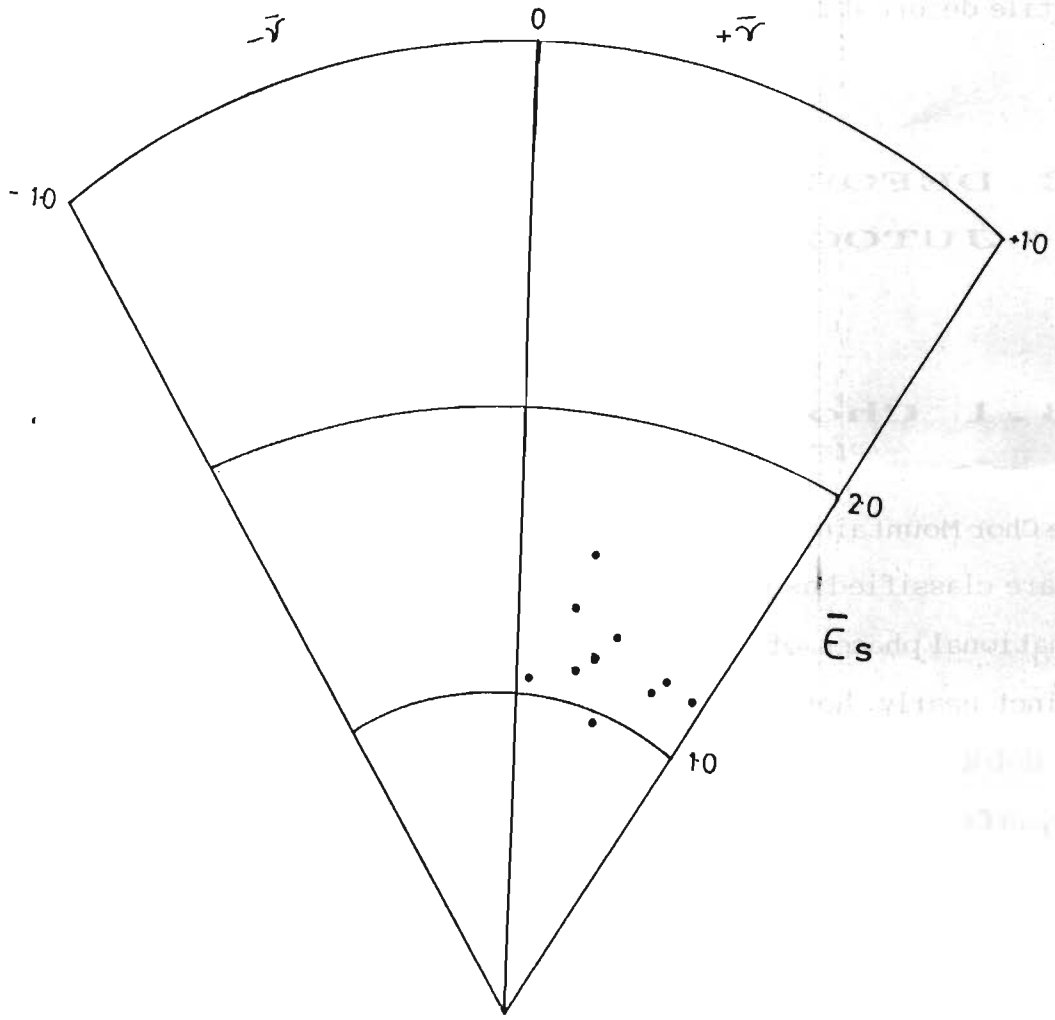

Figure 3.29 : Hsu plot showing strain data of samples lying in flattening field.

progressive deformation (Fig. 3.30). It is, therefore, evident that the contact between the Wangtu granite gneiss with garnetiferous mica schist appears to be a ductile shear zone, which is indicated by the presence of many characters of ductile deformation regime described above.

3.3 DEFORMATION PATTERN OF THE JUTOGH NAPPE

3.3.1 Chor Mountain region

The Chor Mountain region comprises granitoid and associated metamorphics, which are classified as the Jutogh Group. This region exhibits three distinct deformational phases, of which the most prominent and first D_{C1} phase produces a distinct nearly horizontal E or W plunging folds and a coaxial lineation. As this deformational phase corresponds to D_2 deformation of the Higher Himalayan Crystalline (HHC) and inner parts of the Jutogh Nappe along the Sutlej Valley, deformational history of the frontal Chor Mountain area have been described with D_C connotation.

a. First deformational phase (D_{C1}): This deformation phase is most penetrative and widespread in frontal parts of the Jutogh Nappe and has also been recognised by earlier workers from the Jutoghs of the Simla Hills (Naha and Ray, 1970, 1971, 1972; Dubey and Bhatt, 1991) and the Chor Mountain (Kanwar and Singh, 1979; Kishor and Kanwar, 1984, 1986). During this deformational phase, a series of minor folds are formed. Recumbent, gently inclined to reclined-type F_{C1} folds have been observed on the bedding planes S_{C0} and are prominently seen in quartzite schist alternations (Fig. 3.31 a) and marble bands along the Nauhra-Shamra section. The F_{C1} folds are tight to isoclinal folds with thickened

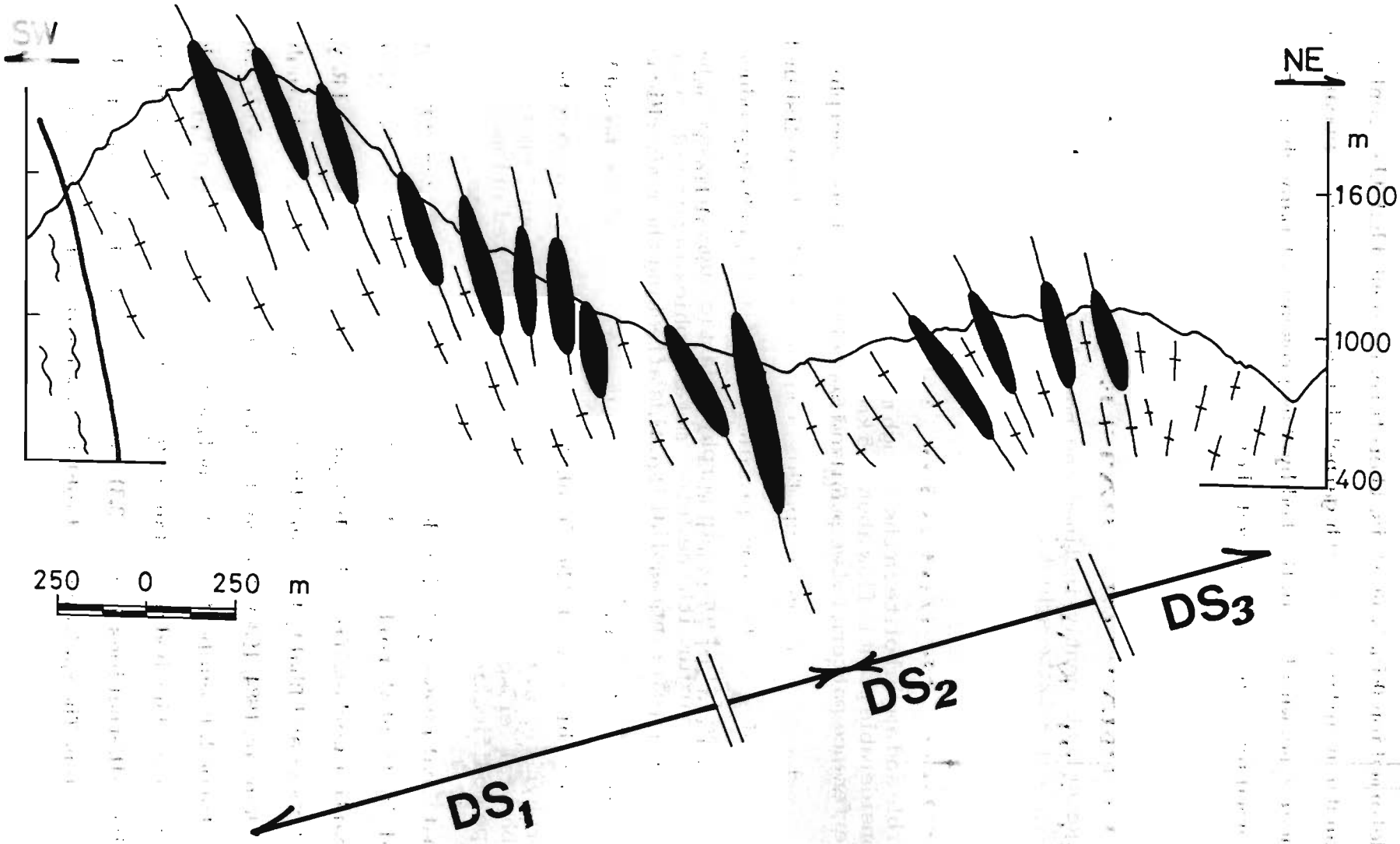

Figure 3.30 : Cross-section of the ductile shear zone DS_1, DS_2 and DS_3, regional foliation and orientation of XZ plane of strain ellipsoid in parts of porphyroclastic Wangtu gneissic complex near the Chaura Thrust along the Sutlej valley.

Figure 3.31 a : Recumbent, gently inclined and non-plunging F_{C1} folds on the bedding planes S_{C0} in quartzite-schist alterations of the Jutogh metamorphics along Nauhra-Shamra section, Chor Mountain.

Figure 3.31 b : Marble and amphibolite in the Jutogh metamorphic having isoclinal F_{C1} folds with considerable plastic flow about 1.5 km towards Shamra from Nauhra. Note type-3 interference pattern between F_{C1} and F_{C2} folds.

Figure 3.31 c : Axial plane foliation S_{C1} in porphyroclastic augen gneiss of the Chor granitoids near the margin with the Jutogh metamorphics along the Raundar Ka Khata nala. Note small-scale intrafolial F_{C1} folds affecting the megacrysts.

Figure 3.31 d : Porphyritic granite of the Chor granitoid body about 5 km ENE of Nauhra. Many subhedral feldspar megacrysts show strong prefered orientation without any shape modification in foliated fine grained groundmass.

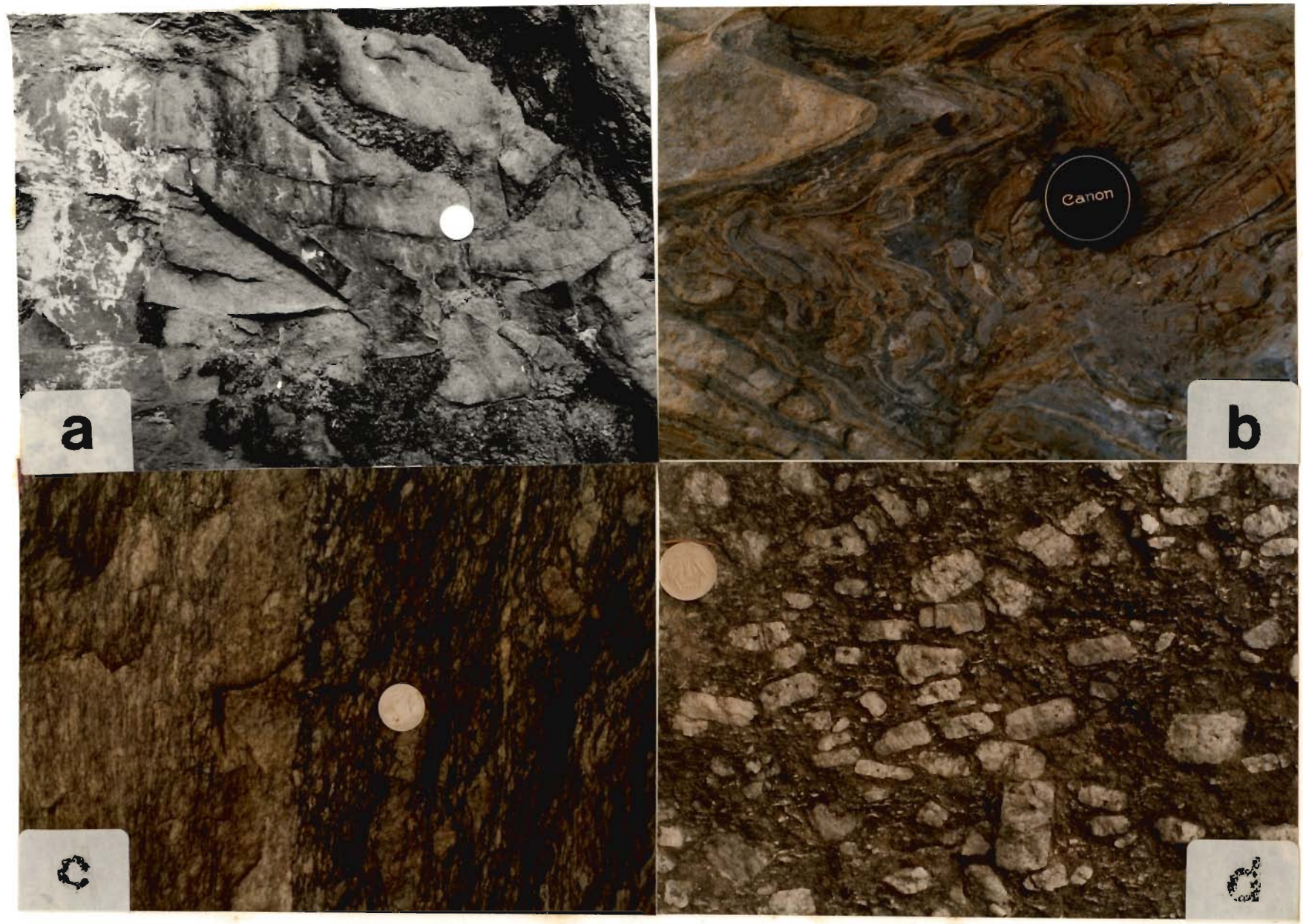

FIG. 3.31

hinge zones and mostly of Class 1C to 2 (cf. Ramsay, 1967). F_{C1} folds plunge at gentle to moderate angles, both E or W and have more or less constant orientation in the area. Limbs of these isoclinal folds in marble bands have undergone considerable plastic flow (Fig. 3.31 b). The coaxial mineral/stretching lineation F_{L1} is associated with F_{C1} folding and marked by preferred orientation of mica, amphibole, stretched quartz and feldspar grains in the country rock. Axial plane foliation S_{C1} dips gently on a regionl scale (Fig. 3.31 a), but is also nearly vertical at places. It is marked by preferred orientation of phyllosilicates and feldspar. S_{C1} subparallels the bedding surface S_{C0} on the limbs of F_{C1} folds.

The axial plane foliation S_{C1}, related to D_{C1} deformation event, is most prominent and found throughout the area in metapelites and metapsammites as well as in the granitoid along the margin with Jutogh metamorphics (Fig. 3.31 c). This foliation can also be designated as main foliation S_{Cm} and is seen throughout the area (Fig. 3.32 a). The pattern of π S_{C1} defines almost a complete girdle whose axis plunges towards E, indicating the effect of subsequent F_{C2} folding. However, S_{C1} foliation trends almost E-W regionally and dips both towards N and S at moderate to steep angles (Fig. 3.32 b). The L_{C1} lineation is mostly found on the main foliation S_{Cm} and plunges coaxially to F_{C1} folds towards east or west at gentle angles (Figs. 3.32 c, d). On the macroscopic scale, the L_{C1} lineation is considerably homogeneous in its amount and trends, which is almost parallel to the strike of the main foliation S_{Cm}, unlike the leneation pattern in the HHC and interior parts of the Jutogh Nappe (Table 3.4).

<u>Main foliation in the Chor granitoid</u>: The main foliation S_{Cm} in the Jutogh metamorphics and the Chor granitoid is subparallel to each other. The Chor granitoid body has developed a very prominent mylonitic foliation due to intense shearing along the contact with the Jutogh metamorphics. This foliation

Figure 3.32 a : Structural map of Chor Mountain region showing main foliation S_m and lineation L_{C1} in the Jutogh metamorphics.

Figure 3.32 b : Synoptic π - diagram of main foliation S_{CM}/S_{C1} from the Chor Mountain.

Figure 3.32 c : Synoptic stereoplot of mineral lineation L_{C1} from the Jutogh metamorphics around Nauhra and Shamra area.

Figure 3.32 d : Scattered plot of a few F_{C1} folds from Chor Mountain area.

Figure 3.32 e : Scattered plot of a few poles to crenulation foliation S_{C3} from Chor area.

Figure 3.32 f : Crenulation fold F_{C3} from the Chor Mountains showing a high scatter due to later folding.

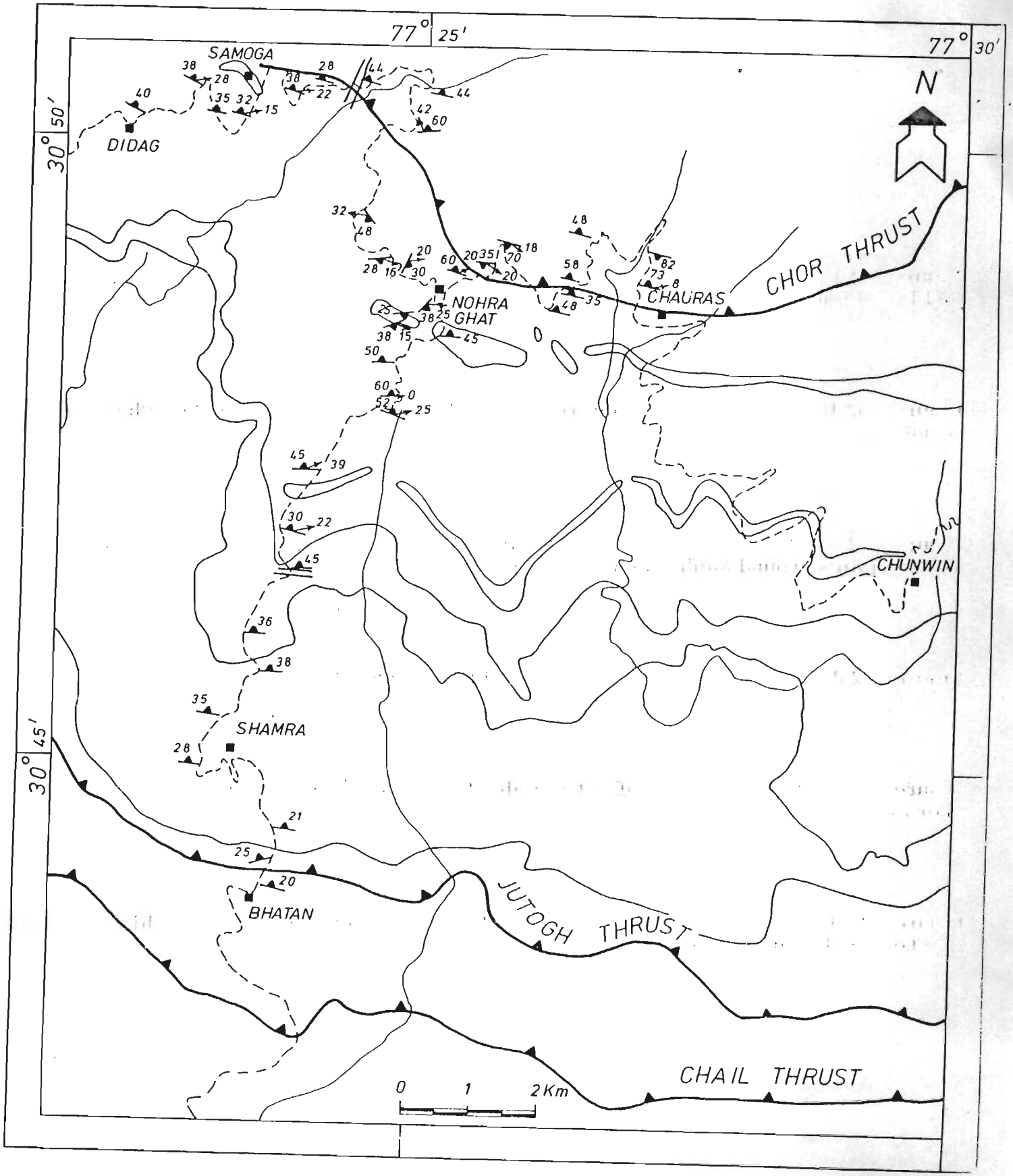
77° 25'
77° 30'
30° 50'
30° 45'
N
SAMOGA
DIDAG
NOHRA GHAT
CHAURAS
CHOR THRUST
CHUNWIN
SHAMRA
BHATAN
JUTOGH THRUST
CHAIL THRUST
0 1 2Km

a

Table 3.4 : Deformational history of the HHC in the root zone and the Jutogh Nappe in the frontal part, Himachal Pradesh, India.

DEFORMATIONAL PHASES	AREA	
	SUTLEJ VALLEY (Singh, 1987)	SHIMLA-CHOR AREA (Naha and Ray, 1972; & Kishor and Kanwar, 1984)
D_1	F_1 : tight to isoclinal with longdrawn limbs, rare with tightly appressed narrow hinge. S_1 : parallels the lithological layering of metamorphic/sedimentary origin	ABSENT
D_2	F_2 : developed on S_1 close to isoclinal, reclined, plunging down the dip either NNE/SSW L_2 : mineral/stretching lineation parallels the F_2 developed on S_2 foliation plane or composite S_0, S_1, S_2 plane designated as main foliation Sm S_2 : most prominent planar fabric striking ESE-WNW dipping NNE or SSW	F_1 : reclined to recumbent fold plunging moderatly E or W most prominent L_1 : mineral/stretching lineation mostly E-W horizontal in attitude S_1 : axial plane dipping at high angle nearly vertical most prominent in the area
D_3 — D_{3a}	F_{3a}: isoclinal inclined to recumbent type plunging ESE/WNW at low angle L_{3a}: parallels F_{3a} folds S_{3a}: gentle to moderatly inclined	F_2 : gentle nearly upright nearly horizontal plunging E or W folding feeble to insignificant L_2 : parallels F_2 folds which is coaxial to F_1 S_2 : steep in nature
D_3 — D_{3b}	F_{3b}: crenulation folds plunging ESE/WNW at low angle parallels F_{3a} folds mostly asymmetric with southward vergence L_{3b}: very prominent and parallels the axis of crenulation S_{3b}: steeply dipping axial plane of the F_{3b} fold	F_3 : crenulation folds open and upright folds L_3 : parallels the F_3 folds S_3 : steeply dipping towards SE or ENE

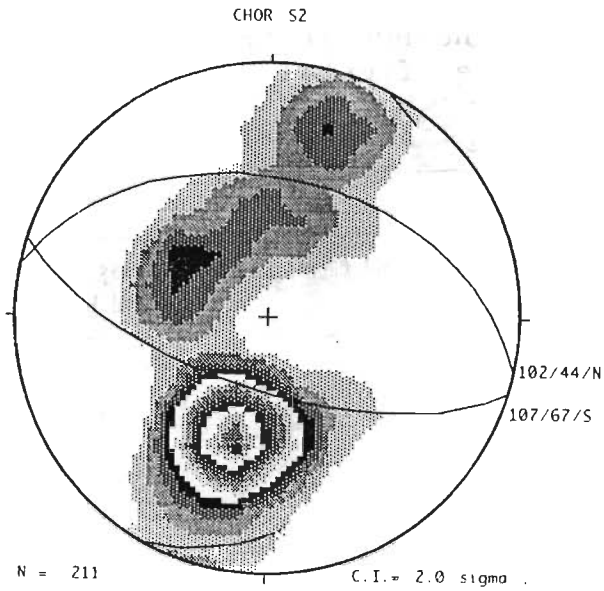
CHOR S2
102/44/N
107/67/S
N = 211
C.I.= 2.0 sigma

b

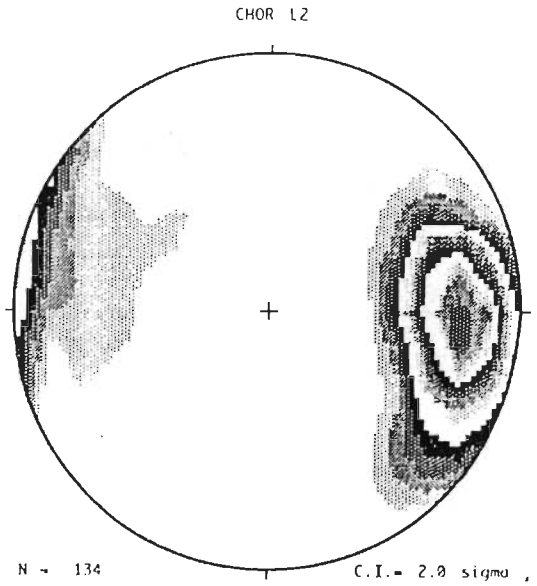
CHOR L2
N = 134
C.I.= 2.0 sigma

c

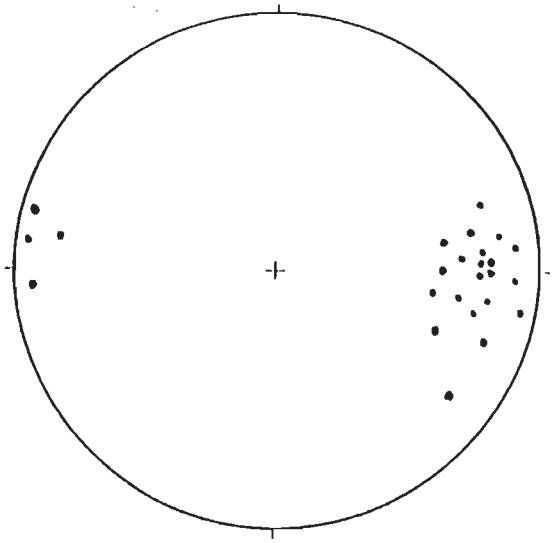

d

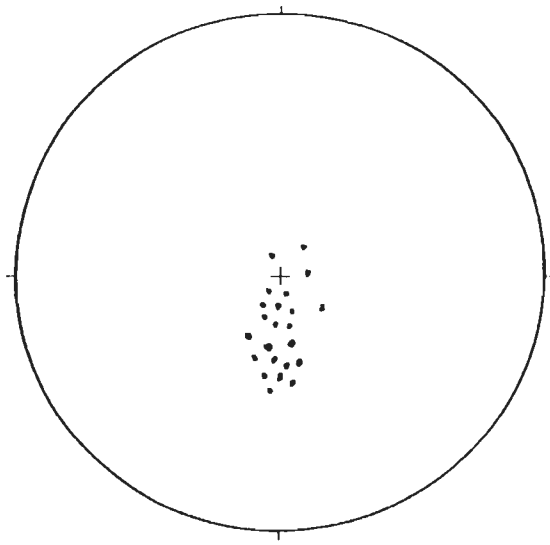

e

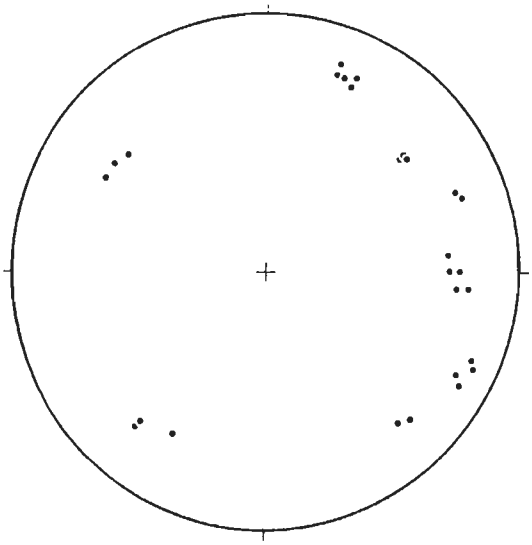

f

Table 3.4 continued

DEFORMATIONAL PHASES	AREA	
	SUTLEJ VALLEY (Singh, 1987)	SHIMLA-CHOR AREA (Naha and Ray, 1972; & Kishor and Kanwar, 1984)
D_4	Thrust faults cutting across S_{3b} Shear bands and shear lenses Quartz filled tension gashes Culmination and depression affecting the D_3 deformation	

is defined by preferred orientation of phyllosilicates and feldspar (Figs. 2.56; 3.31 c). The marginal parts of the granitoid are characterised by general increase in the grain size resulting into the development of porphyritic granite (Fig. 3.31 d). Complete gradation from undeformed coarse granite to well foliated mylonitic augen gneiss to fine grained gneiss has been observed on the outcrop scale (Fig. 3.33 a). In such cases, feldspar megacrysts have undergone gradual elongation and asymmetric rotation (Fig. 3.33 b). Towards the margin of the Jutogh metamorphics, the megacrysts are extremely elongated with grain size reduction (Fig. 3.33 a). S-C shear fabric is developed with asymmetric feldspar augen and their tails indicating a consistent SW-shear vergence (Figs. 3.33 a, b). These megacrysts also define a prominent stretching lineation parallelling the main L_{C1} lineation in the Jutogh metamorphics.

b. Second deformational phase (D_{C2}): This deformational phase is not very prominent in the area, but a few occurences are notable and provide clues to the structural relationship with the D_{C1} phase. In the southern portion of the Chor granitoid, signatures of the second deformation D_{C2} have not been observed, whereas these are present at a few localities in the Jutogh metamorphics. D_{C2} deformational phase is characterised by the isoclinal folding of the earlier axial plane foliation S_{C1}, forming a coaxial F_{C2} fold with F_{C1}. The angle between the limbs of F_{C2} folds ranges between less than 10° to about 40°. These folds are isoclinal to tight, Class 1C-type (cf. Ramsay, 1967), nearly upright to inclined with gentle, almost horizontal E or W plunging hinges (Fig. 3.33 c). The related L_{C2} mineral lineation is also not very widespread in the area, but it can well be seen in the hinge zone of F_{C2}. Otherwise, all the linear structure of D_{C1} and D_{C2} deformational phase are parallel to each other. The overprinting of F_{C2} fold on F_{C1} give rise to type-3, hook-shaped interference pattern (Fig. 3.31 b). The F_{C2} folds have also been affected by plastic flow within the marble band along with F_{C1} (Fig. 3.31 b). The associated S_{C2} axial plane foliation of the F_{C2} fold is steeper in nature.

c. Third deformational phase (D_3): The third deformational phase is prominent in the schistose rock of the Jutogh metapelites and metapsammites and nearly absent in mylonitic rock and granitoid body. The crenulation fold F_{C3} are seen in the metapelite and metapsammite alterations with variable interlimb angles and wavelength-amplitude relation depending upon the lithological contrast (Fig. 3.33 d). The F_{C3} folds are mostly asymmetric, upright in character and have southwestward-vergence (cf. Butler, 1982). Synoptic diagram of poles of axial plane foliation S_{C3} of crenulation fold shows that S_{C3} foliation strikes nearly E-W with moderate dips towards N (Fig. 3.32 e). F_{C3} fold axes in southern portion of the Chor Mountain clearly depict a spread in plunge, orientation and amount, probably due to late folding (Fig. 3.32 f).

3.3.2 Anni-Dalash region

The Jutogh Nappe of the Anni-Dalash area is thrust over the Shali Formation and contain Cambro-Ordovician granitoids, which represent the off-shoots of the Mandi-Karsog pluton (545 ± 12 Ma) of late D_1 deformation (Fig. 2.1). These gneissose granite bodies have caused contact metamorphism during Early Paleozoic on low grade Jutogh metamorphics (Gururajan and Virdi, 1984). Subsequently, these have been remobilised and deformed during the Himalayan Orogeny (Woldai, 1987; Wolde, 1987).

The Jutogh Nappe in this part of the Sutlej Valley represents the souhwestern limb of a large-scale synform and reveals four distinct deformational phases.

a. First deformational phase (D_1): The first deformational structures are rarely encountered in the area. The F_1 folds have 'flame-type', irregular hinges and long-drawn stretched limbs, as has been noticed in the HHC. These folds are

Figure 3.33 a : Complete gradation from undeformed coarse Chor granitoid to well foliated mylonitic augen gneiss and fine-grained gneiss with S-C shear fabric development having SW-shear vergence about 4 km NNW of Nauhra.

Figure 3.33 b : Gradual elongation and asymmetric rotation of feldspar megacryts in mylonitised augen gneiss near margin of the Chor granitoid with the Jutogh metamorphics. Loc. : Raundar Ka Khata nala.

Figure 3.33 c : Isoclinal, recumbent F_{C2} folds of class 1C-type in quartzite of the Jutogh Group about 1 km towards Bandal village from Nauhra.

Figure 3.33 d : Crenulation folds F_{C3} with variable interlimb angles and wavelength-amplitude relation depending upon lithological contrast of metapelite and metapsammite alterations. Loc. : About 6 km south along the Nauhra-Shamra road.

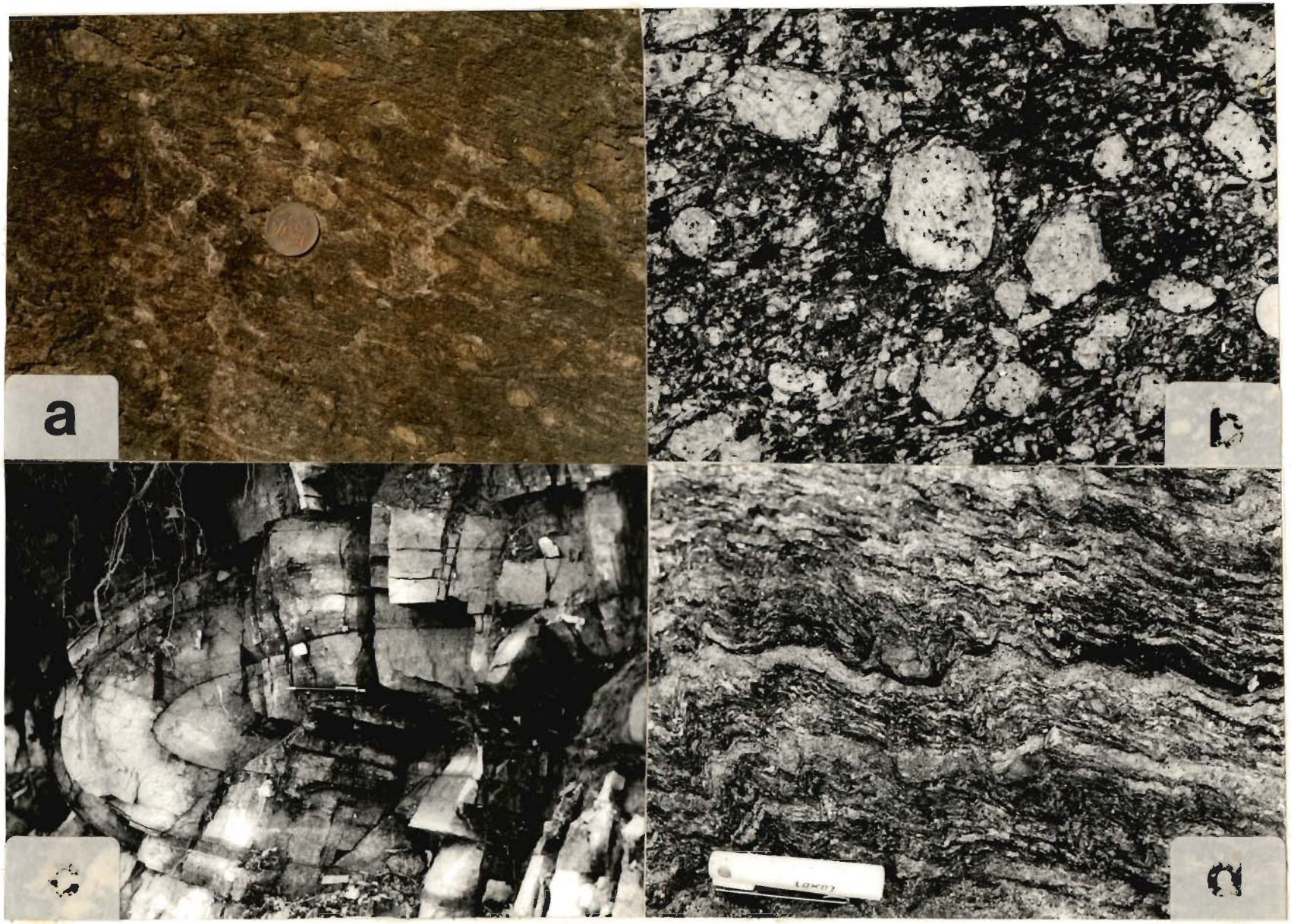

FIG. 3 .33

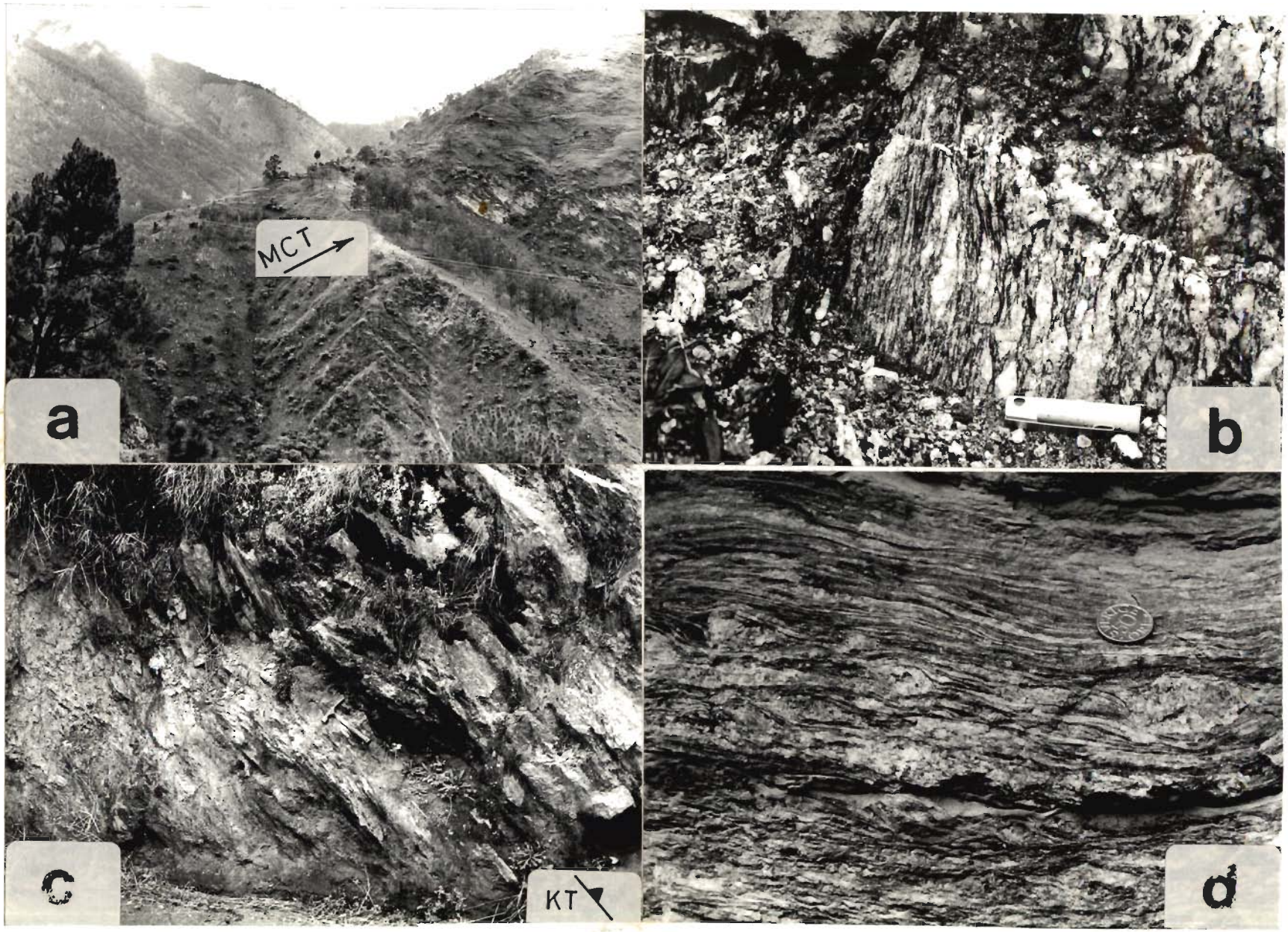

FIG. 3 .34

Figure 3.34 a : Panoramic view of the Main Cental Thrust (MCT) between low grade metamorphosed orthoquartzite on footwall and hangingwall pelitic schist with gneissos bodies. View from Jakhri towards right bank of the Sutlej valley.

Figure 3.34 b : Foliation within the porphyroclastic augen gneiss marked by stretched quartz and feldspar augen, which appear to be mylonitised near Chaura village. Note development of elongated megacryst and banded gneiss on left side of photograph due to ductile shearing.

Figure 3.34 c : Intensely mylonitised augen gneiss of the Bajura/Kulu Nappe with elongated megacryts and grain size reduction with development of blasto-mylonite and ulteramylonite bands near Luhri village. Note development of S-C shear fabric and asymmetrical feldspar augen having vergence towards left.

Figure 3.34 d : Mylonitised augen gneiss of the Bajura/Kulu Nappe overlying the carbonaceous phyllite of the Rampur Group along the Kulu Thrust (see hammer), marked by brittle frible rock powder. Loc. : Kali miti Ka Nala near Chareota on the national highway 22.

observed on quartz veins and interbanded lithologies, such as quartzite and mica schist. These early F_1 folds are appressed, tight to isoclinal and of small wavelength, with obscured or obliterated hinges due to shearing along short limbs. The axial plane foliation S_1 of the F_1 fold is parallel or subparallel to the metamorphic/lithological layering (S_0). At some places, the earliest fabric has angular relationship with S_1 foliation. Despite the presence of the F_1 folds, the L_1 lineation is less common due to subsequent deformational event.

b. Second deformational phase (D_2): The second deformation D_2 is most prominent and produces F_2 folds, its axial plane foliation S_2 and coaxial mineral/stretching lineation L_2. The F_2 folds are mostly reclined-type and less often inclined or recumbent-type. F_2 folds are characterised by long limbs and rounded hinges with interlimb angles varying between less than 10 to 35°. F_2 folds plunge consistently towards NE at low angles and are developed in schist, granite gneiss, pegmetite and quartz veins all over the area. However, these locally deflect from this particular trend. The axial plane foliation S_2 of these folds is marked mainly by preferred oriented quartz and phyllosilicates. In a few instances, biotite-rich layers are often crenulated in hinge zones, where pelites are interbanded with semipelitic or psammmitic bands. This foliation is also designated as the main foliation (Sm) due to subparalellism of both S_1 and S_2 planar surfaces. The Sm foliation generally trends WNW to NW and to a lesser extent towards NE. The consistent WNW to NW trend of the main foliation Sm indicates that the rocks form the limb of a larger fold (Woldai, 1987), while later cross-folds have caused some minor deflections from the general persistent WNW and NW trend.

The L_2 mineral/stretching lineation is coaxial to the F_2 folds and, at places, also represented by mullions, quartz rods and boudins. L_2 lineation plunges consistently NNE to NE at moderate angles, even in the granitoids (Wolde, 1987). In a few instances, this lineation also plunges SW, possibly due to later F_3

folds. The type and nature of the minerals defining the mineral/stretching lineation depends upon the composition of the lithological units. The L_2 lineation maintains consistent orientation and parallelism in all the lithological units, including the mylonite augen gneiss of the Bajura/Kulu Nappe (Faiya, 1987). It indicates that the development of L_2 lineation is unrelated to the thrusting and have possibly developed in ductile shear strain regime during the D_2 deformational event.

c. Third deformational phase (D_3): On the basis of mutual structural relationships, D_3 phase has been classified into the early D_{3a} and late D_{3b} deformation phases.

D_{3a} deformation phase incorporates F_{3a} folds having recumbent to gently inclined geometry with subhorizontal to inclined axial surfaces. These are developed on earlier foliation $S_0/S_1/S_2$. The axial plane foliation S_{3a} of these folds is marked by preferred alignment of quartz and mica at low to moderate angle to the curved S_2 foliation. F_{3a} folds are also characterised by less prominent nearly NW-plunging coaxial L_{3a} lineation of mica at moderate to high angles to the main L_2 lineation.

Late D_{3b} deformational event has produced F_{3b} folds, which are mostly close to tight, moderately to steeply inclined and crenulation-type. Their hinges form a prominent lineation L_{3b}. These folds are coaxial to F_{3a} folds and produce type-3 interference pattern. These folds plunge gently to moderately towards NW or SE. F_{3b} folds have variable interlimb angles and wavelength-amplitude relationship and are mostly asymmetric in character with southward vergence geometry. The crenulation foliation S_{3b}, associated with F_{3b} folds, is well developed in pelitic schist and less commonly in quartz-mica schist. It is marked by faint alignment of mica flakes. The foliation mostly trends NW having moderate dips towards NE.

d. Fourth deformational phase (D_4): In the last deformation phase, axial planes S_4 of associated kink folds F_4 are developed in garnetiferous mica schist at a few places. S_4 foliations have trend N to NE with moderate to steep dips. A series of sporadically developed brittle and brittle-ductile shear zones have also been observed to offset the continuity of earlier foliation.

3.4 MAJOR TECTONIC BOUNDARIES

The area along the Sutlej valley and Chor Mountain contains the following major tectonic boundaries:

(i) Main Central Thrust (MCT),

(ii) Kulu Thrust (KT),

(iii) Chaura thrust,

(iv) Jutogh Thrust (JT)

(v) Chor thrust

3.4.1 Main Central Thrust (MCT)

The Main Central Thrust (MCT) lies between the Lesser Himalayan Proterozoic foreland Kulu-Rampur Window and the Higher Himalayan Crystalline (HHC) along the Sutlej Valley. The HHC is thrust southwestward along the MCT and now rests over the quartzite-volcanic sequence, where the metavolcanics yields a Sm-Nd 2509 ± 94 Ma whole rock age (Bhat and Le Fort, 1991). The HHC consists of metapelites and metapsammites with granite and gneiss of about 2000 Ma and 1800 Ma (see Chapter 6). The HHC wraps around the Manikaran Quartzite of the Rampur Window towards southeast and merges with the Kulu Thrust near Taklech village along the Nogli Gad (Fig. 2.2). Here, the quartzite-volcanic sequence directly

comes in contact with the mylonitised augen gneiss of the Bajura/Kulu Nappe, and the latter is overlain by the HHC.

Along the Sutlej Valley, the MCT is defined as a thick zone on left bank of the Sutlej river at Jakhri along northeastern margin of the Kulu-Rampur window along the Barauni Gad and is tracable for a considerable distance towards Gaura village. From the Nogli Gad, it is traceable near Deothi village along the Bati-Gandri Khad. The MCT swings near Bahli village and extends towards Kasha-Pat villages and then loops back to the south of Taklech. It either merges with the Kulu Thrust or overlaps this thrust (Fig. 2.2). On the right bank of the Sutlej River, the contact is sharp between low grade metamorphosed orthoquartzite and pelitic schist having gneissic bodies (Fig. 3.34 a). The MCT parallels the main folation, both in the window zone and the overlying metamorphic pile.

Heim and Gansser (1939) designated the boundary between the Lesser Himalayan sedimentary zone (Berinag quartzite and/or Calc Zone of Tejam) and low to medium grade metamorphics of the Higher Himalaya in Kumaon as the Main Central Thrust (MCT). In Nepal Himalaya, the French workers placed this tectonic boundary between medium grade and high grade metamorphic rocks (Bordet, 1973; Le Fort, 1975). Valdiya (1980) did not follow this nomenclature of the MCT in Kumaon, but redesignated it as the Munsiari Thrust. The latter delimits the base of the Munsiari unit of medium grade metamorphics and deformed granite gneiss. Valdiya (1980) has also delineated another tectonic boundary between Munsiari Formation and high grade Vaikrita Group and designated it as the Vaikrita Thrust on the basis of an abrupt break in the metamorphic grade.

3.4.2 Chaura Thrust

It lies between the Jeori Formation and Wangtu granite gneiss of the HHC along the Sutlej Valley. This tectonic contact has been worked out on the basis of strain analysis on feldspar augen from porphyroclastic granite gneiss (section 3.2.4). The conatct between the metasediments of the Jeori Formation and porphyroclastic granite gneiss is concealed below the soil cover on the road section, but is exposed at higher elevation. The contact between these two units is sharp. Foliation within the porphyroclastic gneiss becomes very intense towards the contact and is marked by stretched quartz and feldspar augen, which appear to be mylonitised (Fig. 3.34 b). The strain analysis shows that the contact has developed during ductile shear regime of main deformational event.

The Chaura thrust separates two lithotectonic unit of HHC with distinct uplift rates, as has been worked out on the basis of Fission Track Dating on apatite and zircons from these units (Kumar, 1992).

3.4.3 Kulu Thrust

This tectonic boundary is present in between the Lesser Himalayan sedimentary foreland windows and the Bajura/Kulu Nappe of the Proterozoic mylonitised augen gneiss. The thrust is basal to the Bajura/Kulu Nappe and is a subsidiary thrust to the MCT.

In the Nirath-Baragaon area, the Kulu Thrust is distinct by the presence of highly mylonitised and lineated 800 m thick dismembered augen gneiss of the Bajura/Kulu Nappe over carbonaceous phyllite/slate of the window rock. Due to intense deformation, mylonitised augen gneiss is characterised by elongated megacyrysts and grain size reduction with development of blastomylonite and

ultramylonite bands (Fig. 3.34 c). Numerous discrete ductile shear zones reveal discordant relationships to the main mylonitic foliation within the nappe unit, wherein coarse augen-rich bands are progressively reduced in size from the shear zone walls towards the centre of the shear zone (Fig. 3.34 d). This reflects the overall geometry of the nappe.

Along the Kulu Thrust near Luhri footwall encompasses carbonaceous phyllite/slate and interbedded thin black massive quartzite of the Rampur Window, and the hangingwall of the overlying mylonitised augen gneiss of the Bajura/Kulu Nappe. In the window zone, dolomitic limestone is deformed and crushed during thrust movements. The trend of foliations in window rocks and overthrust mylonitised augen gneiss is mostly concordant. However, this structural concordance is lost towards Luhri, where intense shearing and rotation in mylonite have resulted in diverse attitude of structures. This is evident from a series of thrust slabs stacked on top of each other thus forming duplex structure along the Luhri-Dalash road (Fig. 3.35 a).

In the Cheorata window, the thrust lies between carbonaceous phyllite/slate and interbedded quartzite and mylonitised augen gneiss along the Kali Mitti Nala (Fig. 3.34 c). The contact is very sharp between mylonisied augen gneiss and friable carbonaceous quartzite with development of fault gauge along planes striking N 115° and dipping 50° S. Here, main foliation in mylonitised augen gneiss strikes N 142° and dips at 45° S.

In the main Rampur Window, the Bajura/Kulu Nappe pinches out south of Taklech, and at the same time, the Kulu Thrust is concealed beneath the MCT/JT (Fig. 2.2). On the southern slope of Nogli Gad the Kulu Thrust lies between carbonaceous slate/phyllite and mylonitised augen gneiss. This contact can be traced from a distance on the basis of distinct sparse vegetation pattern in cabonaceous phyllite.

Figure 3.35 a : Thrust slab, stacked on top of each other forming duplex structure within the Bajura/Kulu nappe along the Luhri- Daish road. Loc. : Near Luhri. For scale see man standing on road.

Figure 3.35 b : Localised quartz fibre growth in down-the-dip direction and chlorite-sericite lineation in a 500 m wide zone within the Chail Nappe. Loc. : Near Bhatan on Nauhra-Shamra road section.

Figure 3.35 c : Panoramic view of the Jutogh thrust oblique to the main foliation within the Nirath-Baragaon mylonite gneiss demarcating footwall , with the Jutogh Group metamorphics. Loc. : About 500 m from the Baragaon village towards Basantpur.

Figure 3.35 d : Sharply demarcated and imbricated Manikaran Quartzite (Q) with the Rampur Volcanic (V) within the Kulu-Rampur Window. Viewed from the national highway 22 about 3 km from Rampur town. Also note a normal fault displacing contact of quartzite and volcanics for scale note men working for the road construction.

FIG. 3.35

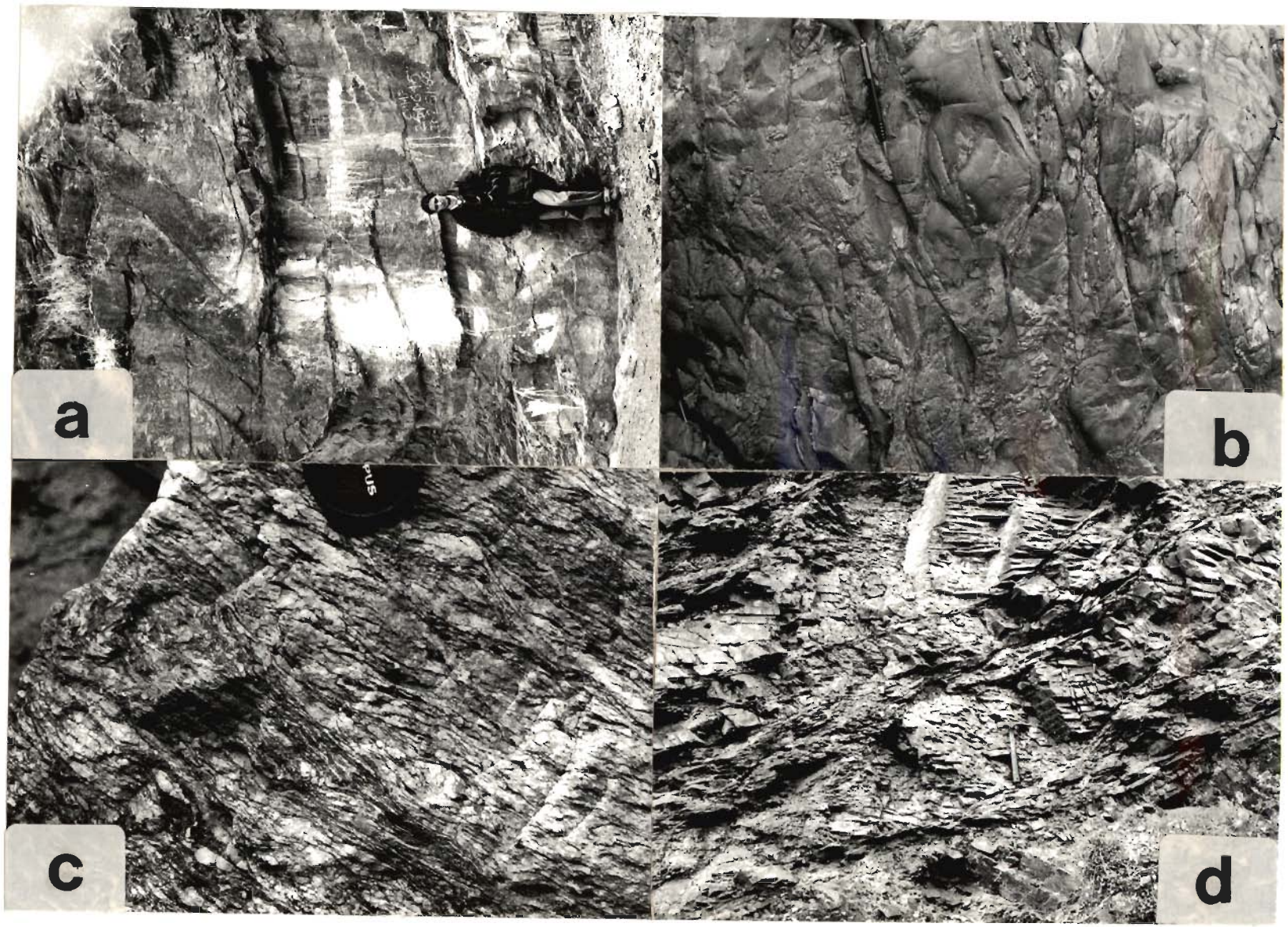

FIG. 3 .36

Figure 3.36 a : E-W trending recumbent, isoclinal tightly folded quartzite and overlying carbonaceous having S-vergence beneath the Bajura/Kulu Nappe Loc. : Kali Miti, Ka Nala near Chareota on the national highway 22.

Figure 3.36 b : Conglomerate containing large rounded quartzite boulders embedded in arenaceous matrix, having elongated pebbles with down-the-dip lineation. Pitted boundaries enhanced elongation of grains due to pressure solution near Chareota village.

Figure 3.36 c : Small-scale shear zone as a penetrative foliation due to intense ductile shearing within the Bajura/Kulu Nappe about 5 km downstream from Nirath. Note development of extensional foliation showing displacement towards right-hand side in the normal sense.

Figure 3.36 d : Numerous discrete brittle-ductile to brittle duplex thrust within the Bajura/Kulu Nappe at Kali Miti Ka Nala near Chareota village on the national highway 22.

Earlier, this thrust was designated as the Chail Thrust (Virdi, 1971, 1976, 1980; Gururajan and Virdi, 1984; Gururajan, 1985). Frank *et al.* (1977) introduced the term "Bajura Nappe" for a typical lithological association of highly mylonitised augen gneiss, having typical acid volcanic affinity for a basal thrust sheet to the "Crystalline Nappe" in the Kulu area, but they did not name it. Later, Bhargava *et al.* (1991) termed it as the Kulu Thrust Sheet and the basal contact as the Kulu Thrust after considering this unit as a part of much extensive nappe.

On the regional scale, it appears the Kulu Thrust has transgressed over the Chail Thrust of the frontal part of the Jutogh Nappe (Fig. 1.2).

3.4.4 Jutogh Thrust (JT)

Defining the base of the frontal Jutogh Nappe in Simla Hill and Chor Mountain regions, the Jutogh Thrust seperates the Lesser Himalayan metamorphic belt from the Chail Group metamorphics. However, the Jutogh Nappe is thrust over the Bajura/Kulu Nappe along this thrust in the interior.

The Jutogh Thrust can be located between carbonaceous phyllite of the Jutogh Group and chlorite-sericite-bearing quartzite of the Chail Formation near Pidiya Ghat along the Nauhra-Shamra section (Fig. 2.3). The emplacement of the Jutogh Nappe over the Chails has probably caused localised quartz fibre growth in down-the-dip direction and chlorite-sericite lineation in a 500 m wide zone within the footwall (Fig. 3.35 b). Within fine-grained quartzite of the Chail Formation, kinks with gently south-dipping axial planes are seen in the thrust zone, which can be interpreted as a gravity collapse structure. Within the Chail Formation, late-stage brittle fractures are also developed and post-date the kink development. The presence of discrete shears, fault gouge

and brittle overthrusts within the Jutogh Thrust zone reveals its shallow-level structural development in a high strain regime.

Between Nirath-Luhri-Baragaon, the Jutogh Thrust demarcates the contact between the Jutogh Group metamorphics and augen mylonite of the Bajura/Kulu Nappe (Fig. 3.35 c). Graphitic schist nearly always demarcate the Jutogh Thrust and serves as a key horizon for distinguishing the two formations from each other. The S- and C-shear fabric is very prominently developed within the Bajura/Kulu Nappe. The angles between S- and C- fabric planes gradually decrease from 30° to less than 10° towards the Jutogh Thrust. Approximately 2 km NW from Baragaon on the Kingal-Basantpur road, the Jutogh Thrust is exposed on the road with about 50 m strike-section (Fig. 3.35 c). Here, NE-trending contact between mylonite augen gneiss and dark grey biotite schist approximately dips 20° towards NW. One can observe this contact oblique to the trend of main foliation within these sequences, indicating gradual truncation of the Bajura/Kulu subnappe (Fig. 3.35 c). The Jutogh Thrust is also very sharply exposed along the Luhri-Dalash road , where it is characterised by almost identical oblique relationships.

3.4.5 Chor thrust

The Chor granitoid body reveals localised development of mylonite containing a very prominent mylonitic foliation due to intense ductile shearing along its contact with the Jutogh metamorphics (Fig. 3.33 a). The mylonitic foliation is defined by preferred orientation of phyllosilicates and feldspar (Fig. 3.31 c). This contact has been locally termed as the Chor thrust. The mylonitised augen gneissose granite is characterised by many shear indicators e.g. S-C shear fabric, asymmetrical augen and presssure shadows having top-to-southwest vergence on the southern side of the Chor Mountain (Fig. 3.33

a). It is apparent that the Chor granitoid has initially intruded the Jutogh metamorphics and subsequently sheared during the Himalayan Orogeny.

3.5 LARGE-SCALE STRUCTURES

3.5.1 Lesser Himalayan foreland window zone

The Lesser Himalayan para-autochthonous Proterozoic foreland sequence is exposed in numerous windows due to the deep erosion of the overlying metamorphic nappes. Along the Sutlej river bed, the Kulu-Rampur and Shali Windows are characterised by low grade metamorphosed sedimentary rocks having metavolcanic intercalations.

The **Kulu-Rampur Window** occurrs as a doubly plunging antiform with a closure towards SE. The existence of a tectonic 'window' around Rampur in the Sutlej Valley was first indicated by Berthelsen (1951). Chakrabarti (1973, 1976, 1979) is of opinion that the so-called window is open to the southeast of Rampur along the Nogli Gad. Bhargava (1982) remarked that the Manikaran Quartzite extends as a thin narrow band upto Karcham, then sweeps around towards N and NW around the Wangtu gneissic complex. Bhargava (1982) has interpreted the latter as a tectonic inlier within the Kulu-Rampur Window with a distinct 1800-2000 Ma igneous activity. On the contrary, Sharma (1977) mapped the window closure towards ENE of Rampur (also Virdi, 1981). In the present study, it has been observed that the Manikaran Quartzite extends around Kasa and Pat villages beneath the HHC, thus demarcating the closure of the Kulu-Rampur Window. Here, garnetiferous mica schist of the HHC wraps around the window zone rocks.

Imbrication of the Manikaran Quartzite and Rampur Volcanic within the

window has also been noteworthy, which could possibly be due to the presence of ramping within the window zone (Fig. 3.35 d). Traversing from Jakhri downstream from the MCT zone towards Rampur within the window zone, a thick sequence of massive quartzite with a few metavolcanic bands are developed on northern limb of the Kulu-Rampur Window. Further downstream, metavolcanics are imbricated with white massive quartzite near Rampur town, where atleast two tectonic lenses of metavolcanics within the quartzite can be observed (Fig. 3.35 d). It is likely that main antiformal structure of the window is associated with ramping along such many imbricate zones.

The Cheorata Window, lying to the west of the main Kulu- Rampur Window, is characterised by a doubly-plunging, E-W trending open anticline. The mylonitic augen gneiss of the Bajura/Kulu Nappe completely covers the window rocks. Within the window, quartzite and the overlying carbonaceous slate are tightly folded into large-scale E-W trending recumbent isoclinal folds having S-vergence beneath the Bajura/Kulu Nappe (Fig. 3.36 a). Within the window zone, quartzitic conglomerate contains large rounded quartzite boulders, which are embedded in arenaceous matrix. Elongated pebbles define a strong down-the-dip lineation, which plunges steeply towards NE (Fig. 3.36 b). Pressure soloution along boundaries of large boulders caused pitted boundaries and may have enhanced elongation of grains (Fig. 3.36 b). The siltstone are locally graded in character and support the orthoquartzite boulders. Stretching lineation of pyrite nodules is also present in the carbonaceous slate/phyllite and parallels the pebble lineation.

The rocks of the Cheorata Window have been regarded equivalent to the Basantpur Formation of the basal Simla Group (Srikantia and Sharma, 1971). Bhargava *et al.* (1972) used the cobble bed, associated with the dolomitic limestone, for the identification of the Basantpur Formation in the Cheorata Window. The succession of dolomitic limestone, cobble bed, carbonaceous

slate/phyllite and quartzite may also represent a part of the Mandhali Formation, lying near the base of the Jaunsar Group (Srikantia and Bhargava, 1984). Virdi (1976) proposed that the correlation of these rocks with the Rampur Formation is more appropriate than the Simla Group, due to nearest exposure present in the area. According to him, a change in sedimentary facies from carbonates through euxenic to orthoquartzite with basic volcanics is a typical shallow water assemblage.

The Luhri village is flanked by two distinct windows, therefore, they have been designated as the Luhri-I and Luhri-II windows. The Luhri-I window is located about 0.5 km east from the village and exposes carbonaceous phyllite and quartzite beneath the Bajura/Kulu Nappe. The main foliation of the foreland rocks and overlying allochthonous mylonite is parallel with each other. The Luhri-II window is partially bounded by Kulu thrust, which can be traced on the right flank of the Sutlej river and is not observed on the other side of the river. Within the overlying allochthonous nappe, dip of the main foliation varies from 10° to almost vertical near the boundary, while underlying phyllite is gently dipping in the window. This window pinches out in a narrow zone to the west of Luhri and eventually disappear beneath the Bajura/Kulu Nappe. Apart from these small windows, westernmost parts of the area also exposes the extreme eastern margin of the main Shali Window (Fig. 2.2) with outcrops extending along the river courses at the lower elevations. The window-zone rocks are highly crushed and fractured due to local cataclastism.

3.5.2 Bajura/Kulu Nappe

The Nirath-Luhri-Baragaon section along the Sutlej Valley, comprises a 800 m-thick intermittently exposed, dismembered and highly mylonitic augen gneiss. The nappe is bounded by the Kulu Thrust at its base and the Jutogh Thrust at

its top. In the Parvati valley in western Himachal Pradesh, this nappe is traced from west to Pechha, north of Bhuntar to Gangyasi. To the east of Beas river, this gneissic band can be traced from north of Khokhan village in the north to south of Patogi in the south and again from east of Aut to Baragaon in Sutlej Valley (Sharma, 1977), and further eastward towards Luhri, Nirath to Taklech in the northeast along the Nogli Gad.

Frank *et al.* (1977) coined the term Bajura Nappe for a thin tectonic unit in Kulu area for calc-schist, muscovite schist and microcline augen gneiss, which has been considered equivalant to the Chail Nappe of Fuchs (1967). Sharma (1977) opined the main mylonitised augen gneiss unit of this nappe as the Garh member of the Kulu Formation. It consist of quartzose, banded and streaky gneiss with augen structure. Quartz and feldspar augen are wrapped around by biotite. He described its contact with the underlying Khamrade member (carbonaceous and graphitic slate/phyllite and schist with limestone bands) and overlying Kulu member (garnetiferous biotite and chlorite schist with quartzite and porphyritic granites) as conformable and gradational.

Gururajan (1990) used the term Chail Thrust Zone, in which mylonitic augen gneiss is only a part of the sequence. The lower contact of the Chail Thrust Sheet with autochthonous Shali Formation was demarcated by him as the Chail Thrust. He noted that mylonite augen gneiss grades into phyllite, quartzite and garnet-mica schist.

Bhargava *et al.* (1991) described this unit as the Kulu Thrust Sheet with distinct granitoid activity of 1430 ± 150 Ma age. The upper contact of this thrust sheet with the Jutogh was termed by them as the Jutogh thrust, while the lower contact with autochthonous window rocks was termed as the Kulu Thrust.

Within the Bajura/Kulu Nappe, intense ductile shearing has produced

small-scale shear zones as a penetrative planar fabric, probably at deeper crustal levels (Fig. 3.36 c; Faiya, 1987; Gururajan, 1990).Detailed shear strain analysis of numerous such zones within the augen mylonite of this unit has revealed alternating zones of high and low shear displacements (Faiya, 1987). This pattern is subsequently superposed by numerous discrete brittle-ductile to brittle duplex thrusts within the nappe (Fig. 3.36 d).

3.5.3 Lesser and Higher Himalayan Metamorphic Belt

The metamorphic belt overlies the allochthonous Bajura/Kulu Nappe in the inner parts of the Higher Himalaya and the Chail Nappe in frontal parts of the Lesser Himalaya. The metamorphic belt is mainly characterised by the Higher Himalayan Crystalline (HHC) in the inner part and the Jutogh Nappe (JN), both in the inner as well as frontal parts.

The HHC is a monotonous NE-dipping belt with different pre-Himalayan granitoid intrusions, as is evident from deformational history and also from U-Pb zircon ages of ~2000 Ma and ~1800 Ma (Chapter 6). On the basis of the magmatic activity, it is noteworthy that the HHC is characterised by atleast three distinct zones, containing younger granitoids towards higher structural level. The basal parts are characterised by 2000 Ma magmatic activity, which is seperated from younger zone of 1800 Ma activity by the Chaura thrust. The uppermost belt is of Tertiary age and lies near the contact with the Tethyan Sedimentary Belt.

The Jutogh Nappe occurs into two main outcrops; Chor Mountain in the frontal parts as a tongue in the Lesser Himalaya, with its continuation as a folded succession towards north around Narkanda and Luhri-Dalash area, and

Shimla Hills exposing isolated pear-shaped klippe. The Chail Nappe lies below this nappe in the frontal tongue-like and pear-shape outcrops. However, the Jutogh Nappe is underlain by the Bajura/Kulu Nappe along the Sutlej Valley in the inner parts. There is a marked difference in frontal and inner parts of the Jutogh Nappe with respect to the deformational histories. The earliest deformational event of the frontal part coincides with the second deformational phase of the inner parts. Both the areas are emplaced by the pre-Himalayan granitoids, now occuring as gneissic granitoids of different ages. The contact of the Chor granitoid with the underlying metamorphics appears to be a thrust contact, as is evident from the presence of the mylonite along this contact, having shear indicators revealing top-to-SW displacements.

3.6 SHEAR CRITERIA AND SENSE OF DISPLACEMENT

Numerous shear criteria have recently been used to decipher the sense of displacement in orogenic belts and reveal complex movement histories during various deformational phases (Berthe *et al.*, 1979; Gapais *et al.*, 1987). In the Himalayas, application of these criteria have indicated large-scale southwestward verging movements of the metamorphic nappes, followed by a phase of extensional tectonics (Burg *et al.*, 1984; Burchfield and Royden, 1985; Brunel, 1986; Herren, 1987; Kunding, 1989; Jain *et al.*, 1991; Patel *et al.*, 1993).

Most relevant shear criteria in ductile shear zones, useful in deciphering the sense of movement in rocks are asymmetric structures like augen, pressure shadows, shear bands, S-C- fabrics, tension gashes, asymmetric folds, rotational textural fabric of porphyroblastically growing minerals etc. (Ramsay and Graham, 1970; Berthe, *et al.*, 1979; Simpson and Schmid, 1983; Gapais *et al.*, 1987). In thrust system, sense of shear has been equated with transport direction

(Bouchez and Pecher, 1981). A common attempt is to make use of S- and C- fabric relationships and other shear criteria in determining the general transport direction in the orogenic belts.

The following numerous shear criteria have been analysed in the HHC and Jutogh Nappe and classified as follows for better kinematic analysis:

3.6.1 Ductile non-coaxial deformational structures

These structures show a consistent top-to-southwest overthrust sense of displacement during the most pervasive deformation in the metamorphic belts.

a. S-C composite planar fabric (Berthe *et al.*, 1979; Lister and Snoke, 1984): S-C fabric is charecterised by two sets of planes with foliation planes S- gradually bending sigmoidally due to C- shear planes (Figs. 3.2 c, d; 3.40). The latter are related to displacement discontinuities and/or zones of strain sub-parallel to shear planes during a non-coaxial deformation even within the MCT zone (Fig. 3.37 a). The angular relationship between S- fabric is directly related to rotation of XY-plane of the strain ellipsoid due to shearing (Ramsay, 1980). It is very much evident that angle between S- fabric decreases with increasing strain and predominance of C- shear foliation. The C- shear planes are discrete shear zones during moderate strained domains (Figs. 3.2 c, d), but are continous in high strained zones where S-surfaces also become subparallel to C-shear bands (Figs. 3.2 c; 3.38) and has been widely used as a kinematic indicators for the ductile shear zones.

It has been observed that the S-C composite foliation is a S_2 planar fabric and not oldest S_1 foliation (Fig. 3.37 c). Probably this is the eveidence showing

that the S-C are synchronously developed on S_{C1} fabric. Earlier it was postulated that S- is older to C- planes (Lister and Snoke, 1984). It appears that both S- and C- planes have acted like shear planes (Fig. 3.37 c) in the fabric development due to varying orientation of X and Y axes of the strain ellipsoid.

b. Asymmetrical sheared lenses, augen/megacryst and folds: Both σ-and δ-types of quartz and feldspar augen are very common in granite gneiss and its mylonitised derivatives (Figs. 3.2 d, 3.31 c, 3.33 a, 3.37 d, 3.39 a, b). σ-type augen are characterised by wedge-shaped recrystallised tails on opposite side of a reference plane with the main foliation approximately parallel to the megacryst boundary (Figs. 3.2 d, 3.37 d). In δ-type megacryst, tails lie on opposite side of the plane in augen gneiss and garnetiferous mica schist (Fig. 3.39 a). Further many C- shear planes also bound tightly appressed intrafolial folds within the mylonite having the same SW-vergence geometry (Fig. 3.39 b).

Asymmetrical disposition of quartzo-feldspar augen in the XZ sections typically indicate deformation mechanism in a deep crustal broad ductile shear zone overthrust-type with southward sense of movement of the tectonic pile as has been observed elsewhere in the Himalaya (Bouchez and [illegible]1; Brunel, 1986; Jain and Anand 1988; Jain *et al.*, 1991; Patel *et al.*, 1993).

[illegible] pressure shadows (Simpson and Schmidt, 1983): Rigid megacryst of quartz, feldspar and rotated garnet crystals show sigmoidal inclusion tails parallel to top-to-southwest overthrust sense of shear displacement (Figs. 3.33 a, 3.37 d). These shadows mostly are of quartz and biotite aggregates.

d. Fractured and displaced rigid grains: Feldspar augen in mylonite of the Bajura/Kulu Nappe are traversed by high angle mesoscopic fractures. These reveal small-scale displacement, like card-deck model, and dip mostly 50° to 60° antithetic to the overall sense of movement towards SW (Fig. 3.37 d).

Figure 3.37 a : S-C fabric characterised by two sets of planes within main foliation. S- gradually bending sigmoidally due to C- shear planes within the HHC near the MCT at Jakhri village.

Figure 3.37 b : S-C fabric in quartzite of the Kulu-Rampur Window showing gradual bending of S- plane due to C- shear planes. Loc. : About 5 km downstream from Rampur town.

Figure 3.37 c . Microphotograph of S-C fabric, characterised by two sets of foliation planes. S- planes gradually bend sigmoidally due to C- shear planes within the Jutogh Nappe of Chor Mountain area showing that the S C are synchronously developed and constitute the S_{C1} fabric of the J h metamorphics. CH_5 : Crossed X 72

Figure 3.37 d : S-C shear fabric showing gradual sigmodal bending of S- planes due to C- shears within the Bajura/Kulu Nappe. Also note -type augen characterised by wedge-shaped recrystallised tails on opposite side of a reference plane with the main foliation. Also note σ-type augen, characterised by wedge shaped recrystalised tails on opposite side of a reference plane with the main foliation. Also showing asymmetric pressure shadow and small-scale card-deck model displacement in feldspar megacrysts antithetic to the overall sense of movement towards left. Loc. : About 5 km downstream from Nirath on right bank of the Sutlej river after crossing the wooden bridge.

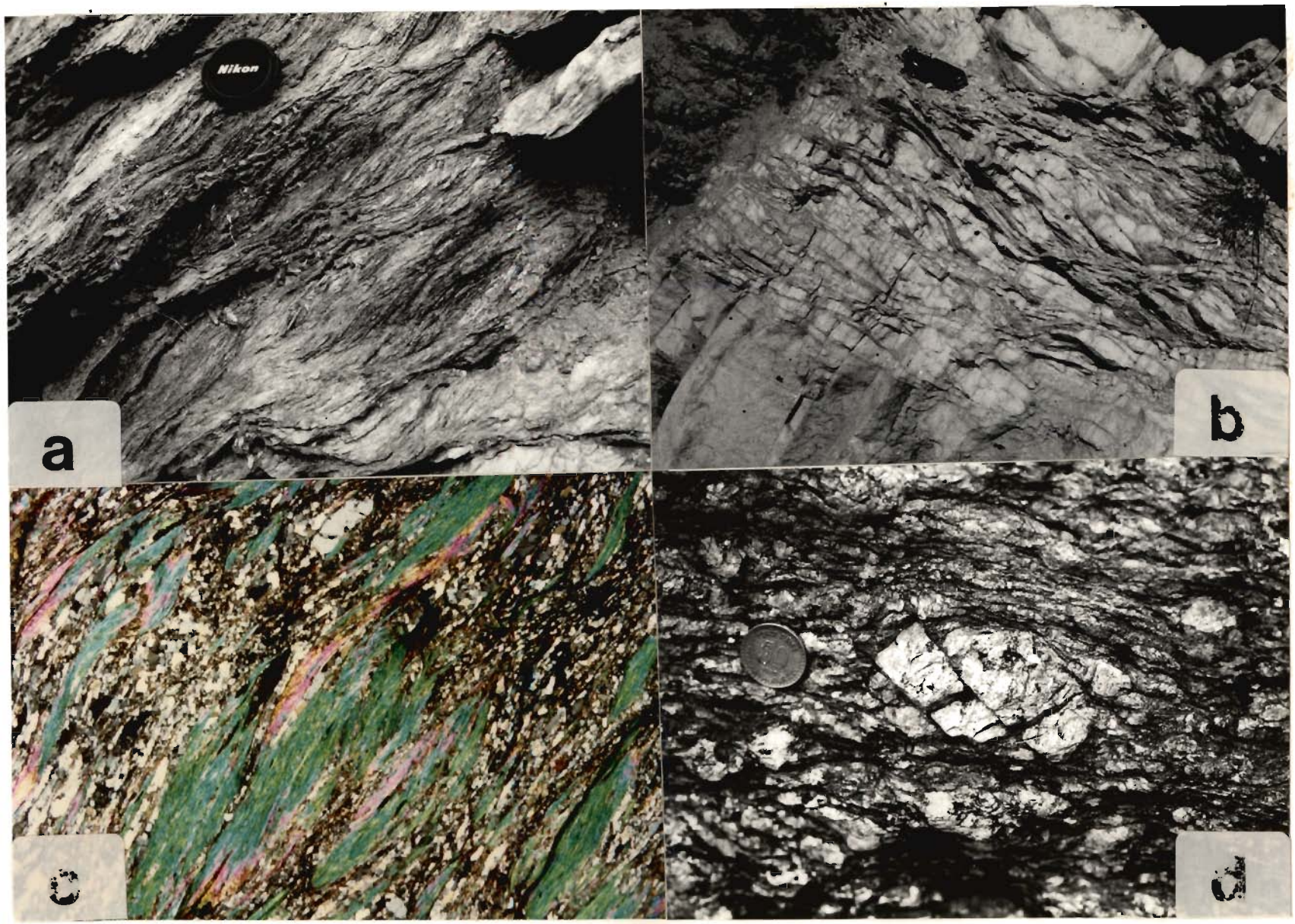

FIG. 3 .37

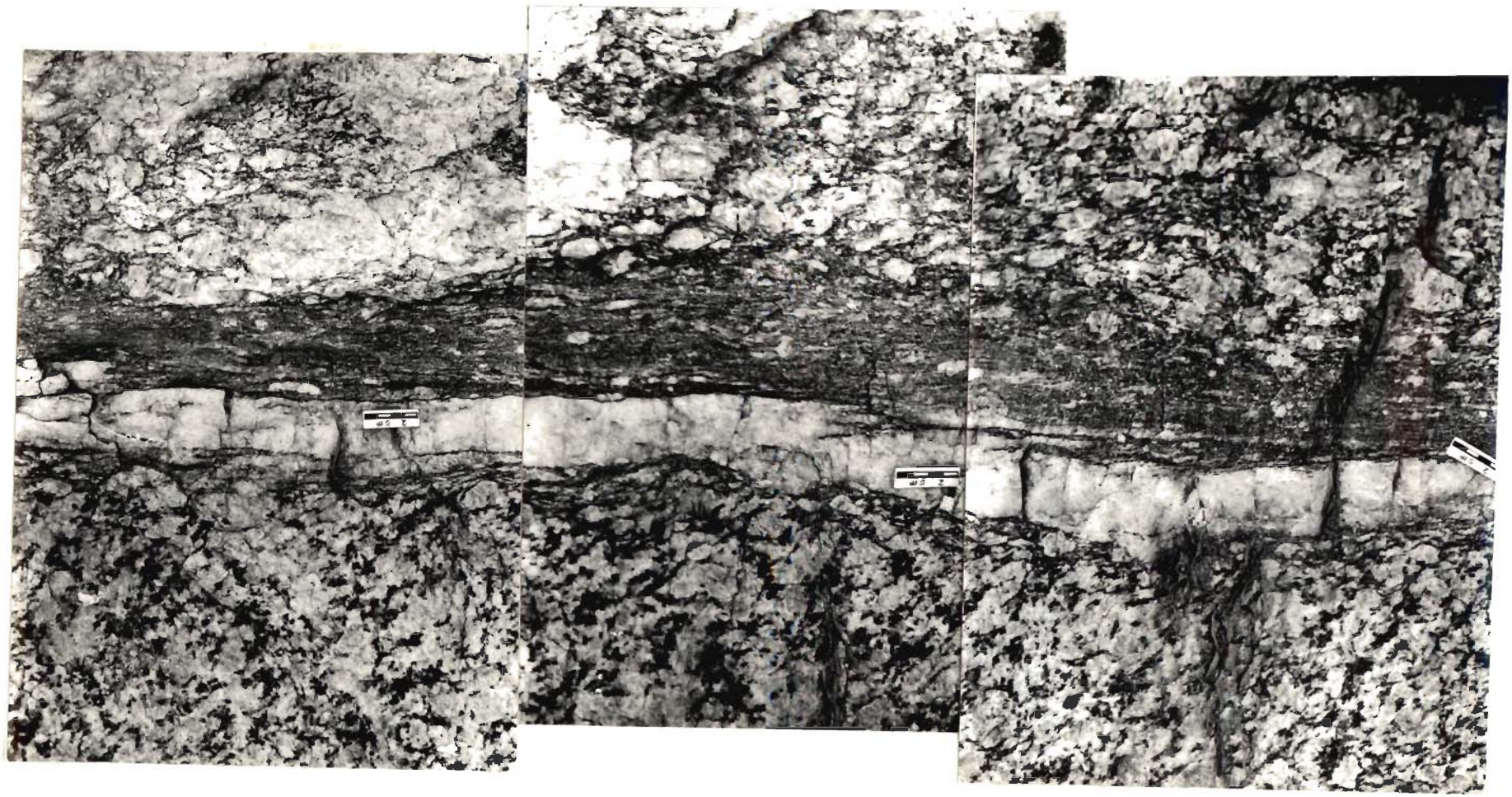

FIG. 3.38

Figure 3.38 : Discrete S-C shear fabric within the Wangtu granitoid body, characterised by development of intense localised fabric within the shear zone from undeformed granitoid. Due to high strain, S-surface become almost subparallel to C-shear fabric. Loc. : Near Wangtu bridge.

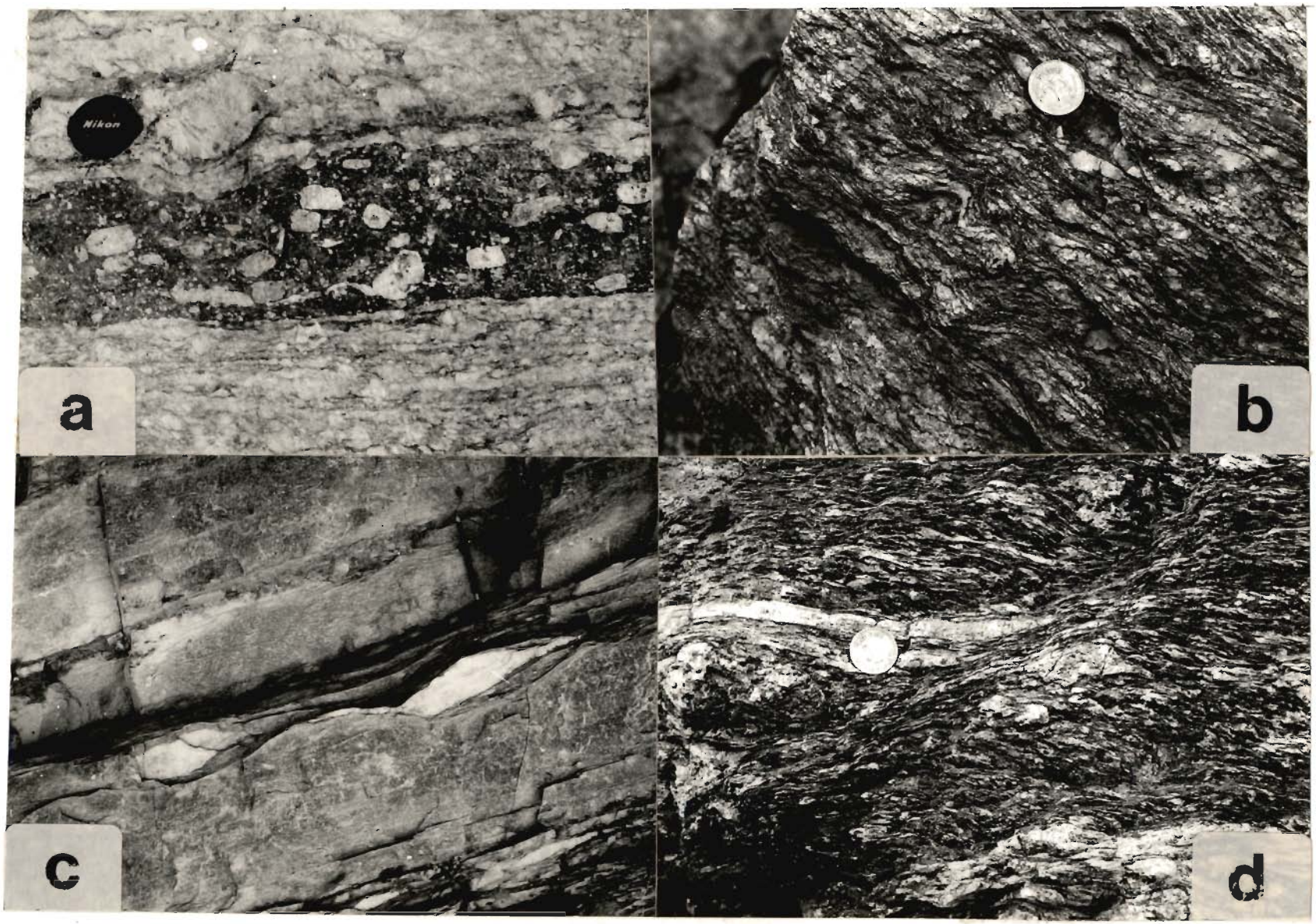

FIG. 3.39

Figure 3.39 a : δ-type megacrysts with tails lying on oppsite side of the plane in augen gneiss nera Nauhra village.

Figure 3.39 b : Late close to tight folds within the Nirath-Baragaon mylonite superposed upon S-C shear fabric. Loc. : Near Nirath vilage on the national highway 22.

Figure 3.39 c : Symmetrical and asymmtrical boudinage on pre-existing main foliation, and characterised by ductile shear trending obliquely in normal fault-sense. Loc. : The Nauhra-Shamra section.

Figure 3.39 d : Single discrete narrow shear band within the mylonite augen gneiss with normal fault-sense of movement showing overall extension within the Chor granitoid near Nauhra village.

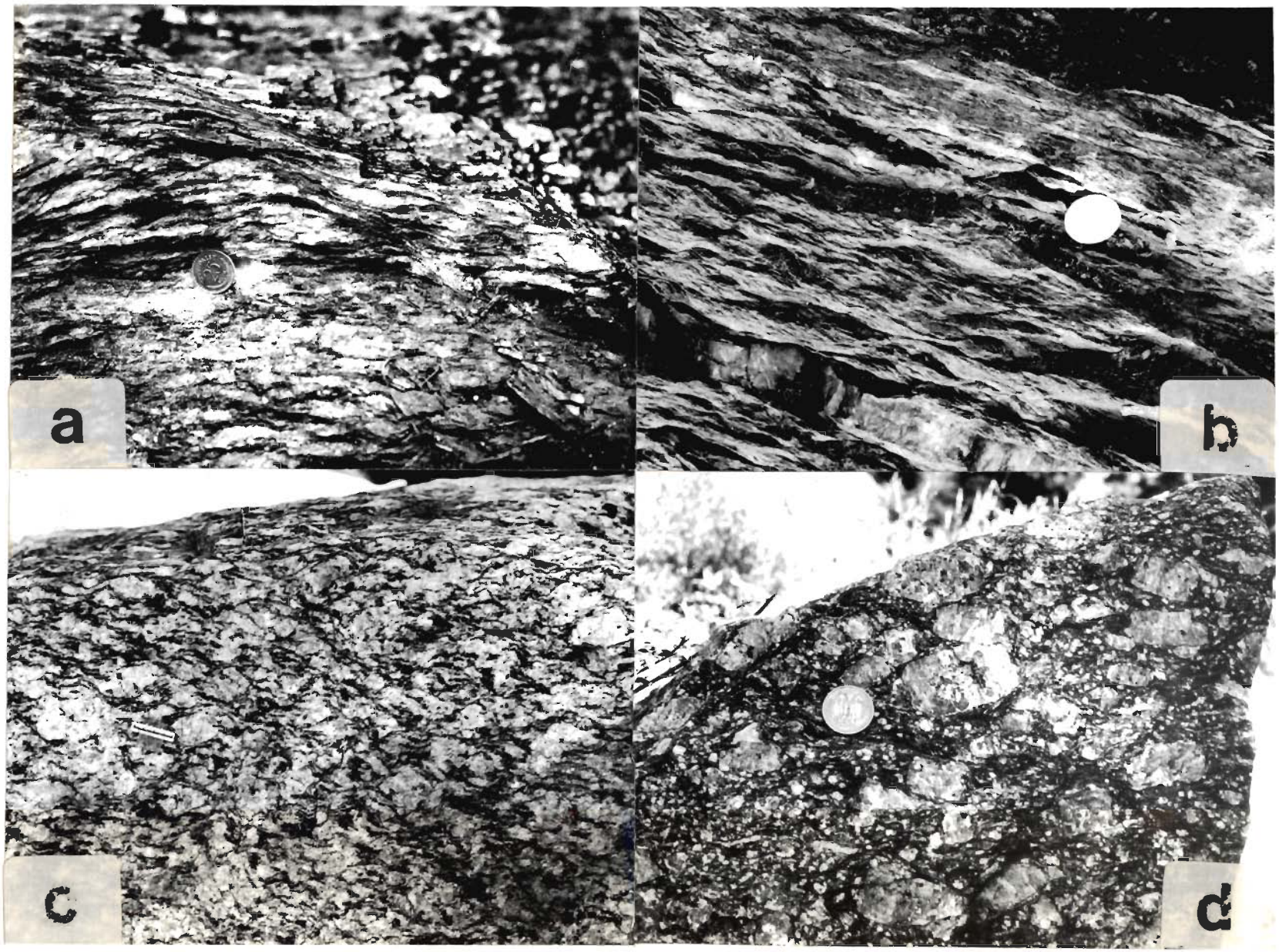

FIG. 3 . 40

Figure 3.40 a : Single discrete narrow shear band within the mylonite augen gneiss with the normal fault sense of movement showing overall extension within the Chor granitoid. Loc. : About 4 km ENE of Nauhra village.

Figure 3.40 b : Conjugate set of extensional crenulation foliation prominetly developed in metapelites and gneiss along the Nauhra-Shamra section within the Jutogh Nappe.

Figure 3.40 c : Conjugate set of extension crenulation foliation (ECC) having opposite sense of normal extension displacement, superposed upon shear criteria ECC_1 plane dipping NE (towards left) at steeper angles are ubiquitously more prominent than the westerly gently dipping ECC_2 plane revealing overall shortening normal to pre-exsisting foliation and extension parallel to it within the Wangtu granitoid. Loc. : Near Wangtu bridge.

Figure 3.40 d : Conjugate set of extension crenulation foliation (ECC) having opposite sense of normal displacement. Planes dipping NE at steeper angles (towards left) are more prominent than the westerly and gently-dipping planes revealing an overall extension parallel to pre-existing foliation. Loc. : Near Chhog village in the Chor Mountain area.

3.6.2 Superposed layer-parallel extensional structures

Ductile non-coaxial deformational phase is superposed by a consistent NE-SW extension across the HHC and the Jutogh Nappe. Most of these structures represent superposed deformation upon orogen-parallel NW/SE trending folds and their axial plane foliation.

a. Symmetrical and asymmetrical boudinage: In the symmetrical boudinage foliation pinchs out towards the cuspate region (Fig. 3.39 c). The asymmtrical boudinage on pre-existing main foliation is characterised by ductile shear, which trends obliquely in normal-fault sense (Fig. 3.39 c).

b. Narrow shear bands (White, 1979 b): Single discrete set is best developed in the HHC gneisses and mylonite gneiss of the Bajura/Kulu Nappe, along which pre-existing main foliation is relative displaced with the normal fault sense with hanging wall moving down and showing the overall extension (Figs. 3.39 d; 3.40 a). Shear bands strike NW-SE and dip steeply towards NE at about 20° to 40°.

c. Extension Crenulation cleavage (ECC - Platt and Visser, 1980): In the HHC and the Jutogh Nappe, single and conjugate sets of cleavage/foliation provide undisputed eveidences of extension parallel to the pre-existing foliation and shortening normal to it. Single set of ECC is prominently developed in metapelites and gneiss (Fig. 3.40 b). Minor changes in their orientation indicate gradual rotation during the overall non-coaxial deformation (Platt and Visser, 1980).

Conjugate set of extension crenulation cleavage with opposite sense of normal extension displacement is one of the most important structure superposed upon earlier described shear criteria in the HHC (Figs. 3.40 c,d). ECC_1

planes dip NE at steeper angle and are ubiquitously more prominent than the westerly, gently-dipping ECC_2 planes. This structure leads to overall shortening normal to pre-existing foliation and extension parallel to it (Figs. 3.39 c, 3.40 c, d).

CHAPTER 4: METAMORPHISM

4.1 INTRODUCTION

The Lesser and Higher Himalayan metamorphic belt commonly exhibit polyphase Barrovian-type metamorphism throughout the orogenic belt (Windley, 1983; Sandhu, 1985; Das, 1987; Pecher, 1989; Staubli, 1989). The Lesser Himalayan Proterozoic Foreland, exposed in Kulu-Rampur Window, and in frontal parts of the Shimla Hills, is made up of quartzite, metavolcanics, carbonaceous phyllite and granite gneiss and has mostly remained within greenschist facies metamophic condition (Pilgrim and West, 1928; Naha and Ray, 1970). The hanging walls of the Main Central Thrust (MCT)and Jutogh Thrust incorporates pelite, psammite, and quartzite sequence are metamorphosed under upper greenschist to almandine-amphibolite facies condition in the Higher Himalayan Crystalline (HHC) and the Jutogh Nappe (Pilgrim and West, 1928; Berthelsen, 1951; Roy and Mukherjee, 1976; Sharama, 1977, Chakrabarti, 1976; Bhargava, 1980, 1982).

To understand the characters of this metamorphism, petrological investigations were carried out along a few cross-sections on the hanging wall side of the Jutogh Thrust and MCT. These sections include (a) Nauhra-Shamra section in the Chor area and (b) Jakhri to Wangtu section in the Sutlej valley, NE of Kulu-Rampur Window (Fig. 1.2). Detailed sampling was carried out along these sections to investigate texture and mineral paragenesis as well as microprobe analysis to determine the P-T conditions.

4.2 METAMORPHIC EPISODES

It has been observed that various metamorphic minerals have developed in

different lithotectonic units of the HHC along the Sutlej Valley and Jutogh Nappe of Chor Mountain area. On the basis of mineral assemblages and textural relationship, three metamorphic episodes are identified viz., i) Early Pre-Himalayan metamorphism, ii) Main Himalayan metamorphism, and iii) Late to post-Himalayan metamorphism.

4.2.1 Pre-Himalayan Metamorphism

The earliest M_1 metamorphism, is pre-Himalayan and largely been superposed and obliterated by later Himalayan metamorphism. The evidences of M_1 metamorphism are found only in the HHC along the Sutlej valley and absent in the frontal parts of the Jutogh Nappe in Chor Mountain region. In the Sutlej valley, metamorphic layering is coeval with the F_1 folds, where tiny mica flakes trend uniformly across the hinge and parallel the lithological layering on the limbs (Fig. 3.1 a). S_1 foliation has been observed in the hinge zones of rootless intrafolial F_2 folds indicating intense transportation of the earlier structures (Fig. 3.1 b). Crystallisation of minerals such as quartz, muscovite, chlorite, biotite, feldspar, etc., occurred during the development of F_1 folds and preferably oriented along the axial plane foliation S_1 and are, therefore, related to D_1 deformation. The presence of quartz, chlorite, biotite, muscovite and quartz in the assemblage along F_1 folds suggests greenschist facies for pre-Himalayan metamorphism M_1.

4.2.2 Main Himalayan Metamorphism

The HHC rocks in Sutlej valley seem to have undergone main Himalayan M_2 metamorphism during strong penetrative D_2 deformation. However, this metamorphism is considered as M_{C1} in the frontal parts of the Jutogh Nappe in

Chor area and related to D_{C1} deformation (see Chapter 3). S_2/S_{C1} foliation is developed during this deformation with the syntectonic porphyrobalstic mineral growth like garnet, staurolite, chloritoid, kyanite etc. (Figs. 4.1, 4.2, 4.3 a, b). Presence of kyanite, staurolite etc. in the assembalge suggest that these rocks have attained amphibolite facies metamorphism.

Syntectonic minerals are often overgrown by the subidioblastic inclusion-free post-tectonic minerals mainly garnet (Figs. 4.1, 4.2) during late to post D_2/D_{C1} deformation and $M2/M_{C1}$ metamorphism. S- and C- shear fabric marking the S_2/S_{c1} foliation in schistose and gneissose rocks are developed throughout the region irrespective of the major tectonic boundaries (Figs., 4.3, c, d). The S- surface turn progresively into C- surface (Berthe *et al.*, 1979) with sense of displacement showing top-to-SW overthrust sense of movement (Fig. 4.4 a) in the HHC as well as in the Jutogh Nappe (Figs., 4.3 c, d; 4.5 a, b). Along with this S-, and C- shear fabric, asymmetric pressure shadows along rigid porphyroblasts of garnet are also observed indicating the same sense of overthrust movement (Figs. 4.5 c, d).

4.2.3 Late to Post-Himalayan Metamorphism

Minerals developed during main M_2/M_{C1} metamorphism are later affected by D_3/D_{C2} deformation during late M_2/M_{C1} metamorphism. This is manifested by post-kinematic growth of quartz, muscovite and greenish biotite along the S_{3a} foliations in the hinge zones of F_{3a} folds. Along the S_{3b} foliation, new mica flakes are developed parallel to the axial traces of F_{3b} folds. Retrograde metamorphism has taken place during D_{3b} deformation and has resulted in development of chlorite and muscovite at the expense of biotite garnet and staurolite respectively (Fig. 4.3 b).

Figure 4.1 : Syntectonic garnet stringers along the main foliation S_m, overgrown by subidioblastic inclusion-free rim in garnetiferous mica schist. Internal fabric S_i in garnet parallels external S_e fabric of the main foliation from one end to other. Note post-garnet crenulation of mica-quartz-rich foliation on left margin. Sample W11. Oblique extinction X 72.

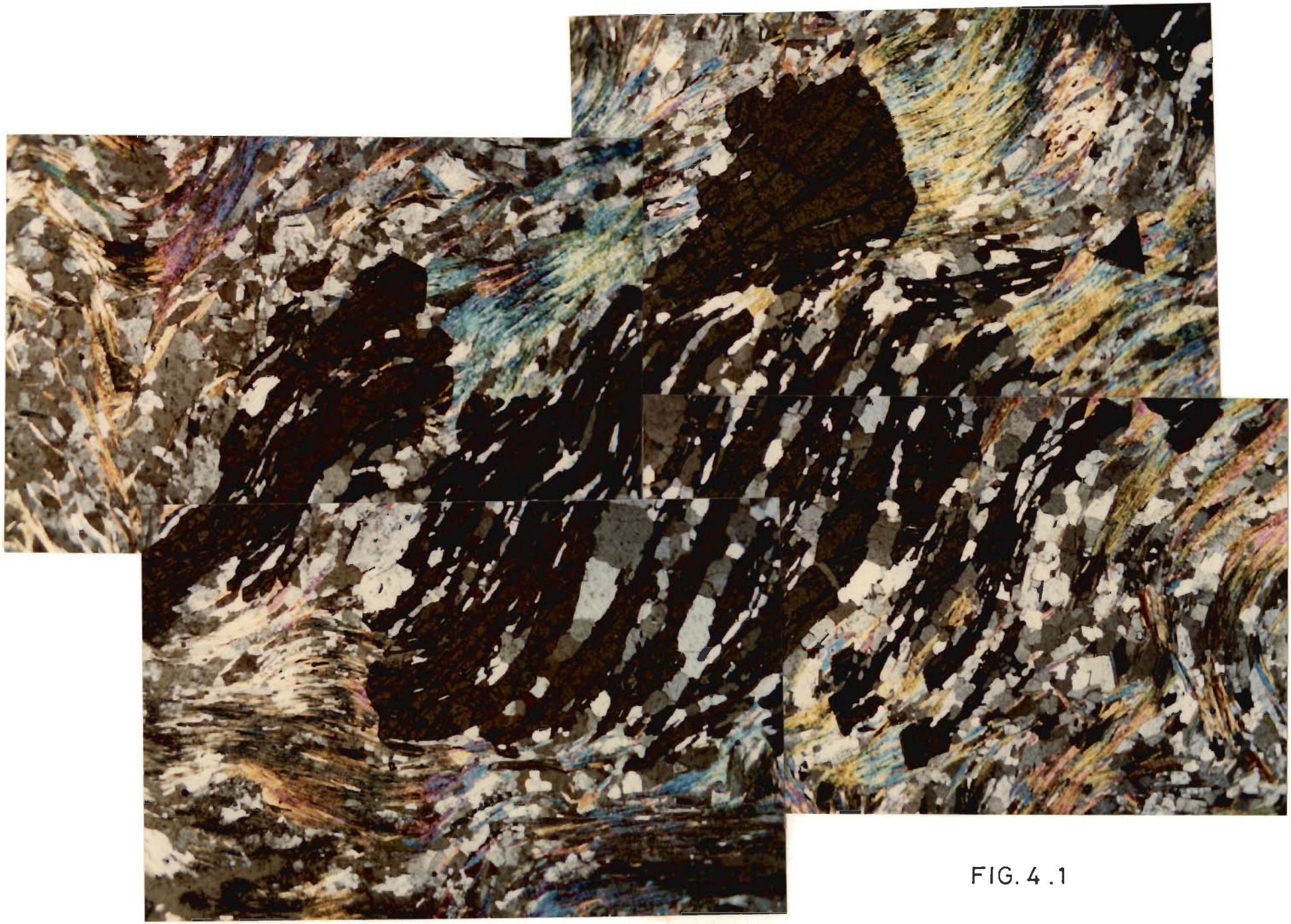

FIG. 4 .1

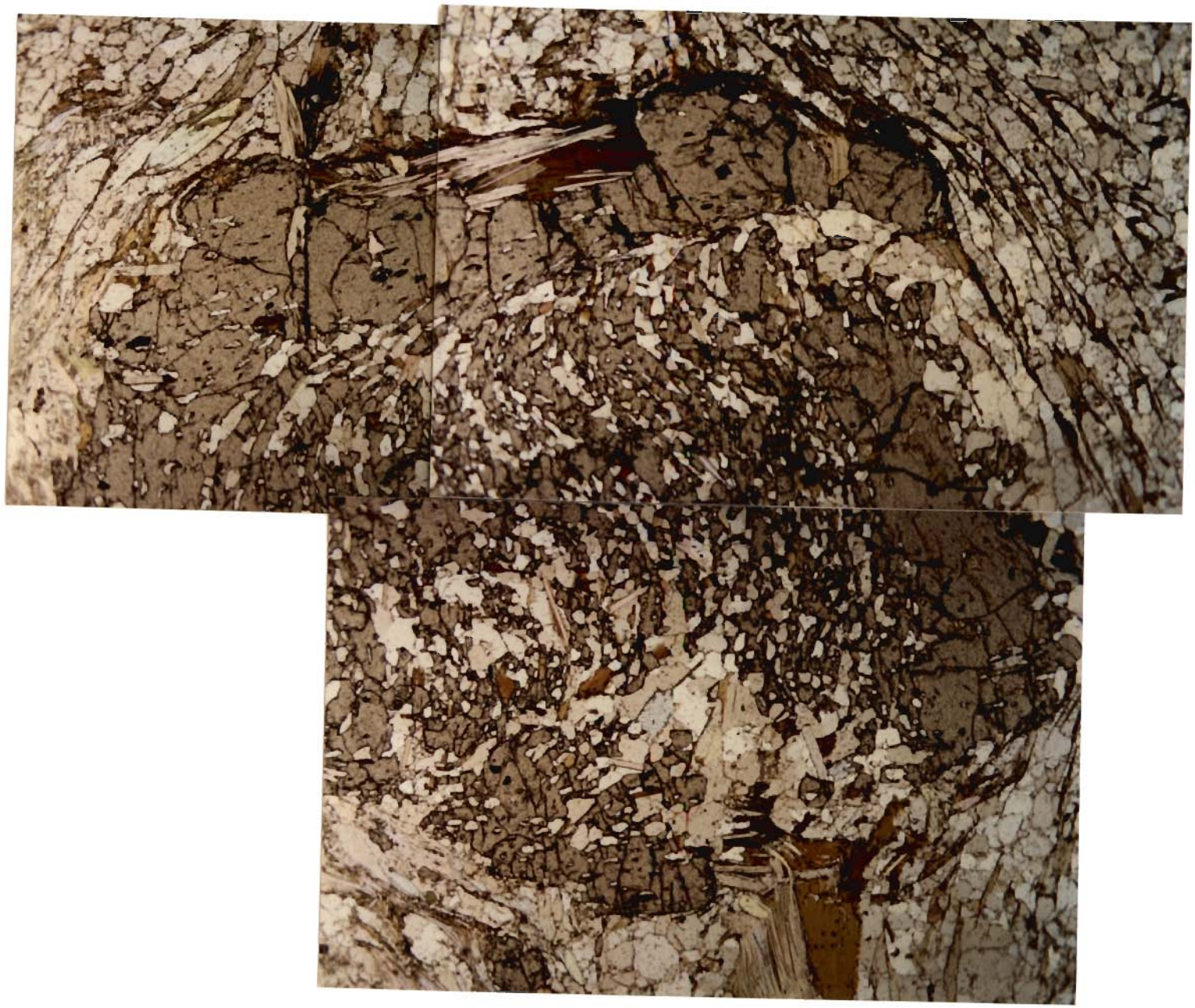

FIG. 4.2

Figure 4.2: Syntectonically growing rotated garnet core having quartz, biotite, muscovite, rutile inclusions, overgrown by subidioblastic inclusion-free post-tectonic garnet in garnetiferous-staurolite-kyanite schist from the Chor Mountain region (CH 7/7). PL X 72.

Figure 4.3 a : Syntectonic grown non-rotational staurolite and chloritoid porphyroblasts along the main foliation S_m from staurolite-chloritoid-mica schist along the Sutlej valley. Within 50 m of the MCT zone (W 2/5). Biotite alters to chlorite in pressure shadow zone. PL X 112.5.

Figure 4.3 b : Syntectonic staurolite and chloritoid along the main foliation in the Chor Mountain region in staurolite-chloritoid-mica schist (CH 10/10). Devlopment of chlorite and sericite felt mainly due to retrogression of biotite and staurolite. PL X 72.

Figure 4.3 c : S-and C- shear fabric having mainly mica (biotite + muscovite) with tail of tourmaline grain along S- surface, rotated by C- shear surface in tourmalinised garnetiferous mica schist (CH 2/5). Note small garnet along S-surface bent along C-shear plane. Upper margin of photo is marked by tiny streak of tourmaline crystals along C-planes. Oblique extinction X 72.

Figure 4.3 d : Mylonitised mica schist (CH 3/13) from Chor Mountain containing S- and C- shear zone with porphyroblastic muscovite growth along S-surface truncated and bent by C-shear planes at both ends, thus providing mica fish. Crossed X 72.

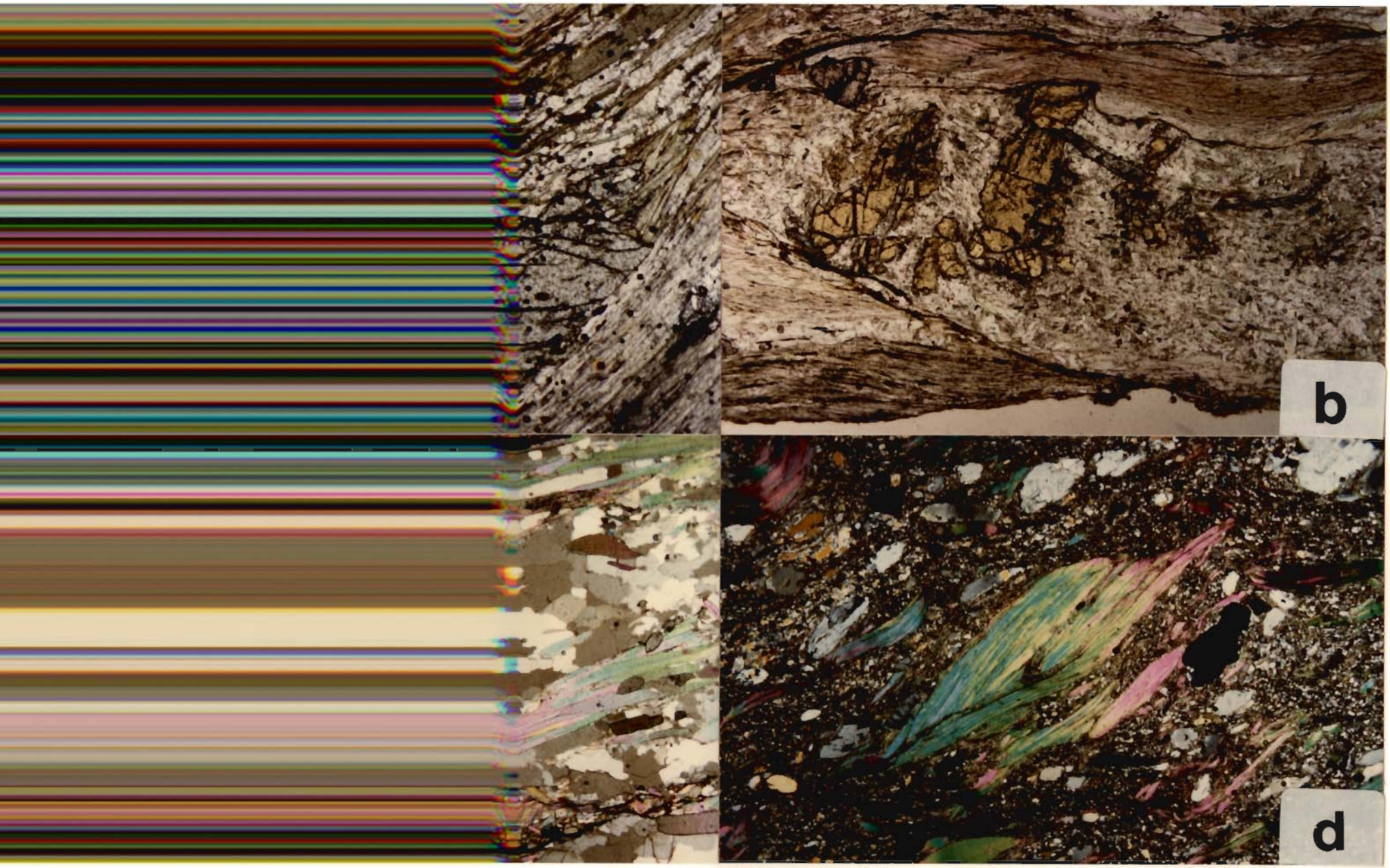

FIG. 4.3

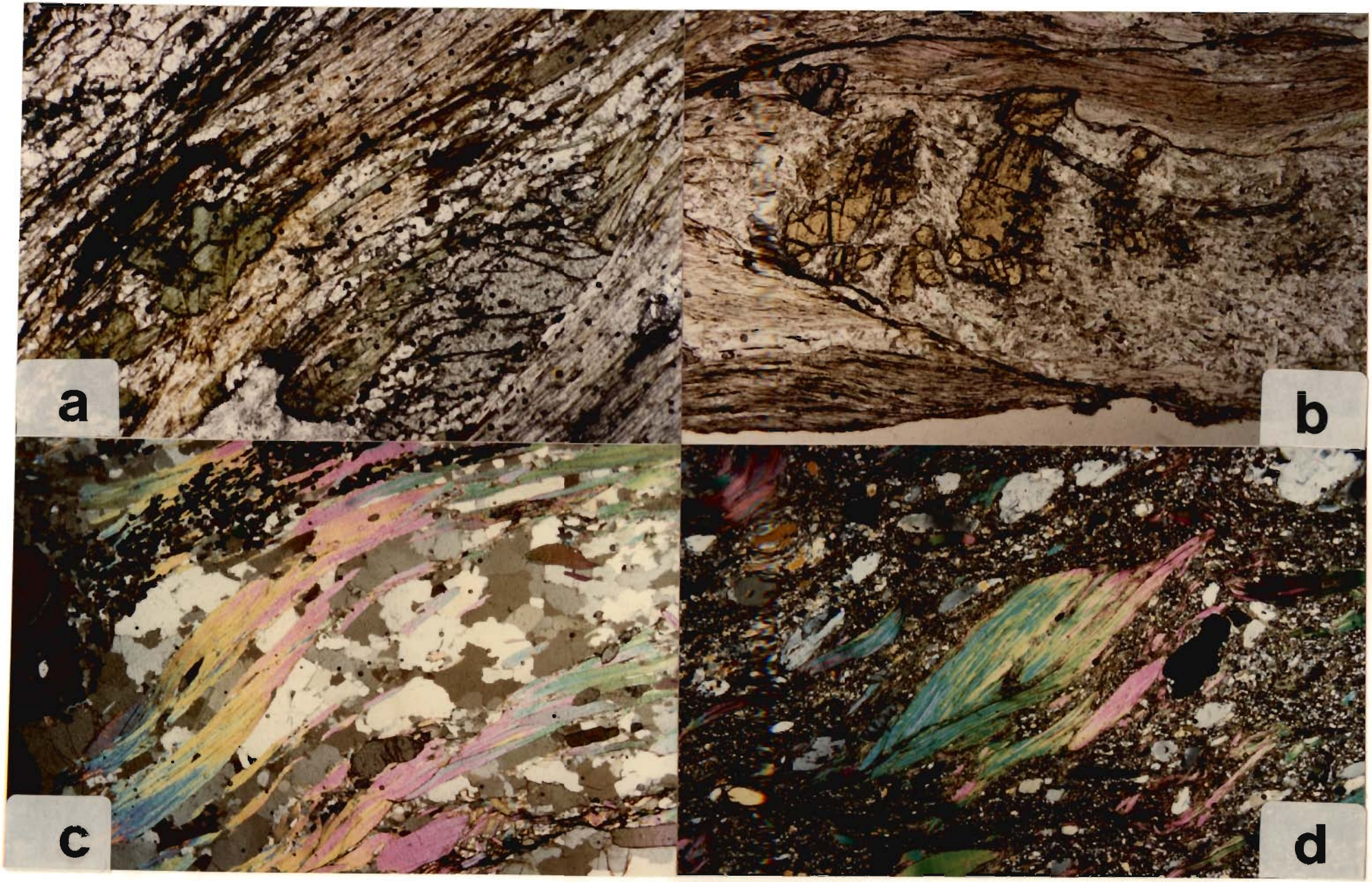

FIG. 4.3

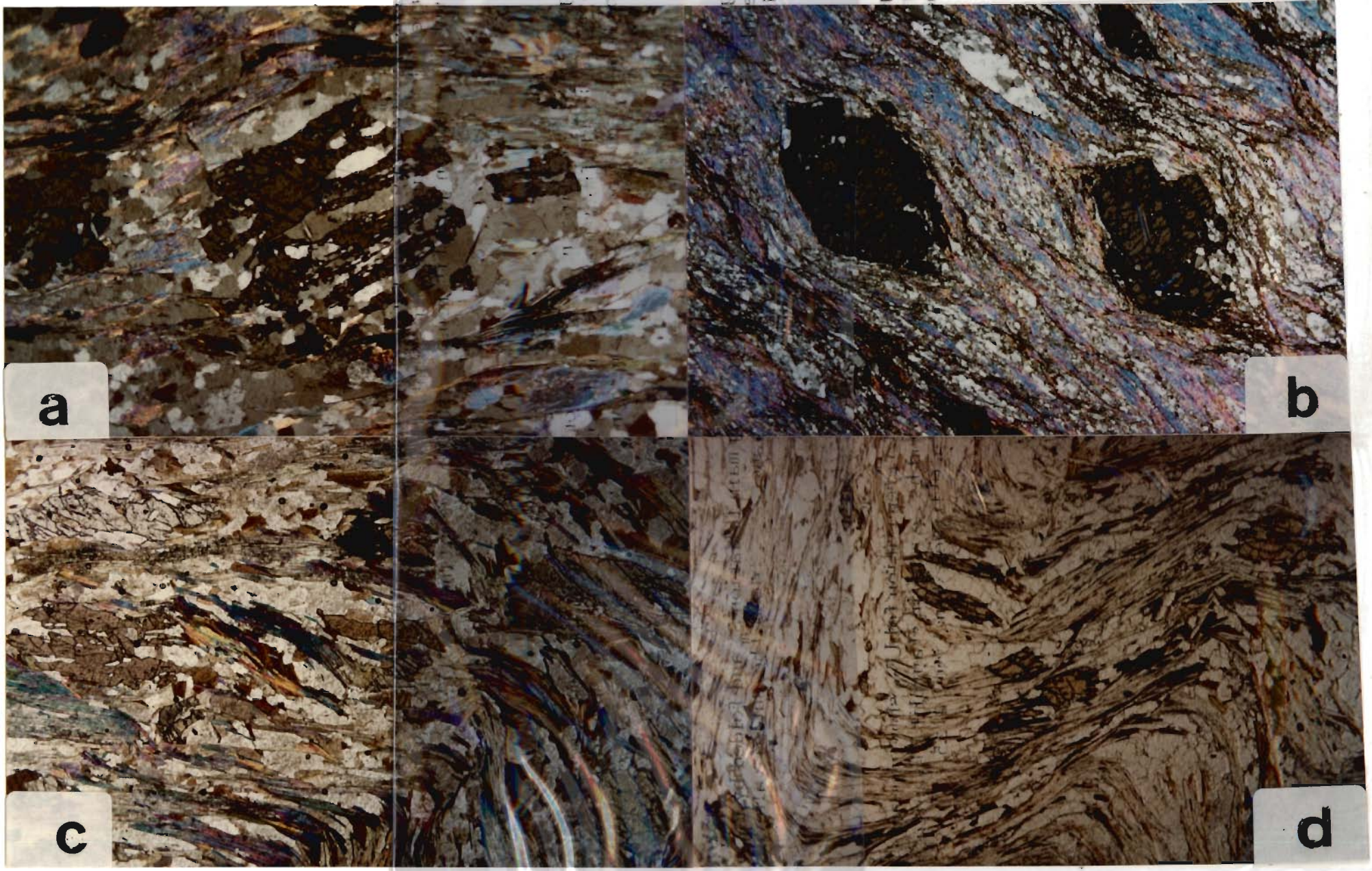

FIG. 4.4

Figure 4.4 a : S-and C- shear fabric (CH 2/5 A) with skeltal syntectonic growth of garnet along S- surface being slightly rotated due to C-shear in the Chor Mountain region in garnetiferous schist. Oblique extinction X 72.

Figure 4.4 b : Very fine grained S-C mylonitised garnetiferous mica schist (CH 11/21) with highly fractured garnet indicating post-metamorphic shearing in the Chor Mountain region. Oblique extinction X 72.

Figure 4.4 c : Syntectonic staurolite along main foliation S_m and folded by F_{3b} crenulation fold in staurolite-kyanite zone (W 13) along the Sutlej valley. Oblique extinction X 72.

Figure 4.4 d : Folded main foliation S_m due to crenulation fold F_{3b} showing many porphyroblasts of staurolite curving around hinge zone in staurolite-kyanite zone (W 12/10) along the Sutlej valley section. Oblique extinction X 112.5.

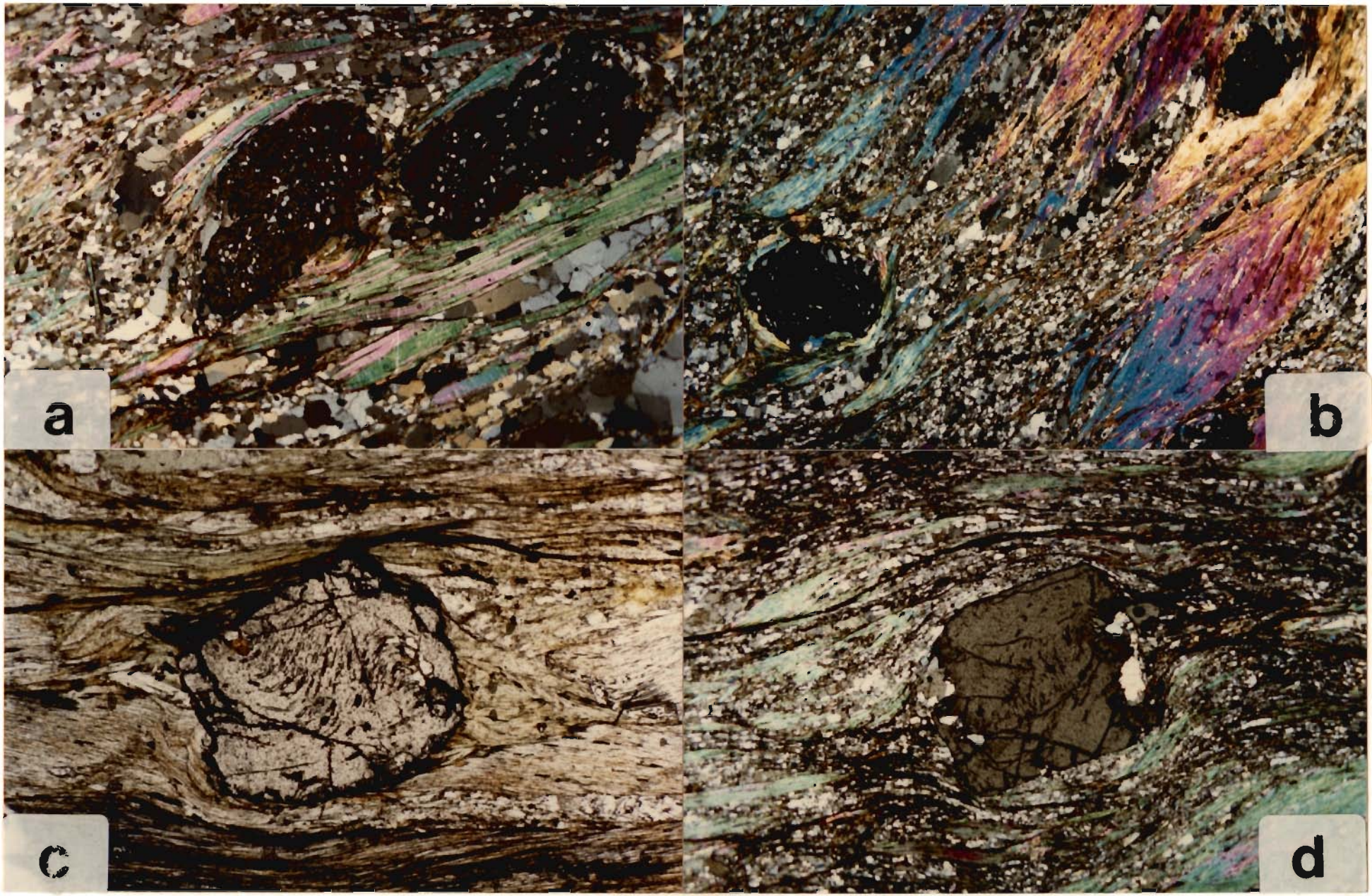

FIG. 4.5

Figure 4.5 a : S- and C- fabric in (CH 2/5 A) with rotational garnet along S- surface gradually turning along C-shear surface, the sense of the displacement is top-to-right overthrust movement. The internal S_i is rotated is continuous with the external foliation S_e in the Chor Mountain area. Oblique extinction X 112.5.

Figure 4.5 b : S- and C- shear fabric in (CH 10/20) showing asymmtric presure shadow along rigid porphyroblasts of garnet with top-to-right overthrust sense of movement. Crossed X 72.

Figure 4.5 c : Growth of syntectonic snowball garnet (CH 10/10) with S-shape spiral inclusions (S_i of quartz, mica and opaque minerals) in garnetiferous mica schist. C-shear plane almost subparallel to main foliation. PL X 112.5.

Figure 4.5 d : Suidioblastic garnet (CH 10/19) with S_i fabric development in the Chor Mountain region in garnetiferous mica schist. S- and C- shear fabric along with asymmtric presure shadow are evident along rigid porphyroblasts of garnet with top-to-right overthrust sense of movement. Oblique extinction X 72.

Table 4.1 summarises the mineral paragenesis mainly of the HHC and the Jutogh Nappe in relation to distinct metamorphic episodes.

4.3 METAMORPHIC GRADES

In the hanging wall of the MCT within the HHC and the Jutogh Nappe, metamorphism remains within garnet to staurolite-kyanite grades of upper greenschist to amphibolite facies conditions. In both the areas, the rocks are mainly pelites and psammites, and sometimes, intercalated with very thin layers of quartzite and amphibolite. Locations of the samples used are given in Figures 4.6 and 4.7. Table 4.2 provides detailed mineral assemblages from various metamorphic isograds.

4.3.1 Garnet Zone

Garnet zone rocks are found at the base of the Jutogh Nappe adjacent to the JT farthest from the Chor granitoid (Figs. 4.6). The main foliation S_{C1} is made up of muscovite, quartz, and sometimes by biotite, chlorite and chloritoid. Chloritoid-bearing samples usually have very less amount of biotite; instead chlorite is commonly associated in these rocks. Garnet is mostly syntectonic having mineral inclusions, and sometimes, overgrown by post-tectonic rims devoid of any inclusions (Fig. 4.2). Coexisting chlorite and garnet are rarely found in these rocks. Chloritoid and staurolite are associated together in some of the samples (Fig. 4.3 b). Epidote, tourmaline, zircon, apatite and ilmenite are found as accessories. Chloritisation of biotite, garnet etc. are noticeable in some of the samples from these regions. Close to the thrust contact the rocks are crushed, mylonitised and recrystallised (Fig. 4.4 b).

TABLE 4.1 Minerals associated with different metamorphic phases from the HHC and the Jutogh Nappe in Himachal Pradesh

	EARLY	MAIN	LATE
QUARTZ			
CHLORITE			
MUSCOVITE			
BIOTITE			
GARNET			
STAUROLITE			
KYANITE			
K-FELDSPAR			
PLAGIOCLASE			

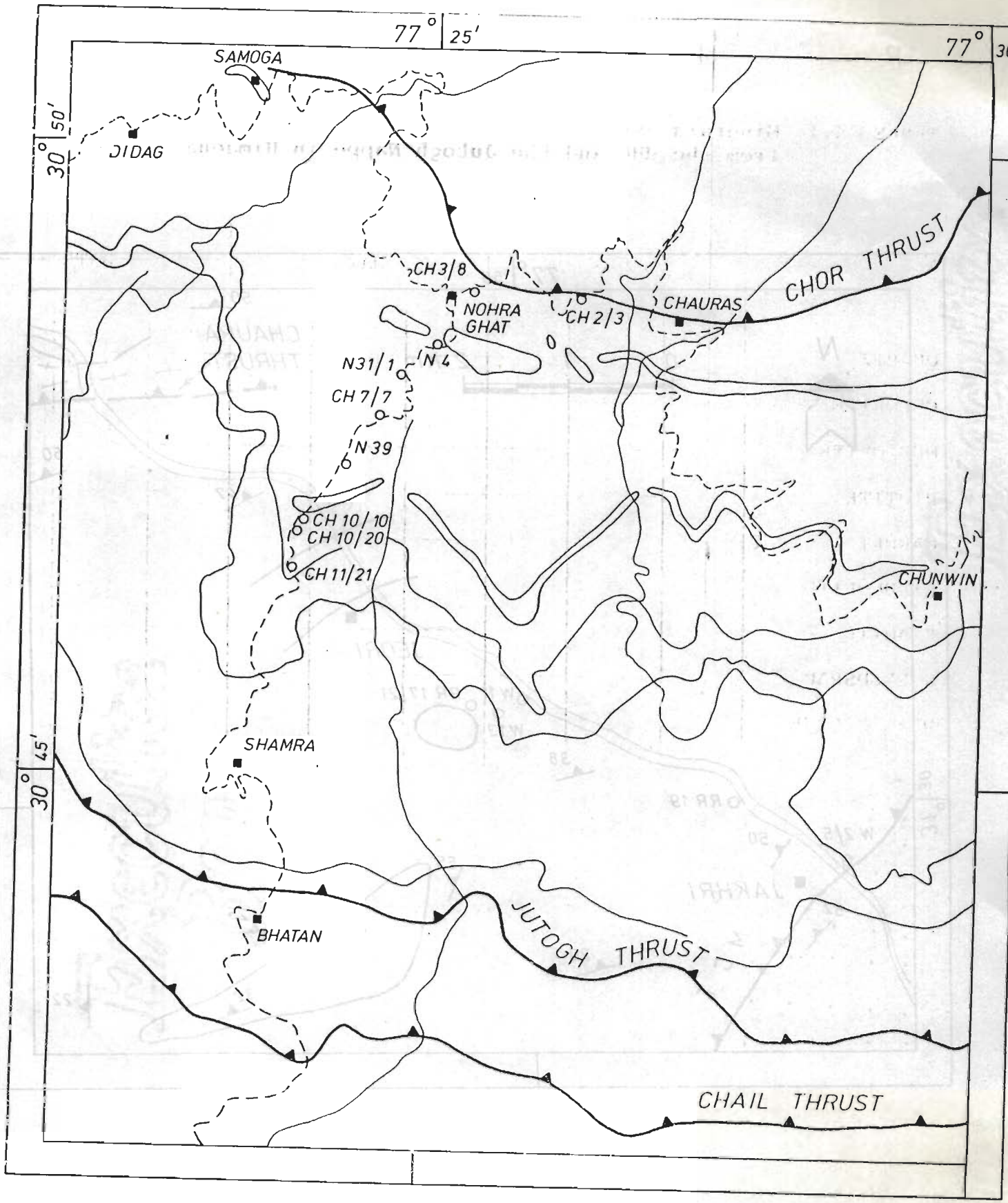

Figure 4.6 : Location map of samples used in microprobe analysis for the P-T estimation in the Chor Mountain region.

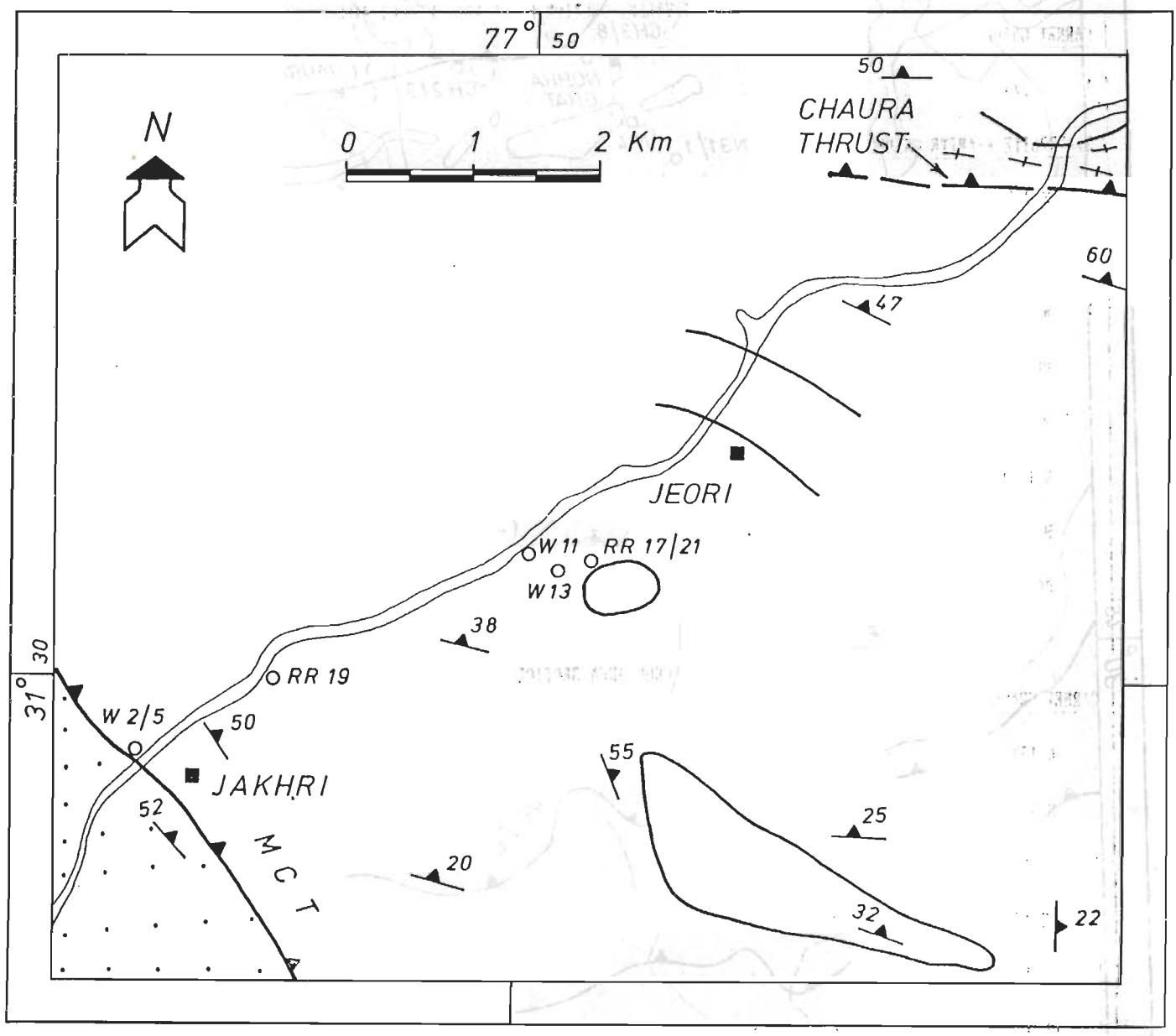

Figure 4.7 : Location map of samples used in microprobe analysis for the P-T estimation along the Sutlej valley section.

TABLE 4.2 Mineral assemblages in different metamorphic grades of the HHC and the Jutogh Nappe in Himachal Pradesh

S.NO.	SAMPLE NO.	CHLORITE	BIOTITE	MUSCOVITE	GARNET	STAUROLITE	KYANITE	CHLORITOID	K-FELDSPAR	PLAGIOCLASE	QUARTZ
					SUTLEJ VALLEY SECTION NE OF KULU-RAMPUR WINDOW						
GARNET GRADE											
1	W 2/3	X	X	X	X				X	X	X
STAUROLITE-KYANITE GRADE											
2	W 2/5	X	X	X	X	X		X			X
3	W 3/6	X	X	X	X	X	X		X	X	X
4	W 6/7		X	X					X	X	X
5	RR 19		X	X	X	X					X
6	W 11		X	X	X	X	X				X
7	W 12/10	X	X	X	X	X	X				X
8	W 13	X	X	X	X	X	X				X
9	RR 17/22		X	X	X						X
					CHOR AREA SECTION						
GARNET GRADE											
1	N 17/1		X	X	X					X	X
2	N 8/1		X	X	X				X	X	X
3	CH 17/36		X	X	X				X	X	X
4	CH 17/35		X	X	X				X	X	X
5	CH 17/33		X	X	X				X	X	X
6	CH 15/27		X	X	X				X	X	X
7	CH 11/21		X	X	X				X	X	X
8	CH 10/20		X	X	X				X	X	X
STAUROLITE-KYANITE GRADE											
1	CH 10/10	X	X	X	X	X		X	X	X	X

Table 4.2 continued

S.NO.	SAMPLE NO.	CHLORITE	BIOTITE	MUSCOVITE	GARNET	STAUROLITE	KYANITE	CHLORITOID	K-FELDSPAR	PLAGIOCLASE	QUARTZ
2	CH 7/7		X	X	X				X	X	X
3	N 31/1	X	X	X	X				X	X	X
4	N 39		X	X	X				X	X	X
5	CH 5/13		X	X	X				X	X	X
6	N 4		X	X	X				X	X	X
7	CH 5	X	X	X	X					X	X
8	CH 4		X	X	X					X	X
9	CH 3/9		X	X	X				X	X	X
10	CH 3/8		X	X	X				X	X	X
11	CH 2/5		X	X	X				X	X	X
12	CH 2/2	X	X	X	X				X	X	X

The mineral assemblage, observed in pelites, include:

Biotite - Muscovite - Garnet - Plagioclase - Quartz - K-feldspar ± Chlorite ± Chloritoid.

4.3.2 Garnet/staurolite-kyanite grade transition zone

Rocks of this zone characterise the basal part of the HHC in the Sutlej valley, while a narrow zone of this sequence is also been observed in the Chor Hills. In this zone, staurolite, chloritoid, garnet, biotite, muscovite, quartz and opaque are present in the pelitic assemblage from both the regions. The coexistence of staurolite and chloritoid in the assemblage indicate the transition zone between garnet and staurolite-kyanite grade (Fig. 4.3 a; Winkler, 1979)

4.3.3 Staurolite-kyanite grade

Staurolite-kyanite grade rocks in both the sections are medium to coarse grained. Porphyroblastic growth of syntectonic garnet, staurolite and kyanite are present in these rocks from the Sutlej valley (Fig. 4.7), while the Nauhra-Shamra section has not revealed any kyanite sofar.

Along the Sutlej valley and away from the MCT towards Jeori, the metapelites contain muscovite, biotite, quartz, staurolite and kyanite in the assemblage (Fig. 4.4 c). Kyanite is present in substantial quantities with limited occurrence of staurolite in the assemblage. Biotite and muscovite form the main foliation and reveal characteristic S-C shear fabric having micas crystallised along S- foliation gradually deflected towards southwards by C- shear foliation

(Fig. 4.4 a). The Chor section contains staurolite in almost negligible amount, but essentially reveals garnet, muscovite, biotite, K-feldspar, plagioclase and quartz in the assemblage. In both the sections, the following observations are evident:

(a) Biotite and muscovite vary sympathetically, and in general, muscovite is the most predominent mineral,

(b) Plagioclase is variable, more in the Chor section and negligible in the Sutlej valley section,

(c) Chlorite is mostly retrograded after biotite and garnet,

(d) Syntectonic garnet with spiral mineral inclusions, is often overgrown by post-tectonic garnet without mineral inclusions and

(e) Accessories include apatite, zircon, tourmaline and ilmenite.

The mineral assemblages found in this grade in pelitic rocks include:

Biotite + Muscovite + Garnet + Quartz + Plagioclase + K-feldspar ± Staurolite ± Kyanite

The relation between individual mineral fabric and deformation in these metamorphic grades are explained below.

a. Garnet: Garnet is a common mineral found in all the metamorphic grades. Growth of embryonic or skeletal, snowball and subhedral garnets are observed in the HHC and the Jutogh metamorphics (Figs. 4.1; 4.2; 4.4 a, b; 4.5). Garnet stringers are either parallel to main foliation S_2/S_{Cl} (Fig. 4.4 a) or display bowing out-like structures at almost normal to the foliation (Fig. 4.4 d; cf., Misch, 1971). Some samples show deflection of the S_2 foliation due to porphyroblastic garnet stringers (Fig. 4.4). All these observations suggest an incipient stage of garnet growth during D_2/D_{Cl} deformation and main M_2/M_{Cl} metamorphism in both the areas.

In the main D_2/D_{C1} deformation and M_2/M_{C1} metamorphism, growth of syntectonic garnet with S-shaped spiral inclusions (S_i) of quartz, mica and opaque minerals are observed (Figs. 4.5 c, d). Internal fabric S_i is rotated but continuous with the external foliation S_e (Fig. 4.5 a). Sometimes, continuity is maintained at one end but disturbed at the other end (Fig. 4.1). During late to post-deformation, idioblastic-to-subidioblastic garnet devoid of mineral inclusions is often overgrown on syntectonic garnet (Figs. 4.1; 4.5 c, d).

b. Staurolite: Staurolite porphyroblasts are faintly pleochroic, having quartz, mica and opaque mineral inclusions, where S_i continues undisturbed with S_e fabric (Figs. 4.4 c, d). However, these inclusions are occassionally arranged in a sigmoidal pattern indicating syntectonic rotation and growth during main D_2/D_{C1} deformation (Fig. 4.4 c). A few subidioblastic staurolite crystals, devoid of mineral inclusions are also found in these samples. Staurolite growth is essentially syn kinematic to main D_2/D_{C1} deformation and subsequently folded by F_{3b} folds in the Sutlej valley (Figs. 4.4 c, d).

c. Feldspar: Both K-feldspar and plagioclase porphyroblasts are present in these samples. In Chor section, K-feldspars are mainly microperthitic having sometimes inclusions of quartz and altered sericite. Myrmekite intergrowth of quartz and feldspar are common, giving evidence of partial melting and recrystallisation. Sometimes, rims of albite around K-feldspar are noticed. Large porphyroblasts of plagioclase are mostly untwinned and sericitised. Both K-feldspar and plagioclase porphyroblasts are developed syn-kinematically along main foliation.

d. Chloritoid: It is commonly found in Sutlej valley and is mostly fine to medium grained (Fig. 4.3 a). It is associated with muscovite and chlorite in the main foliation. Simetimes, at places, it is found in association with staurolite in the transistion zone, where the staurolite replaces the chloritoid (Fig. 4.3 b).

e. Mica: Both muscovite and biotite are invariably associated with the pelites from both the rgions. These are found with garnet as tiny inclusions and crystallise along the main foliation S_2/S_{C1} (Figs. 4.1; 4.2; 4.3 a; 4.8; 4.9). Mica crystalise in large porphyrobalstic syntectonically grown minerals like garnet, staurolite, kyanite, quartz and feldspar and marks the main metamorphic event M_2/M_{C1} (Figs. 4.5 a, b). It is characterised by S-C shear fabric and crystallises both along S- and C- shear planes (Figs. 4.5 a, b, d; 4.8 d) and predates the grain-size reduction associated with later C- shear zone or MCT/JT/Chor thrust-controled mylonitic foliation (Figs. 4.5 b, d; 4.8 a, d). Transposition of earlier-grown mica as rootless folds by later S_2 mica-rich foliation is occasionally seen in the Chor Hills (Figs. 4.8 a, 4.9), while at places, both muscovite and biotite randomly-oriented flakes are distinctly post-tectonic (Figs. 4.5 a, 4.9).

It is noteworthy that later deformation of mica either due to D_{C2}/D_3 in chor hills and Sutlej valley produces kinks and displace/rotated and newly crystallised flakes along S_3/S_{3b} crenulation foliation (Figs. 4.4 c, d; 4.8 a, b, c).

4.4 PROBE ANALYSIS

Many polished thin sections of suitable samples have been examined under transmitted and reflected light to ascertain texturally the equilibrium mineral assemblage for the analysis. Altered and retrograde samples were discarded for this purpose. Metamorphic textures were used to distinguish different generations of garnet, mica etc.. Microprobe analysis was carried out mainly on minerals, which have grown syntectonically during main metamorphic event or immediately after this event. In each thin section, many grains belong to the same generation of a particular mineral were analysed and each grain contained a number of points to check the compositional variation. All the

analysed points were checked carefully for the stoichiometry and the points with incorrect analysis were discarded in the P-T calculation. In the studied area, core temperature could only be determined in 2 samples, while core pressure could not be determined due to paucity of suitable mineral inclusions. Therefore, P-T determination has been done mainly from garnet rim and coexisting matrix mineral compositions. Thus, five samples have been found suitable from the Sutlej valley and nine samples from the Chor area for the microprobe work.

4.4.1 Anaytical Procedure

Samples have been analysed, using an automated JEOL JXA-8600M Electron Probe X-Ray Microanalyser. The instrument was operated upon at an accelerating voltage of 15 kV and sample current of 2×10^{-8} ampere, having beam size between 1 µm (for garnet, staurolite, ilmenite, chloritoid and rutile) and 10 µm (for biotite, muscovite, and plagioclase). For qualitative and quantitative analyses, three channel Wavelength Dispersive Spectrometers (WDS) were used. Highly polished samples were coated with carbon to a thickness of about 100 Ax. Natural mineral standards (SPI Standard, Canada), such as almandine and pyrope garnets, biotite, plagioclase, sanidine, hematite, rutile and wherever necessary, multi-mineral standards were used in the analysis. ZAF correction was applied for X-ray absorption, X-ray fluorescence, atomic number effects, back scatter and ionization-penetration losses during data acquisition.

Composition close to the rim of unzoned coexisting minerals have been analysed for P-T calculation. For zoned minerals like garnet, staurolite and chloritoid, rim and core and intermediate points in some cases, were analysed for determining the variation in chemical composition. Quantitative line analyses were performed in garnet for zoning. Inclusion minerals such as

Figure 4.8 a : Isoclinal F_{C2} fold with lower limb marked by microscopic thrust characterised by mylonitisation and grain size reduction. Mylonitic foliation cuts across obliquely to main foliation and is post metamorphic fabric in the Chor Mountain region. Also note later upright kink affecting the fold and thrust. Crosed X 72.

Figure 4.8 b : Isoclinal fold F_{C2} superposed by crenulation fold F_{C3} folds and developed on main foliation S_{C1}. Note post-F_{C2} mylonitic streaks in hinge zone of and kink development. Mica schist (CH 2/5 B) from Chor Mountain region. Crossed X 72.

Figure 4.8 c : Crenulation folds F_{C3} having kinked muscovite-biotite and incipient mica growth along axial plane foliation S_{C3} (CH 7/7). Crossed X 72.

Figure 4.8 d : Mica fish development along S- and C- shear fabric in garnet-mica schist (CH 11/21) in the Chor Mountain region. Also note stteply dipping extensional crenulation towards right and characterised by fine grained streaks of mica and quartz. Crossed X 72.

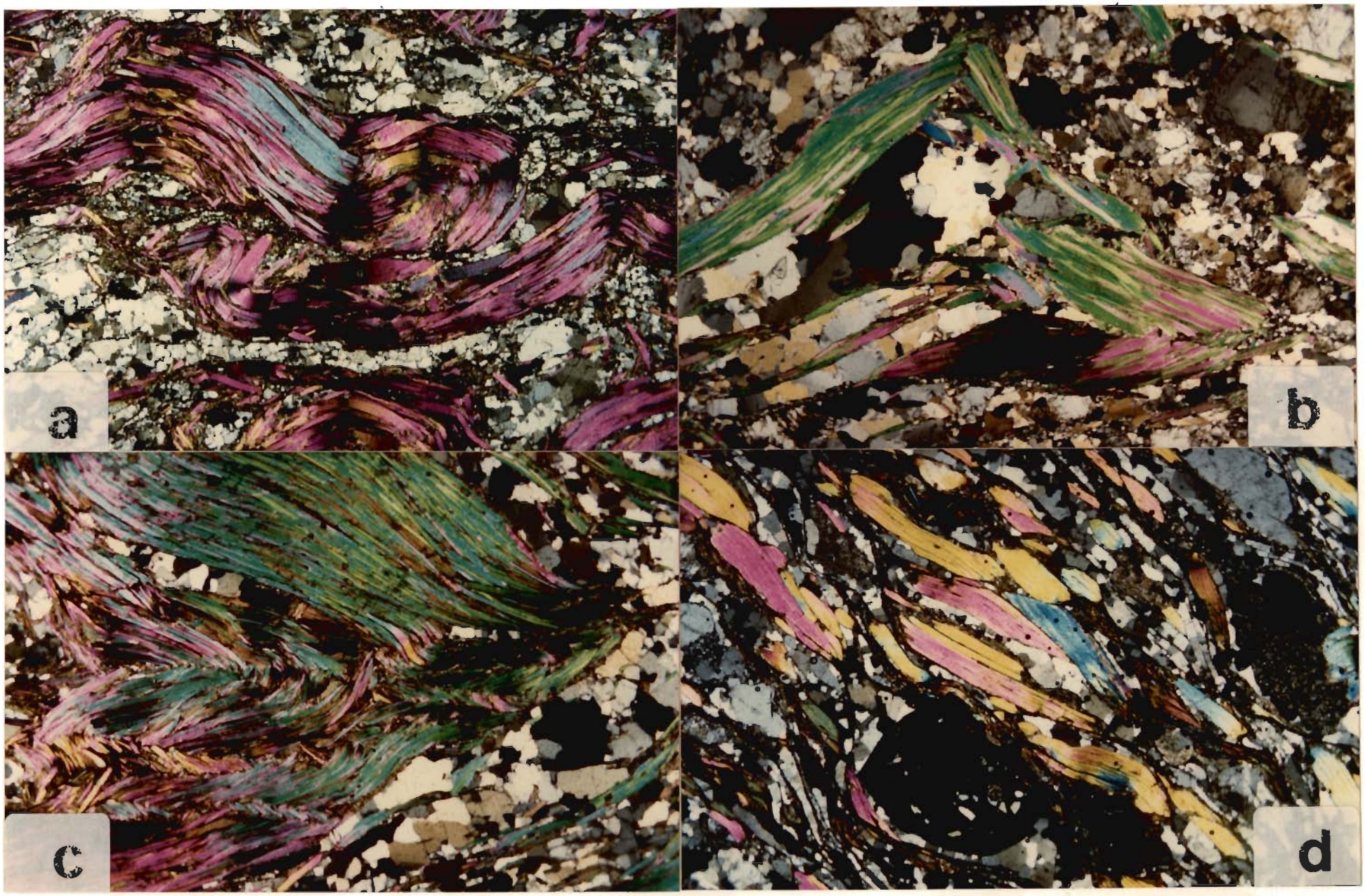

FIG. 4.8

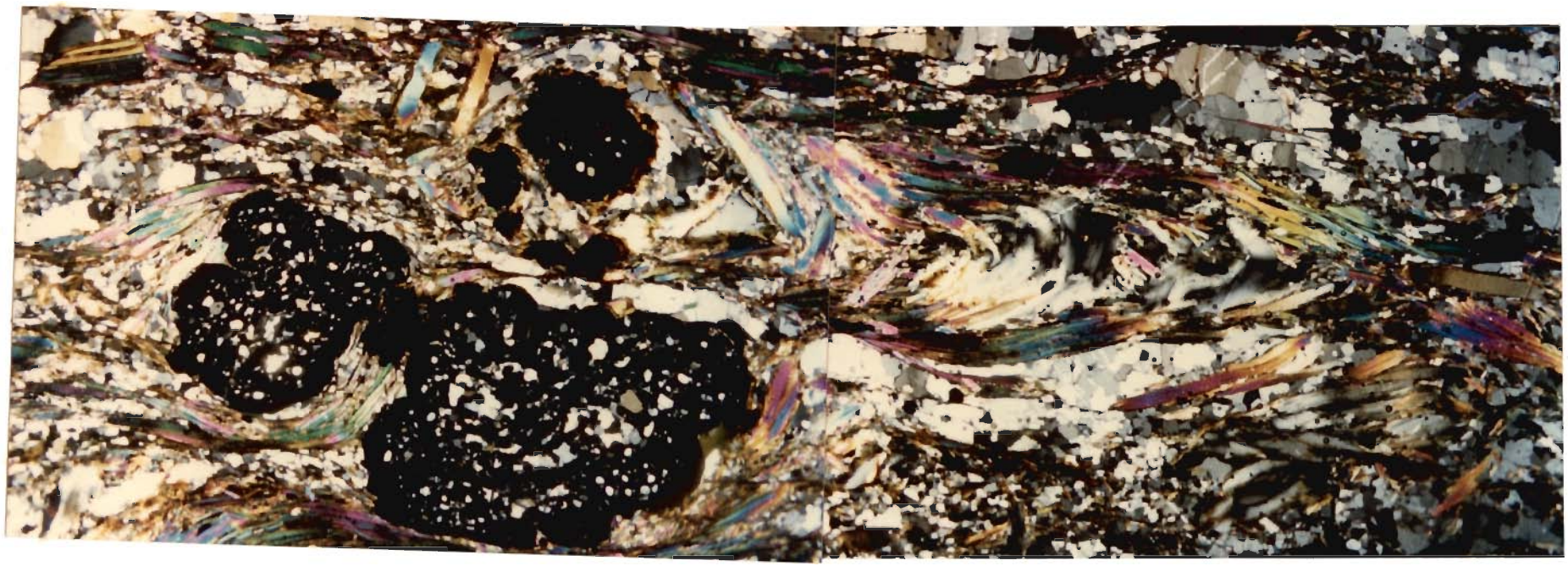

FIG. 4.9

Figure 4.9 : Rootless fold F_{C2} showing preserved earlier foliation S_{C1} within two main foliation planes. Porphyroclastic garnet riddled with quartz-mica inclusions in mica schist (CH 2/5) from Chor Mountain. Crossed X 72.

Table 4.3 Microprobe analysis of garnet from Chor Mountain area

ELEMENTS	CH 7/7					CH 10/20			CH 10/10		N 31/1	
	RIM	CORE	RIM	RIM	RIM	RIM	RIM	RIM	RIM	RIM	RIM	RIM
						WEIGHT%						
OXIDES												
SiO_2	38.688	37.440	37.632	37.357	36.868	37.943	37.511	37.182	37.571	37.366	37.652	37.800
Al_2O_3	22.263	21.573	21.800	21.755	21.354	21.697	21.534	21.386	21.699	21.441	21.664	21.570
CaO	4.301	2.411	3.960	4.438	3.943	2.757	4.057	3.849	3.768	2.788	1.311	2.427
FeO	31.810	31.821	32.409	32.994	32.067	33.966	32.592	32.120	33.691	33.446	35.688	35.636
MgO	2.013	1.747	2.090	2.146	1.972	1.577	1.617	1.302	2.730	2.500	3.020	2.549
MnO	2.513	5.403	2.569	2.213	3.961	3.580	3.465	4.334	0.732	2.788	1.511	0.909
Total	101.588	100.403	100.460	100.903	100.165	101.519	100.776	100.172	100.192	100.317	100.826	100.891
						CATION (on the basis of 12 oxygen)						
Si	3.0328	3.0070	3.0016	2.9766	2.9726	3.0155	3.0000	2.9991	2.9975	2.9957	3.0001	3.0098
Al	2.0571	2.0422	2.0495	2.0432	2.0294	2.0325	2.0299	2.0332	2.0405	2.0261	2.0328	2.0244
Ca	0.3612	0.2075	0.3384	0.3789	0.3407	0.2348	0.3477	0.3326	0.3221	0.2395	0.1119	0.2070
Fe	2.0855	2.1374	2.1619	2.1987	2.1624	2.2576	2.1799	2.1668	2.2480	2.2426	2.3781	2.3731
Mg	0.2353	0.2102	0.2485	0.2549	0.2370	0.1868	0.1928	0.1565	0.3247	0.2988	0.3586	0.3025
Mn	0.1668	0.3676	0.1736	0.3789	0.2706	0.2410	0.2347	0.2961	0.0495	0.1885	0.1020	0.0613
Total	7.9387	7.9719	7.9736	8.0018	8.0127	7.9682	7.9851	7.9843	7.9823	7.9912	7.9835	7.9781

Table 4.3 - continued

ELEMENTS	N 4		CH11/21	N 39	CH 2/3				CH 3/8	
	RIM	RIM	RIM	RIM	RIM	RIM	RIM	RIM	RIM	CORE
				WEIGHT%						
OXIDES										
SiO_2	36.754	37.487	37.716	37.039	37.868	38.662	38.167	38.144	36.778	36.118
Al_2O_3	21.059	21.563	21.555	22.046	21.587	22.024	21.768	21.832	21.197	20.511
CaO	9.233	6.677	2.761	0.636	2.188	5.860	2.931	5.006	7.417	4.102
FeO	25.130	24.118	34.825	35.312	34.164	32.595	34.370	33.447	26.717	27.172
MgO	0.761	0.798	1.886	2.373	2.246	1.945	2.079	2.021	0.831	0.888
MnO	6.213	9.643	0.971	1.209	2.613	0.859	2.384	0.973	6.753	10.012
Total	99.149	100.285	99.714	98.615	100.670	101.945	101.692	101.424	99.693	98.803
				CATION (on the basis of 12 oxygen)						
Si	2.9791	3.0034	3.0323	3.0066	3.0217	3.0238	3.0169	3.0102	2.9763	2.9803
Al	2.0119	2.0363	2.0426	2.1093	2.0304	2.0304	2.0281	2.0307	2.0220	1.9949
Ca	0.8019	0.5732	0.2378	0.0553	0.1871	0.4911	0.2482	0.4233	0.6431	0.3627
Fe	1.7035	1.6160	2.3415	2.3973	2.2800	2.1321	2.2721	2.2074	1.8082	1.8752
Mg	0.0920	0.0953	0.2260	0.2871	0.2671	0.2267	0.2442	0.2378	0.1003	0.1092
Mn	0.4266	0.6544	0.0661	0.0831	0.1769	0.0569	0.1596	0.0650	0.4629	0.6998
Total	8.0150	7.9785	7.9464	7.9388	7.9631	7.9610	7.9691	7.9745	8.0128	8.0222

Table 4.3 continued

Microprobe analysis of garnet from the Sutlej valley section

ELEMENTS	W 2/5	W 11	W 13		RR 17/22		RR 19		
	RIM	RIM	RIM	RIM	RIM	RIM	RIM	RIM	RIM
OXIDES	WEIGHT%								
SiO_2	37.840	37.990	31.112	33.304	37.909	38.169	37.100	36.956	37.993
Al_2O_3	21.640	21.809	17.919	21.781	21.631	21.766	21.152	20.699	21.530
CaO	1.690	2.445	5.915	5.607	7.234	6.397	2.846	2.360	3.044
FeO	35.838	36.924	31.302	30.443	28.985	30.415	34.431	35.396	34.478
MgO	2.001	2.108	2.022	2.084	2.114	2.636	2.822	2.985	2.965
MnO	2.753	0.651	0.435	0.440	3.196	1.658	0.395	0.286	0.312
Total	101.760	101.927	88.703	93.659	101.069	101.041	98.746	98.682	100.323
	CATION (on the basis of 12 oxygen)								
Si	3.0064	3.0045	2.8762	2.8533	2.9945	3.0045	3.0084	3.0100	3.0226
Al	2.0266	2.0330	1.9525	2.1995	2.0141	2.0195	2.0217	1.9872	2.0190
Ca	0.1438	0.2072	0.5859	0.5148	0.6122	0.5396	0.2473	0.2059	0.2595
Fe	2.3813	2.4422	2.4201	2.1813	1.9148	2.0023	2.3350	2.4111	2.2941
Mg	0.2369	0.2485	0.2786	0.2662	0.2490	0.3093	0.3411	0.3625	0.3516
Mn	0.1853	0.0436	0.0340	0.0319	0.2139	0.1105	0.0272	0.0197	0.0211
Total	7.9803	7.9790	8.1475	8.0469	7.9985	7.9857	7.9807	7.9964	7.9679

Table 4.4 Microprobe analysis of biotite from Chor Mountain area

ELEMENTS	CH 7/7			CH 10/20			CH 10/10		N 31/1	CH 3/8	
	INC.									INC.	
						WEIGHT%					
OXIDES											
SiO_2	34.759	34.890	34.974	34.090	35.275	33.811	33.096	33.576	33.767	34.673	53.951
Al_2O_3	18.511	18.298	18.179	18.406	19.033	18.371	19.024	19.775	17.785	17.765	11.979
K_2O	8.504	9.027	8.731	8.491	8.740	7.893	6.253	5.379	7.518	8.610	6.026
Na_2O	0.354	0.267	0.330	0.489	0.361	0.410	0.293	0.304	0.459	0.172	0.207
CaO	0.099	0.041	0.102	0.065	0.058	0.256	0.488	0.376	0.201	0.059	0.182
FeO	18.841	20.516	18.745	20.349	20.769	19.668	18.673	19.364	18.232	23.322	17.931
MgO	9.572	8.874	9.549	8.460	8.658	8.040	8.956	11.091	9.6121	6.199	3.911
MnO	0.113	0.203	0.086	-	0.036	0.028	0.201	0.039	-	0.227	0.384
TiO_2	2.208	2.414	2.617	1.581	1.576	1.670	1.278	1.249	1.527	2.289	1.841
Cl	0.110	0.086	0.104	0.262	0.144	0.274	0.168	0.148	0.066	0.037	0.094
Total	93.314	94.804	93.438	92.534	95.065	90.893	88.391	91.269	89.374	93.344	96.485
						CATION (on the basis of 22 oxygen)					
Si	5.4018	5.3910	5.4181	5.4075	5.4320	5.4383	5.7792	5.6291	5.4642	5.4934	7.5484
Al	3.3908	3.3325	3.3196	3.4415	3.4547	3.4829	3.2259	3.2270	3.4273	3.3175	1.9755
K	1.6861	1.7794	1.7256	1.7184	1.7171	1.6197	1.5565	1.6851	1.6364	1.7404	1.0756
Na	0.1068	0.0799	0.0991	0.0111	0.1078	0.1279	0.0391	0.0407	0.1294	0.0528	0.0563
Ca	0.0165	0.0069	0.0169	0.0048	0.0096	0.0441	0.0480	0.0081	-	0.0188	0.0273
Fe	2.4488	2.6512	2.4286	2.6995	2.6748	2.6456	2.2561	2.3200	2.2843	3.0902	2.0981
Mg	2.2175	2.0440	2.2053	2.0005	1.9876	1.9277	2.0314	2.3928	2.2907	1.4641	0.8158
Mn	0.0149	0.0266	0.0113	-	0.0047	0.0038	0.0054	0.0156	0.0152	0.0305	0.0456
Ti	0.2581	0.2805	0.3049	0.1886	0.1825	0.2020	0.2320	0.1509	0.2287	0.2728	0.1937
Cl	0.0290	0.0474	0.0273	0.0703	0.0376	0.0747	0.0175	0.0262	0.0037	0.0100	0.0222
Total	15.7979	15.7525	15.5951	16.0346	15.9838	16.0363	15.1911	15.4956	15.4800	15.4817	13.8583

Table 4.4 continued

ELEMENTS	CH 2/3		N 4			CH 11/21	N 39
			WEIGHT%				
OXIDES							
SiO_2	35.174	36.858	35.287	33.541	34.884	35.433	34.135
Al_2O_3	17.300	21.092	17.399	17.408	17.551	19.793	18.426
K_2O	8.438	0.016	8.515	8.832	9.331	6.664	7.232
Na_2O	0.209	0.003	0.401	0.057	0.105	0.313	0.293
CaO	0.214	2.474	0.188	0.206	0.140	0.156	0.172
FeO	20.810	32.583	19.962	22.641	22.510	19.310	19.542
MgO	9.409	2.549	9.864	5.885	6.584	9.112	9.413
MnO	0.043	2.931	0.088	0.284	0.204	-	-
TiO_2	1.180	-	1.454	3.371	3.690	1.029	0.930
Cl	0.111	0.006	0.119	0.150	0.119	0.142	0.019
Total	92.863	99.374	93.699	92.523	95.584	92.491	90.335
		CATION	(on the basis of 22 oxygen)				
Si	5.5277	5.5085	5.5051	5.3944	5.4288	5.4949	5.4535
Al	3.2046	3.7155	3.1994	3.3001	3.2195	3.6180	3.4699
K	1.6917	0.0031	1.6947	1.8123	1.8527	1.3184	1.4741
Na	0.0635	0.0008	0.1214	0.0178	0.0317	0.0943	0.0907
Ca	0.0360	0.3962	0.0315	0.0356	0.0234	0.0259	0.0294
Fe	2.7351	4.0726	2.6045	3.0453	2.9298	2.5044	2.6111
Mg	2.2043	0.5679	2.2941	1.4109	1.5273	2.1064	2.2418
Mn	0.0057	0.3710	0.0116	0.0388	0.0269	-	-
Ti	0.1395	-	0.1705	0.4078	0.4319	0.1200	0.1118
Cl	0.0295	0.0014	0.0315	0.0408	0.0313	0.0373	0.0052
Total	15.6377	15.3418	16.0473	15.6623	15.9216	15.8050	15.6426

Table 4.4 continued

Microprobe analysis of biotite from the Sutlej valley section

ELEMENTS	W 2/5	W 11	W 13		RR 17/22	RR 19		
			WEIGHT%					
OXIDES								
SiO_2	35.389	33.692	34.672	35.205	32.436	34.037	33.851	34.189
Al_2O_3	19.238	19.065	18.592	19.492	20.457	18.538	18.566	18.925
K_2O	8.883	8.761	8.590	9.166	7.229	9.138	8.810	8.715
Na_2O	0.259	0.319	0.155	0.242	0.129	0.381	0.334	0.336
CaO	0.077	0.237	0.163	0.141	0.599	0.054	0.131	0.081
FeO	21.453	21.532	18.927	18.739	20.634	19.678	18.685	18.310
MgO	9.170	7.755	10.117	9.640	8.129	9.445	9.469	9.071
MnO	0.101	0.052	-	0.008	0.455	0.044	0.016	0.088
TiO_2	2.964	1.594	0.585	0.172	0.699	1.235	1.121	1.548
Cl	-	0.081	0.354	0.163	0.897	-	-	-
Total	95.534	93.218	92.882	93.204	91.633	92.583	91.595	91.814
			CATION (on the basis of 22 oxygen)					
Si	5.4090	5.3228	5.4559	5.4770	5.1999	5.3664	5.3944	5.4081
Al	3.4658	3.5502	3.4483	3.5742	3.8656	3.4450	3.4874	3.5287
K	1.7321	1.7659	1.7245	1.8192	1.4786	1.8381	1.7912	1.7588
Na	0.0769	0.0978	0.0471	0.0731	0.0400	0.1165	0.1031	0.1124
Ca	0.0127	0.0402	0.0274	0.0235	0.1029	0.0092	0.0224	0.0138
Fe	2.7423	2.8849	2.4908	2.4381	2.7666	2.5947	2.4903	2.4223
Mg	2.0893	1.8263	2.3732	2.2356	1.9426	2.2197	2.2493	2.1390
Mn	0.0131	0.0070	-	0.0011	0.0617	0.0058	0.0021	0.0118
Ti	0.1108	0.1894	0.0693	0.0201	0.0843	0.1465	0.1344	0.1842
Cl	-	0.0217	0.6937	0.2317	0.2437	-	-	-
Total	15.6518	15.7935	16.4247	15.9367	15.9363	15.7698	16.2069	16.0285

Table 4.5 Microprobe analysis of plagioclase from Chor Mountain area

ELEMENTS	CH 7/7		CH 10/20		CH 10/10	N 31/1	CH 3/8	N 4	CH 2/3		
					WEIGHT%						
OXIDES											
SiO_2	60.799	60.589	59.953	63.019	63.241	66.957	62.890	60.531	61.554	57.541	61.786
Al_2O_3	24.195	24.133	24.963	23.099	23.198	21.187	23.618	25.484	23.858	25.795	23.713
K_2O	0.122	0.084	0.353	0.079	0.057	0.049	0.171	0.217	0.073	-	0.055
Na_2O	8.436	8.379	8.198	9.569	9.766	11.405	9.133	8.408	11.623	10.095	8.745
CaO	5.642	5.636	6.134	4.079	4.395	1.913	4.768	6.825	5.146	5.022	5.321
FeO	-	0.049	0.240	0.119	0.099	0.010	0.049	0.026	-	-	0.069
MgO	0.015	0.028	0.007	-	0.013	0.041	0.012	-	-	0.165	-
TiO_2	0.043	0.009	0.036	0.013	0.038	-	-	-	-	-	0.028
Total	99.290	99.933	99.884	99.985	100.807	101.592	100.662	101.491	102.253	98.618	99.717
					CATION (on the basis of 8 oxygen)						
Si	2.7216	2.7207	2.6795	2.7903	2.7827	2.9018	2.7692	2.6645	2.7039	2.6140	2.7495
Al	1.2766	1.2773	1.3151	1.2055	1.2031	1.0823	1.2258	1.3222	1.2353	1.3812	1.2439
K	0.0069	0.0048	0.0201	0.0045	0.0037	0.0027	0.0107	0.0122	0.0041	-	0.0031
Na	0.7323	0.7295	0.7105	0.8215	0.8333	0.9584	0.7798	0.7176	0.9900	0.8892	0.7546
Ca	0.2706	0.2712	0.2937	0.1935	0.2072	0.0889	0.2250	0.3219	0.2422	0.2445	0.2537
Fe	-	0.0019	0.0090	0.0044	0.0036	0.0004	0.0018	0.0010	-	-	0.0026
Mg	0.0010	0.0019	0.0004	-	0.0009	0.0027	0.0008	-	-	0.0112	-
Ti	0.0024	0.0005	0.0020	0.0007	0.0021	-	-	-	-	-	0.0016
Total	5.0121	5.0083	5.0303	5.0207	5.0360	5.0376	5.0131	5.0393	5.1755	5.1401	5.0089

Table 4.5 continued

MICROPROBE ANALYSIS OF PLAGIOCLASE FROM SUTLEJ VALLEY SECTION

ELEMENTS	W 11	RR 17/22
	WEIGHT%	
OXIDES		
SiO_2	60.115	57.741
Al_2O_3	25.309	26.140
K_2O	0.376	0.119
Na_2O	8.319	8.074
CaO	5.973	6.306
FeO	0.161	0.054
MgO	0.048	0.069
TiO_2	-	-
Total	100.301	98.573
CATION (on the basis of 8 oxygen)		
Si	2.6734	2.6167
Al	1.3267	1.3962
K	0.0213	0.0069
Na	0.7174	0.7095
Ca	0.2846	0.3062
Fe	0.0060	0.0020
Mg	0.0032	0.0046
Ti	-	-
Total	5.0326	5.0434

Table 4.6 Microprobe analysis of muscovite from Chor Mountain area

ELEMENTS	CH 7/7		CH 10/20	CH 10/10	N 31/1	CH 3/8	N 4	CH 2/3		
					WEIGHT%					
OXIDES										
SiO_2	44.937	44.662	49.114	45.714	44.816	45.470	45.783	44.367	44.788	51.872
Al_2O_3	33.634	33.654	29.262	35.129	35.128	31.470	33.155	30.375	31.969	28.601
K_2O	10.193	10.118	5.816	8.520	7.536	10.514	10.984	8.790	9.441	8.407
Na_2O	0.991	1.026	4.699	1.968	3.135	0.540	0.446	1.223	1.340	1.194
CaO	0.037	0.069	1.755	0.020	0.060	0.001	0.020	0.084	0.102	0.111
FeO	1.345	1.263	4.556	0.972	1.639	2.532	1.919	4.779	3.248	2.482
MgO	0.842	0.920	0.627	0.681	0.407	0.742	0.897	1.139	1.206	0.846
MnO	0.060	0.036	0.040	-	0.032	0.064	-	-	0.032	-
TiO_2	0.447	0.505	0.185	0.143	0.314	0.690	0.615	0.458	0.458	0.780
Cl	-	0.001	0.103	-	0.013	0.015	-	0.012	0.014	0.014
Total	92.487	92.306	93.185	93.349	93.078	92.188	94.327	91.225	92.798	94.315
					CATION (on the basis of 22 oxygen)					
Si	6.1809	6.1577	6.6428	6.1721	6.0813	6.3261	6.2362	6.2688	6.2065	6.9263
Al	5.4529	5.4691	4.6650	5.5905	5.6184	5.1608	5.3232	5.0587	5.2217	4.5014
K	1.7887	1.7797	1.0035	1.4676	1.3046	1.8662	1.9088	1.5845	1.6692	1.4322
Na	0.2644	0.2743	1.2322	0.5152	0.8250	0.1457	0.1178	0.3350	0.3599	0.3090
Ca	0.0055	0.0101	0.2544	0.0029	0.0087	0.0001	0.0029	0.0127	0.0152	0.0159
Fe	0.1547	0.1457	0.1760	0.1097	0.1860	0.2946	0.2186	0.5679	0.3764	0.2771
Mg	0.1727	0.1891	0.1265	0.1372	0.0823	0.1540	0.1821	0.2349	0.2491	0.1684
Mn	0.0070	0.0042	0.0046	-	0.0037	0.0076	-	-	0.0038	-
Ti	0.0463	0.0524	0.0188	0.0145	0.0320	0.0722	0.0630	0.0487	0.0477	0.0316
Cl	-	0.0003	0.0237	-	0.0030	0.0036	-	0.0030	0.0034	0.0059
Total	14.0730	14.1213	14.1848	14.1585	14.1453	14.1475	14.4303	14.1160	14.3068	14.0089

Table 4.6 continued

MICROPROBE ANALYSIS OF MUSCOVITE FROM SUTLEJ VALLEY SECTION

ELEMENTS	W 11		RR 17/22	
	WEIGHT%			
OXIDES				
SiO_2	44.862	45.389	51.099	45.216
Al_2O_3	34.912	34.637	30.867	34.802
K_2O	9.647	9.430	5.137	10.071
Na_2O	1.230	1.179	5.013	1.121
CaO	0.100	0.108	3.101	0.129
FeO	1.293	1.422	0.873	1.566
MgO	0.621	0.569	0.379	0.736
MnO	0.049	-	-	-
TiO_2	0.236	0.282	0.188	0.403
Cl	-	0.306	0.084	-
Total	92.487	92.306	96.721	94.045
CATION (on the basis of 22 oxygen)				
Si	6.1176	6.1733	6.6203	6.1168
Al	5.6117	5.5528	4.7136	5.5493
K	1.6839	1.6362	0.8490	1.7381
Na	0.3252	0.3110	1.2594	0.2941
Ca	0.0145	0.0158	0.4305	0.0187
Fe	0.1474	0.1617	0.0946	0.1772
Mg	0.1262	0.1154	0.0731	0.1485
Mn	0.0057	-	-	-
Ti	0.0242	0.0289	0.0183	0.0410
Cl	-	0.0705	0.0184	-
Total	14.0779	14.0656	14.0773	14.0837

Table 4.7 Microprobe analysis of staurolite

ELEMENTS	W 11		W 2/5		CH 10/10	
	RIM	CORE	RIM	CORE	RIM	CORE
			WEIGHT%			
OXIDES						
SiO_2	28.054	27.686	27.852	26.816	27.480	27.355
Al_2O_3	52.455	51.147	52.205	50.283	51.823	51.812
FeO	11.804	12.158	11.824	11.353	10.820	11.915
MgO	1.365	1.493	1.285	1.218	1.209	1.418
MnO	0.038	0.065	0.016	0.038	0.024	0.063
CaO	0.015	-	0.002	0.007	-	-
TiO_2	0.461	0.402	0.554	0.472	0.527	0.690
ZnO	0.347	0.161	0.149	0.025	2.639	2.356
Cr_2O_3	0.071	0.190	0.071	0.035	-	-
Total	94.610	93.303	93.956	90.247	94.522	95.609
CATION (on the basis of 48 oxygen)						
Si	8.3205	8.3475	8.3113	8.3228	8.2337	8.1441
Al	18.3379	18.1769	18.3626	18.3952	18.3025	18.1820
Fe	2.9278	3.0658	2.9508	2.9469	2.7113	2.9668
Mg	0.6036	0.6712	0.5717	0.5633	0.5401	0.6294
Mn	0.0095	0.0166	0.0041	0.0099	0.0060	0.0159
Ca	0.0049	-	0.0006	0.0022	-	-
Ti	0.1027	0.0911	0.1242	0.1102	0.1187	0.1544
Zn	0.0759	0.0358	0.0327	0.0058	0.5840	0.5179
Cr	0.0167	0.0452	0.0167	0.0087	-	-
Total	30.3995	30.4503	30.3748	30.3651	30.4963	30.6105

Table 4.8 Microprobe analysis of chloritoid

ELEMENTS	W 2/5		CH 10/10	
	RIM	CORE	RIM	CORE
	WEIGHT%			
OXIDES				
SiO_2	24.136	23,905	24.204	23.665
Al_2O_3	38.050	38.278	38.021	38.102
FeO	20.241	21.019	20.346	21.141
MgO	2.525	2.595	2.623	2.699
MnO	0.387	0.408	0.652	0.806
CaO	0.035	0.012	0.043	0.021
TiO_2	0.009	0.006	0.010	0.007
ZnO	0.011	-	-	-
Cr_2O_3	0.331	0.057	0.451	0.069
Total	85.725	86.280	86.350	84.510
CATION	(on the basis of 48 oxygen)			
Si	8.4553	8.3530	8.4861	8.3821
Al	15.7116	15.7654	15.6987	15.7241
Fe	5.9304	6.1425	5.9501	6.1642
Mg	1.3188	1.3515	1.3215	1.3710
Mn	0.1148	0.1207	0.2210	0.2401
Ca	0.0131	0.0046	0.0152	0.0079
Ti	0.0023	0.0015	0.0029	0.0018
Zn	0.0028	-	-	-
Cr	0.0917	0.0157	0.1012	0.0189
Total	31.6408	31.7549	31.7967	32.0101

higher grade rocks (Tracy, 1982). Calculated diffusion models on garnet growth and homogenisation suggest that garnet > 1 mm size can preserve growth zoning even in upper amphibolite facies condition. However, garnet of < 1 mm size undergoes intragranular volume diffusion and experiences complete homogenisation in these grades (Spear, 1988; Jiang and Lasaga, 1990; Florence and Spear, 1991). Similarly, it is observed that garnet of > 0.4 mm size preserves growth zoning in staurolite-kyanite grade and is not affected by diffusional homogenisation at this temperature condition (Florence and Spear, 1991).

To evaluate garnet zoning in pelitic rocks from the Jutogh Nappe, syntectonic garnets were analysed. The analyses were carried out along garnet diameters parallel and perpendicular to the main foliation. Analysis reveals the presence of growth zoning, having Mn-rich core and Mn-poor rim producing typical bell-shaped profile, with enrichment of Fe and Mg ratios towards the rim, indicating normal growth zoning in garnet (Fig. 4.10 a, b; Ch 10/10 and Ch 10/20). Ca shows enrichment from core to near- rim, but it shows depletion at the rim. Towards the edges, garnet shows reversal with enrichment of Mn and depletion in Mg (Fig. 4.10 a; Ch 10/10). The reversal in zoning at the rim may be because of post-metamorphic requilibration during cooling. This is evidenced from the reduction in temperature at the rim with respect to the inner rim of garnet and also by presence of retrograde chlorite replacing the garnet at the edges and biotite in the assemblage.

4 - 6 GEOTHERMOMETRY AND GEOBAROMETRY

The regional metamorphic condition is deciphered from mineral paragenesis, and by the determination of pressure and temperature, using relevant exchange or discontinuous mineral reactions for which thermo-chemical and phase

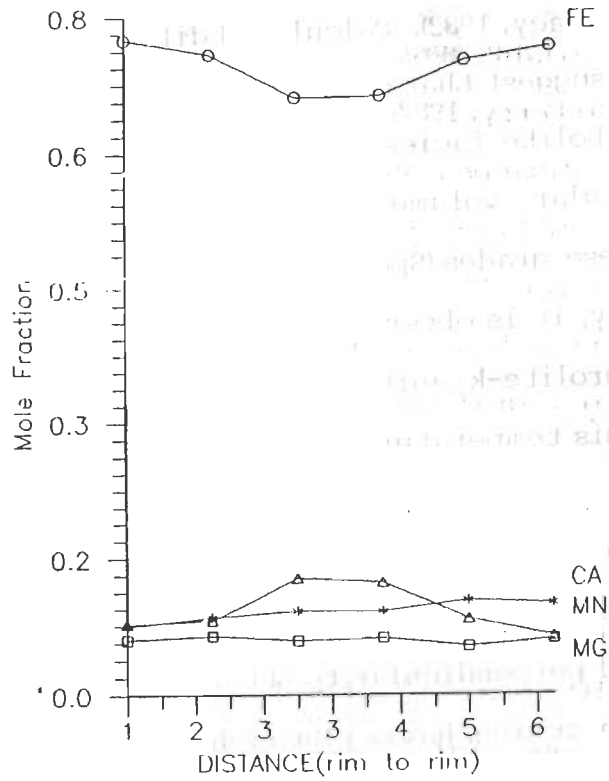

Figure 4.10 b : Garnet zoning showing bell-shaped pattern of Fe and Mn indicating normal growth zoning in sample CH 10/20 from the Chor Mountain region.

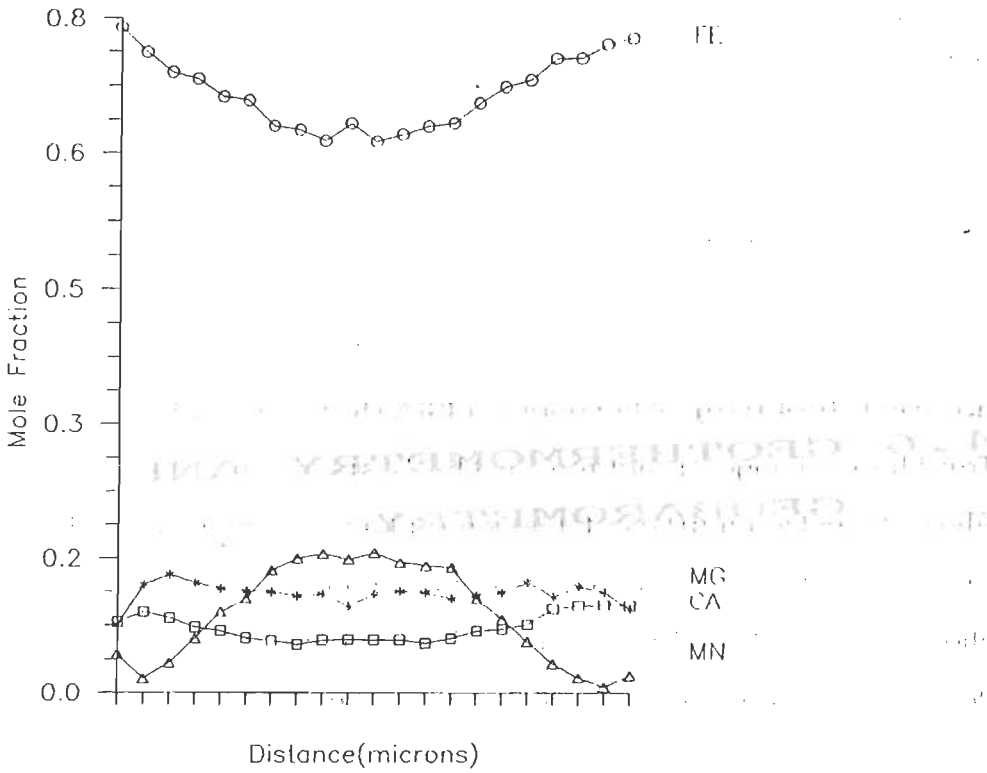

Figure 4.10 a : Garnet zoning showing bell-shaped pattern of Fe and Mn indicating normal growth zoning in sample CH 10/10 from the Chor Mountain region.

equilibria data are available (Robie *et al.*, 1966, 1978; Helgason *et al.*, 1978; Winkler, 1979; Turner, 1981; Ferry, 1982; Berman, 1988). Earlier studies emphasised more on the appearance/disappearance of index minerals and metamorphic facies, where mineral assemblages are repeated in space and time (cf., Winkler, 1979; Turner, 1981). However, P-T condition of metamorphism is evaluated thermodynamically and through phase equilibria studies in recent years, using compositions of coexisting equilibrium mineral assemblages. For this purpose, microprobe analysis of coexisting minerals, thermochemical and phase equilibria data of specific mineral systems/reactions are essential.

In the study area, the metamorphic rocks are mainly made up of metapelites and quartzites. Only pelites are considered, as these rocks contain suitable minerals such as biotite, muscovite, garnet, staurolite, kyanite, plagioclase, K-feldspar for geothermobarometric work. Metamorphism in the study area ranges from upper garnet to staurolite-kyanite grades, and therefore, garnet-biotite thermometer and garnet-plagioclase- sillimanite/kyanite-quartz and garnet-plagioclase-biotite- muscovite barometers are used for P-T determination.

4.6.1 Geothermometer

a. Garnet-biotite geothermometer (GB): The metamorphic temperature is evaluated for the exchange reaction on the basis of intracrystalline distribution of elements between sites of the same phase or intercrystalline distribution of elements between two or more coexisting phases. The exchange reactions, which show very little volume change, large entropy , insensitivity to pressure and do not reset during cooling, are ideal thermometers (Essene, 1982).

The GB geothermometer is an intracrystalline exchange reaction and applied widely in pelitic rocks, as this is a common assemblage in almost all metamorphic grades. This geothermometer has been calibrated empirically and through phase equilibria studies by number of workers, such as Thompson (1976), Goldman and Albee (1977), Ferry and Spear (1978), Ganguly and Saxena (1984) and Indares and Martignole (1985).

The intercrystalline exchange reaction is expressed as:

$KMg_3Si_3AlO_{10}(OH)_2 + Fe_3Al_2Si_3O_{12} = KFe_3Si_3AlO_{10}(OH)_2 + Mg_3Al_2Si_3O_{12}$ ---(4.1)

Phlogopite + Almandine = Annite + Pyrope

and the $K_D = (Fe/Mg)^{Bio}/(Fe/Mg)^{Gt}$.

Caliberation by Thompson (1976) and Ferry and Spear (1978) are based on ideal Fe-Mg mixing of garnet and biotite. Since garnet has variable Ca and Mn content, Ganguly and Saxena (1984) have modified Ferry and Spear's calibration, considering non- ideal mixing in garnet. However, presence of high Ti and Al^{VI} in high grade granulites led Indras and Martingole (1985) to reformulate this thermometer, considering non-ideal mixing in both the phases. In the present work, temperature has been calculated using mainly the calibrations of Ferry and Spear (1978) and Ganguly and Saxena (1984) due to the presnce of low Mn and Ca in garnet and Ti and Al in biotite. Temperatures, calculated using Ganguly and Saxena (1984) method, seem to be more realistic, while considering activities of minor elements and the overall mineral assemblages and bulk composition. The P-T data are presented in Table. 4.9.

Table 4.9 P-T data for the HHC and the Jutogh Nappe samples from the Himachal Himalaya

S.NO.	SAMPLE NO.	TEMPERATURE (°C)	PRESSURE (Kbar)
		CHOR AREA	
GARNET GRADE			
1	CH 11/21	484	
2	CH 10/20	505	5.5
3	CH 10/10	513	7.10
STAUROLITE-KYANITE GRADE			
4	CH 7/7	515	7.0
5	N 39	512	
6	N 31/1	525	7.8
7	N 4	555	7.8
8	CH 3/8	540	-
9	CH 2/3	543	6.35
		SUTLEJ VALLEY SECTION	
STAUROLITE-KYANITE GRADE			
1	W 2/5	519	-
2	RR 19	564	-
3	W 11	570	-
4	W 13	515	-
5	RR 17/22	654	-

4.6.2 Geobarometry

The metamorphic pressure is calculated using mainly the solid-solid reactions, as these reactions are not dependent on composition or presence of a fluid phase. Although solid- solid reactions generally are temperature and pressure dependent, most of the reactions are primarily used for pressure calculation, as the temperature is determined by exchange reaction. The selection of suitable reaction for pressure calculation is based on large V and H values. Many of commonly applied reactions involve minerals like plagioclase, pyroxene, garnet, sillimanite/kyanite, quartz, rutile, ilmenite etc. Since most of the minerals involved in reactions are complex solid solutions, pressure calculation is dependent on standard thermodynamic and well constrained activity-composition data of participating minerals in a reaction (Essene, 1982).

a. Garnet-plagioclase-Al_2SiO_5-quartz (GASP) geobarometry: This assemblage is widely used as a geobarometer due to its common occurrence in medium-to high-grade rocks. Ghent (1976) calibrated this geobarometer through experimental phase equilibria study for the end-member reaction:

$$3CaAl_2Si_2O_8 = Ca_3Al_2Si_3O_{12} + 2Al_2SiO_5 + SiO_2 \quad ---(4.2)$$

Anorthite Grossular Sillimanite Quartz

In this reaction, activity of grossular content in garnet is considered to be its mole fraction assuming ideal mixing and activity coefficient of anorthite is taken as 1.276 for calculating pressure (Orville 1972). However, this model has been modified later by Newton and Haselton (1981), Hodges and Spear (1982) and Koziol and Newton (1988), using different activities for grossular in garnet and anorthite in plagioclase. For the pressure calculation, only Newton and Haselton (1981) calibration has been used because of its better activity

model.

b. Garnet-muscovite-plagioclase-biotite geobarometry: Ghent and Stout (1981) developed alternative geobarometers for the medium grade, using the commonly occurring garnet-muscovite-plagioclase-biotite assemblage of pelitic rock. The end-member reactions for this assemblage are:

$$Mg_3Al_2Si_3O_{12} + Ca_3Al_2Si_3O_{12} + KAl_3Si_3O_{10}(OH)_2 = 3CaAl_2Si_2O_8 + KMg_3AlSi_3O_{10}(OH)_2 \quad ---(4.3)$$

Pyrope + Grossular + Muscovite = Anorthite + Phlogopite

$$Fe_3Al_2Si_3O_{12} + Ca_3Al_2Si_3O_{12} + KAl_3Si_3O_{10}(OH)_2 = 3CaAl_2Si_2O_8 + KFe_3AlSi_3O_{10}(OH)_2 \quad ---(4.4)$$

Almandine + Grossular + Muscovite = Anorthite + Annite

Ghent and Stout (1981) calibrated these equilibria, using pressure and temperature values, derived from GASP (Ghent *et al.*, 1979) and GB (Ferry and Spear, 1978) equilibria and also the K_D values obtained from natural assemblages. This model was modified further by Hodges and Crowley (1985), in solving uncertainities through empirical method. However, they concluded that much of the uncertainties in P-T estimation stem from uncertainities in enthalpy and entropy rather than by microprobe analysis.

Among the various geobarometers mentioned, Newton and Haselton (1981) geobarometer has been applied for rocks having garnet - plagioclase - sillimanite/kyanite - quartz assemblage. In the absence of aluminosilicate, garnet - plagioclase - biotite - muscovite barometer of Hodges and Crowley (1985) is used.

4.7 GEOTHERMOBAROMETRIC RESULTS

4.7.1 Chor Area

In the Nauhra-Shamra section of this area and close to the Chor granite, the pelitic rocks contain muscovite-biotite-quartz-garnet-staurolite-K-feldspar-plagioclase-opaque-tourmaline assemblage in the staurolite-kyanite grade. In this grade, syntectonic garnet core and rim show temperatures of about 625° C and 550° C respectively, while only the garnet rim reveal pressures of 6.4 to 7.8 kbar (Table 4.9).

While moving down towards Shamra, staurolite, chloritoid and chlorite assemblages are found with substantial reduction in feldspar and biotite in the garnet/staurolite-kyanite grade transitional zone. Garnet rim from these assemblages record temperature and pressure of 505-525° C and 5.5-7.8 kbar (Table. 4.9). Further down in the section, garnet grade rocks record a temperature of about 480° C, which is also evidenced by the presence of garnet, chlorite, muscovite and biotite in the assemblage. The section reveals disappearence of key metamorphic minerals, such as staurolite and chloritoid from top to bottom of the section near to the base of the Jutogh Nappe. Difference in rim temperatures of about 60°C from top to bottom of this section appears to real rather than apparent, hence is indicatve of the metamorphic inversion in the Jutogh Nappe.

4.7.2 Sutlej Valley Area

At the base of the hanging wall of the MCT, the pelitic rocks contain staurolite-chloritoid-garnet-chlorite-muscovite-quartz-biotite-opaque-tourmaline in the assemblage. The samples are almost completely devoid of any

feldspar. The absence of plagioclase either as inclusion in garnet or matrix assemblage does not permit calculation of pressure along this valley, and therefore, only temperaure has been calculated. Syntectonic garnet rim in staurolite-chloritoid transition zone at the base records temperature of ~520°C in these rocks (W 2/5) on the hanging wall in immediate vicinity of the MCT. While moving towrads ENE towards Jeori, chloritoid disappears with appearance of kynaite in the assemblage. The rim temperature is increased to about 50°C from the base (RR 19 to W 11) and increased further and reached a maximum temperature of ~650°C near Jeori (RR 17/22). The change in mineral assemblage corresponds with the rim temperature data. This section also provides evidences of possible metamorphic inversion in the HHC, from its base near the MCT to higher structural levels.

4.8 DISCUSSIONS

In the present areas of study, mineralogical and P-T data suggest that metamorphism remains in garnet to staurolite-kyanite grade conditions. The base of the HHC, occurring NE of Kulu-Rampur Window marks garnet and staurolite-kyanite grade transition zone, while the Jutogh Nappe is characterised by garnet zone at its base. This is evident from the presence of garnet, chloritoid, and chlorite in the garnet zone, and sometimes, by the presence of staurolite and chloritoid in the the transition zone. Chloritoid-bearing samples give temperature of about 520°C, which is less than the temperature for chloritoid-breakdown reaction. The experimental chloritoid-breakdown reactions suggest break-down temperature of 540°C to 575° C for water-pressures of 4 to 8 kb (Richardson, 1968; Hoschek, 1967). Considering the overall pressure for the study area, the rim temperature should be around 550°-560°C for this transition zone. However, the reduced rim temperatures appear to be an effect of retrograded garnet rims, as evidenced

from Mn and Mg reversals in garnet zoning. Maximum temperature of 650°C for rocks occurring further NE from the MCT in the Sutlej valley indicate that these rocks have been formed in the upper amphibolite facies condition. It is indicated by the absence of chloritoid and staurolite and the presence of significant amount of kyanite. In such temperature conditions, staurolite is no longer stable and breaks down to produce almandine and aluminosilicates (Pigage and Greenwood, 1982). Regional prograde Barrovian-type metamorphism for the studied region is evidenced from the assemblage, garnet zoning and P-T data.

CHAPTER 5: GRANITE GEOCHEMISTRY

5.1 INTRODUCTION

The Himalayan orogenic belt is characterised by numerous granite bodies of different dimensions in many tectonic zones. Strachey (1851), Oldham (1883), McMahon (1884) and Stoliczka (1866) are the pioneers in the study of Himalayan granites, which have different field relationships, ages and modes of emplacement. Based on different tectonic environment, the Himalayan plutonic bodies are broadly divided into two groups:

(a) Pre-Himalayan granitoids of Proterozoic to Paleozoic ages, and

(b) Syn- and post-tectonic Himalayan granitoids of Late Mesozoic to Miocene ages.

The Himalayan plutons constitute five major belts (Le Fort, 1988) with characteristic magmatic events. From north to south, these belts include the following :

(a) The Karakoram belt has distinct calc-alkaline to sub-alkaline magmatic activity having quartz diorite to granite rocks of Eocene to Miocene age.

(b) The Trans-Himalayan belt, lying north of the Indus- Tsangpo Suture Zone (ITSZ), is characterised by batholiths of gabbro to granite composition with ages ranging from 60 to 100 Ma.

(c) The North-Himalayan belt consists of two-mica adamalite of Early Paleozoic age.

(d) The Higher Himalayan belt of Proterozoic gneiss and contains mainly two-mica granite and biotite-tourmaline leucogranite, the latter occur close to the contact of the HHC with the Tethyan Sedimentary Zone (TSZ) and belongs to Late Cenozoic age.

(e) The Lesser Himalayan belt has concordant granite sheets of pre-Himalayan age (~ 500 Ma), characterised by discontinuous gneissic and non-gneissic granite. Granite bodies of ~ 500 Ma are also present in overthrust slab of the MCT having almost similar petrological and geochemical characters.

To understand the genetic relationships and evolutionary history of granitoid bodies from Himachal Pradesh, geochemistry of a few such bodies of the Higher Himalayan Crystalline (HHC) and the Jutogh Nappe (JN) has been carried out.

5.2 CLASSIFICATION OF GRANITE

In general, granites are classified into four main types, based on major, trace and REE geochemistry and tectonic environment. Of these, two types of granite occur more frequently (Chapple and White, 1974; White and Chapple, 1977) namely:

(i) I-type granite - broadly corresponding to biotite-hornblende tonalite association, and considered to be of igneous origin, and

(ii) S-type granite - broadly corresponding to the two-mica granite association, considered to be of sedimentary origin.

I-and S- granite classification has been further extended by White (1979 a) to A-type and M-type granites. All orogenic alkaline granites are related to A-type and calc-alkaline plagiogranite to M-type.

The I-type granite is generally derived by underplating at ocean-continental convergence plate margins and the partial melting of the subducted plate. S-type granite is characteristic of continental collision zones and encratonic ductile shear belts. In both the cases, the crust is tectonically thickened to cause the temperature at depth to rise and promote crustal melting (Pitcher, 1983). The A-type granite is present in rift-zones of the shield areas (anorogenic) and also in an orogenic belt. On the other hand, M-type granite is derived from the parental magma directly or from the subducted oceanic crust beneath the volcanic arcs.

5.3 GEOLOGICAL SETUP OF GRANITE BODIES

In NW-Himalaya, biotite- and tourmaline-bearing leucogranite regionally occurs immediately below the Tethyan Sedimentary Zone (TSZ) within Vaikrita Group of the HHC (Valdiya, 1973, 1977; Sharma, 1976), such as Leopargil, Gangotri, Badrinath, Manaslu, Makalu, Chomolhari, Thimpu and Chacha leucogranites. Besides these tourmaline-bearing granites, the HHC belt also contains biotite granite of older ages such as Karcham granite along the Baspa valley and the Kinnar Kailash granitoid having Rb-Sr isochron ages of 494 ± 50 Ma and 675 ± 70 Ma respectively (Sharma, 1983). Other nappes coeval with this unit are characterised by Proterozoic pre-Himalayan granites e.g., Wangtu, Munsiari, Dhakuri, Ramgarh, Champawat, Ranikhet, Almora, Kulu, Chor, Dalhousie, Chamba, Mandi, Rohtang etc. (Table 1.1).

Along the Sutlej Valley and Chor Mountain regions, different granites are delineated on the basis of the field relationships. Dark-coloured biotite-rich paragneiss along the Sutlej Valley is intruded by grey granite with associated aplite and pegmetite during early to syn-D_1 deformation (Chapter 3). Subsequently, grey granite and associated phases are affected by D_2 deformation producing gneissosity within the granite (Figs. 5.1 a, b). Further in the northeast, the metapelite sequence of the HHC is intruded by the Wangtu granite gneiss and porphyroclastic granite gneiss, containing metapelitic xenoliths. However, porphyroclastic granite gneiss, Wangtu granite gneiss and associated pegmatitic phase appear to be genetically related to each other. In many places, the porphyroclastic granite gneiss intrudes into the Wangtu granite and the metamorphics, thus predating the most pervasive Himalayan deformation (D_2) and metamorphism.

The grey granite is mainly found along the Maglad Khad near Jeori village, as small bodies within the garnetiferous mica schist of the Jeori Formation. This body is fine grained, almost undeformed and light grey in colour. Along the margins, it shows development of the foliation, whereas the central part is almost undeformed.

The undeformed Wangtu granite is monotonous, fine to coarse grained and is well exposed near the Wangtu bridge (Figs. 2.4 d; 3.40). Along with this granite, the associated porphyroclastic component occurs downstream along the Sutlej river. Both the granites are made up of K-feldspar, plagioclase and quartz, which are wrapped by flakes of biotite-muscovite. Feldspar porphyroclasts are buff-coloured and slightly weathered.

In the Chor Mountain area, the granite is exposed in an elliptical-shaped outcrop and is surrounded by metamorphics of the Jutogh Group (Fig. 2.2). Towards the central parts, granite becomes coarser and almost undeformed

massive body. However, approaching towards its margin with the Jutoghs, it is porphyritic, deformed and well foliated (Figs. 2.5 b; 3.35 a, b). The foliation of the deformed granitoid body is parallel to the main foliation of the metamorphic rocks (Fig. 3.33 c) and marks the D_{C1} deformation, thus emplacement of the Chor granitoid, appears to pre-date this deformation event. However, no noticeable pegmatitic activity, associated within the Chor granitoid, has been observed sofar. The Chor granitoid consists of biotite granite gneiss, porphyroclastic granite gneiss and non-foliated homogeneous granite. These granitoids are buff to grey and fine to coarse grained.

5.4 PETROGRAPHY

Grey granite from the Sutlej Valley is fine-grained, containing mainly quartz and albite with less amount of K- feldspar and microcline (Fig. 5.2 a; quartz > plagioclase > K- feldspar > microcline). Muscovite and biotite are present in significant amounts. Coarse and fine grained muscovite is common in this rock. Poorly-developed main foliation is made up of fine-grained muscovite, biotite and quartz (Fig. 5.1 a). Feldspars show minor alteration to sericite. Considering qualitatively the overall modal percentage of minerals, it falls within the tonalite field of quartz-orthoclase-plagioclase diagram (cf. Streikeisen, 1976).

The Wangtu granite body predominently contains plagioclase with less amount of K-feldspar, quartz and biotite (Fig. 5.2 b). The accessory minerals include apatite, zircon and small amount of opaques. Normative plot of this granite in a quartz-orthoclase- plagioclase diagram, falls within the quartz-monzodiorite field (cf. Streikeisen, 1976). However, qualitative modal mineralogy suggests that this rock should be more of tonalite rather than quartz-monzodiorite. Green biotite is present having inclusions of apatite and

Figure 5.1 a and b : Photograph and sketch of grey granite body intruding the dark coloured biotite paragneiss along the Sutlej valley during early to syn-D_1 deformation, subsequently affected by main deformational event D_2. Note slight penetrative displacement along gentle dipping S_2 foliation towards top-to-left (southwestward). Also cutting across S_1 foliation are northeasterly dipping. Crenulation foliation S_{3b} planes also indicate displacement. BG/BS - Biotite granite gneiss/Biotite schist, GR - grey granite gneiss.

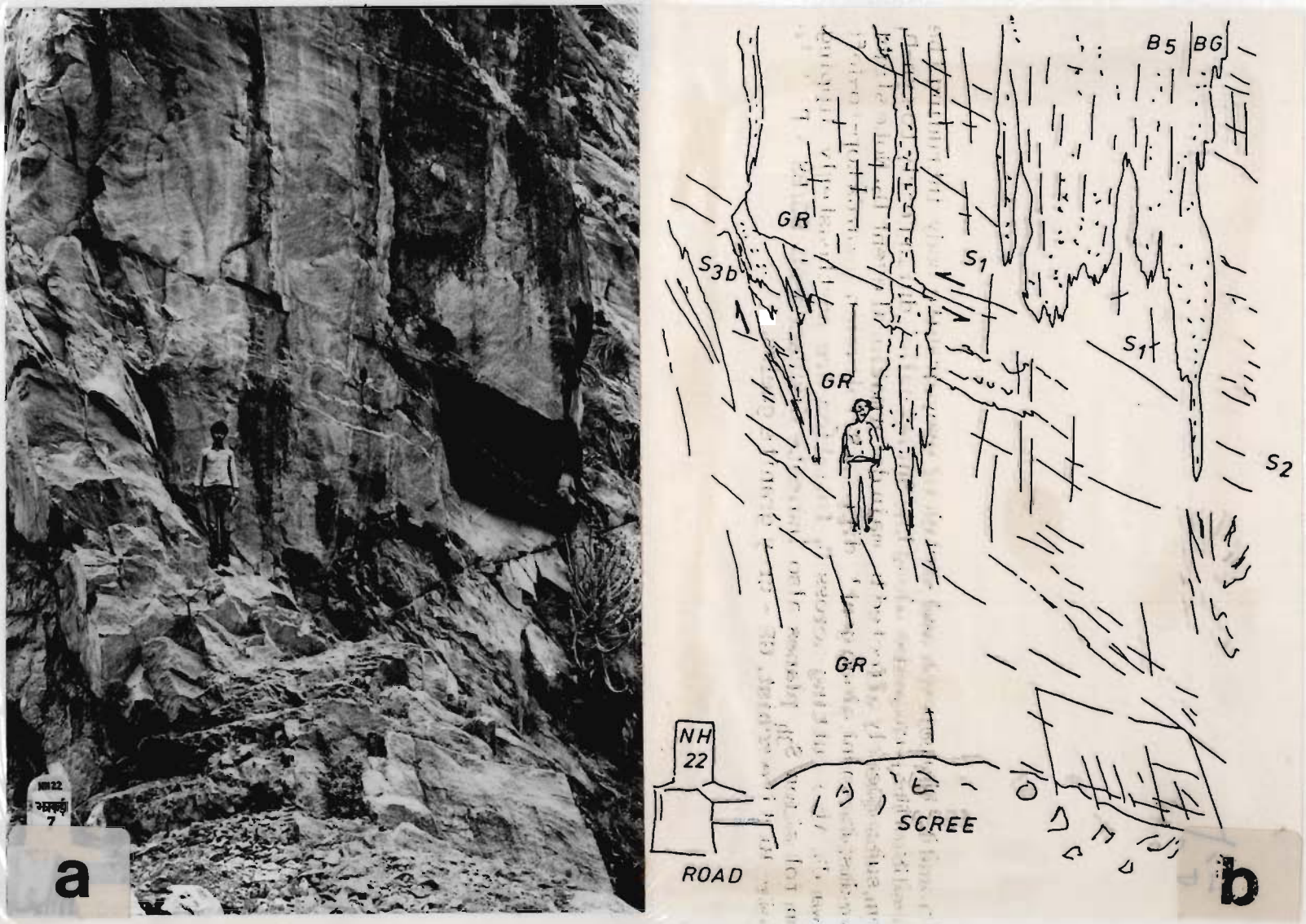

FIG. 5.1

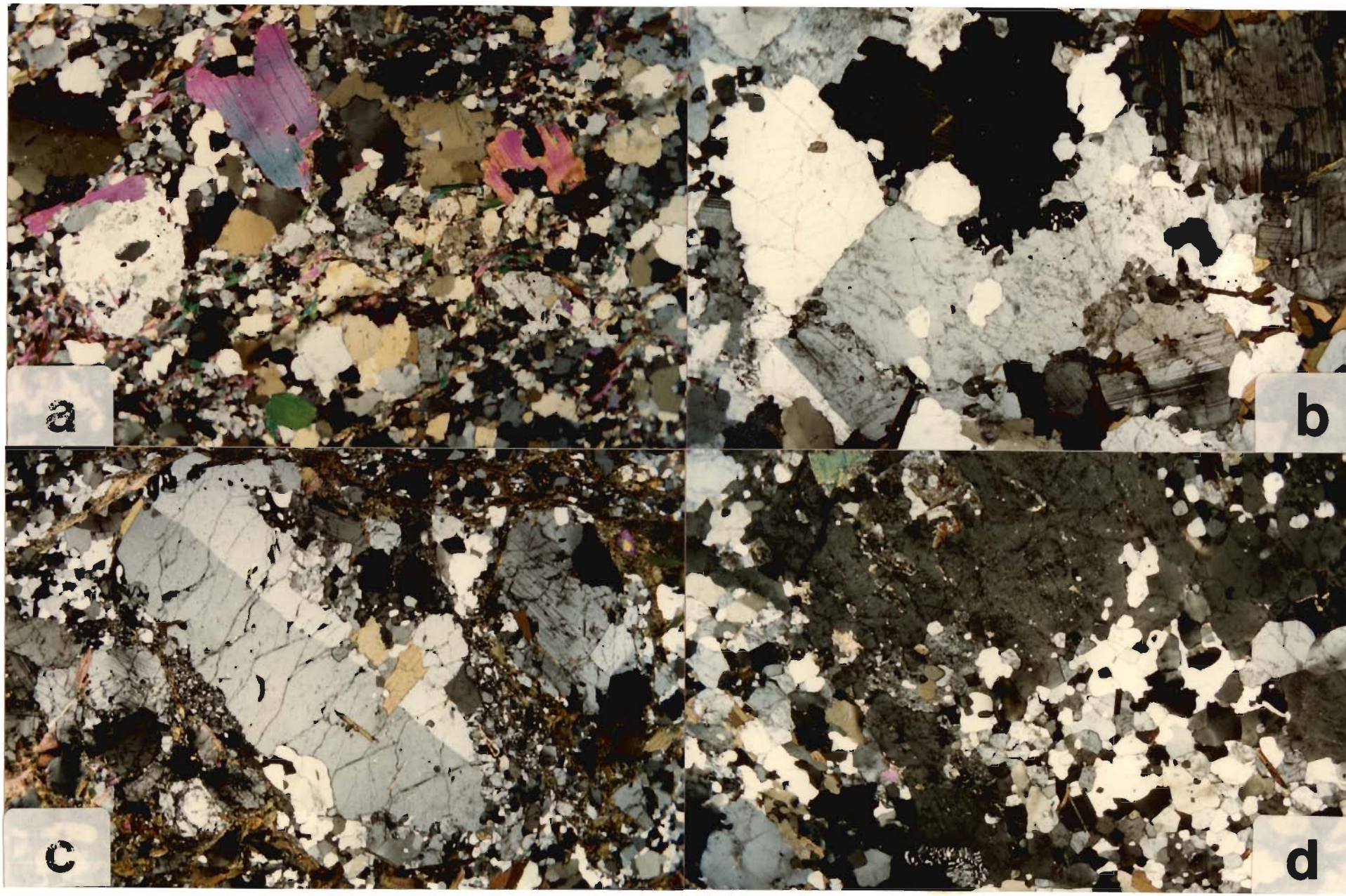

FIG. 5.2

Figure 5.2 a : Grey granite gneiss (W 14/14) with porphyroclastic growth of muscovite and feldspar. Incipient foliation distinct due to mica flakes and quartz. Crossed X 72.

Figure 5.2 b : Wangtu granitoid (W 17/16), hypidiomorphic texture having subhedral to anhedral plagioclase, quartz and green biotite. Note myrmekitic growth around K-feldspar. Crossed X 72.

Figure 5.2 c : Porphyroclastic granite gneiss (C 10) from the HHC having large twinned K-feldspar megacrst. Also containing sodic plagioclase. Note cataclastic margins of feldspars and surrounded by biotite and finely commuted mica along the foliation. Crossed X 72.

Figure 5.2 d : Chor granitoid (CH/RN) showing porphyritic character with inclusions of quartz and sericitised plagioclase in K-feldspar. Groundmass made up of recrsytallised polygonised quartz. Poorly foliated due to preferred orientation of green biotite and elongated quartz. Crossed X 72.

zircon. At places, plagioclase shows development of quartz-feldspar myrmekite, indicating partial melting and recrystallisation of plagioclase (Fig. 5.2 b). Some of the plagioclases are zoned suggesting disequilibrium conditions during its crystallization. Development of epidote is seen at the expense of plagioclase in some places, denoting later fluid activity during subsequent deformation and metamorphism. Feldspars show sericitization indicating minor retrogression.

The porphyroclastic granite is texturally similar to the Wangtu granite, but slightly different in minerological composition. The modal analysis shows that this rock contains plagioclase, K-feldspar and quartz in almost equal amounts (Fig. 5.2 c) and falls within the granite field of the quartz-orthoclase-plagioclase modal plot (cf. Streikeisen, 1976). The rock mostly contains potash feldspars of porphyritic character (Fig. 5.2 c). Biotite is comparetively less, having inclusions of apatite and zircon.

The Chor granite is mineralogically similar to the Wangtu granite. The main constituent is plagioclase, having zoning and alteration in a few cases (Fig. 5.2 d). Quartz is fine grained and occurs mainly in the matrix with little K-feldspar. Green biotite is present in this rock. The modal plot in a quartz-orthoclase-plagioclase diagram suggest that it is a quartz-monzodiorite (cf. Streikeisen, 1976).

5.5 PETROCHEMISTRY

To characterise these granitoids geochemically and to understand their genetic relations, four samples have been collected from each of these granitoid bodies namely, grey granite, porphyroclastic granite gneiss and Wangtu granitoid, while three samples from the Chor granitoid have been analysed for major, trace and REE elements.

5.5.1 Analytical Procedures

Major and trace elemental analyses of these granitoids were carried out using Energy dispersive XRF technique (Philips model: EDEX-EXAM SIX). The instrumental condition used are mentioned in Table 5.1. The emission intensity of this characteristic radiation is measured with the suitable X-ray spectrometer (Potts, 1987) using international reference standard samples (Govindraju, 1989). Pressurised-powder pellets of samples have been used with a measurement accuracy better than 5 % and 10% for major and trace elements respectively.

TABLE 5.1: ANALYTICAL CONDITIONS FOR THE MAJOR AND TRACE ELEMENTAL ANALYSIS

ELEMENTS	TUBE VOLTAGE	TUBE CURRENT	PATH	LIVE TIME
All major elements	12 KV	400 µA	VAC no filter	200 sec.
Ga, Pb, Th, Rb, Sr, U, Y, Zr, Nb	40 KV	250 µA	AIR with Ag filter	500 sec.

The rare-earth-element (REE) analysis was carried out on the Inductively

Coupled Plasma (ICP) spectrometer, using the solutions of dissolved rock samples. Rock JG-2 (GSJ granite; Govindraju, 1989) and synthetic salts were used as standards.

For XRF analysis, 3 gm of rock powder is mixed with two drops of polyvinyl alcohol and stirred thoroughly into a paste in agate mortar. The sample paste is mixed with boric acid and compressed in hydraulic press at 10 kbar for about 3 minutes to make the pellets.

The rare-earth-elements (REE) were analysed following a chromatographic seperation and preconcentration method of Walsh *et al.* (1981) after certain modifications. Approximately 0.5 gm of sample has been taken in a flat-bottom 60 ml teflon beaker and digested with hydrofluoric (HF) acid. After initial acid attack using hydrofluoric-perchloric mixture, the solution is evaporated to incipient dryness to permit all the silica to be lost by volatilisation as silicon tetrafluoride (SiF_4). This step has been repeated to dissolve the sample completely. After drying, the residue is dissolved in 25 ml of 10% HCl and made to 50 ml volume. Mini-fusion has also been carried out on undissolved minerals like zircon, tourmaline etc., in the sample. For the mini-fusion, the solution was filtered on ashless paper and dried in oven. The dried filter paper was burnt in platinum crucible to remove the filter paper and the residue is fused with in 0.2 gm anhydrous lithium tetraborate (LiB_4O_7) with one drop of lithium bromide (LiBr) in FLUXY fusion appratus. The fused flux was dissolved in already prepared sample solution and made to volume.

For the REE separation, the sample solution was loaded on to ion-exchange column containing DOWEX AG 8X (200-400 mesh) resin, which was washed with 450 ml 4 N HCl to remove the major elements. After washing, the column was again eluted with 450 ml 1.7 N HCl to remove some of the trace elements (all Ba, some Sr, Zr, Hf) were retained quantitatively in the column. The REEs were then eluted from the

column with 600 ml 1 N HCl. The eluted REE fraction was then evaporated to dryness and made to a volume of 10 ml. One standard rock sample (JG-2 : GSJ granite; Govindraju, 1989) and a blank were also prepared. Finally, the REEs were determined using the sequential monochrometer of an ICP-AES (make: JOBIN YUON, model JY 70 PLUS).

5.6 RESULTS

5.6.1 Major Element Geochemistry

Analyses of major element data indicate that three distinct types of granite exist in this region. The Wangtu granite and porphyroclastic granite gneiss can be grouped together due to their almost similar geochemical character, whereas the Chor granite and grey granite are different in chemical composition. All the granites have Al_2O_3/Na_2O+K_2O+CaO ratio > 1 and Na_2O/K_2O < 1 indicating their peraluminous and peralkaline character (Table 5.2).

The grey granite is characterised by high silica and alkalis ($Na_2O + K_2O$), low in FeO, CaO and TiO_2 contents (Table 5.2). The Na_2O vs K_2O plot shows that this granite falls in the granodiorite composition field (Fig. 5.3 a), and in granite and quartz-monzonite fields in quartz-orthoclase-plagioclase normative plot (Table 5.3; Fig. 5.3b; Streikeisen, 1976). However, in the Nomenclature and Characteristic mineral diagrams (Table 5.4; cf., Debon and LeFort, 1982), it falls in the granite and quartz-syenite fields (Fig. 5.4 a) and mainly in sector II, except one sample in sector III (Fig. 5.4 b). In the silica variation diagrams, FeO, Na_2O, K_2O, TiO_2 and Al_2O_3 components show negative correlation; CaO and MnO give positive correlation and no correlation for P_2O_5 (Figs. 5.5-5.7).

TABLE 5.2 Major oxides data in wt% of different granitoids from the HHC and the Jutogh Nappe of Himachal Pradesh

	PORPHYROCLASTIC GRANITE				WANGTU GRANITOID				GREY GRANITOID				CHOR GRANITOID		
	C1	C7	C10	J20	RR 7/6	W 17/16	W 17/17	W 17/18	RR 17/21	W 14/13	W 14/14	W 14/15	CH 1/1	CH 3/9	CH /RN
SiO_2	70.92	72.1	69.96	71.14	68.9	63.23	70.32	71.49	72.66	68.47	69.21	67.4	65.23	65.15	64.26
Al_2O_3	14.46	14.24	14.47	15.44	14.98	17.72	14.12	14.35	14.82	17.33	16.22	17.38	15.87	15.43	17.01
Fe_2O_3	0.65	0.6	0.83	0.35	0.9	1.06	0.85	0.47	0.31	0.31	0.39	0.42	1.06	1.01	0.57
FeO	2.61	2.42	3.31	1.39	3.59	4.25	3.39	1.86	1.24	1.24	1.58	1.7	4.23	4.05	2.28
MgO	0.7	0.53	0.96	0.3	0.98	1.45	0.91	0.52	0.00	0.06	0.4	0.42	1.75	2.0	2.85
CaO	1.27	1.49	2.04	0.91	2.33	2.48	2.17	1.22	0.8	0.93	0.5	0.41	1.41	2.75	1.59
Na_2O	3.74	3.02	2.78	4.11	4.27	4.33	3.65	4.21	4.17	5.23	3.97	5.21	3.76	3.81	4.53
K_2O	4.47	5.43	4.93	6.18	4.76	5.6	4.43	6.7	5.46	6.25	5.95	6.23	4.88	4.74	7.75
TiO_2	0.45	0.43	0.62	0.14	0.46	0.6	0.46	0.3	0.1	0.14	0.14	0.12	0.64	0.77	0.64
P_2O_5	0.22	0.25	0.22	0.43	0.26	0.12	0.24	0.1	0.43	0.47	0.45	0.37	0.22	0.44	0.22
MnO	0.04	0.04	0.06	0.04	0.07	0.07	0.07	0.03	0.04	0.02	0.04	0.04	0.11	0.08	0.03
Total	99.52	100.54	100.28	100.44	101.49	100.93	100.62	101.24	100.03	100.44	98.85	99.3	99.16	100.22	100.5
Na_2O/K_2O	0.84	0.56	0.56	0.67	0.90	0.77	0.82	0.63	0.76	0.84	0.67	0.84	0.77	0.80	0.58
$Al_2O_3/(CaO+Na_2O+K_2O)$	1.53	1.43	1.48	1.38	1.32	1.43	1.38	1.18	1.42	1.40	1.56	1.47	1.58	1.37	1.23

Table 5.3 CIPW normative data of different granitiods from the HHC and the Jutogh Nappe of Himachal Pradesh

	PORPHYROCLASTIC GRANITE				WANGTU GRANITOID				GREY GRANITOID				CHOR GRANITOID		
	C1	C7	C10	J20	RR 7/6	W 17/16	W 17/17	W 17/18	RR 17/21	W 14/13	W 14/14	W 14/15	CH 1/1	CH 3/9	CH /RN
Quartz	26.279	27.926	26.564	20.497	17.520	5.788	23.908	17.698	25.546	11.457	20.861	10.810	15.868	13.360	0.00
Orthoclase	26.440	32.118	29.160	36.554	28.155	33.123	26.203	39.630	32.295	36.968	35.194	36.850	28.865	28.037	45.840
Albite	31.609	25.524	23.495	34.736	36.088	36.595	30.848	35.581	34.821	44.202	33.553	44.033	31.778	32.201	38.286
Anorthite	6.044	7.136	9.736	4.256	7.604	11.855	9.016	0.419	3.710	4.486	2.221	1.774	6.282	10.952	3.128
Corundum	1.239	0.761	0.975	0.411	0.000	0.170	0.000	0.000	0.756	0.298	2.417	1.397	2.084	0.000	0.000
Hypersthene	6.472	5.654	8.408	2.560	7.188	11.460	7.681	2.341	1.494	1.652	3.093	3.433	12.082	11.383	8.383
Magnetite	0.942	0.870	1.203	0.507	1.305	1.537	1.232	0.681	0.449	0.449	0.565	0.609	1.537	1.464	0.826
Ilmenite	0.418	0.475	0.608	0.817	0.494	0.228	0.456	0.190	0.817	0.893	0.855	0.703	0.418	0.836	0.418
Apatite	0.095	0.095	0.142	0.095	0.166	0.166	0.166	0.071	0.095	0.047	0.095	0.095	0.260	0.189	0.418
TOTAL	99.538	100.558	100.292	100.434	101.510	100.922	100.620	101.256	99.983	100.453	98.854	99.704	99.175	100.245	101.741
Quartz-(Albite+Anorthite)-Orthoclase Plot															
Quartz	29.1	30.1	29.9	21.3	19.6	6.6	26.6	19.0	26.5	11.8	22.7	11.6	19.2	15.8	0.0
Ab+An	41.7	35.2	37.4	40.6	48.9	55.5	44.3	38.6	40.0	50.1	39.0	49.0	46.0	51.0	47.5
Orthoclase	29.2	34.7	32.7	38.1	31.5	37.9	29.1	42.5	33.5	38.1	38.3	39.4	34.8	33.2	52.5

Table 5.4 Gram atoms * in 100 gm of material data used for Nomenclature Diagram and Characteristic mineral diagram of different granitiods from the HHC and the Jutogh Nappe of Himachal Pradesh

	PORPHYROCLASTIC GRANITE				WANGTU GRANITOID				GREY GRANITOID				CHOR GRANITOID		
	C1	C7	C10	J20	RR 7/6	W 17/16	W 17/17	W 17/18	RR 17/21	W 14/13	W 14/14	W 14/15	CH 1/1	CH 3/9	CH /RN
Si	1182.00	1201.67	1166.0	1185.67	1148.33	1053.83	1172.00	1191.50	1211.00	1141.17	1153.50	1123.33	1087.17	1085.83	1071.00
Al	283.53	279.22	283.73	302.75	293.73	347.45	276.86	281.37	290.59	339.80	318.04	340.78	311.18	361.37	333.53
Fe	40.75	37.75	51.75	21.75	56.13	66.38	53.00	29.13	19.38	19.38	24.63	26.50	66.13	63.25	35.63
Mg	17.50	13.25	24.00	7.50	24.50	36.25	22.75	13.00	0.00	1.50	10.00	10.50	43.75	50.00	71.25
Ca	22.68	26.61	36.43	16.25	41.61	44.29	38.75	21.79	14.29	16.61	8.93	7.32	25.18	49.11	28.39
Na	120.65	97.42	89.68	132.58	137.74	139.68	117.74	135.81	134.51	168.71	128.07	168.07	121.29	122.90	146.13
K	95.11	115.53	104.89	131.49	101.28	119.15	94.26	142.55	116.17	132.98	126.60	132.55	103.83	100.85	164.89
Ti	5.63	5.38	7.75	1.75	5.75	7.50	5.75	3.75	1.25	1.75	1.75	1.50	8.00	9.63	8.00
P	3.10	3.52	3.10	6.06	3.66	1.69	3.38	1.41	6.06	6.62	6.34	5.21	3.10	6.20	3.10
Mn	0.56	0.56	0.85	0.56	0.99	0.99	0.99	0.42	0.56	0.28	0.56	0.56	1.55	1.13	0.42
Al-(Na+K+2Ca) = A	22.42	13.05	16.30	6.18	-28.51	0.05	-12.63	-40.56	11.33	5.00	45.52	25.52	35.70	39.40	-34.28
Fe+Mg+Ti= B	63.88	56.38	83.5	31.00	86.38	110.13	81.5	45.88	20.63	22.63	36.38	38.5	117.88	122.88	114.88
Si/3-(K+Na+2Ca/3)= Q	163.13	169.87	169.81	120.32	116.02	62.93	152.84	104.28	143.46	67.63	123.89	68.95	120.48	105.45	27.05
K-(Na+Ca)= P	-48.22	-8.50	-21.21	-17.34	-78.07	-64.81	-62.24	-15.04	-32.63	-52.34	-10.40	-42.83	-42.64	-71.16	-9.63

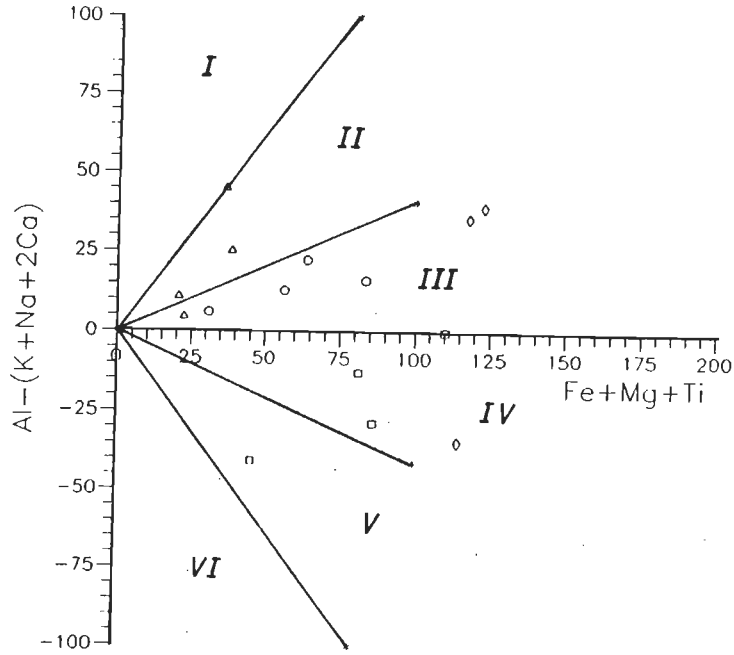

Figure 5.4 b : Characteristic mineral plot showing different granitoid bodies from the Himachal Pradesh (after Debon and Le Fort, 1982).

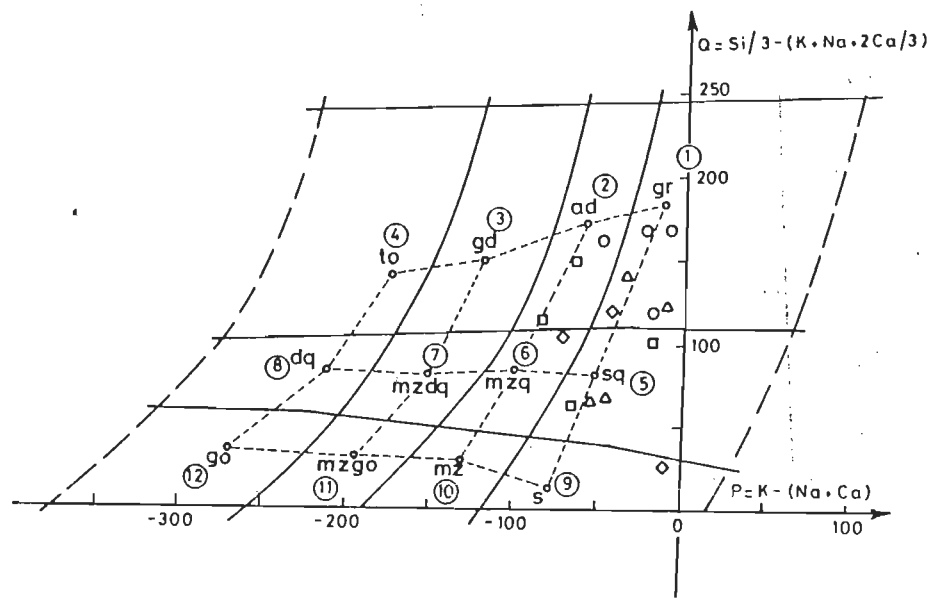

Figure 5.4 a : Nomenclature plot showing different granitoid bodies from the Himachal Pradesh (after Debon and Le Fort, 1982).

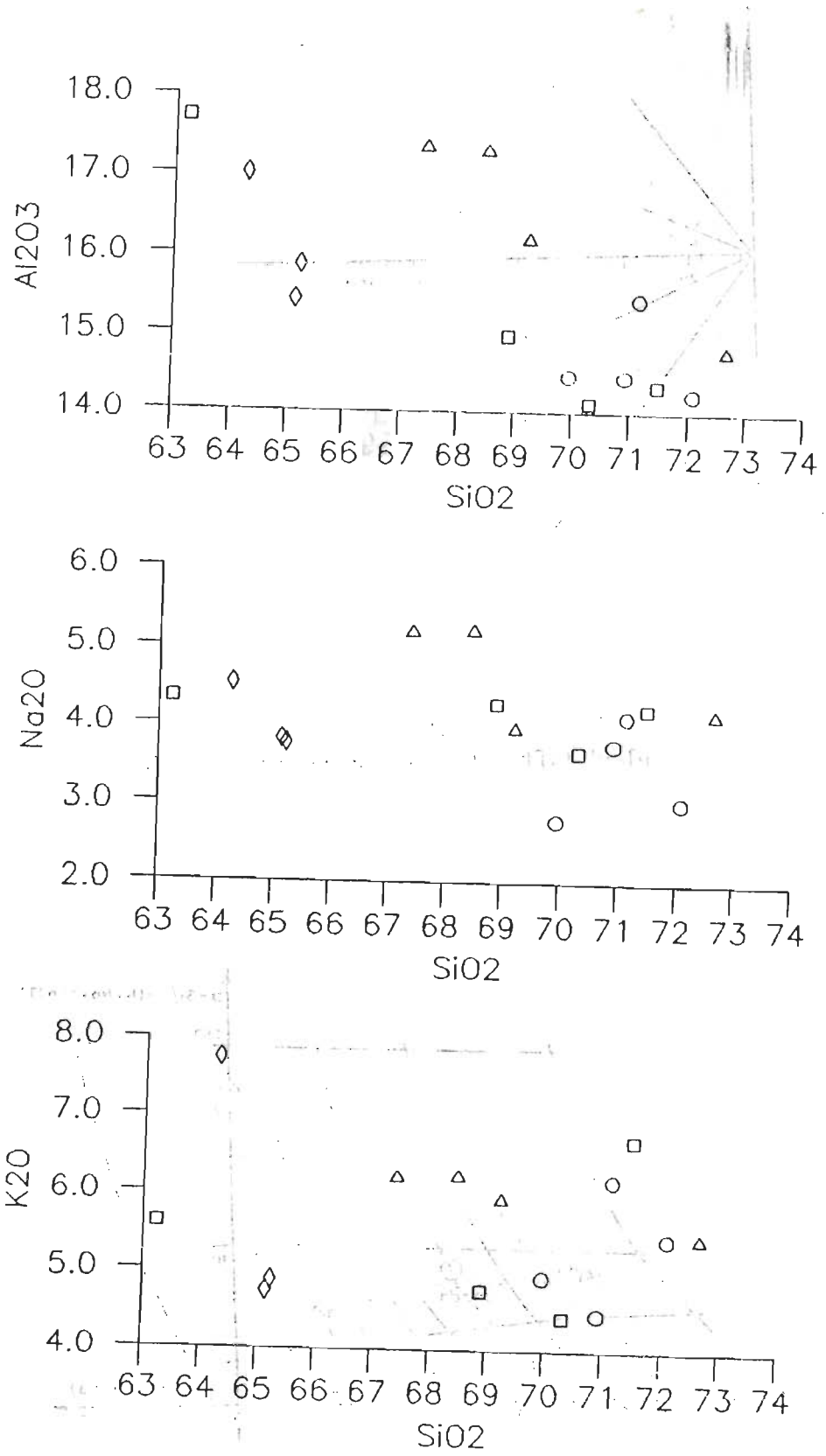

Figure 5.5 : SiO_2 variation vs K_2O, Na_2O and Al_2O_3 diagrams showing trend of different granitoid bodies from the Himachal Pradesh.

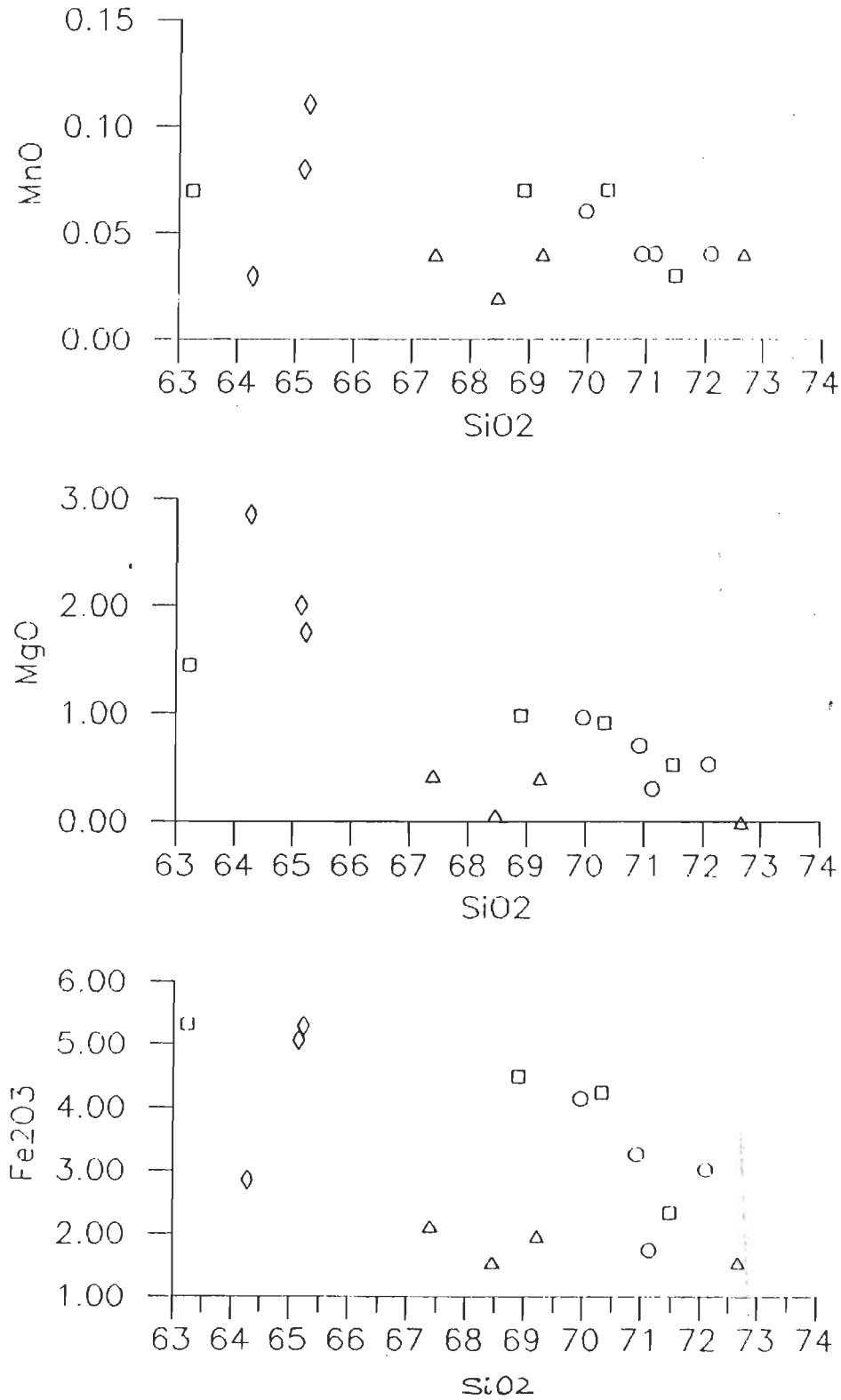

Figure 5.6 : SiO_2 variation vs Fe_2O_3, MgO and MnO plots for different granitoid bodies from the Himachal Pradesh.

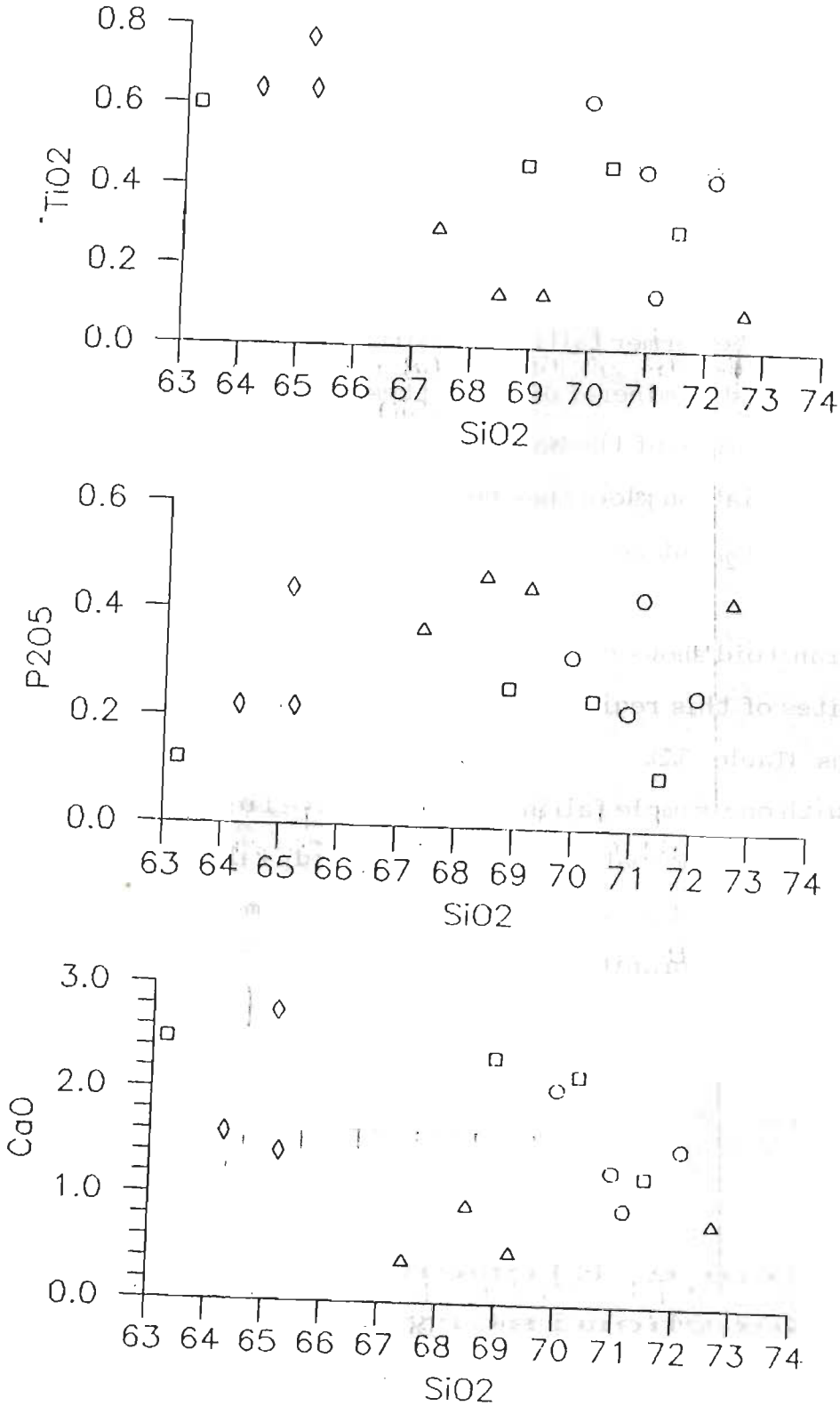

Figure 5.7 : SiO_2 variation vs. CaO, P_2O_5 and TiO_2 plots of different granitoid bodies from the Himachal Pradesh.

The Wangtu granitoid body and porphyroclastic granite are characterised by similar silica and alkalis as that of grey granite (Table 5.2). However, on the Na_2O vs K_2O plot, these bodies fall in granodiorite and tonalite fields (Fig. 5.3 a). In quartz-orthoclase-plagioclase normative plot, these are in granite and quartz-monzonite fields respectively (Table 5.3; Fig. 5.3 b; Streikeisen, 1976). In the Nomenclature diagram, these plot in adamellite and granite fields, except for two samples of the former falling in quartz-syenite field (Table 5.4; Fig. 5.4 a). In the Characteristic mineral diagram, these samples plot in sector III and IV, except for one sample of the Wangtu body falling in sector V (Table 5.4; Fig. 5.4 b). The silica variation plots show negative correlation with Na_2O, Al_2O_3, FeO, MgO, MnO, CaO and TiO_2, but no correlation with K_2O and P_2O_5 (Figs. 5.5-5.7).

The Chor granitoid shows comparatively low silica content, when compared to other granites of this region and has appreciably higher FeO, MgO and TiO_2 concentrations (Table 5.2). The Na_2O vs K_2O plot indicates granodiorite composition, with one sample falling in the tonalite field (Fig. 5.3 a). In quartz-orthoclase-plagioclase normative plot, the Chor body falls in quartz-monzonite and monzonite fields (Table 5.3; Fig. 5.3 b). In the Nomenclature diagram, this granitoid falls close to granite and quartz monzonite field (Table 5.4; Fig. 5.4 a), whereas this falls in sector III and IV in the Characteristic mineral diagram (Table 5.4; Fig. 5.4 b). The silica variation diagram does not reveal clear correlation with any of the oxides (Figs. 5.5-5.7).

5.6.2 Trace Elemental Geochemistry

Trace element data have been frequently used in quantitative modelling of petrogenetic processes and are well established in studies of oceanic basalts (Hanson, 1980). Although trace element modelling is more difficult in rocks of

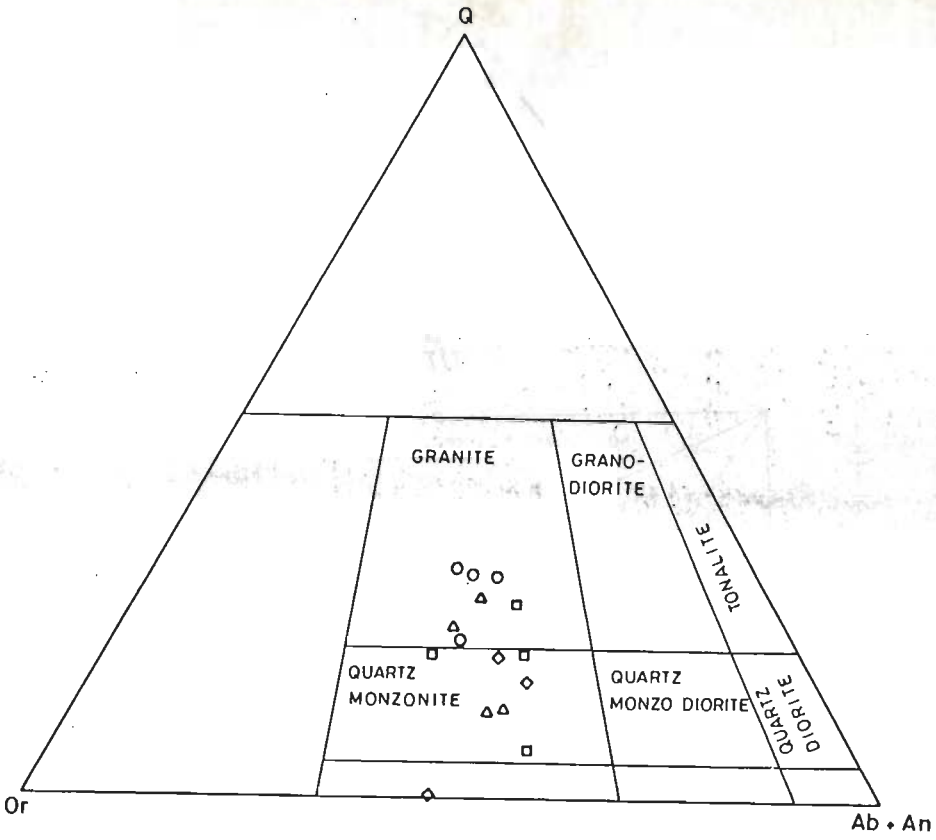

Figure 5.3 b : Quartz-orthoclase-plagioclase normative plot showing different granitoid bodies from the Himachal Pradesh (after Streikeisen, 1976).

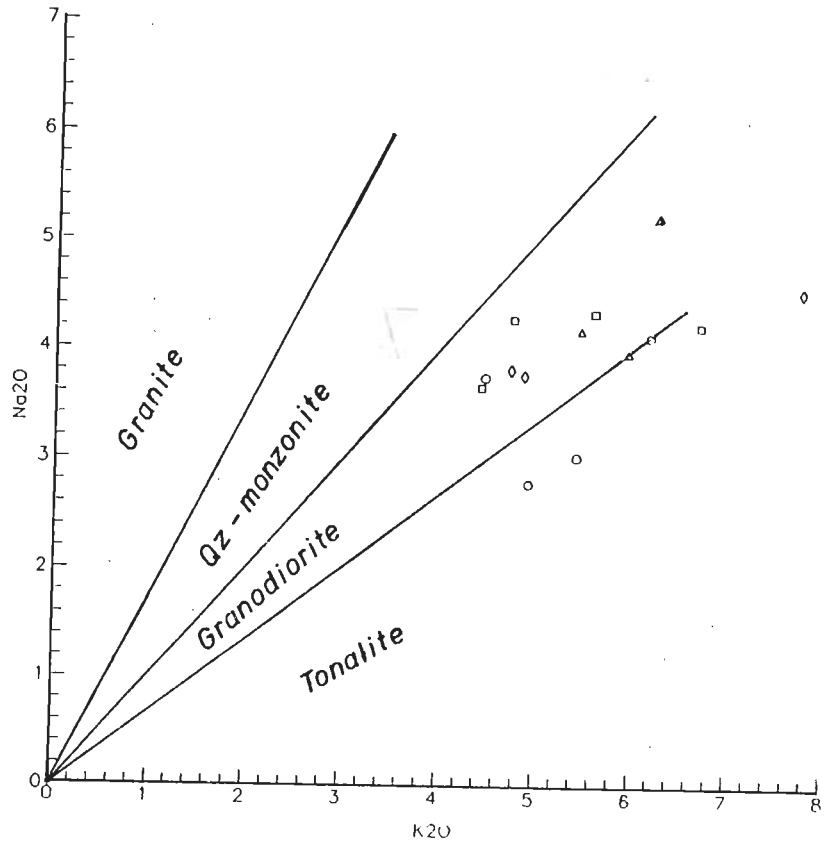

Figure 5.3 a : Na_2O vs K_2O plot showing different granitoid bodies from the Himachal Pradesh.

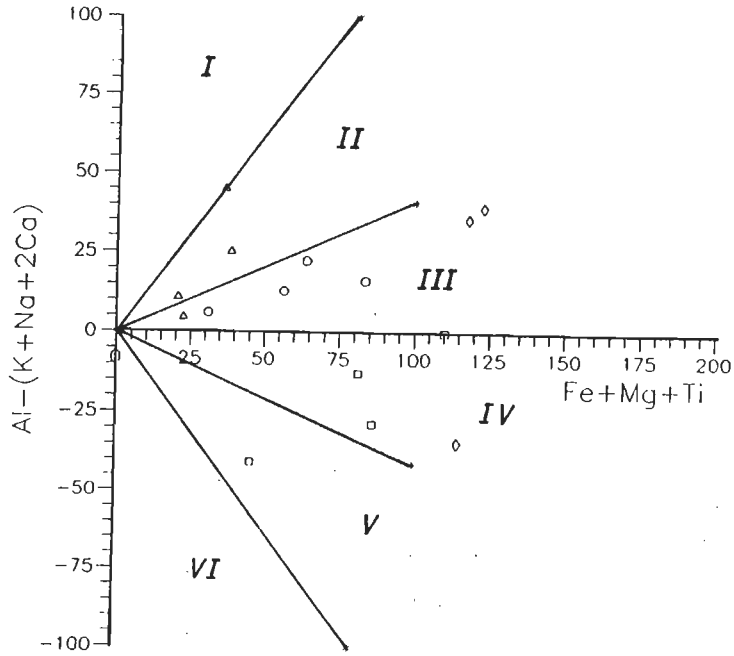

Figure 5.4 b : Characteristic mineral plot showing different granitoid bodies from the Himachal Pradesh (after Debon and Le Fort, 1982).

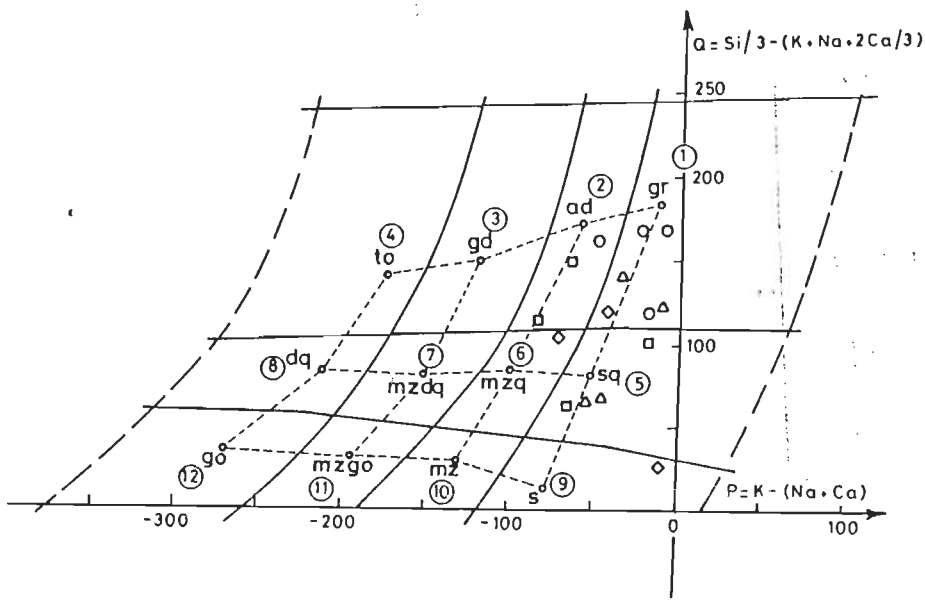

Figure 5.4 a : Nomenclature plot showing different granitoid bodies from the Himachal Pradesh (after Debon and Le Fort, 1982).

other compositions, particularly in granites, some attempts have recently been made to model granite petrogenesis (Chappel and White, 1974; Hanson, 1980). Limited trace element data of these Proterozoic granitoids have been used to understand the petrogenesis (Table 5.5).

All the samples of the grey granitoid body of the HHC have a consistent pattern (Fig. 5.8 a) and a distinctly lower abundance in Pb, Th, Nb, Sr and Ti and possess higher Ga, Rb, U, K, P and Y values and consistent Rb/Sr ratio (Table 5.5; Fig. 5.8 a). However, the spidergram plot shows lower values for Th, Nb, Ce, Sr, Sm, Ti and similar abundances in Rb, U, K, P Zr and Y with each other (Fig. 5.8 a). This body possesses distinctive negative anomalies for Th, Nb, Sr and Ti (Fig. 5.8 a).

Four samples from the Wangtu body also reveal a good and consisitent pattern (Fig. 5.8 b). This body has similar trace element abundances in Ga, Pb, Th, Rb, Sr, U, Zr, Nb, K, P and moderate K/Rb ratio (Table 5.5). The Spidergram plot shows similar abundances in Rb, U, K, Sr, and Y; lower values of Nb, Sr, P and Ti and moderate variations in the abundances of Th, Nb, P and Zr. This body posseses negative anomalies in distinctive Sr, P and Ti (Fig. 5.8 b)

The porphyroclastic granite gneiss possesses consistent trend in many trace elements, except sample J 20 revealing anomalous trend in some of the elements (Table 5.5; Fig. 5.8 c). Similar abundance can be noticed in Ga, Pb, Rb, Sr, U, K and Y and moderate K/Rb ratio in all the samples (Table 5.5; Fig. 5.8 c). The spidergram shows identical abundances in all the samples for Rb, U, K, Sr and Y; lower values in K, Nb, Sr and Ti with variation in values of Th, Nb, P, Zr and Ti (Fig. 5.8 c). This body reveals a distinctive Sr and Ti negative anomalies (Fig. 5.8 c).

The Chor granitoid body reveals three distinct rock units: (a) large portion of the body is made up of undeformed granite (sample CH 1/1), (b) marginal porphyritic granite (CH R/N) and (c) deformed mylonitised augen gneissose

TABLE 5.5 Trace elemental data in ppm of different granitiods from the HHC and the Jutogh Nappe of Himachal Pradesh

	PORPHYROCLASTIC GRANITE				WANGTU GRANITOID				GREY GRANITOID				CHOR GRANITOID		
	C1	C7	C10	J20	RR 7/6	W 17/16	W 17/17	W 17/18	RR 17/21	W 14/13	W 14/14	W 14/15	CH 1/1	CH 3/9	CH /RN
Fe	2.76	2.64	3.73	1.45	3.91	5.27	3.69	2.18	1.31	1.34	1.53	1.64	4.85	5.05	3.05
Ga	19.85	20.27	20.69	18.13	19.72	23.15	21.21	20.98	20.86	18.89	18.96	19.59	21.42	25.09	21.15
Pb	43.53	43.45	50.04	42.83	36.15	46.7	36.07	47.53	26.3	20.93	17.52	24.04	24.99	60.64	54.65
Th	53.46	48.19	57.0	14.65	24.78	43.31	24.34	48.73	9.3	1.88	2.34	4.73	34.3	55.86	1.62
Rb	243.92	350.61	290.06	276.81	243.54	352.3	252.12	326.43	252.23	282.72	292.95	271.5	258.91	205.61	197.36
Sr	105.54	112.18	140.19	91.18	156.95	187.00	138.00	108.29	80.79	82.27	64.66	57.97	168.94	799.31	1093.25
U	9.85	14.89	11.62	10.76	9.32	15.12	9.83	13.81	9.6	11.0	11.25	10.05	10.04	10.21	10.1
Y	38.54	41.06	36.18	35.46	28.1	46.56	32.56	39.48	32.68	37.8	35.92	30.94	34.44	31.34	26.45
Zr	208.86	193.7	278.09	82.39	272.89	439.91	271.13	161.59	76.74	80.99	80.34	74.43	190.08	324.51	136.96
Nb	24.76	20.44	25.24	6.51	15.26	29.27	21.86	16.44	4.43	10.87	8.86	3.84	20.15	38.28	15.86
Na	27745.1	22403.8	20623.4	30489.9	31676.9	32122.0	27077.5	31231.8	30935.1	38798.7	29451.4	38650.3	27893.5	28264.4	33605.7
K	37111.3	45081.5	40930.4	51308.3	39518.9	46492.9	36779.2	55625.5	45330.6	51889.4	49398.7	51723.4	40515.3	39352.9	64342.90
Na/K	0.75	0.50	0.50	0.60	0.80	0.70	0.74	0.56	0.68	0.75	0.60	0.75	0.69	0.72	0.52
K/Rb	152.2	128.6	141.1	185.4	162.3	131.9	145.9	170.4	179.7	183.5	168.6	190.5	156.5	191.4	326.0
Rb/Sr	2.31	3.13	2.07	3.04	1.55	1.88	1.83	3.01	3.12	3.44	4.53	4.68	1.53	0.26	0.18
Rb/Y+Nb	3.85	5.70	4.72	2.68	5.62	4.65	4.63	5.84	6.80	5.81	6.54	3.41	4.74	2.95	4.67

Table 5.6 Trace elements data in ppm used in Spidergram of different granitiods from the HHC and the Jutogh Nappe of Himachal Pradesh

	Wangtu Granitoid	Chor Granitoid	Porphyro-clastic Granite	Grey Granitoid	Primordial Mantle
Rb	243.54	258.91	290.06	252.23	0.86
Th	24.78	34.3	57.00	9.3	0.096
U	9.32	10.04	11.62	9.6	0.027
K	39519.0	40515.3	40930.4	45330.6	252.0
Nb	15.26	20.15	25.24	4.43	0.62
La	53.12	68.23	88.47	9.6	0.71
Ce	111.4	133.9	186.4	21.8	1.90
Sr	156.95	168.94	140.19	80.79	23.0
Nd	45.52	51.65	68.95	16.19	1.29
P	1134.7	960.1	960.1	1876.6	90.4
Zr	272.89	190.08	278.09	76.74	11.0
Sm	10.97	12.94	15.69	2.03	0.385
Ti	2757.2	3836.2	3716.3	599.4	15526
Y	28.10	34.44	36.18	32.68	4.87

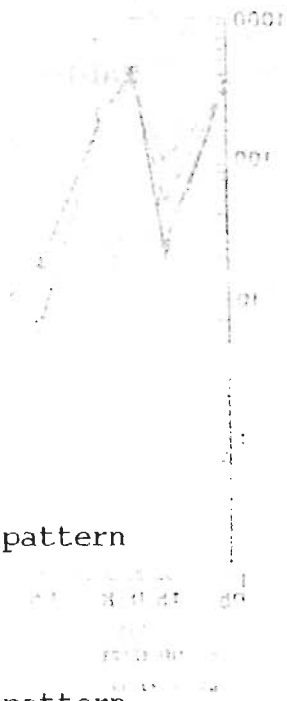

Figure 5.8 a : Spidergram plot normalised to primordial mantle showing pattern of the grey granitoid body.

Figure 5.8 b : Spidergram plot normalised to primordial mantle showing pattern of the Wangtu granitoid body.

Figure 5.8 c : Spidergram plot normalised to primordial mantle showing pattern of the porphyroclastic granite body.

Figure 5.8 d : Spidergram plot normalised to primordial mantle showing pattern of the Chor granitoid body.

Grey Granitoid

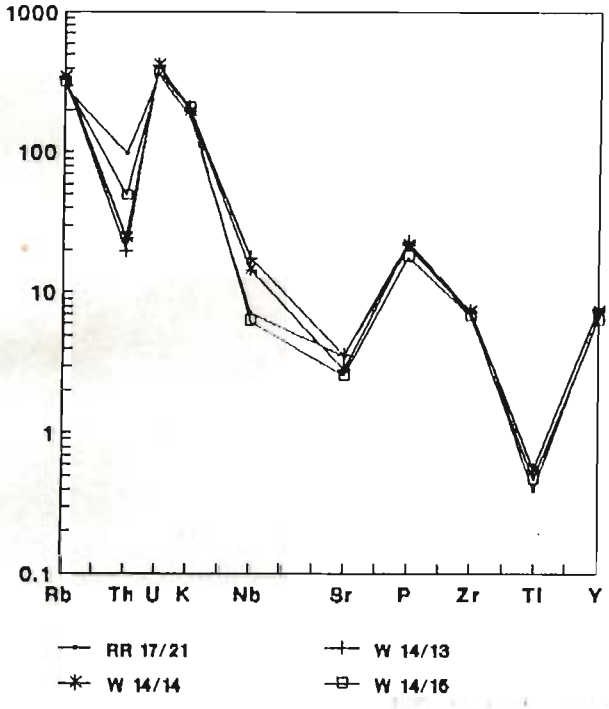

Wangtu Granitoid

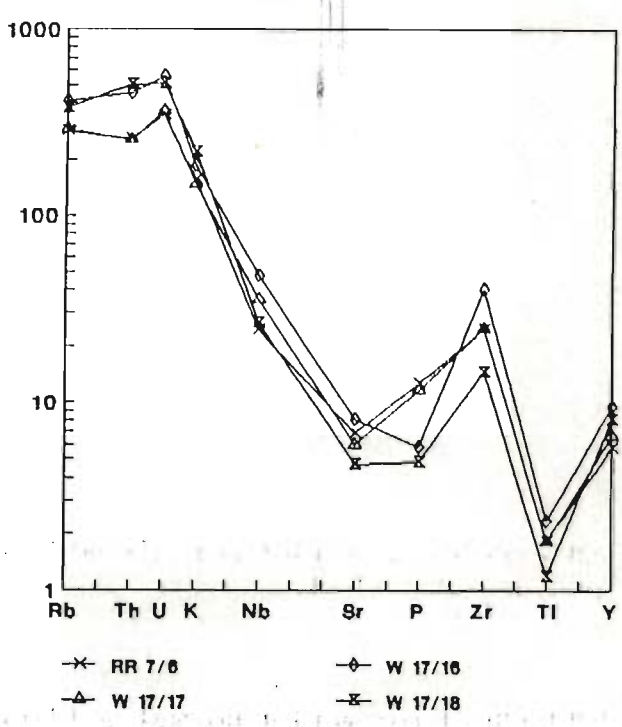

Porphyroclastic Granite

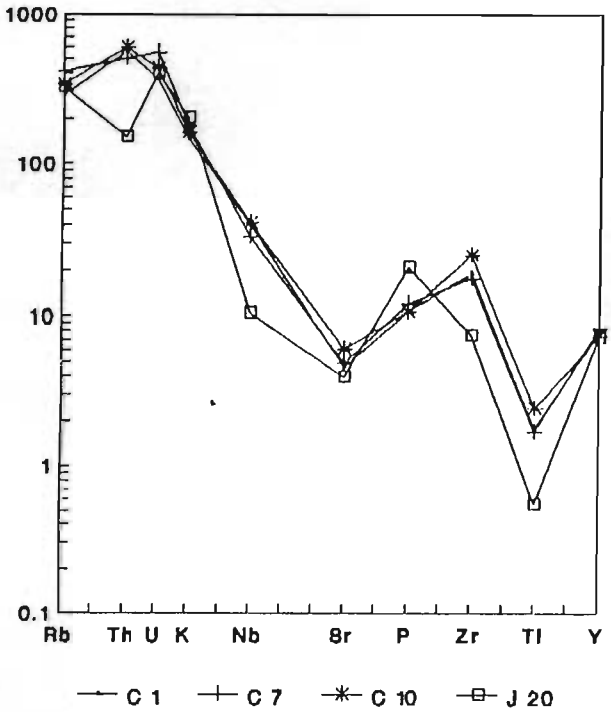

Chor Granitoid

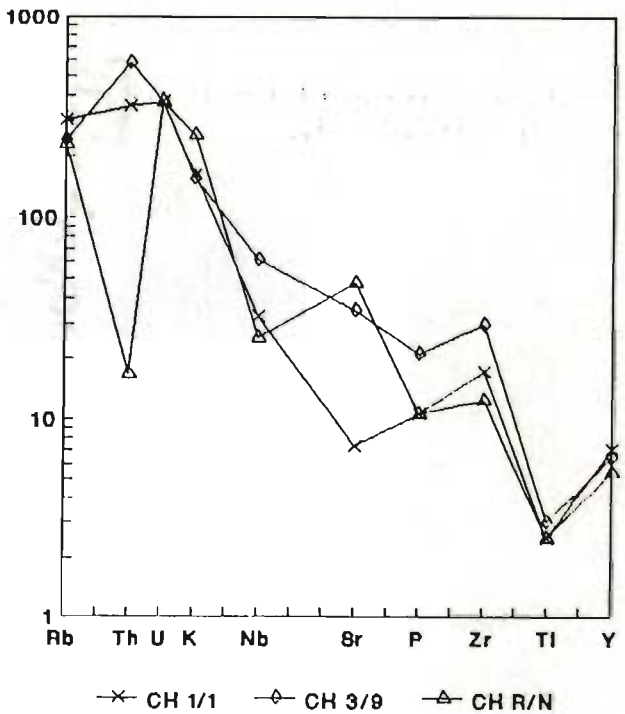

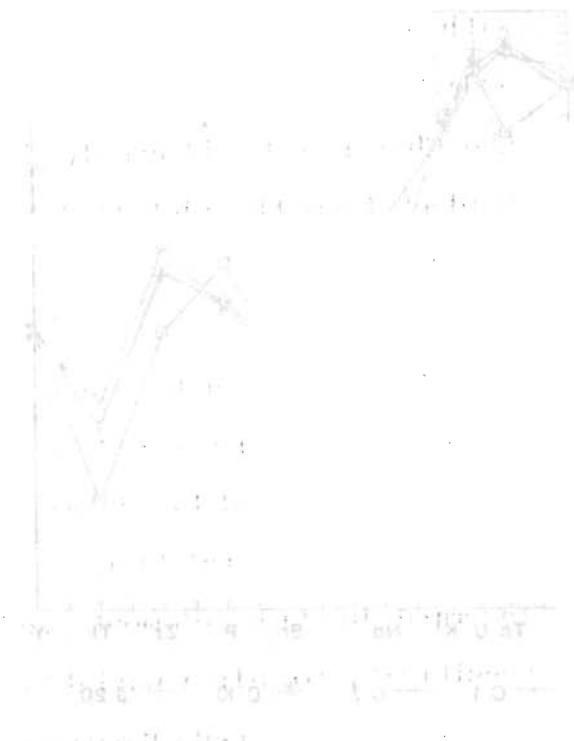

granite (CH 3/9). Trace element geochemistry of these varieties reveal an inconsistent trend except for a few elements. Ga, Rb, U, Ti Y and Na have consistent values with moderate K/Rb ratio (Table 5.5). The spidergram reveals lower values of Nb and Ti; higher variation in Th, Sr, P and Zr; and a distinct Ti negative anomaly (Fig. 5.8 d).

Four least deformed and representative samples from these bodies, used for REE analysis and geochronology, have been selected for comparison of trace element patterns of these bodies (Table 5.6; Fig. 5.9 a).

The grey granitoid has a distinctive lower abundances in the trace elements as compared to other bodies from this area (Table 5.6; Fig. 5.9 a). This body possesses a distinctive negative anomalies in Th, Nb, Sr and Ti, indicating a typical crustal contamination and/or crustal affinity. Other bodies from the HHC and the Jutogh Nappe show higher abundances in concentration of the trace elements. The porphyroclastic granite gneiss has a slight positive Th anomally with strong negative Nb, Sr, P and Ti anomalies. The Wangtu granitoid also has a slight negative Th anomally with strong Nb, Sr, P and Ti negative anomalies and the Chor granitoid has only Nb, Sr, P and Ti anomalies (Table 5.6; Fig. 5.9 a). It is evident from the plot that the overall trend is almost similar except in abundances.

To have better understanding of fractionation processes, trace element data of these bodies are normalised with hypothetical Oceanic Ridge Granite (ORG) data, as suggested by Pearce *et al.* (1984). Also, for inferring the granite petrogenesis in relation to the different tectonic environment, more incompatible trace elements such as Rb, Y, Nb, Ta and Yb are used, due to their sensitivity to silica variation and their variable abundances in different tectonic environments (Pearce *et al.*, 1984).

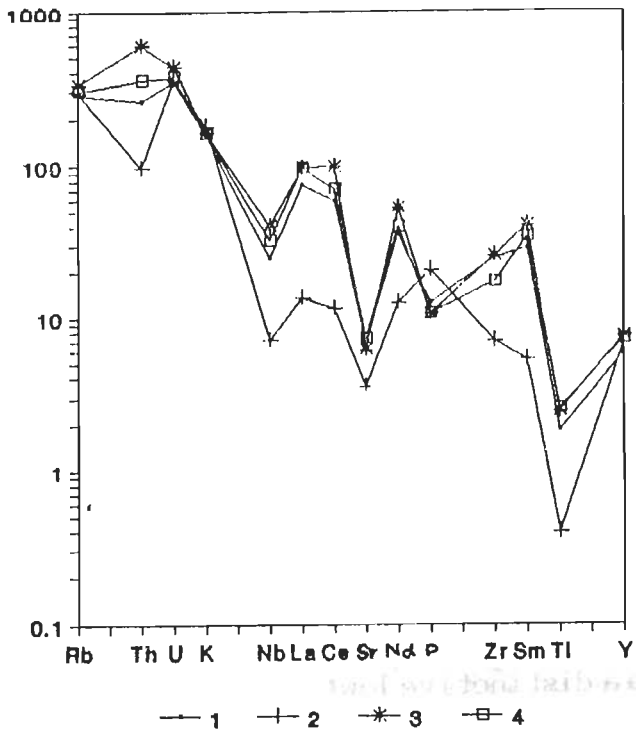

Figure 5.9 a : Spidergram plot normalised to primordial mantle showing pattern for different granitoids of the Himachal Pradesh. 1- Wangtu granitoid, 2- Grey granitoid, 3- Porphyroclastic granite gneiss and 4- Chor granitoid.

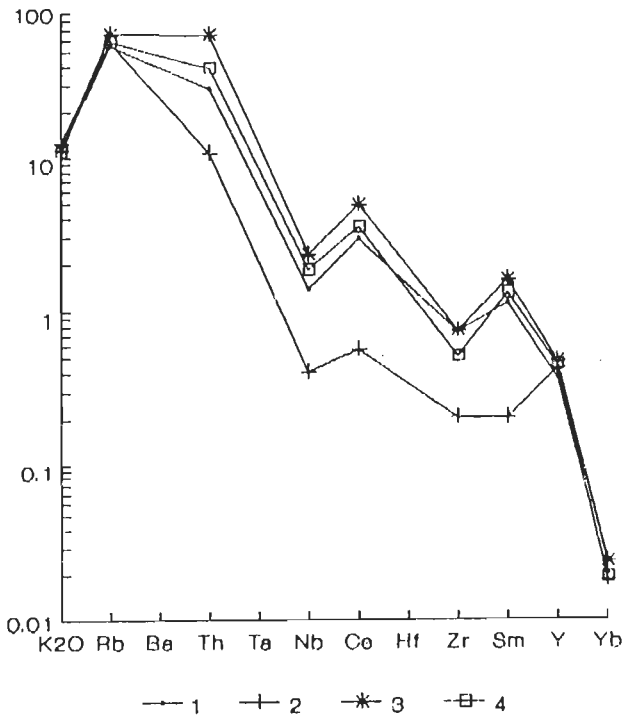

Figure 5.9 b : ORG-normalised vs compatible and incompatible elements plot showing pattern for differnt granitoids of the Himachal Pradesh. 1- Wangtu granitoid, 2- Grey granitoid, 3- Porphyroclastic granite gneiss and 4- Chor granitoid.

The ORG-normalised plot with compatible and incompatible element gives more or less the similar pattern as that of Spidergram plot, but with moderate variations in Th, Nb, Ce, Zr and Sm (Fig. 5.9 b). Similarly, all these trace elements from these granitoid bodies are plotted in silica variation diagrams. Among those plots, only Rb vs SiO_2 variation plot is distinct and falls in the field of Within Plate granite. Likewise, Rb vs Y+Nb discrimination plot also shows that these granitoids are derived from Within Plate environment (Figs. 5.10 a, b; cf. Pearce *et al.*, 1984).

5.6.3 REE Geochemistry

The REE are a group of 15 elements with atomic numbers ranging from 57 (Lanthanum - La) to 71 (Lutenium - Lu). Out of these, 14 elements occur naturally. The REE are generally classified as the light REE (LREE) and middle or heavy REE (HREE), based on their atomic numbers. The raw REE data are normalised with C1 Chondrite in order to refine the data (Sun and McDonough, 1989). In the present study, all the REE analyses (Table 5.7) were normalised to C1 Chondrite values and plotted in Fig. 5.11 a.

Grey granite has very low LREE and HREE abundances as compared to the other granites of this region (Table 5.7; Fig. 5.11 a). The plots of the porphyroclastic granite, Wangtu granite and Chor granite show almost similar trends and are enriched in LREE and depleted in HREE (Table 5.7; Fig. 5.11 a). However, among these three granitoids; the porphyroclastic granitoid has more LREE and HREE abundances than the Wangtu granite. The Chor granitoid has also more LREE and HREE abundances than the Wangtu granitoid, but poorer in relation to porphyroclastic granite (Fig. 5.11 a). REE-normalised plot of grey granite gives very gentle slope suggesting nearly an unfractionated nature of the parent material. However, plots for porphyroclastic granite, Wangtu granitoid and Chor

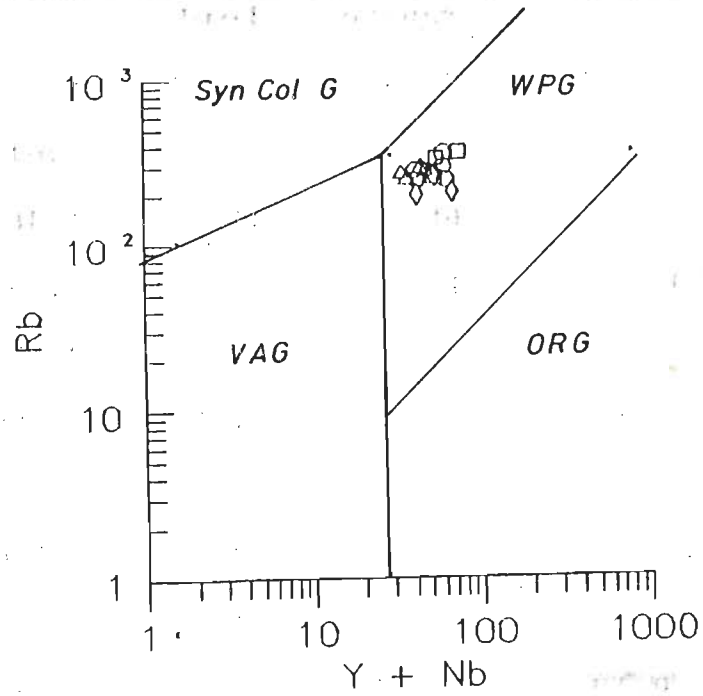

Figure 5.10 b : Rb vs Y + Nb discrimination plot for granitoids from Himachal Pradesh.

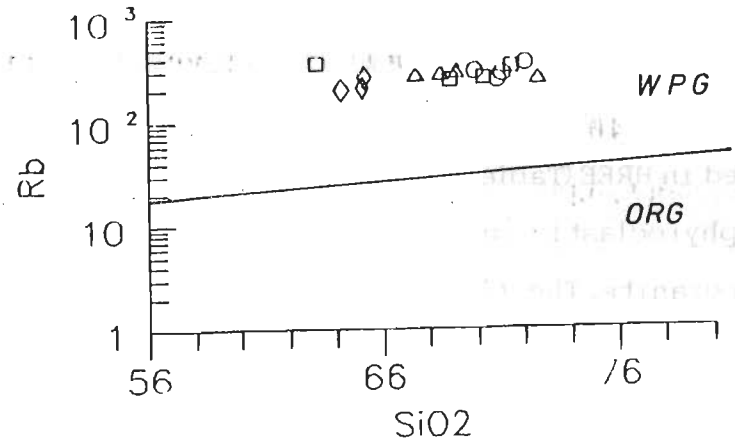

Figure 5.10 a : Rb vs SiO_2 discrimination plot for granitoids from Himachal Pradesh.

TABLE 5.7 REE data in ppm of different granitiods from the HHC and the Jutogh Nappe of Himachal Pradesh

	Wangtu Granitoid	Chor Granitoid	Porphyro-clastic Granite	Grey Grani-toid	C I Condrite
La	53.12	68.23	88.47	9.6	0.237
Ce	111.4	133.9	186.4	21.8	0.612
Nd	45.52	51.65	68.95	16.19	0.467
Sm	10.97	12.94	15.69	2.03	0.153
Eu	1.28	1.46	1.42	0.73	0.058
Gd	7.27	7.55	8.39	1.8	0.206
Dy	4.63	5.34	5.84	2.86	0.254
Er	2.05	2.15	2.74	3.12	0.166
Yb	1.60	1.53	1.93	1.45	0.17
Lu	0.21	0.19	0.24	0.265	0.025
$(Ce/Yb)_N$	19.34	24.31	26.83	4.18	
$(Ce/Sm)_N$	2.54	2.59	2.97	2.69	
$(Dy/Lu)_N$	2.21	2.77	2.40	0.84	
$(Eu/Eu^*)_N$	0.44	0.42	0.37		
$(La/Lu)_N$	27.11	37.88	38.89	3.88	32.20
$(La/Sm)_N$	3.13	3.40	3.64	3.05	5.61
Σ REE	238.05	284.94	380.07	59.845	280

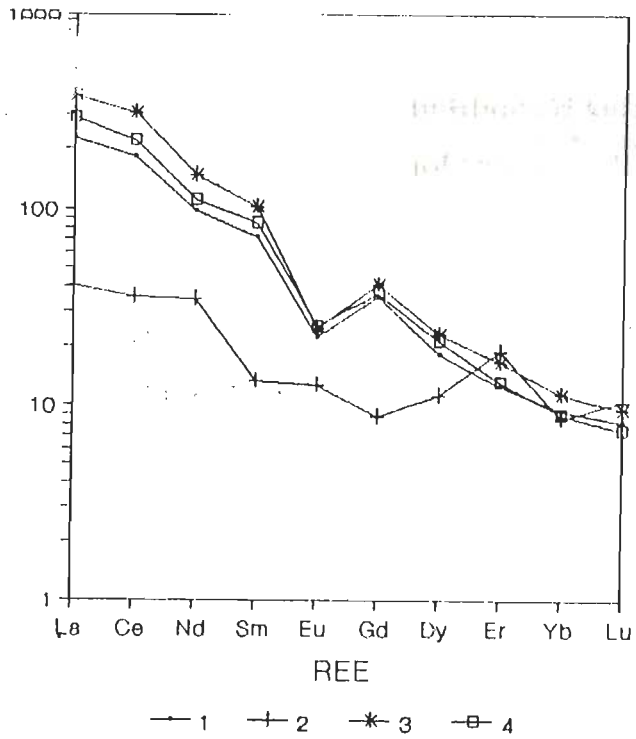

Figure 5.11 a : REE normalised plot, normalised to C1 Chondrite, for the Granitoids form The Himachal Pradesh. 1- Wangtu granitoid, 2- Grey granitoid, 3- Porphyroclastic granite gneiss and 4- Chor granitoid.

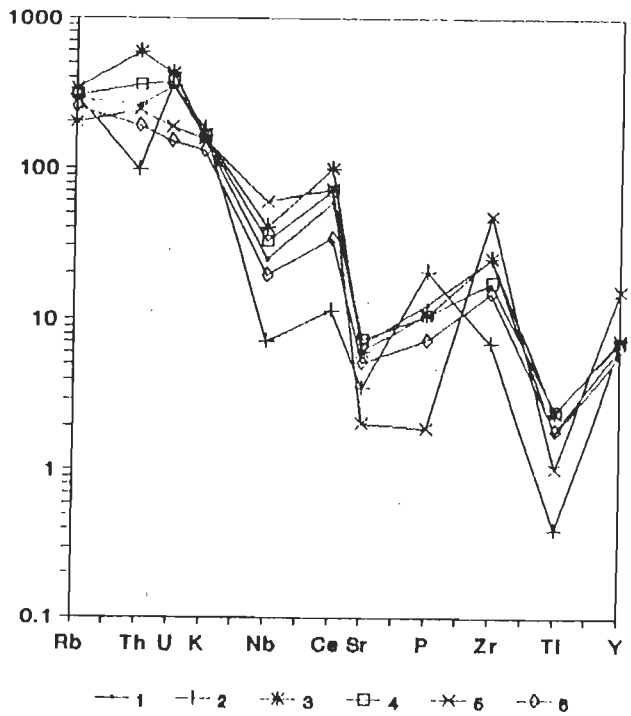

Figure 5.11 b : Spidergram plot normalised to primordial mantle showing comparision of granitoids from Himachal Pradesh. 1- Wangtu granitoid, 2- Grey granitoid, 3- Porphyroclastic granite gneiss, 4- Chor granitoid with 5- A-type granite and 6- S-type granite.

granitoid give similar LREE and HREE fractionation pattern and trend with steeper slope in LREE and gentler slope in HREE having slight concave trend (Fig. 5.11 a). These bodies are moderately fractionated in HREE with respect to LREE, having $(Ce/Sm)_N$ ratio ranging from 2.54 to 2.97. These possess a moderate negative Eu anomaly, having $(Eu/Eu^*)_N$ ratio from 0.37 to 0.44. Low Yb concentration and moderately fractionated REE pattern suggest that these granites are derived from crustal source.

5.7 DISCUSSIONS

In the Himalaya, three major granitoid types have been envisaged and classified on the basis of their tectonic setting, petrography and whole-rock geochemistry. These belts include:

(a) Collision-related granites of ~15-20Ma age, e.g. the Manaslu granite (Nepal), the Bhagirathi and the Badrinath granites (Garhwal and Kumaon Himalaya) (Vidal *et al.*, 1982; Stern *et al.*, 1989).

(b) Subduction-related granitoids-granodiorite of 60 to 100 Ma age, e.g. the Hunza and the Baltoro granitoids (Karakoram) and the Ladakh batholith of the NW-Himalaya (Rex *et al.*, 1988; Searle, 1991; Sharma, 1991).

(c) Pre-collisional granitoids of Proterozoic-Early Paleozoic ages from about 2000 to 500 Ma such as Dalhousie, Mandi, Wangtu, Chor granitoids of Himachal Pradesh and elsewhere (Le Fort *et al.*, 1983 a).

The total REE of the Wangtu granite, Chor granite and phorphyroclastic granite gneiss are quite high with a negative Eu anomaly (Table 5.7; Fig. 5.11 a). These granites are enriched in LREE in comparision to the HREE. $(La/Lu)_N$, $(La/Sm)_N$ and $(Ce/Sm)_N$ ratios range from 27.11 to 38.89, 3.13 to 3.64 and 2.54 to 2.97 respectively. the HREE $(Dy/Lu)_N$ ratio ranges from 2.21 to 2.77. It is evident from the data that HREE are less fractionated as compared to LREE (Table 5.7). However, the total REE of grey granite is considerably low and show less fractionation trend with respect to both LREE and HREE.

5.7.3 Comparisions with other bodies

a. Comparision with S-type and A-type granite (Fig. 5.11 b): Keeping in mind the peraluminous character of these granitoids from Himachal Pradesh, comparision with A-type and S-type of granite has been done (cf. Wahlen *et al.*, 1989). In spidergram plot, both the A-type and S-types of granites have similar patterns except the abundances of the elements. It is evident from the plot that the porphyroclastic granite gneiss, the Wangtu granitoid and the Chor granitoid have closer affinity towards the S-type of granite, whereas grey granitoid has closer affinity with the A-type of granite.

b. Comparision with subduction-related granite (Fig. 5.12): When these bodies are compared with subduction-related Hunza granite of 95 Ma and Darkot granite of 111 Ma from North Pakistan on spidergram plot (Table 5.6; Figs. 5.12 a, b) and REE normalised plot (Table 5.7; Fig. 5.12 c, d), these indicate similar geochemical characters, except in the concentration of the trace elements.

granitoid give similar LREE and HREE fractionation pattern and trend with steeper slope in LREE and gentler slope in HREE having slight concave trend (Fig. 5.11 a). These bodies are moderately fractionated in HREE with respect to LREE, having $(Ce/Sm)_N$ ratio ranging from 2.54 to 2.97. These possess a moderate negative Eu anomaly, having $(Eu/Eu^*)_N$ ratio from 0.37 to 0.44. Low Yb concentration and moderately fractionated REE pattern suggest that these granites are derived from crustal source.

5.7 DISCUSSIONS

In the Himalaya, three major granitoid types have been envisaged and classified on the basis of their tectonic setting, petrography and whole-rock geochemistry. These belts include:

(a) Collision-related granites of ~15-20Ma age, e.g. the Manaslu granite (Nepal), the Bhagirathi and the Badrinath granites (Garhwal and Kumaon Himalaya) (Vidal *et al.*, 1982; Stern *et al.*, 1989).

(b) Subduction-related granitoids-granodiorite of 60 to 100 Ma age, e.g. the Hunza and the Baltoro granitoids (Karakoram) and the Ladakh batholith of the NW-Himalaya (Rex *et al.*, 1988; Searle, 1991; Sharma, 1991).

(c) Pre-collisional granitoids of Proterozoic-Early Paleozoic ages from about 2000 to 500 Ma such as Dalhousie, Mandi, Wangtu, Chor granitoids of Himachal Pradesh and elsewhere (Le Fort *et al.*, 1983 a).

5.7.1 Geochemical characters of Himalayan granitoids

Major, Trace and REE geochemistry of a few of collision and subduction-related granitoid bodies have been studied in more detail for their tectonics and petrogenesis.

Most of the collision-related granites, such as Manaslu and Bhagirathi granitoids, intrude the HHC and/or occur close to the Tethyan Sedimentary Zone (TSZ). In the Nomenclature diagram, the Manaslu samples plot in adamellite field and extend to granodiorite and granite fields due to variation in Na/K ratio. The Characteristic mineral diagram for major elements indicate their general peraluminous character in sectors I, II and III (Le Fort *et al.*, 1987). These bodies are characterised by higher SiO_2 content and higher Rb, Ta, Cs and U abundances; lower FeO, MgO, CaO and TiO_2 contents; and extremely low Sr, Ba, Zr, Hf and REE concentrations (Le Fort, 1975, 1986; Vidal *et al.*, 1982, 1984; Cunney *et al.*, 1984; Deniel, 1985; Deniel *et al.*, 1987; Le Fort *et al.*, 1987; Stern *et al.*, 1989). The REE pattern is characterised by low total REE with an enrichment in LREE and negative Eu anomaly. The origin of these granites have been attributed to crustal anatexis, associated with frictional heating along the MCT during the Late Cenozoic collisional processes (Le Fort *et al.*, 1987).

The subduction-related granitoids are mainly confined to the Trans-Himalayan region, such as the Hunza and Baltora granitoids of Karakoram region (Rex *et al.*, 1988). These bodies are calc-alkaline in composition with Andean-type tectonic setting (Rex *et al.*, 1988). These rocks are mainly granodioritic in composition with higher CaO, MgO and FeO, moderate TiO_2 and lower alkalis contents. The characteristic mineral diagram plot suggest that these bodies are peraluminous in character. Also, these are enriched moderately in Rb, Sr, Ba, Th, U, Zr and LREE abundances; but depeleted in most of HREE, except

for a slight increase in Yb and Lu, and negative Eu anomaly (Rex *et al.*, 1988).

The pre-collision granitoids are present in the Higher and Lesser Himalaya and constitute a linear belt in the south such as Dalhousie, Mandi, south Almora, Simchar etc. These bodies are very similar in their structural, petrological and geochemical characters and are generally porphyritic in nature, showing post-magmatic deformation. The Characteristic mineral diagram of these bodies plot in the sectors I, II and III, indicating their peraluminous character (Valdiya, 1962; Shams, 1969; Le Fort *et al.*, 1983 b; Sharma, 1983; Thakur, 1983; Singh *et al.*, 1993). However, limited major and trace element data on these granites indicate higher SiO_2 contents and lower Na_2O, CaO, MgO and TiO_2 content with moderate Ba, Rb and Sr concentration (Le Fort *et al.*, 1986)

5.7.2 Granitoids from Sutlej Valley and Chor Mountain region

The granitoids from the HHC and Jutogh Nappe are similar in geochemical character as that of the pre-collision granites. Na_2O/K_2O and $Al_2O_3/CaO+Na_2O+K_2O$ ratios suggest that these bodies are peralkaline and peraluminous in nature (Table 5.2), indicating the involvement of upper crustal material (cf. McDonald *et al.*, 1987). In the quartz-orthoclase-plagioclase modal plot, these granites fall in tonalitic (grey granite), quartz-monzodiorite (Wangtu and Chor granitoid) and granite (porphyroclastic granite gneiss) fields. However, in the quartz-orthoclase-plagioclase normative plot, these are plotted in granite, quartz-monzonite and monzonite fields respectively (Table 5.3; Fig. 5.3 b). In the Nomenclature diagram, these bodies fall in granite, adamelite, quartz-syenite and syenite fields (Table 5.4; Fig. 5.4 a), whereas in the Characteristic mineral diagram, these fall in sectors II, III and IV respectively (Table 5.4; Fig. 5.4 b).

The total REE of the Wangtu granite, Chor granite and phorphyroclastic granite gneiss are quite high with a negative Eu anomaly (Table 5.7; Fig. 5.11 a). These granites are enriched in LREE in comparision to the HREE. $(La/Lu)_N$, $(La/Sm)_N$ and $(Ce/Sm)_N$ ratios range from 27.11 to 38.89, 3.13 to 3.64 and 2.54 to 2.97 respectively. the HREE $(Dy/Lu)_N$ ratio ranges from 2.21 to 2.77. It is evident from the data that HREE are less fractionated as compared to LREE (Table 5.7). However, the total REE of grey granite is considerably low and show less fractionation trend with respect to both LREE and HREE.

5.7.3 Comparisions with other bodies

a. Comparision with S-type and A-type granite (Fig. 5.11 b): Keeping in mind the peraluminous character of these granitoids from Himachal Pradesh, comparision with A-type and S-type of granite has been done (cf. Wahlen *et al.*, 1989). In spidergram plot, both the A-type and S-types of granites have similar patterns except the abundances of the elements. It is evident from the plot that the porphyroclastic granite gneiss, the Wangtu granitoid and the Chor granitoid have closer affinity towards the S-type of granite, whereas grey granitoid has closer affinity with the A-type of granite.

b. Comparision with subduction-related granite (Fig. 5.12): When these bodies are compared with subduction-related Hunza granite of 95 Ma and Darkot granite of 111 Ma from North Pakistan on spidergram plot (Table 5.6; Figs. 5.12 a, b) and REE normalised plot (Table 5.7; Fig. 5.12 c, d), these indicate similar geochemical characters, except in the concentration of the trace elements.

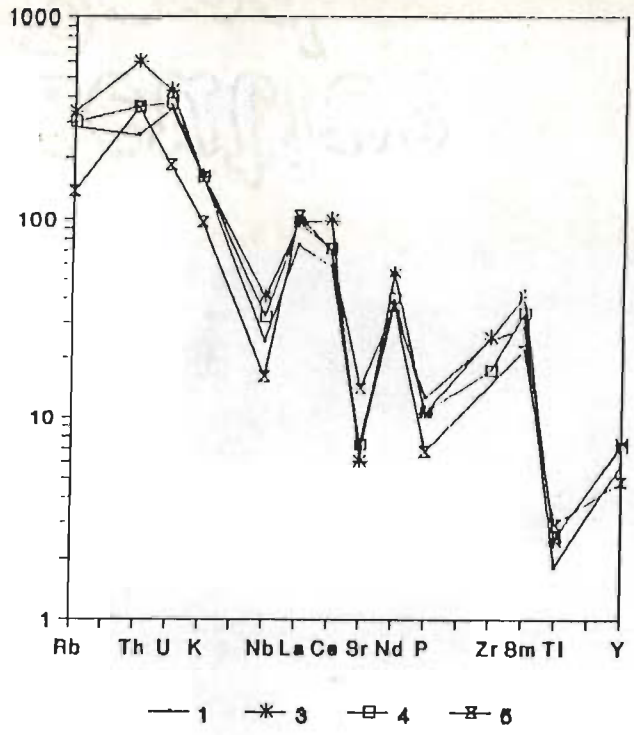
1000
100
10
1
Rb Th U K Nb La Ce Sr Nd P Zr Sm Tl Y
1 3 4 5

a

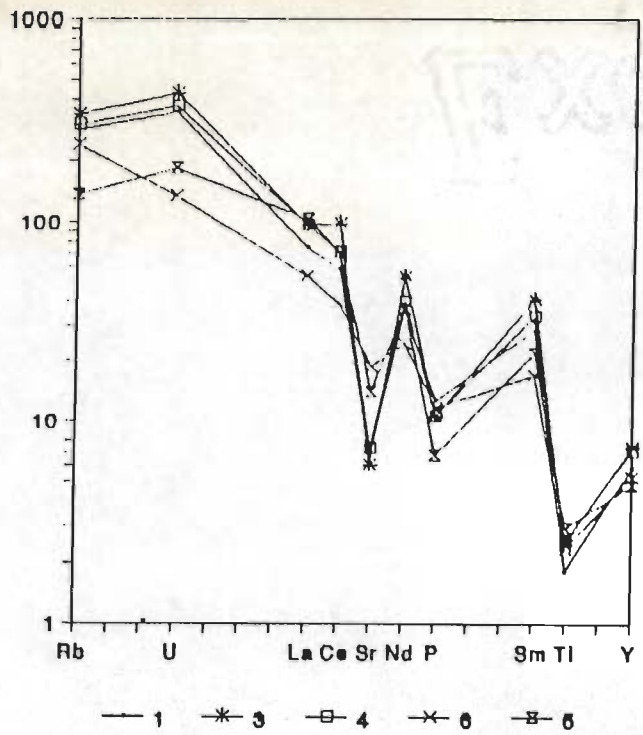
1000
100
10
1
Rb U La Ce Sr Nd P Sm Tl Y
1 3 4 6 5

b

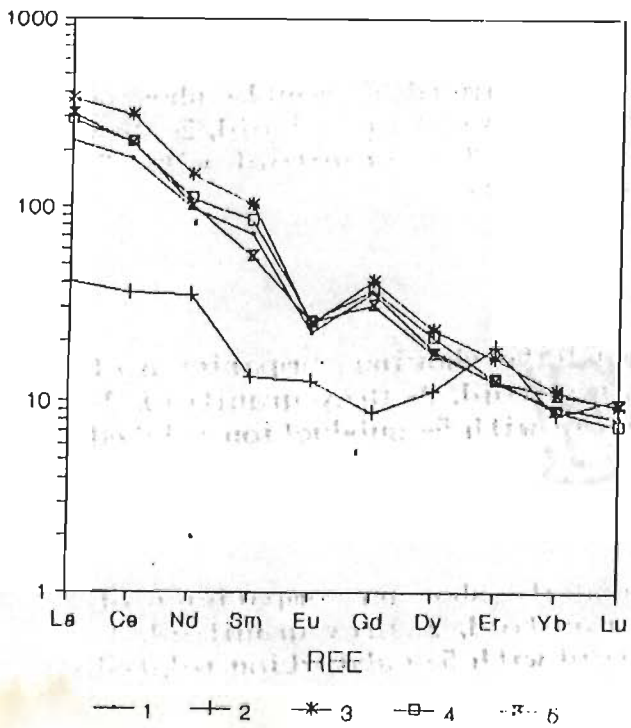
1000
100
10
1
La Ce Nd Sm Eu Gd Dy Er Yb Lu
REE
1 2 3 4 5

c

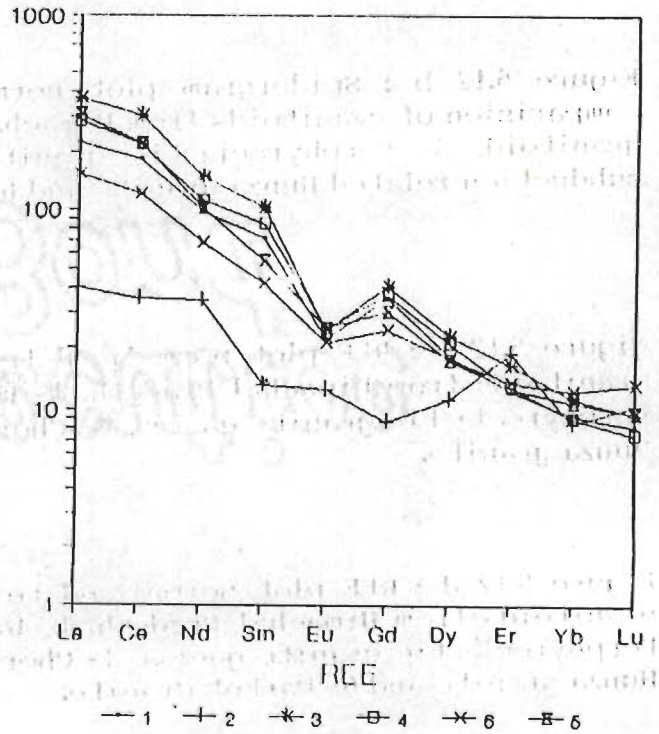
1000
100
10
1
La Ce Nd Sm Eu Gd Dy Er Yb Lu
REE
1 2 3 4 6 5

d

Figure 5.12 a : Spidergram plot normalised to primordial mantle showing comparision of granitoids from Himachal Pradesh. 1- Wangtu granitoid, 2- Grey granitoid, 3- Porphyroclastic granite gneiss, 4- Chor granitoid with 5- subduction related Hunza granite.

Figure 5.12 b : Spidergram plot normalised to primordial mantle showing comparision of granitoids from Himachal Pradesh. 1- Wangtu granitoid, 2- Grey granitoid, 3- Porphyroclastic granite gneiss, 4- Chor granitoid with 5- subduction related Hunza granite and 6- Darkot Granite.

Figure 5.12 c : REE plot normalised to C1 Chondrite showing comparision of granitoids from Himachal Pradesh. 1- Wangtu granitoid, 2- Grey granitoid, 3- Porphyroclastic granite gneiss, 4- Chor granitoid with 5- subduction related Hunza granite.

Figure 5.12 d : REE plot normalised to C1 Chondrite showing comparision of granitoids from Himachal Pradesh. 1- Wangtu granitoid, 2- Grey granitoid, 3- Porphyroclastic granite gneiss, 4- Chor granitoid with 5- subduction related Hunza granite and 6- Darkot Granite.

c. Comparision with collision-related Cenozoic leucogranites (Fig. 5.13): A comparision of collision-related leucogranites with these bodies from the HHC and the Jutogh Nappe shows that the collision-related bodies - the Manasalu leucogranite from Nepal (Vidal *et al.*, 1982) and the Bhagirathi leucogranite from Garhwal (Stern *et al.*, 1988) have lower concentration of trace elements and REE (Table 5.7; Fig. 5.13). Apart from concentration, there is mismatch in pattern both on spidergram (Table 5.6; Fig. 5.13 a) and REE normalised plots (Fig. 5.13 b). Normalised REE plots of the Manasalu and Bhagirathi granites give gentle slopes, while the former also yields negative Eu anomaly.

d. Rb vs Y + Nb plot (Fig. 5.14): One of the most significant discrimination plot out of various examples appears to be Rb vs Y + Nb plot (Pearce *et al.*, 1984) for the Himalayan granitoids including those from the present area. All the four bodies from this area plot distinctively Within Plate Granite (WPG) field with Rb/(Y + Nb) ratios ranging between 2.68 to 6.80 (Table 5.5; Figs, 5.10 b, 5.14). Likewise, another pre-collisional and Proterozoic to Early Paleozoic Champawat granitoid body falls distinctively within WPG field, and compares with the granitoids from Himachal Pradesh.

On the other hand, Late Cenozoic leucogranites from Bhagirathi lie distinctly in the field of syn-collisional granite, while the Hunza and Baltoro complexes have a tendecy to fall nearer to Volcanic Arc Granite field (Fig. 5.14). Overall field relations, petrography and geochemical characters strongly support these petrogenetic provinces for the bodies.

Considering the petrography and overall geochemical pattern of the granites from the Chor and Sutlej Valley regions of Himchal Pradesh, the following points are imminent:

1. Petrographically, the grey granite is tonalitic in nature, whereas the

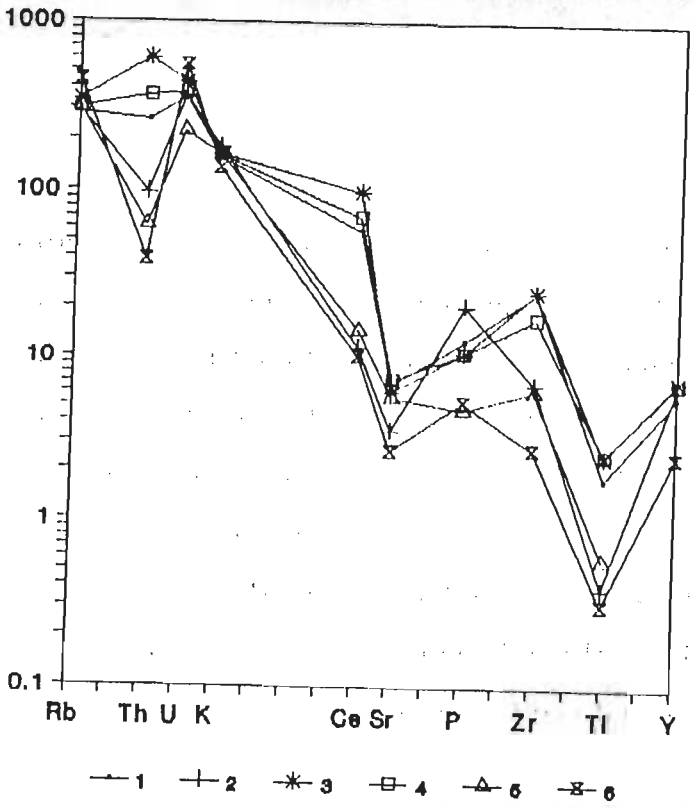

Figure 5.13 a : Spidergram plot normalised to primordial mantle showing comparision of granitoids from Himachal Pradesh. 1- Wangtu granitoid, 2- Grey granitoid, 3- Porphyroclastic granite gneiss, 4- Chor granitoid with collision related Cenozoic leucogranites: 5- Manasalu and 6- Bhagirathi.

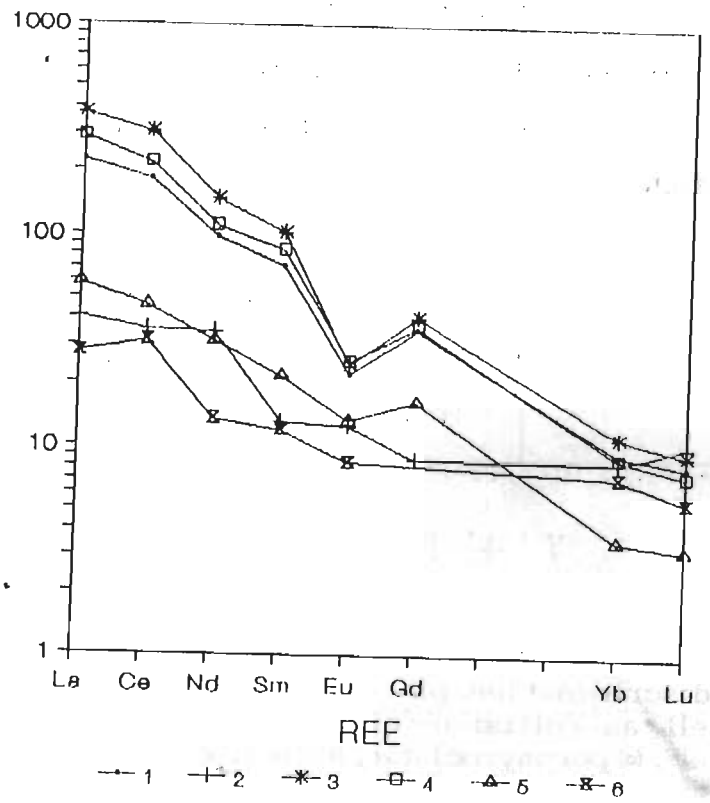

Figure 5.13 b : REE plot normalised to C1 Chondrite showing comparision of granitoids from Himachal Pradesh. 1- Wangtu granitoid, 2- Grey granitoid, 3- Porphyroclastic granite gneiss, 4- Chor granitoid with collision related Cenozoic leucogranites: 5- Manasalu and 6- Bhagirathi.

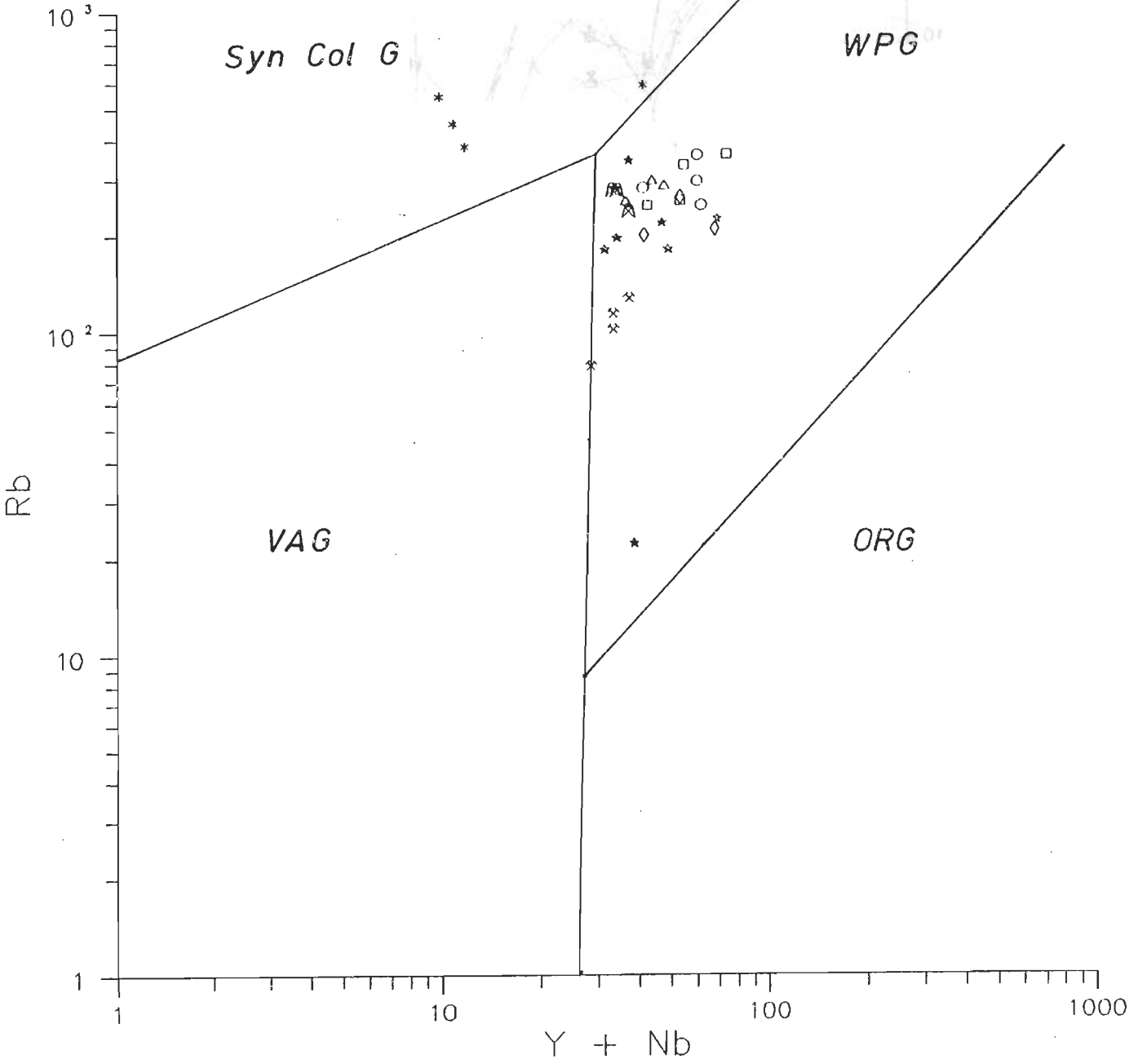

Figure 5.14 : Rb vs Y+Nb discrimination plot showing granitoid bodies from subduction-related as well as collision-related zones from Himalaya. (★) Champawat, (▫) Wangtu, (▵) grey , (○) porphyroclstic, (◇) Chor, (✕) Hunza, (✕) Baltoro, and (✱) Bhagirathi.

Porphyroclastic, Wangtu and Chor granites are granite to quartz-monzodiorite in character.

2. The major element chemistry suggest that these granites are peraluminous and peralkaline in nature, which is similar to other Himalayan granites of younger ages. The quartz-orthoclase-plagioclase normative plot shows that these granites are mainly of granite to quartz-monzonite composition.

3. The negative anomally in Nb, Sr, P and Ti of these bodies in spidergram and low Yb concentration and moderately fractionated REE pattern suggest a typical crustal contamination and/or crustal affinities for these bodies. LREE enriched and HREE depleted pattern with negative Eu anomally indicate that the source material for these bodies might have had enrich LREE.

4. The overall trace element pattern on spidergram plot is similar to S- and A-type granites. The grey granitoid having more affinity towards A-type granite, otherwise rest of the bodies show affinity towards S-Type granite.

5. The similar geochemical pattern of these bodies suggest that, although these bodies are different in geological and geographical entity, the source material and the genesis processes appear to be identical.

6. The trace element variation and discrimination plots suggest that these Proterozoic granites fall in Within Plate Granite environment, whereas other younger subduction related and collision-related granites have close affinity towards volcanic arc and syn-collisional environments respectively.

7. The WPG category of these bodies in the discrimination plot suggest that these bodies are of A-type.

8. Higher LREE and lower HREE abundances are characteristics of these granites, suggesting moderate to higher fractionation, except grey granite which is depleted both in LREE and HREE and is less fractionated. Other younger granites of the Himalaya are relatively poorer in REE abundances than all these granites of this region of Proterozoic age.

CHAPTER 6 : GEOCHRONOLOGY

6.1 INTRODUCTION

The Himalaya lacks precise geochronological dates in general and by U-Pb method in particular, where time of crystallisation of numerous granitoids can be constrained and the Himalayan orogenesis better understood. Exceptions to this are a few 100 Ma U-Pb zircon ages from the Trans-Himalayan belt (Honeger *et al.*, 1982; Scharer *et al.*, 1984; Debon *et al.*, 1981, 1986; Maluski *et al.*, 1988) and a few dates from the Higher Himalayan metamorphic belt (Copeland *et al.*, 1988; Scharer *et al.*, 1986; Parrish, 1990; Pognante *et al.*, 1990).

To provide better geochronological constraints to the overall tectonics of the Higher Himalayan Crystalline (HHC) and the Jutogh Nappe in parts of Himachal Pradesh, U-Pb zircon age determination was actively supported by Prof. D. G. Gee, Department of Mineralogy and Petrology, Institute of Geology, University of Lund, Sweden and at Laboratory for Isotope Geology, Swedish Museum of Natural History , Stockholm, Sweden with Prof. S. Claesson during 1990. In this connection, field investigations and sample collection were done jointly in Himachal Pradesh

6.2 U-Pb GEOCHRONOLOGY : AN INTRODUCTION

Applications of the U-Pb geochronology to granitic rocks has largely been restricted to date zircon ($ZrSiO_4$) and to some extent monazite [(Ce, La, Di)PO_4], and sphene ($CaTiSiO_5$). Although the U-Pb ages calculated from zircon are almost invariably discordant, this method has been considered as most reliable for

establishing meaningful crystallisation age of granitoids due to early formation of zircon and its refractory character during subsequent events.

Isotopic U-Pb investigations on zircon was started only thirtyeight years ago, when early works were followed by the poineering efforts of Tilton *et al.* (1955). Decay of U and Th to stable isotopes of Pb is the basis of this dating method. The concentration of U in common rock-forming silicates is generally low of the order of a few ppm or even less. U is strongly enriched in certain accessory minerals in which it is either a major constituent or replaces other elements.

Uranium has two naturally-occurring radioactive parent isotopes, ^{238}U and ^{235}U. The half life of these isotopes are different from each other and falls into the range of geological time. The decay of ^{238}U gives rise to the "Uranium Series", which includes ^{234}U as an intermediate daughter and ends in stable ^{206}Pb. Each atom of ^{238}U, that decays with a half life of $4.468 * 10^{9}$ yrs (decay constant $1.55125 * 10^{-10}$ y^{-1}), ultimately produces one atom of ^{206}Pb by emission of 8 α particles and 6 β particles. The decay of ^{235}U gives rise to the "Actinium Series", which ends with stable ^{207}Pb. Each atom of ^{235}U, that decays with a half life of $0.7038 * 10^{9}$ yrs (decay constant $9.8486 * 10^{-10}$ y^{-1}), ultimately produces one atom of ^{207}Pb by emission of 7 α particles and 4 β particles.

The decay of ^{238}U and ^{235}U allows us to determine the ages of any mineral containing uranium. The coupled decay of ^{238}U to ^{206}Pb and ^{235}U to ^{207}Pb gives rise to three different ratios from which ages can be calculated; namely $^{206}Pb/^{238}U$, $^{207}Pb/^{235}U$ and $^{207}Pb/^{206}Pb$. Of these three, only two are independent, whereas the third ratio can be obtained by simple calculation from the first two. These ratios can be obtained from the isotopic composition of Pb and the concentrations of Pb and U, which are determined using the isotope dilution technique.

The U-Pb analytical data are generally presented and evaluated by a graphical method known as the concordia-discordia plot (Fig. 6.1 a; Wetherill, 1956 b). The $^{207}Pb/^{235}U$ atomic ratio is plotted on the X-axis and $^{206}Pb/^{238}U$ on the Y axis. The locus of points with equal $^{206}Pb/^{238}U$ and $^{207}Pb/^{235}U$ ages define a curve called CONCORDIA. The age of a sample is said to be concordant when the data points fall on this curve. Otherwise, the age relationships are said to be discordant. Discordant age patterns are mostly evaluated with reference to this concordia diagram (Fig. 6.1 b). Only when the following conditions have been fulfilled, the data point will fall on the curve.

a. The mineral has remained closed to U-Pb and all intermediate daughters throughout its history.
b. Correct values of initial isotopic ratios are to be used.
c. The decay constants are known accurately.

The great advantage of the U-Pb system is that there are two coupled systems with different decay constants. This offers a simple method for testing the assumption of a closed U-Pb system with a single analysis. At the time of crystallisation, U-bearing minerals contain no radiogenic Pb and the system is represented by a point at the origin. This point will move along the concordia curve as long as the system is closed to U and its daughter isotopes. The age of the system is indicated by the location of point on the curve. Due to loss of radiogenic Pb, there may be a change in coordinates of the point representing the system and it will move back along a chord connected to the origin. If all the radiogenic Pb in the system is lost, the system will return to its origin and will get reset to zero with all its earlier memory lost. The system will once again move along the concordia, if it becomes closed to U and to all its daughter isotopes afterwards. If the system loses only a fraction of its radiogenic Pb, it will be represented by a point somewhere on the chord, which will have discordant dates. The chord will be referred to as the discordia. The

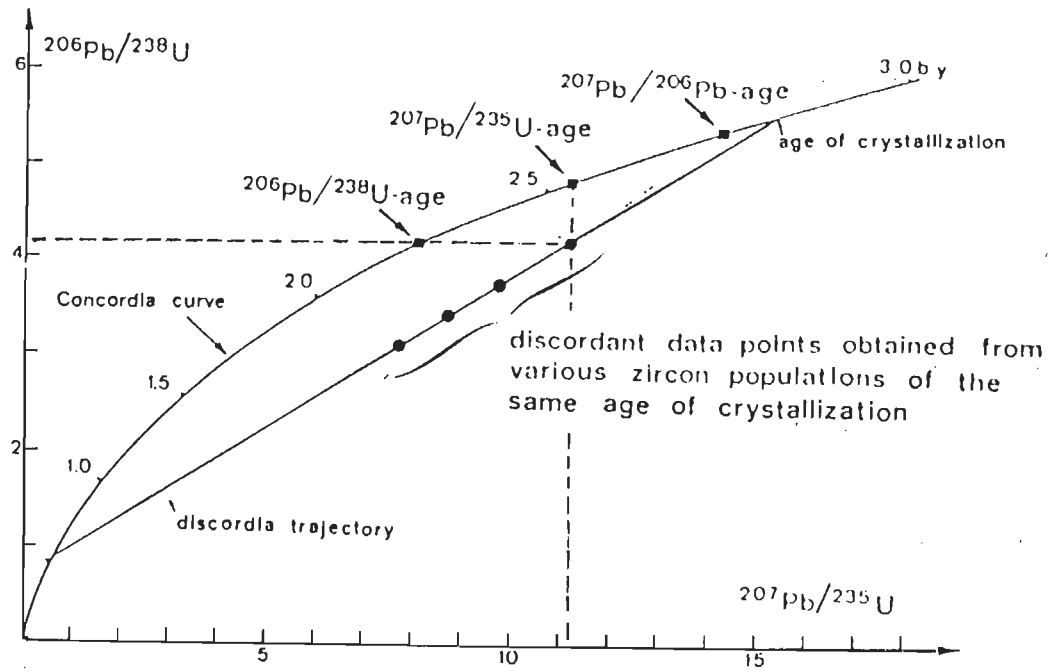

Figure 6.1 b : Concordia diagram showing data points of four zircon population with the apparent U/Pb ages as well as the Pb/Pb age (Gebeuer and Grunenfelder, 1979).

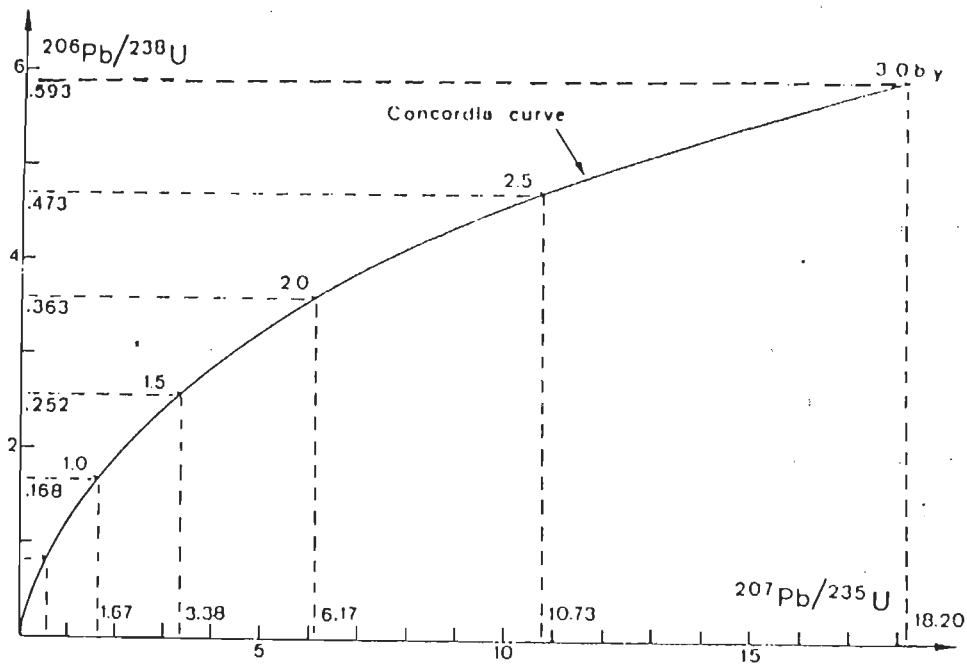

Figure 6.1 a : Conventional concordia diagram. Concordia curve is locus of points for which $^{206}Pb/^{238}U$ age equals $^{207}Pb/^{235}U$ age. It is curved due to the different half-lives of ^{238}U and (Gebeuer and Grunenfelder, 1979).

exact position of the U-Pb system on the discordia depends upon the fraction of radiogenic Pb remaining in the system.

It is quite possible to recover several fractions of zircons from a single rock sample and these will plot as a series of data points. With several data point plotting along a discordia line, one can get two points of intersection with the concordia curve by extrapolation. The upper intersection will give the time elapsed since the original crystallisation of the mineral, and the lower intersection will give the time elapsed since closure of the system following an episode of Pb loss or U gain (Figs. 6.1 b).

Generally, U-bearing minerals lose a variable fraction of their radiogenic Pb, depending upon the size of the crystals, U concentration and the radiation damage in the crystal. Experience have shown that there is generally a very strong relation between the U content of zircon, the magnetic susceptibility and grain size (Fig. 6.2 a). Smaller grains and those having higher U concentrations may suffer greater Pb losses than larger grains and grains containing less U. Zircon crystals in a sample of igneous rock may thus lose varying fractions of their radiogenic Pb, even though all of them have experienced the same type of conditions. Such lead losses may be explained by varios models:

a. Episodic lead loss model (Fig. 6.2 b; Wetherill, 1956 a,b)
b. Diffusion model (Fig.6.3 a; Nicolaysen, 1957; Tilton, 1960; Wasserburg, 1963)
c. Complex model (Fig. 6.3 b; Wetherill, 1963; Allegre et al. 1974)
d. Dilatancy model (Fig. 6.4 a; Goldich and Mudrey, 1972)
e. Alteration model (Fig. 6.4 b; Krogh and Davis, 1975)
f. Low temperature annealing model (Fig. 6.5 a; Gebauer and Grunenfelder, 1976)
g. Mixing model (Fig..6.5 b; Gebauer and Grunenfelder, 1979)

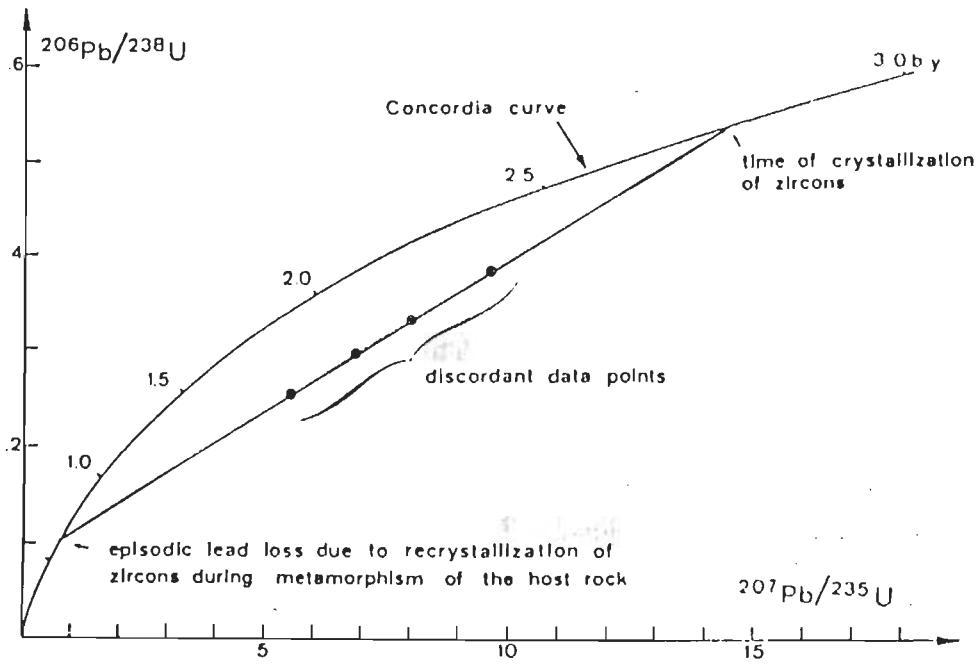

Figure 6.2 b : Concordia diagram showing the effect of episodic lead loss on a cogenetic zircon suit. Lead loss due to recrystallisation is often thought to be the most important mechanism to produce discordant ages (Gebeuer and Grunenfelder, 1979).

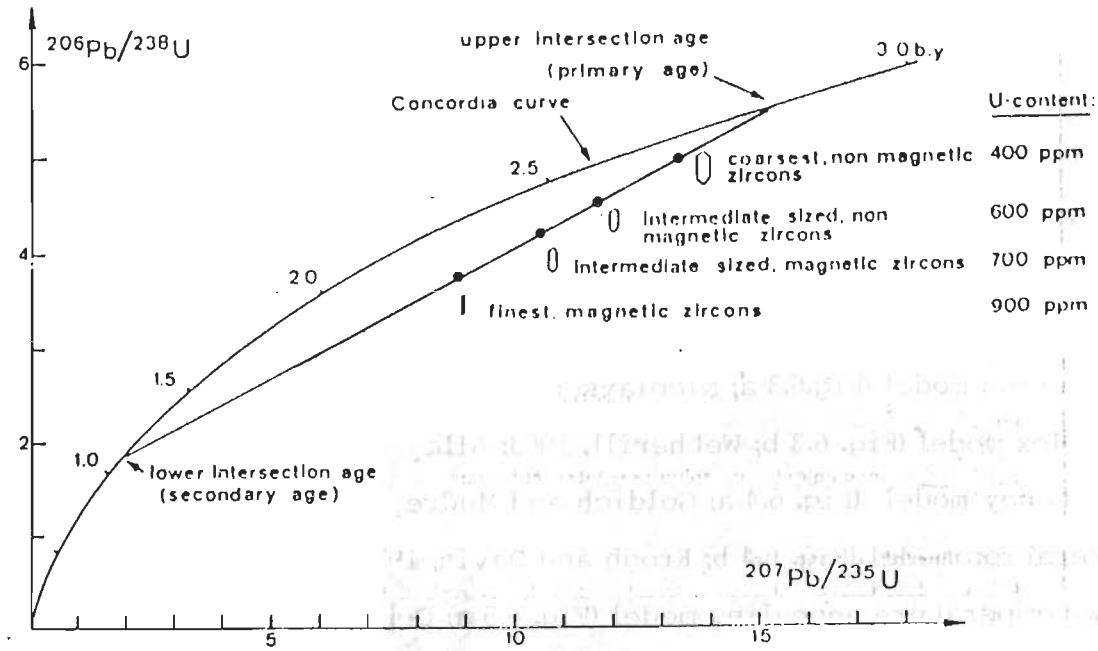

Figure 6.2 a : Concordia diagram showing the influence of U- content, grain size and magnetic susceptibility on degree of discordace (Gebeuer and Grunenfelder, 1979).

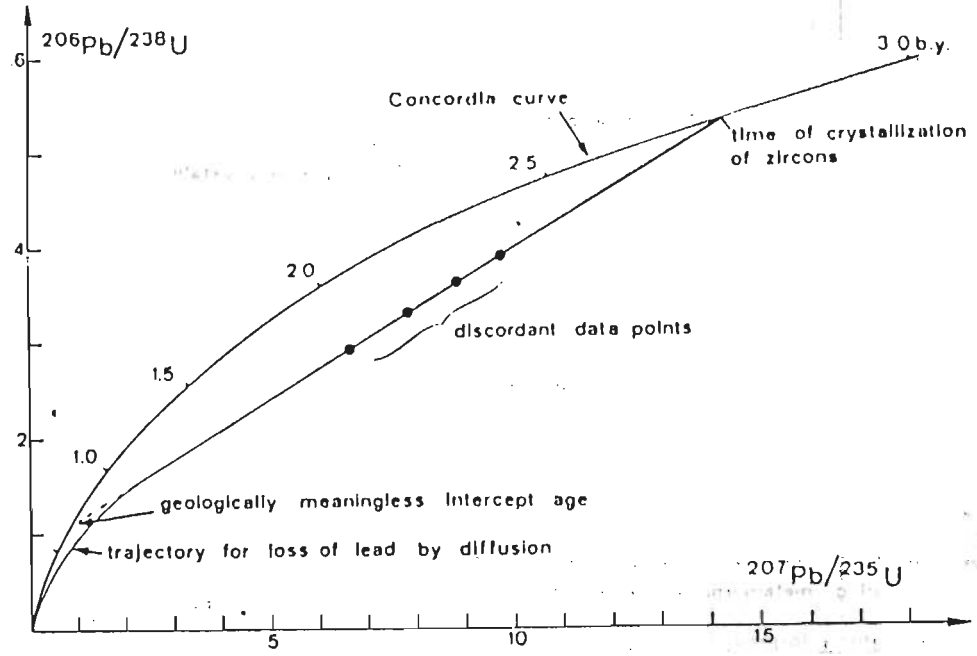

Figure 6.3 a : Concordia diagram showing a diffusion trajectory through the experimental data points. As diffusion curves, based on either on continous (Tilton, 1960) or time-dependent (Wasserburg, 1963) diffusion are very similar, their application will result in practically the same primary ages (Gebeuer and Grunenfelder, 1979).

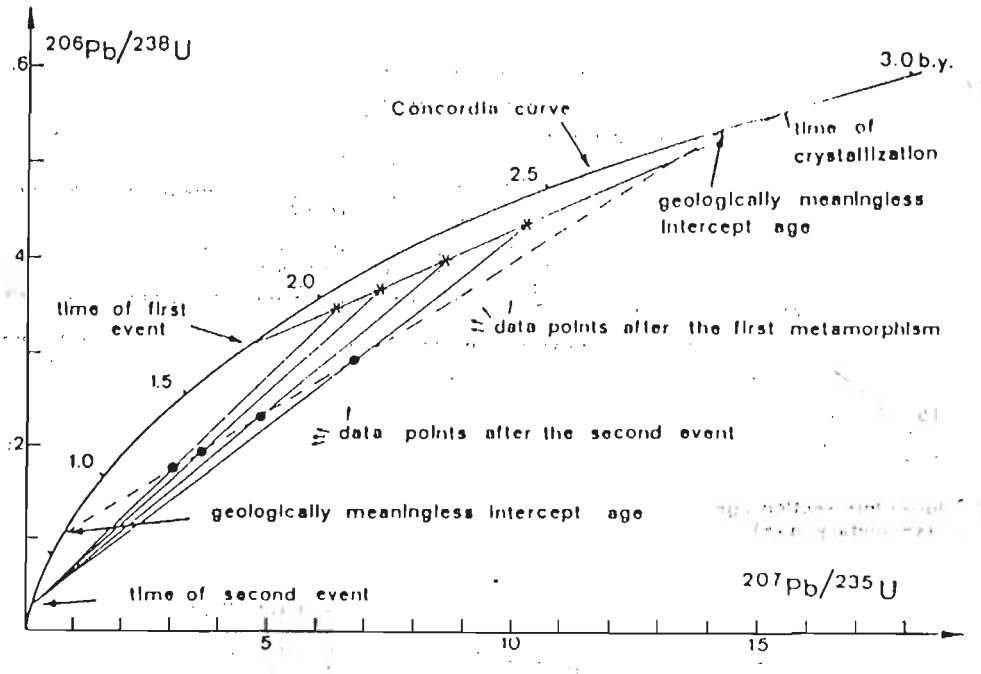

Figure 6.3 b : Concordia diagram showing data points, whose position is a result of a two-stage opening of U-Pb zircon systems. Crosses mark the positions of data points of today, if the second event would have reopened the U-Pb systems (Gebeuer and Grunenfelder, 1979).

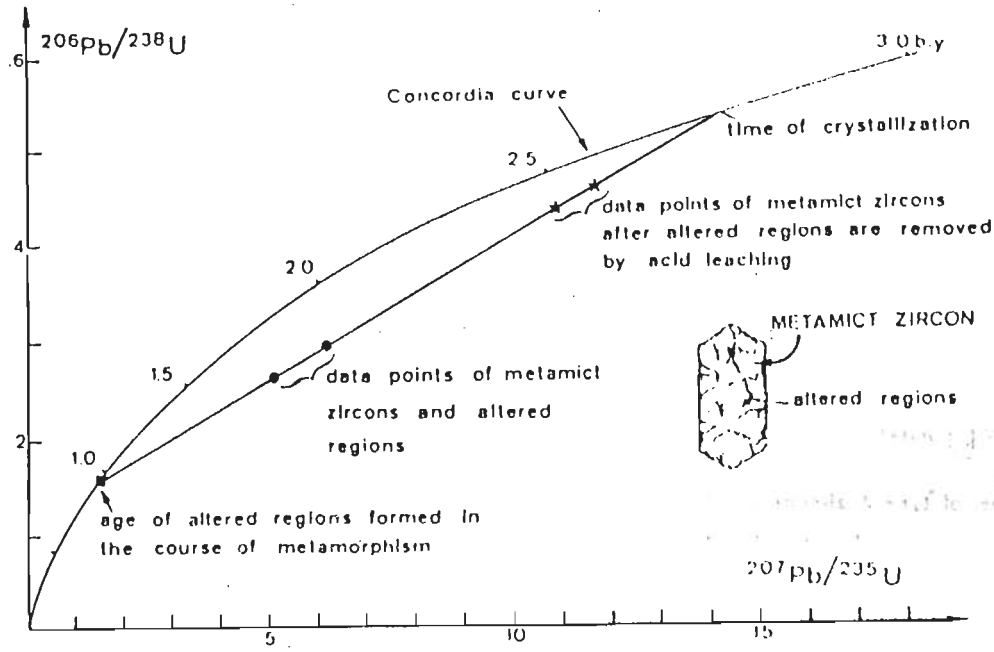

Figure 6.4 b : Concordia diagram with data points of zircon fractions containing variable amounts of altered regions (Gebeuer and Grunenfelder, 1979).

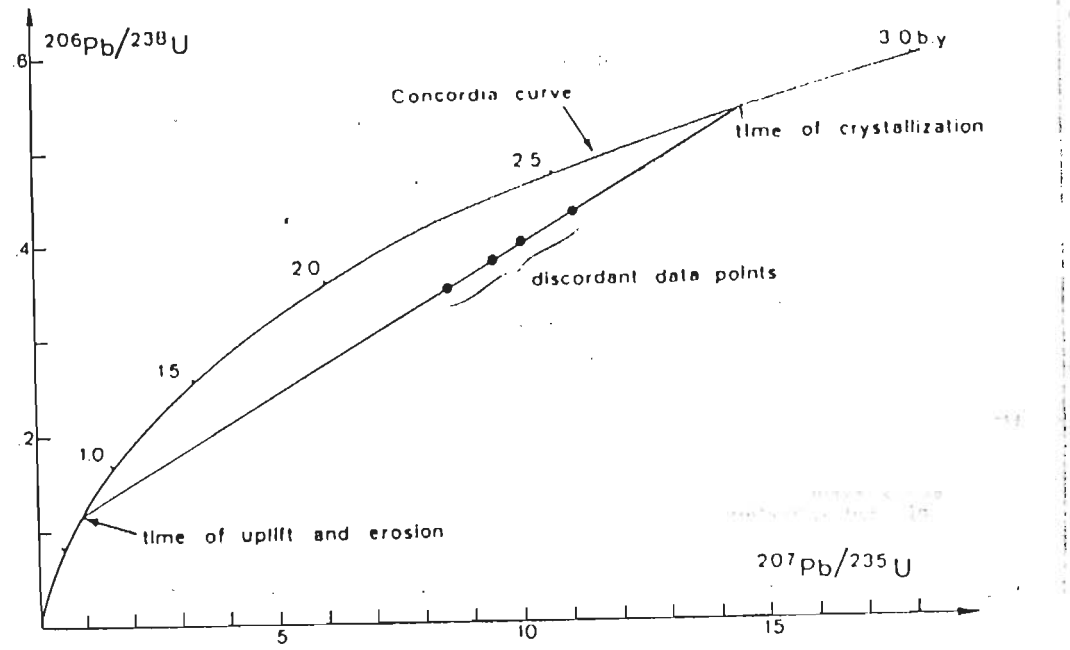

Figure 6.4 a : Concordia diagram with data points of zircon fractions with the discordia line, lower intersection showing the age of uplift and erosion (Gebeuer and Grunenfelder, 1979).

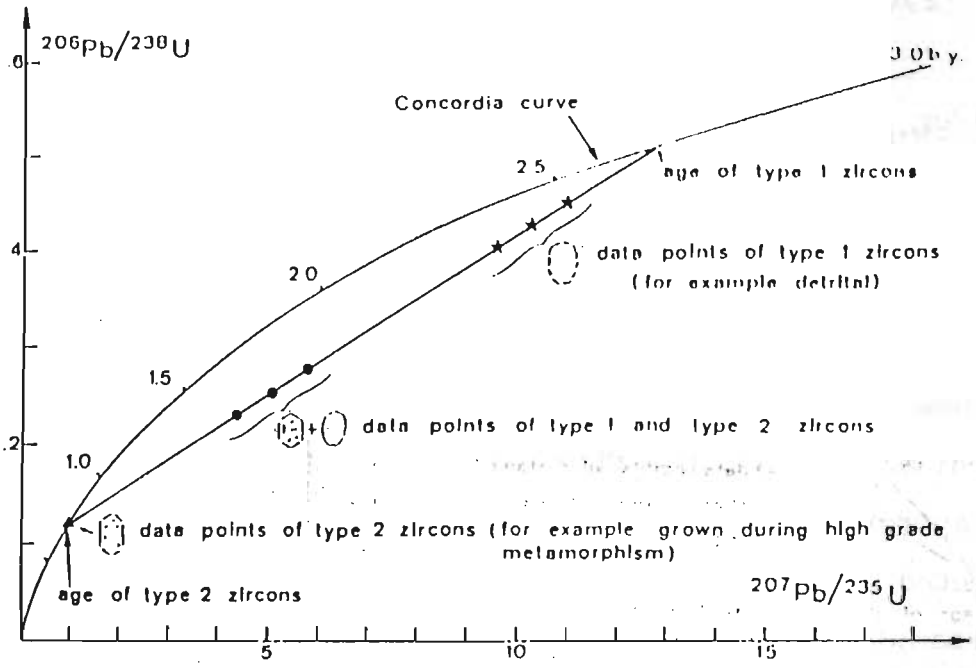

Figure 6.5 b : Concordia diagram with the data points of zircon suit consisting of mixed population. Such data pattern might occur in high-grade metamorphic terranes, in which zircon is newly formed during metamorphism (Gebeuer and Grunenfelder, 1979).

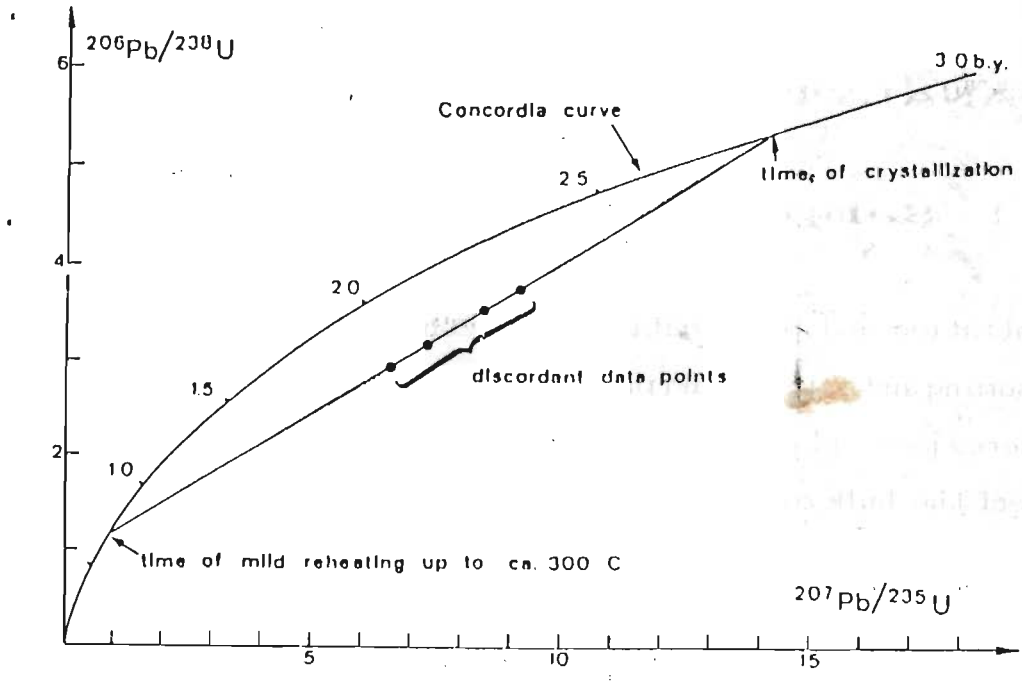

Figure 6.5 a : Concordia diagram with data points of zircon suit, which lost lead due to low-temerature recrystallization at or below ca. 300° C. The condition to anneal zircon at these low temperature is the existence of a strongly radiation-damaged crystal structure (Gebeuer and Grunenfelder, 1979).

6.3 SAMPLE COLLECTION

In order to obtain the best results, fresh, completely unaltered, unmetamorphosed and undeformed rocks should be very carefully selected in the field and collected. Carefully selected regions in the HHC along the Sutlej valley have yielded two undeformed samples of the grey granite (sample no. RR 17/21 or 90056; Fig. 6.6) and Wangtu granitoid (sample no. RR 7/6 or 90054; Fig. 6.6), though these bodies have otherwise undergone extensive deformation and metamorphism. Likewise, the Chor granitoid has revealed its undeformed chracter approximately 5 km from its contact with the Jutogh metamorphics has been selected for U-Pb geochronology (sample no. CH 1/1 or 90055; Fig. 6.6). One deformed sample has also been selected (sample no. CH 4/11 or 90067; Fig. 6.6) near the contact with the Jutogh metamorphics to analyse the effect of deformation and metamorphism on the U-Pb systematics. Each samples weighed approximately 30 kg. Extreme case was undertaken to pick up unweathered, fresh and undeformed samples.

6.4 ANALYTICAL METHODS

6.4.1 Sample preparation

Concentration and purification of zircon crystals from the rocks is a time-consuming and painstaking process. At the beginning, the sample is washed and weathered parts if present, are removed. A piece of each sample is selected to represent the bulk rock type. The dried sample is first crushed by a large jaw crusher into 2-3 cm size rock chips and then to another jaw crusher to obtain even finer pieces. Before performing crushing, each active surface of the jaw crusher has been thoroughly cleaned with vacuum cleaner, steel brush, and compressed air in order to avoid contamination between sample processing.

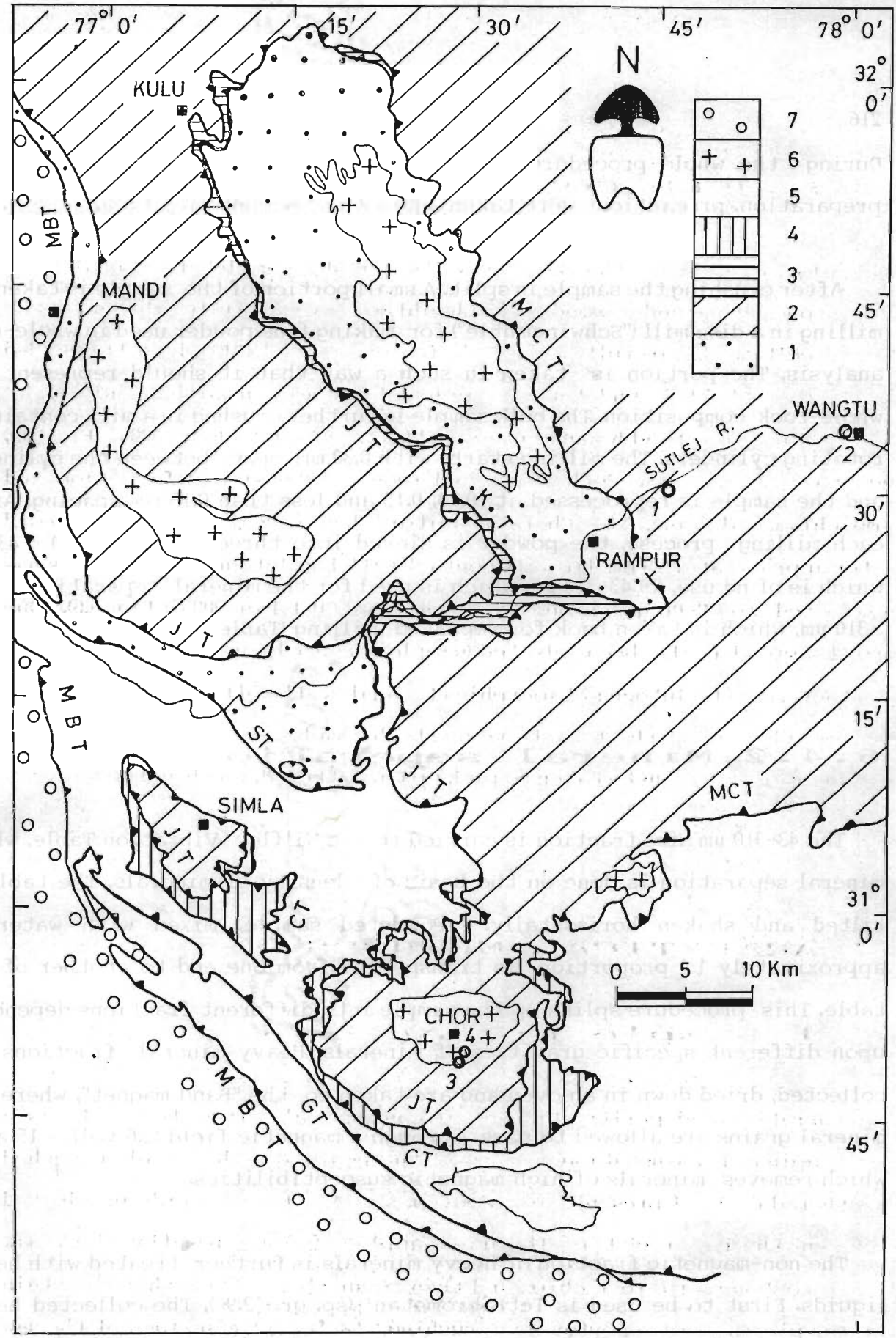

Figure 6.6 : Location map of granitoid bodies used for the geochronological purpose in present work. 1 : grey granitoid, 2 : Wangtu granitoid, 3 : deformed Chor granitoid and 4 : undeformed Chor granitoid.

During the whole procedure of sample treatment and subsequent chemical preparation, precautions were taken against cross-contamination.

After crushing the sample is split. A small portion of the sample is taken for milling in a disc mill ("Schwingmuhle") for making fine powder used in whole-rock analysis. The portion is taken in such a way that it should represent the whole-rock composition. The bulk sample is further crushed in a mill containing rotating cylinders. The milling starts with 0.30 mm space between the cylinders and the sample is reprocessed at 0.20, 0.15 and less than 0.15 mm spacing. After each milling process, the powder is sieved into three fractions: (a) < 43 µm, which is of no use, (b) 43-310 µm, which is used for the mineral separation and (c) > 310 µm, which is taken back for repeated milling (Table 6.1).

6.4.2 Mineral seperation

The 43-310 µm size fraction is carried to the Wilfley Vibration Table, where mineral separation is done on the basis of density of minerals. The table is tilted and shaken horizontally. Powdered sample, mixed with water in approximately 1:4 proportion is transported from one end to another of the table. This procedure splits up the sample into different fractions depending upon different specific gravities of minerals. Heavy mineral fractions are collected, dried down in an oven and are taken to the "Band magnet", where the mineral grains are allowed to pass through a magnetic field (2.6 volt - 15 amp), which removes minerals of high magnetic susceptibilities.

The non-magnetic fraction of heavy minerals is further treated with heavy liquids. First to be used is Tetrabrometan (sp. gr. 2.96). The collected heavy portion is washed in alcohol and later in 3 * distilled water and dried in oven at 70° C. During this initial step of heavy liquid separation, the following

TABLE 6.1 : FLOW CHART FOR CRUSHING-MILLING-SEIVING PROCESS FOR ZIRCON SEPERATION

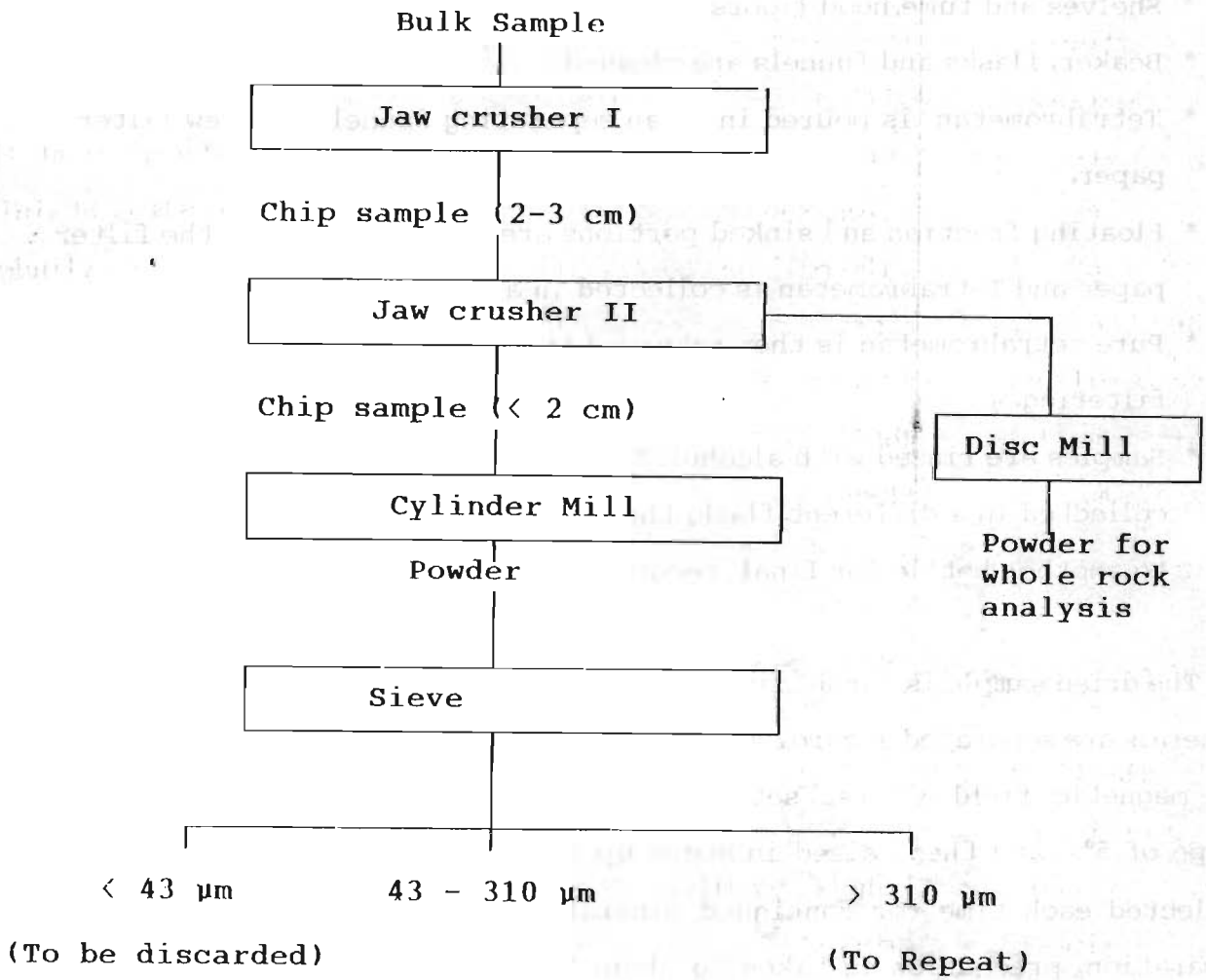

precautions are taken :

* Shelves and fume hood floors are cleaned.
* Beaker, flasks and funnels are cleaned.
* Tetrabrometan is poured in clean separating funnel with new filter paper.
* Floating fraction and sinked portions are drained through the filter paper and Tetrabrometan is collected in a flask below.
* Pure tetrabrometan is then returned to the stock bottle after renewed filtering.
* Samples are rinsed with alcohol. Tetrabrometan mixed with alcohol is collected in a different flask; the mixture is washed by water and taken to another bottle for final recovery.

The dried sample is further upgraded by Frantz Isodynamic separator, where minerals are separated according to their different magnetic susceptibilities. The magnetic field is first setup at 0.15 amp with a constant tilt of 10° and a slope of 5°, and then raised in steps up to 0.4 amp. Non-magnetic portion is collected each time for continued mineral seperation. During the magnetic separation, precaution is taken to clean the interior of Frantz Isodynamic separator, chute and magnet thoroughly by compressed air.

After first Frantz magnetic separation, minerals are taken for a second heavy liquid separation using Dijodmetan (sp. gr. 3.34). After centrifuging the sample in plastic tubes, sunk portion along with Dijodmetan is frozen by liquid nitrogen and the float is removed. The sunk portion is washed with alcohol, then with 3 * distilled water and subsequently put into oven at 70° C. During this liquid separation, same precautions are taken as during the first liquid separation. After drying down, the sunk portion is taken to second magnetic separation with settings ranging from 0.5 amp to 1.5 amp with intermediate steps

at 0.6 amp, 0.8 amp, 1.0 amp, 1.2 amp, and 1.35 amp. Each time only the non-magnetic portion is reprocessed through stronger magnetic field. The non-magnetic fraction at 1.5 amp is finally treated with Clerisis solution (sp. gr. 4.03) for liquid seperation. The sunk portion including zircons are washed by 3 * distilled water and dried down in oven at 70° C.

Zircon concentrate is then sieved into five size fractions (i) > 210 µm (ii) 150 - 210 µm (iii) 106 - 150 µm, (iv) 74 - 106 µm and (v) < 74 µm. The best zircons, uncoloured and free from all inclusion, are selected by hand picking from each fraction for the chemical treatment (Table 6.2).

6.4.4 Chemical preparation

After having hand-picked different size fractions of zircon, the following methodology has been adopted for chemical treatment.

a. <u>Cleaning of zircons</u> : The chemical preparation starts with different washing procedures. Each zircon fraction is treated seperately in cleaned pyrex beakers with 6N QD HCl on hot plate for 20 minutes without letting it boil. The following steps are followed in cleaning zircon grains:

* HCl is washed away by 3 * distilled H_2O; alcohol is used for breaking the surface tension of water due to which some zircons are seen floating.
* Zircons are washed with 7 N HNO_3 for 20 minutes on hot plate.
* HNO_3 is washed off with 3 * distilled H_2O.
* Water is removed and beakers are half-filled with ELGA water and put into ultrasonic bath for about 10 minutes. (If the water is not clear, it is changed and the process is repeated until the water is clear).
* The ELGA water is removed and zircons are washed with DB H_2O (double

TABLE 6.2 : FLOW CHART SHOWING VARIOUS STEPS IN MINERAL SEPERATION AT THE ISOTOPE LABORATORY, STOCKHOLM, SWEDEN.

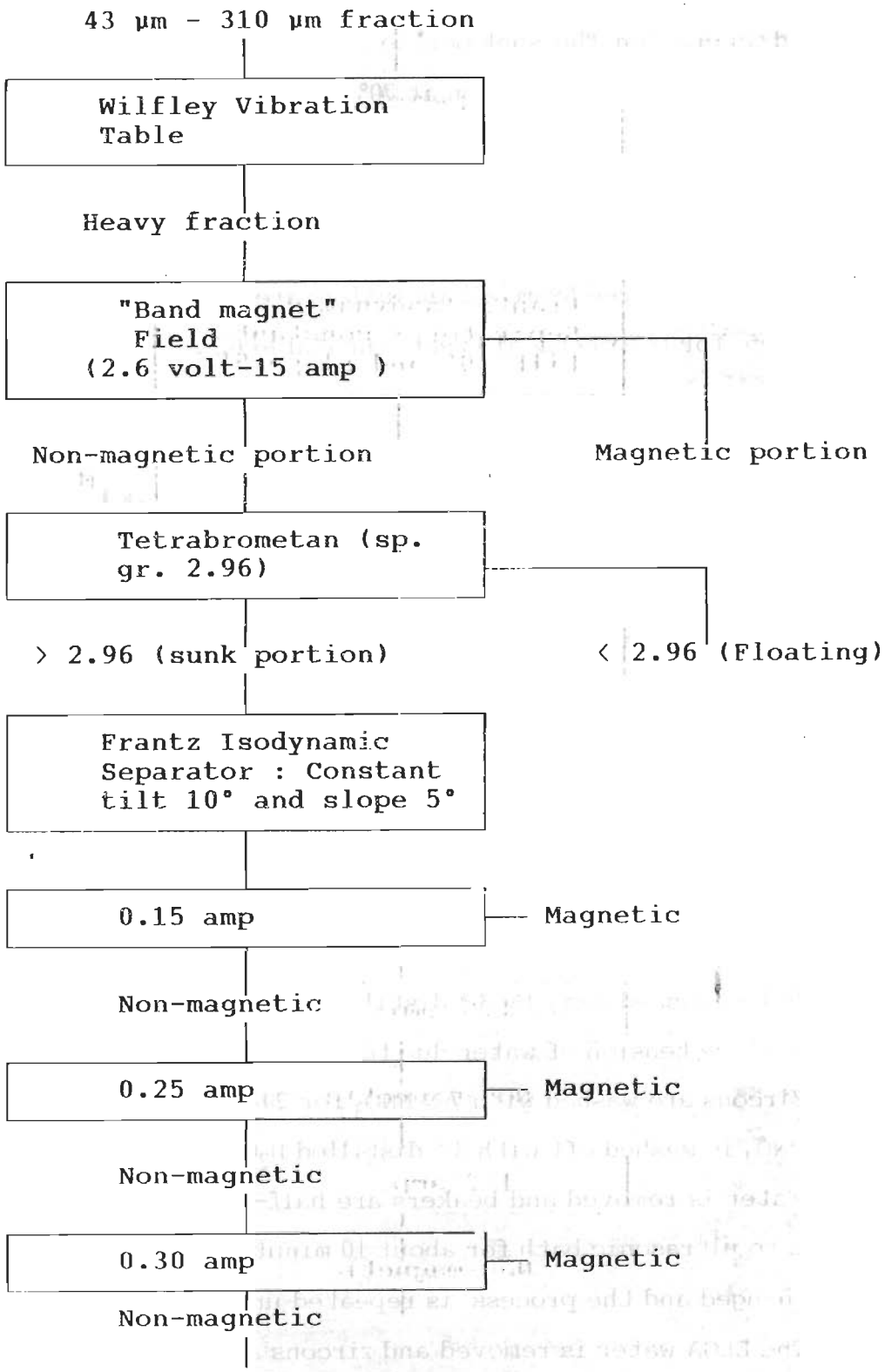

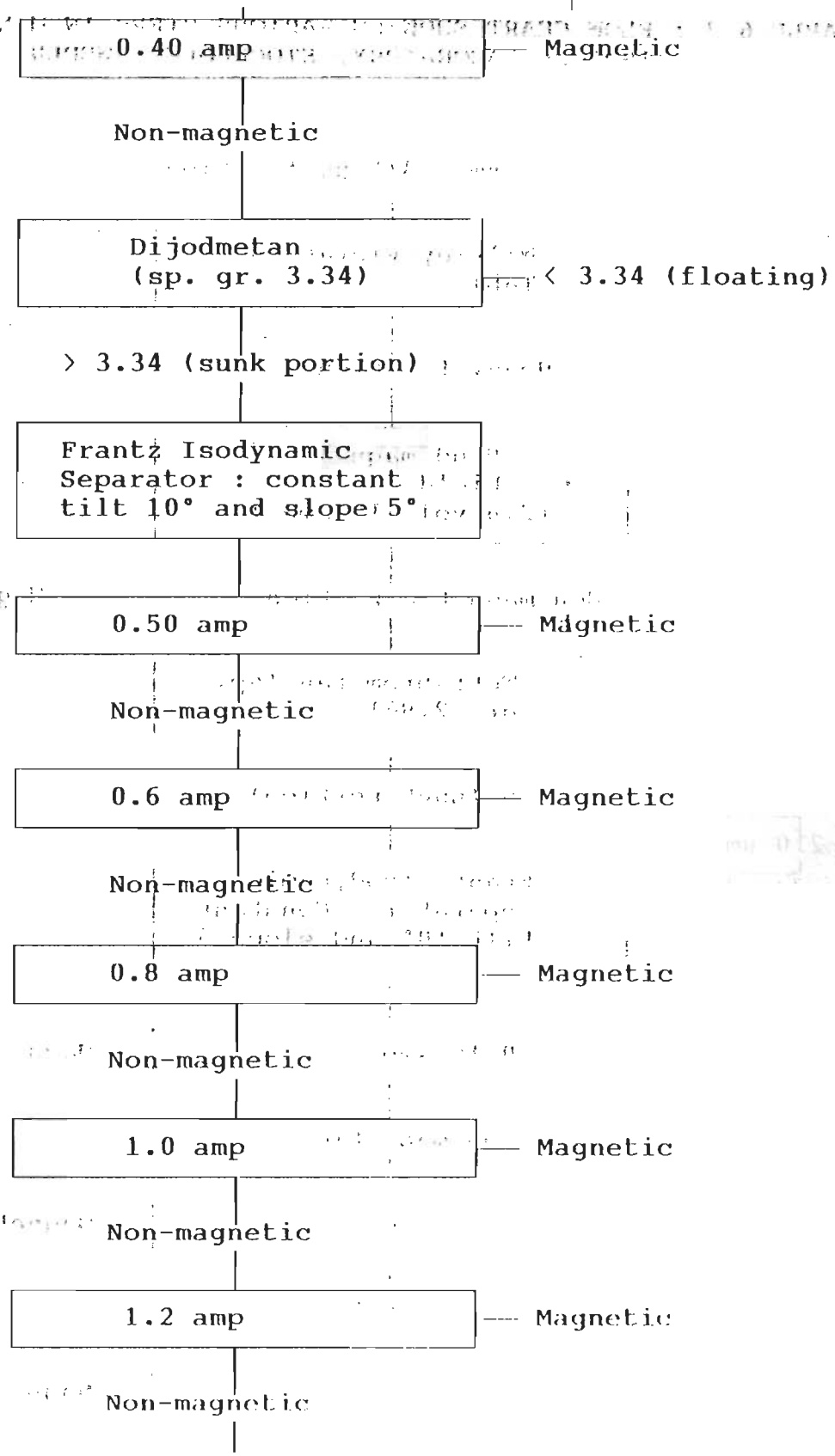
0.40 amp
Magnetic
Non-magnetic
Dijodmetan
(sp. gr. 3.34)
< 3.34 (floating)
> 3.34 (sunk portion)
Frantz Isodynamic
Separator : constant
tilt 10° and slope 5°
0.50 amp
Magnetic
Non-magnetic
0.6 amp
Magnetic
Non-magnetic
0.8 amp
Magnetic
Non-magnetic
1.0 amp
Magnetic
Non-magnetic
1.2 amp
Magnetic
Non-magnetic

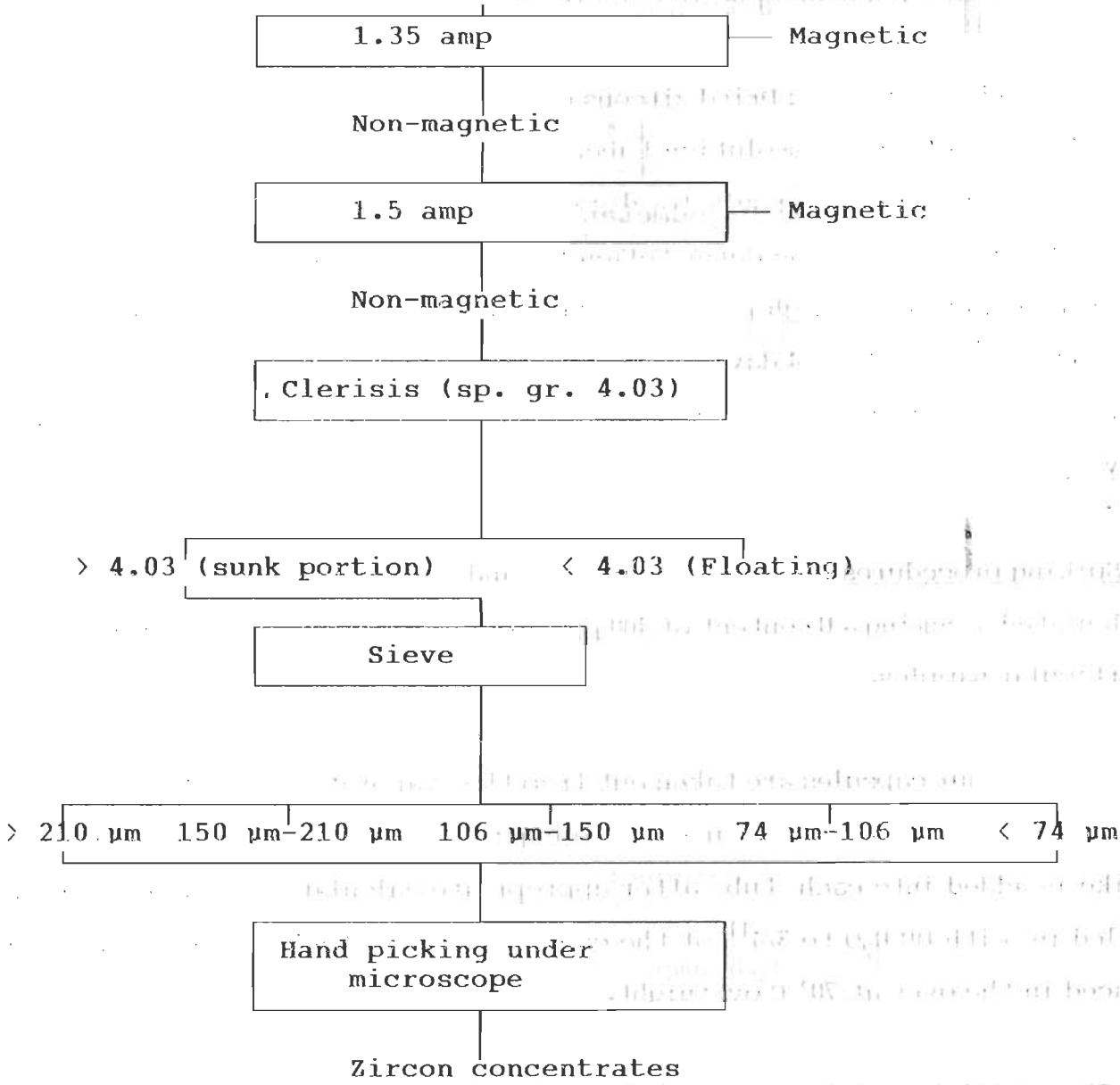
1.35 amp
Magnetic
Non-magnetic
1.5 amp
Magnetic
Non-magnetic
Clerisis (sp. gr. 4.03)
> 4.03 (sunk portion)
< 4.03 (Floating)
Sieve
> 210 µm
150 µm-210 µm
106 µm-150 µm
74 µm-106 µm
< 74 µm
Hand picking under microscope
Zircon concentrates

bottle distilled) and put in oven for drying.

b. Dissolution of zircon : Dried zircons of each fractions are weighed out into double-walled teflon dissolution tube. 0.3 ml HF + HNO_3 (10:1 ratio) is added to each inner dissolution capsule for dissolution, while HF + HNO_3 of same strength and ratio is added to the outer teflon tubes. The outer teflon tube is tightly closed and put into a high pressure teflon-lined steel "bomb". The bomb is put into the oven for about 4 days at 200° C and is later removed from the oven. The capsules are taken out, opened up and put in the evaporation chamber for drying.

c. Spiking procedures : Amount of ^{235}U spike and ^{208}Pb spike for each sample are calculated assuming a U content of 400 ppm and a Pb content of 100 ppm for these particular samples.

All the four capsules are taken out from the evaporation chamber and allow to cool down at room temperature. Sample capsules are then weighed. Weighed ^{235}U spike is added into each tube after appropriate calculations. These are then filled in with DB H_2O to 3/4th of the capsules and put back into the tube and placed in the oven at 70° C overnight.

The capsules are taken out next day and cooled. Each sample is divided into ID (isotope dilution - 1/4 portion) part and IC (isotope composition - 3/4 portion) part. ^{208}Pb spike is added to the ID part. The blank sample, which has been handled extactly in the same way as the zircon sample, is divided into two halfs and ^{206}Pb spike is added to both of these halfs rather than ^{208}Pb. After addition of Pb spike both the ID and IC portions are put into the evaporation chamber.

Dried vessels are taken out from the chamber and 200 ml of HBr (0.4N) is added to them and the samples are left overnight for dissolution.

d. Ion exchange : Ion exchange is carried out by two methods:

(i) Modified traditional method (Krogh,1973) and

(ii) Modified new method (Menhes et al.,1978),

These methods have been used for comparison in getting good intensity of isotopes in mass-spectrometer.

The samples are taken out next day for ion exchange process. Ion exchange separation columns made up of plastic are half-filled in by analytical grade cation exchange resin AG 1-X8 (100-200 mesh) chloride form + DB H_2O. When the resin has settled down, it is washed by 200 µl 0.5 N HNO_3, then two times by 200 µl DB H_2O. The resin is conditioned by putting 150 µl of HBr (0.4N) through the column. After that the sample, dissolved in HBr, is put into the column and U is collected in a separate teflon vessel along with Zr and Fe. This teflon vessel is replaced by a new vessel and the old one is put into the evaporation chamber.

The Pb ions are collected in new vessels by passing 3 * 200 µl DB H_2O through the column. This teflon vessel is also put in the evaporation chamber for drying down and the residue then dissolved again in 200 µl HBr (0.4N) overnight.

A second Pb ion exchange step is performed next day using the same resin and same column, after washing them with 200 µl 0.5 N HNO_3 and two times with 200 µl DB H_2O followed by conditioning with 150 µl HBr (0.4N). After that the sample dissolved in HBr is put into the column and washed with 200 µml HBr (0.4N) once. Then the Pb ions are collected in a new teflon vessel by passing 200 µl DB H_2O three times through the column. After collecting the Pb ions the vessels is taken to the evaporation chamber for drying down. The sample is then ready for mass-spectrometry of Pb.

The sample having U, Zr and Fe are also dissolved but in 0.5 ml 3.1 N DB HCl and is put for dissolution overnight.

After this, a new bigger plastic column is set with analytical grade cation exchange resin AG 1-X8 (200-400 mesh) nitrate form + DB H_2O. When the resin has settled down, it is washed with 1.0 ml DB H_2O and conditioned with 1.0 ml 3.1 DB HCl. After that, the dissolved U, Zr and Fe is put into the column and washed away by 0.25 ml 3.1 N DB HCl twice and then one time 0.5 ml 3.1 N DB HCl. Then elution of U is done by 0.5 ml DB H_2O and 1.0 ml DB H_2O. U is collected in seperate teflon vessel. The vessel is then taken to the evaporation chamber, then dried down. The sample is now ready for mass-spectrometry of U.

6.4.5 Mass Spectrometry

All isotopic measurements are carried out on the Finnigan MAT 261 Mass-Spectrometer. The MAT 261 Mass-Spectrometer is designed for isotope ratio determination using thermal ionization. The precise determination of isotopic ratios of solid samples by thermal ionization requires a highly evacuated analyser system with an ion source for thermal ionisation, which usually generates positive sample ions. The ions are generated, accelerated and focussed within the ion source. The resolution is determined by an ion source slit with a slit width of 0.2 mm. After passing through this slit and the following Y-lens, the ions traverse the free space between the ion source and the magnetic sector field. The ion beam enters and leaves the magnetic sector with an angle of 26.5° with respect to a perpendicular entrance line. Inside the 90° magnetic sector field, each type of ions are affected by a slightly variable force, which is mass and charge dependent. This variable effect causes a seperation of ions of different masses. The ions of different masses (isotopes) can be detected simultaneously with five Faraday detectors and one multiplier detector. The

multiplier detector is used for very small signals, because it can detect signals one hundred times smaller than the detectable level in a Faraday detector. The signals from the detectors are passed through very stable amplifiers, after which these are transformed into digital signals for the computer. Up to thirteen samples can be loaded at the same time and can be automatically run from the computer.

6.5 RESULTS

6.5.1 Zircon morphology

Zircons from the grey granite are euhedral prisms of variable length, averaging about 4:1, with sharp crystal edges and pointed pyramidal terminations. Most crystals are transparent, with some opaque inclusions, and many are strongly zoned. Some crystals include darker coloured central parts, which also are euhedral and oriented parallel to the crysals in which they occur, suggesting that they rather form part of a magmatic zonation pattern in the crystal.

The majority of the zircons in the Wangtu granitoid are well crystaliised euhedral prisms, commonly with sharp edges and pointed pyramidal terminations (Fig. 6.7 a). The average length : width ratio is about 3:1. The crystals are generally transparent, but inclusions are not uncommon (Fig. 6.7 b) and some crystals have internal structure suggesting they may include older cores (Fig. 6.7 c). These are, however, commonly euhedral and oriented parallel to the crystals suggesting the same interpretation like grey granite, as parts of a magmatic zonation pattern (Fig. 6.7 d). Other zircon varieties include twinned crystals, zoned grains, subrounded to rounded grains and terminations, clouded

grains and crystals containing fluid inclusions (Figs. 6.7 b, c, d).

The zircons from the Chor granitoid are generally transparent and some are rich in opaque inclusions (Fig. 6.8 a). Most of the crystals are euhedral but of variable shapes (Fig. 6.8 b) both elongated prism and ellipsoidal crystals with well-developed high-indice surfaces are common (Fig. 6.8 c). No significant, optically distinct cores have been noteworthy in comparision to Wangtu granitoid (Fig. 6.8 d). Other varieties include clouded grains, twinned crystals, grains having fluid inclusions and subrounded grains (Figs. 6.8 b, c, d).

6.5.2 U–Pb zircon ages

The grey granite gneiss, lying near the base of the HHC within the Jeori Formation, occurs as a small stock. A regression line, based on 6-zircon fractions, yields an upper intercept age of 2068 ± 5 Ma (2σ) and a lower intercept age of 379 ± 18 Ma (2σ) having MSWD value 0.93 (Fig. 6.9; Table 6.3). The finer fractions < 74 μm are more discordant, whereas abraded fraction between 106-150 μm moves towards the upper intercept. The upper intercept age of 2068 ± 5 Ma (2σ) indicates the primary crystallisation age. The lower intercept does not have any geological significance and there is no indication of any inherited Pb component or any disturbance in this granitoid body.

The Wangtu granitoid has upper intercept U-Pb zircon age of 1866 ± 10 Ma (2σ) and a lower intercept age of 48 ± 28 Ma (2σ), with a low MSWD value of 0.1, as evident from a regression based on 5-zircon fractions (Fig. 6.10; Table 6.4). Like grey granitoid, the finer fractions are more discordant, whereas the abraded fraction plots closer to the upper intercept. There is no indication of any inherited Pb component or any other disturbance in this body and we interpreted the upper intercept age of 1866 ± 10 Ma (2σ) closely reflecting the primary crystallisation age for the Wangtu granitoid.

Figure 6.7 a : Zircons from the Wangtu granitoid body with well crystallised, euhedral prism commonly with sharp edges and pointed pyramidal terminations. The average length : width ratio is about 3:1. PL X 308.5

Figure 6.7 b : Zircons from the Wangtu granitoid with well-grown tripple twinned, euhedral prism with sharp edges and pointed pyramidal terminations and transparent inclusions. The average length : width ratio is about 3:1. PL X 617.

Figure 6.7 c : Zircons of the Wangtu granitoid with well-grown euhedral prism with sharp edges and pointed pyramidal terminations and transparent inclusions. Zircons also showing darker cores. PL X 617.

Figure 6.7 d : Zircons of the Wangtu granitoid with well-grown euhedral prism and sharp edges and pointed pyramidal terminations and transparent inclusions. Zircons showing darker cores with magmatic zonation pattern. PL X 617.

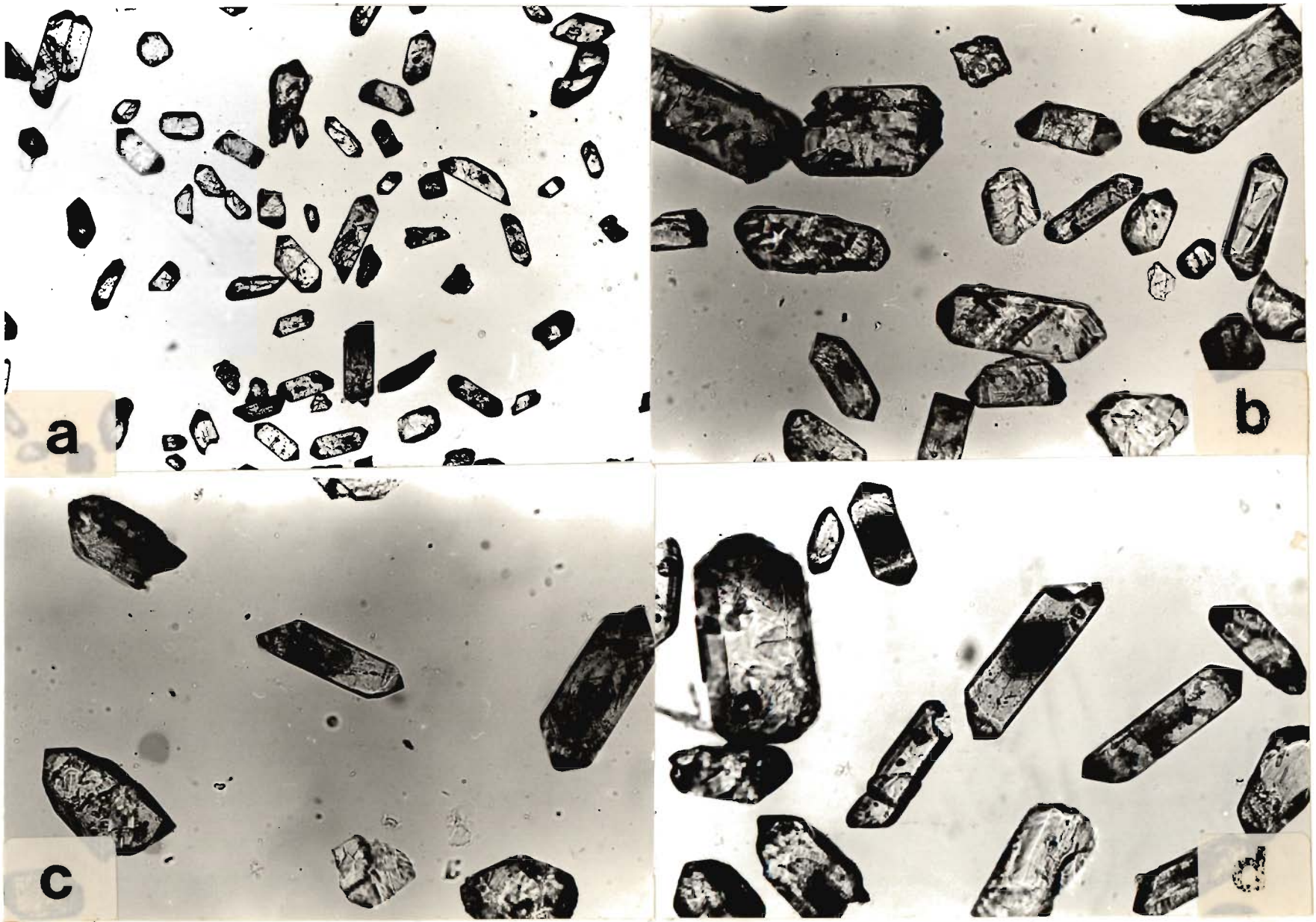

FIG. 6.7

FIG. 6.8

Figure 6.8 a : Zircons of the Chor Granitoid with well developed euhedral prism having sharp edges and pointed pyramidal terminations and transparent to opaque inclusions. PL X 308.5.

Figure 6.8 b : Zircons from the Chor granitoid with variable in shape and well developed euhedral prism and sharp edges, pointed pyramidal terminations and mostly transparent. PL X 617.

Figure 6.8 c : Zircons from the Chor granitoid having variable shape with well developed euhedral prism also ellipsoidal crystals. Also precence of twinned crystal is noted from the crop, which is mostly transparent in nature with a few inclusions. PL X 617.

Figure 6.8 d : Zircons from the Chor granitoid with variable shape and well developed euhedral prism having high indices and also ellipsoidal crystals. Also presence of twinned crystal is noted from the crop, which is mostly transparent in nature with no inclusions. PL X 617.

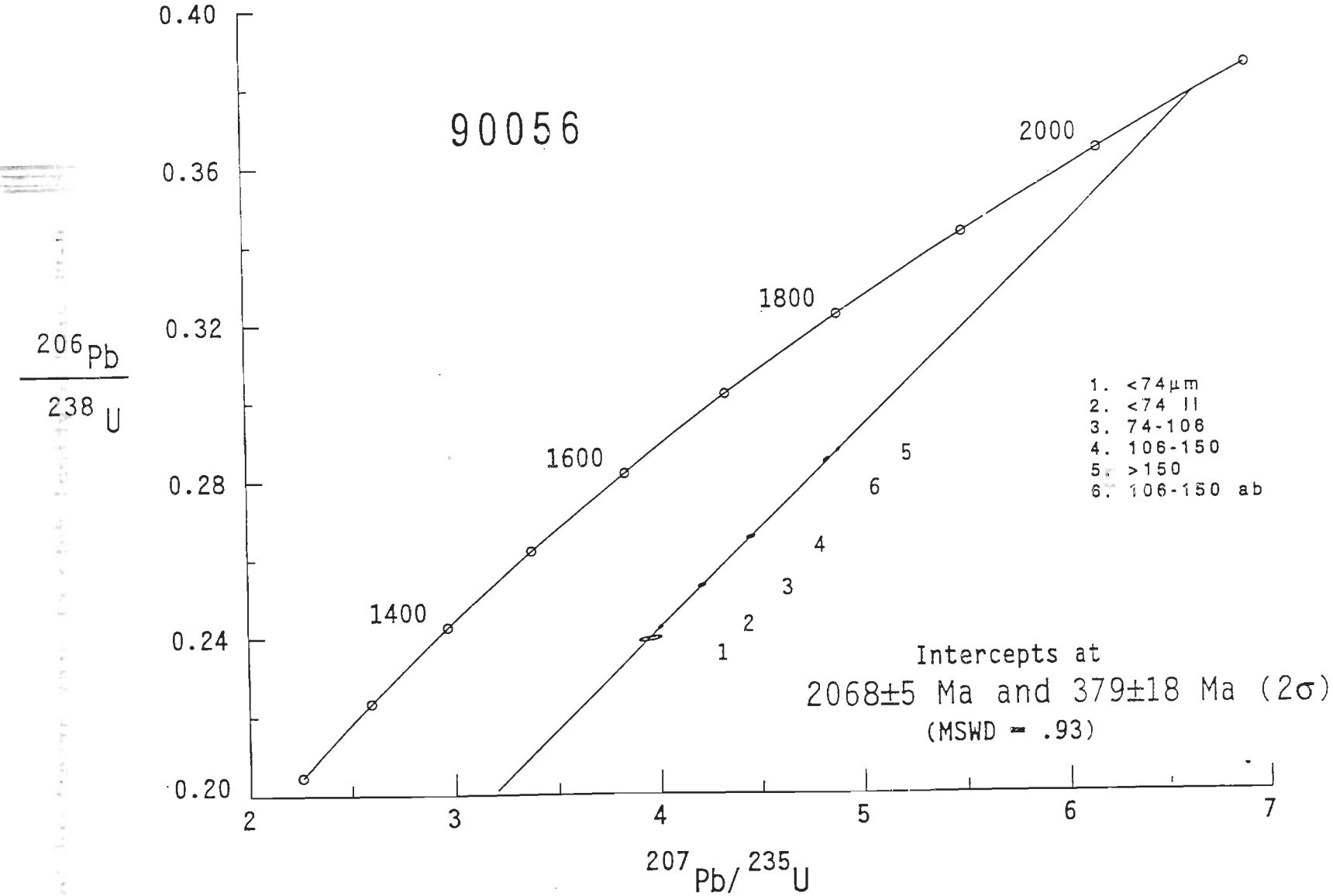

Figure 6.9 : U-Pb concordia diagram for the grey granitoid from the HHC, Sutlej valley.

TBALE 6.3 : U-Pb analyalytical data of grey granitoid form Sutlej valley, Himachal Pradesh

Sample 90056 (fractions)	Concentration in ppm U	Pb_{rad}	^{204}Pb	Atomic ratios[a] and model ages in Ma $^{206}Pb/^{204}Pb$	$^{208}Pb/^{206}Pb$	$^{206}Pb/^{238}U$	$^{207}Pb/^{235}U$	$^{207}Pb/^{206}Pb$
<74 µm	1340	307	1.345	218	0.0303	0.23926±55 1383	3.953±45 1625	0.11984±120 1954
<74 µm ab	1386	325	1.330	230	0.0400	0.24225±44 1398	4.0048±100 1635	0.11990±19 1955
74-106 µm	1101	275	0.128	1865	0.0302	0.25279±40 1453	4.2105±147 1676	0.12080±34 1968
106-150 µm	1059	276	0.189	1275	0.0287	0.26524±40 1517	4.4544±165 1723	0.12180±37 1983
> 150 µm	1016	289	0.216	1165	0.0362	0.28729±43 1628	4.8868± 83 1800	0.12337±10 2005
106-150 µm ab	931	262	0.010	2290	0.0322	0.28476±46 1613	4.8284±126 1790	0.12298±22 2000

(a) $^{206}Pb/^{204}Pb$ corrected for blank and mass discrimination, all other atomic ratios also corrected for initial lead. Errors are given as least significant digits at the 95% confidence level.

Discrimination U 0.05% / AMU Pb 0.12% / AMU
Blank U 0.5 ng Pb 0.2 ng
Common lead $^{206}Pb/^{204}Pb$ 15.1 $^{207}Pb/^{204}Pb$ 15.2
$^{208}Pb/^{204}Pb$ 34.8
(Stacey and Kramer growth curve)

ab - abraded as described by Krogh (1973)

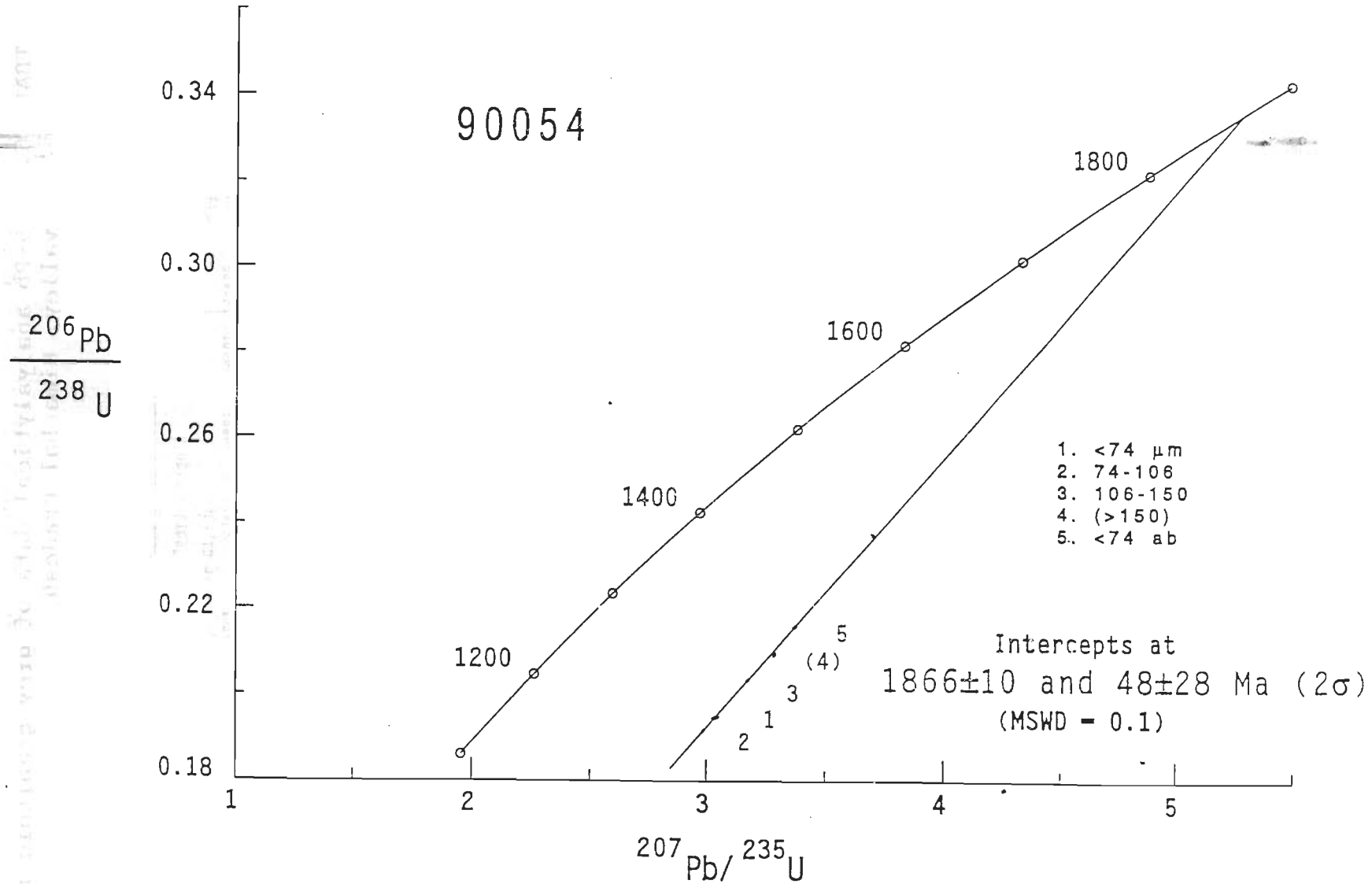

Figure 6.10 : U-Pb concordia diagram for the Wangtu granitoid from the HHC, Sutlej valley.

TABLE 6.4 : U-Pb analyalytical data of the Wangtu granitoid form Sutlej valley, Himachal Pradesh

Sample 90054 (fractions)	Concentration in ppm U	Pb_{rad}	^{204}Pb	Atomic ratios[a] and model ages in Ma $^{206}Pb/^{204}Pb$	$^{208}Pb/^{206}Pb$	$^{206}Pb/^{238}U$	$^{207}Pb/^{235}U$	$^{207}Pb/^{206}Pb$
<74 µm	677	137	0.0129	8680	0.0942	0.19476±31 1147	3.0373±121 1417	0.11311±36 1850
74-106 µm ab	1125	222	0.0045	41000	0.0856	0.19166± 34 1130	2.986± 60 1404	0.11300±09 1948
106-150 µm ab	909	193	0.0297	5500	0.1005	0.20338± 31 1193	3.1730± 54 1451	0.11315±09 1851
< 150 µm	793	172	0.0928	1600	0.0959	0.20934± 31 1225	3.2852± 53 1478	0.11382±07 1861
<74 µm ab	810	182	0.0160	9290	0.0160	0.21586±32 1260	3.3719±78 1498	0.11329±18 1853

(a) $^{206}Pb/^{204}Pb$ corrected for blank and mass discrimination, all other atomic ratios also corrected for initial lead. Errors are given as least significant digits at the 95% confidence level.

Discrimination U 0.05% / AMU Pb 0.12% / AMU
Blank U 0.5 ng Pb 0.3 ng
Common lead $^{206}Pb/^{204}Pb$ 15.6 | $^{207}Pb/^{204}Pb$ 15.3
$^{208}Pb/^{204}Pb$ 35.2
(Stacey and Kramer growth curve)

ab - abraded as described by Krogh (1973)

The U-Pb zircon results for the Chor granitoid present a more complex geological history. Sample CH 4/11 (90067) is slightly deformed due to the presence of ductile shear zone and located near the contact with the Jutogh metamorphics. 3-zircon fractions from this sample yield a regression line with large errors, because there are only limited fractions available, having the upper and lower intercept ages of 859 ± $^{119}_{27}$ Ma (2σ) and 460 ± 264 Ma (2σ) with MSWD value 0.22 (Fig. 6.11; Table 6.5). Whereas 8-zircon fractions of the least deformed sample CH 1/1 (90055) are scattered, these do not form any discordia line (Fig. 6.12; Table 6.6). All the data points, except for the fraction `150-210 μm', plot close to the concordia curve. Five of these cluster close to the discordia line, while the coarsest un-abraded fraction is significantly more discordant (Fig. 6.13). All 8 analyses together yield a reference line with an upper intercept age of c. 910 Ma, but there is a large scatter about this line. After exclusion of the three fraction `> 210 μm', `150- 210 ab μm' and `106-150 redone μm', the remaining five fractions give a discordia line with the upper intercept age 912 ± 6 Ma (2σ) and MSWD of 2.0 (Fig. 6.13; Table 6.6). However, this line has a negative lower intercept age.

6.6 DISCUSSIONS

The U-Pb zircon ages for the grey granitoid sample RR 17/21 (90056) and the Wangtu granitoid sample RR 7/6 (90054) of the HHC are, in principle, very similar and indicate uncomplicated U-Pb isotopic sysytems in zircon crystals from both the rocks. Both zircon populations yield good-fit discordia line, with the exception of the coarsest grain-size fraction from the Wangtu granitoid, which plots slightly to the right of the discordia. The discordancy generally increases with decreasing grain size, and one abraded fraction from each sample is slightly less discordant than the other fractions.

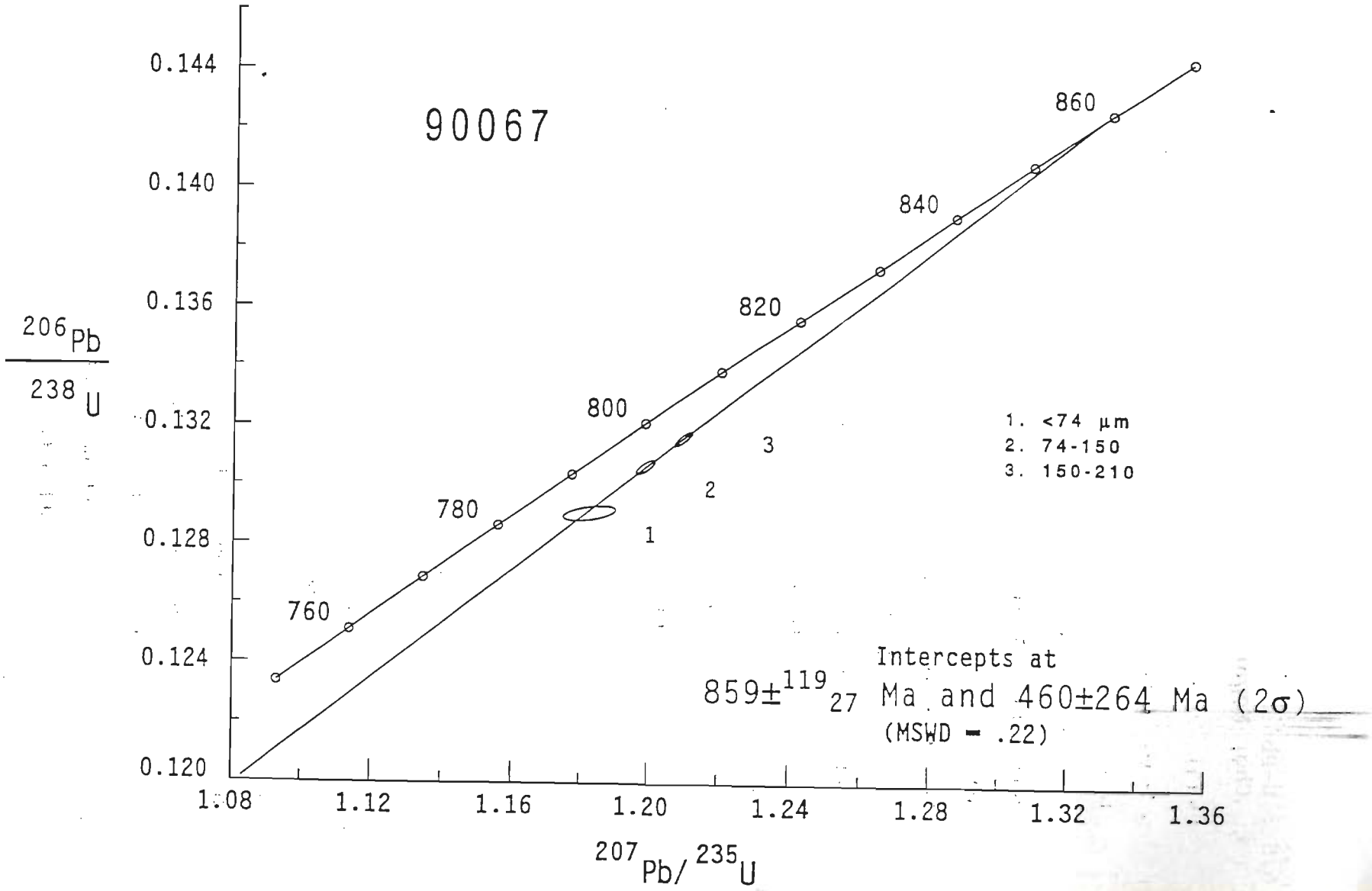

Figure 6.11 : U-Pb concordia diagram for the deformed Chor granitoid from the Chor Mountain.

TABLE 6.5 : U-Pb analyalytical data of the Chor granitoid form Chor Mountain, Himachal Pradesh

Sample 90067 (fractions)	Concentration in ppm U	Pb_{rad}	^{204}Pb	Atomic ratios[a] and model ages in Ma $^{206}Pb/^{204}Pb$	$^{208}Pb/^{206}Pb$	$^{206}Pb/^{238}U$	$^{207}Pb/^{235}U$	$^{207}Pb/^{206}Pb$
<74 µm	633	88	0.0113	6100	0.1852	0.12906±21 782	1.1824±63 792	0.06645±31 820
74-150µm	623	85	0.0119	5800	0.1517	0.13066±20 792	1.1988±23 800	0.06654±08 823
150-210µm	548	75	0.0121	5100	0.1404	0.13163±20 797	1.2098±21 805	0.06665±05 827

(a) $^{206}Pb/^{204}Pb$ corrected for blank and mass discrimination, all other atomic ratios also corrected for initial lead. Errors are given as least significant digits at the 95% confidence level.

Discrimination U 0.18% / AMU Pb 0.12% / AMU
Blank U 0.5 ng Pb 0.1 ng
Common lead $^{206}Pb/^{204}Pb$ 17.4 $^{207}Pb/^{204}Pb$ 15.5
$^{208}Pb/^{204}Pb$ 37.1
(Stacey and Kramer growth curve)

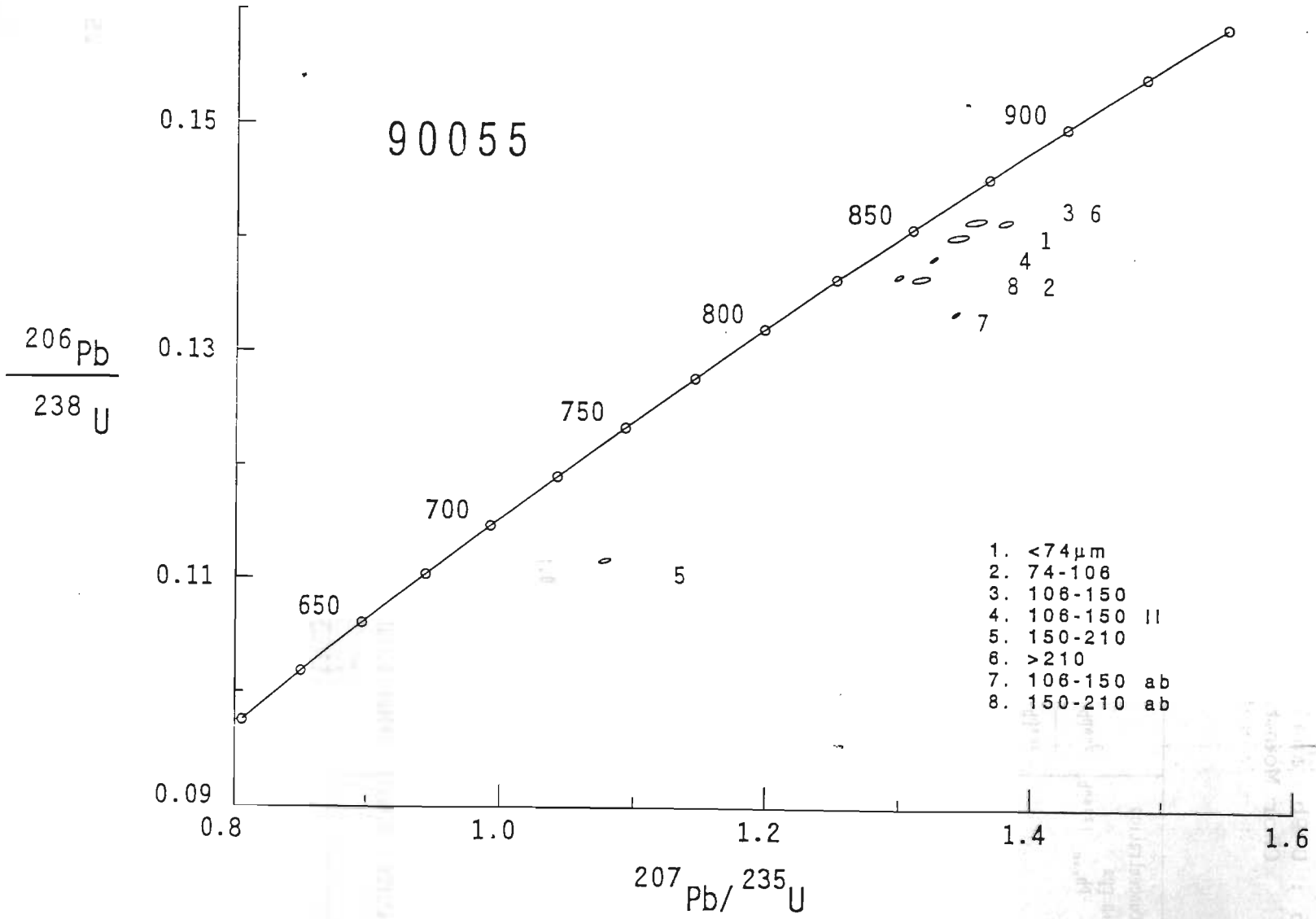

Figure 6.12 : U-Pb concordia diagram for the undeformed Chor granitoid body from the Chor Mountain.

TABLE 6.6 : U-Pb analyalytical data of the chor granitoid from Chor Mountain, Himachal Pradesh

Sample 90055 (fractions)	Concentration in ppm U	Pb_{rad}	^{204}Pb	Atomic ratios[a] and model ages in Ma $^{206}Pb/^{204}Pb$	$^{208}Pb/^{206}Pb$	$^{206}Pb/^{238}U$	$^{207}Pb/^{235}U$	$^{207}Pb/^{206}Pb$
<74 µm	930	127	0.0036	30700	0.0636	0.14029±24 846	1.3433±66 865	0.06945±30 912
74-106µm	887	119	0.0072	14400	0.0690	0.13665±22 826	1.3159±57 853	0.06984±26 924
106-150µm	864	121	0.0034	26100	0.0786	0.14169±24 854	1.3567±66 870	0.06944±30 912
106-150µm II	827	114	0.0006	>100000	0.0921	0.13843±19 836	1.3253±23 857	0.06944±06 912
150-210µm	1122	123	0.0044	24400	0.0762	0.11162±18 682	1.0780±37 743	0.07004±20 930
> 210 µm	692	129	0.0011	75000	0.4553	0.14160±23 854	1.3798±47 880	0.07067±19 948
106-150µm ab	741	97	0.0008	>100000	0.0719	0.13362±20 808	1.3418±24 864	0.07283±07 1009
150-210µm ab	887	125	0.0008	>100000	0.1241	0.13683±21 827	1.2990±27 845	0.06885±10 894

(a) $^{206}Pb/^{204}Pb$ corrected for blank and mass discrimination, all other atomic ratios also corrected for initial lead. Errors are given as least significant digits at the 95% confidence level.
Discrimination U 0.05% / AMU Pb 0.12% / AMU
Blank U 0.5 ng Pb 0.2 ng
Common lead $^{206}Pb/^{204}Pb$ 17.2 $^{207}Pb/^{204}Pb$ 15.5
$^{208}Pb/^{204}Pb$ 36.9
(Stacey and Kramer growth curve)

ab - abraded as described by Krogh (1973)

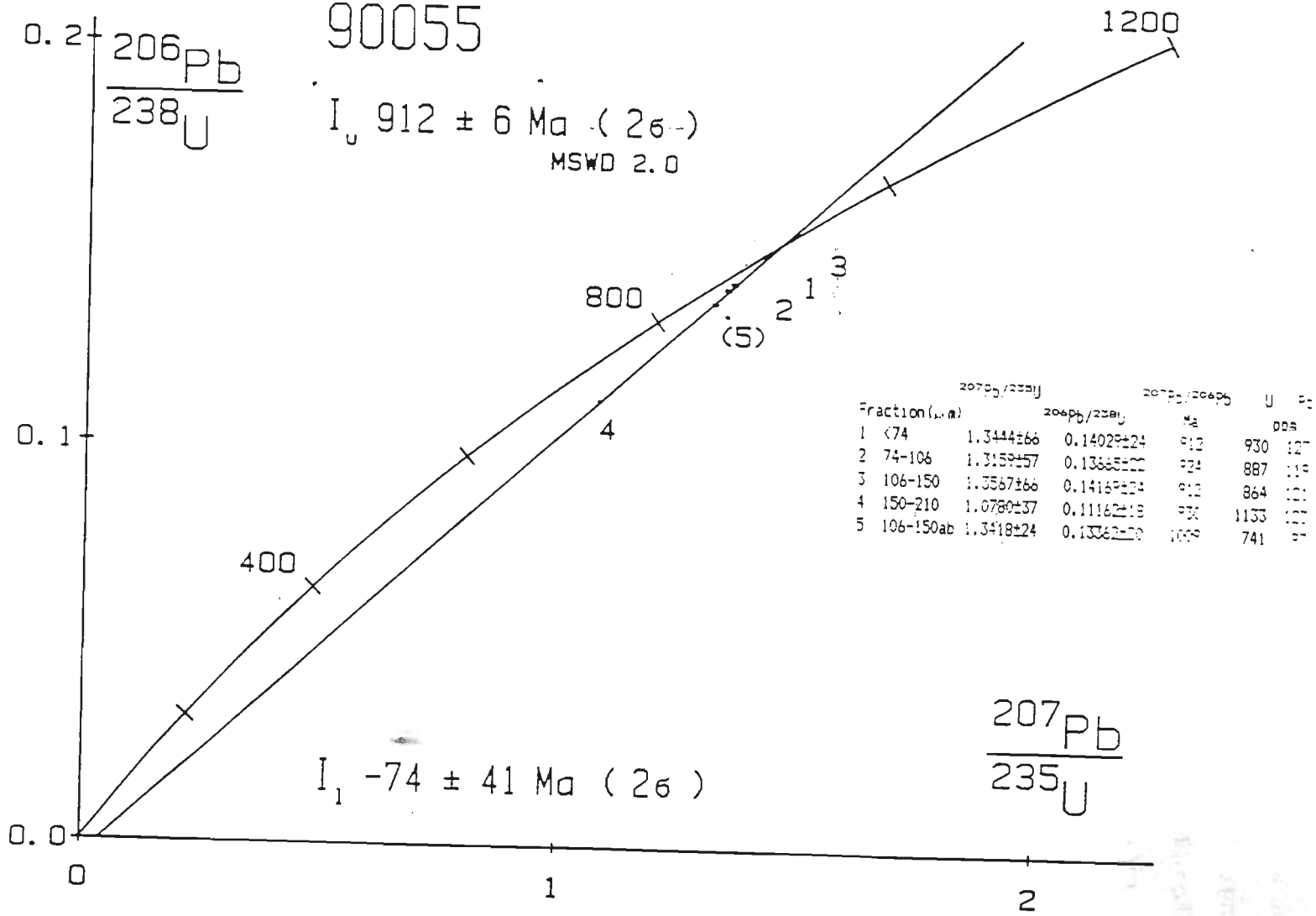

Figure 6.13 : U-Pb concordia diagram for the undeformed Chor granitoid body from the Chor Mountain.

As described previously, both samples include crystals with internal structures, which could be interpreted as cores. These were avoided during handpicking of the analysed fractions, but it is experienced that it can be very difficult to optically identify all such crystals. It is thus possible that the coarse fraction (> 150 µm) from the Wangtu granitoid include a minor component of older inherited Pb. However, the good fit of all other data points, including the abraded fractions, to the discordia line indicates that these internal structures are either related to the zonation of crystals or that older components, which might have been incorporated in crytals, do not significantly affect the analytical results. Since there is no indication in the presented data of any later disturbances, the upper intercept ages have been interpreted as the age of primary crystallisation.

For the grey granitoid, discordia line has a MSWD value of 0.93 and the upper intercept age is 2068 ± 5 Ma. The Wangtu granitoid discordia line with the coarse grain-size-fraction included gives an upper intercept age of 1879 ± 62 Ma and a high MSWD value of 3.2. With the coarse fraction excluded, the five-point discordia line has a MSWD of 0.1 and the upper intercept age is 1866 ± 10 Ma. The latter age has been interpreted to be the best estimate of the primary crystalisation age of the Wangtu granitoid. The lower intercept ages of 379 ± 18 Ma and 48 ± 28 Ma respectively, have probably no direct chronological meaning.

The results for the Chor granitoid are more complex. Seven fractions, including two abraded, were analysed from sample CH 1/1 (90055). Six of these cluster close to the discordia line, while the coarsest un-abraded size-fraction is significantly more discordant. There is no obvious systematic trend in these data. In particular, the relations between the two abraded fractions and the un-abraded fractions of the same grain size vary in an unpredicted manner. All seven analyses together yield a reference line with an upper intercept age of c. 910 Ma, but there is a large scatter about this line. After exclusion of the

fraction i.e., '> 210 μm' and '106-150 ab μm', the remaining five-fractions give a discordia line with the upper intercept age of 912 ± 6 Ma. Therefore, there is no justification for their exclusion. Three slight discordant zircon fractions from the more deformed sample CH 4/11 (90067) define a discordia line with MSWD value 0.2 with an imprecise upper and lower intercept ages of 859 $\pm ^{119}_{27}$ Ma and 460 ± 264 Ma respectively.

The scattering data for the Chor granitoid may be a result of both inherited Pb in zircons and a complex post-crystallisation Pb loss pattern. No exact crystallisation age can be calculated from these data, but the near concordancy, roughly linear arrangement and small spread of most of the data points strongly suggest that the results reflect a major event, which most likely appears to be the primary crystallisation event of the Chor granitoid at c. 0.9 Ga. However, two alternative interpretations require some comments. The Chor granitoid could be either significantly older and the zircon U-Pb isotopic data reflect partial Pb loss at a later time, or it could be significantly younger and the zircons include a large component of inherited Pb. Such model requires that the data points plot along or below a line joining the ages of the two events. Based on published Rb-Sr isotope data for Himalayan granites (Table 1.1), one U-Pb zircon age from the HHC (Pognante *et al.*, 1990) and results of the Wangtu granitoid and grey granitoid of the HHC, 0.5 and 1.8-2.0 Ga would be likely ages for these two events. It is clear from the concordia diagram that the Chor granitoid data plots well above a line joining 1.8 and 0.5 Ga in the concordia diagram (Fig. 6.14). Thus, the Chor data do not allow these two-events scenarios. The three-zircon fractions from the deformed sample CH 4/11 (90067) plot to the left of the seven fractions (Fig. 6.14) from sample CH 1/1 (90055). This could be related to the foliation seen along the margin of the body; the localised deformation may also have caused a partial Pb loss.

High $^{87}Sr/^{86}Sr$ initial ratios, calculated from U-Pb model zircon ages for

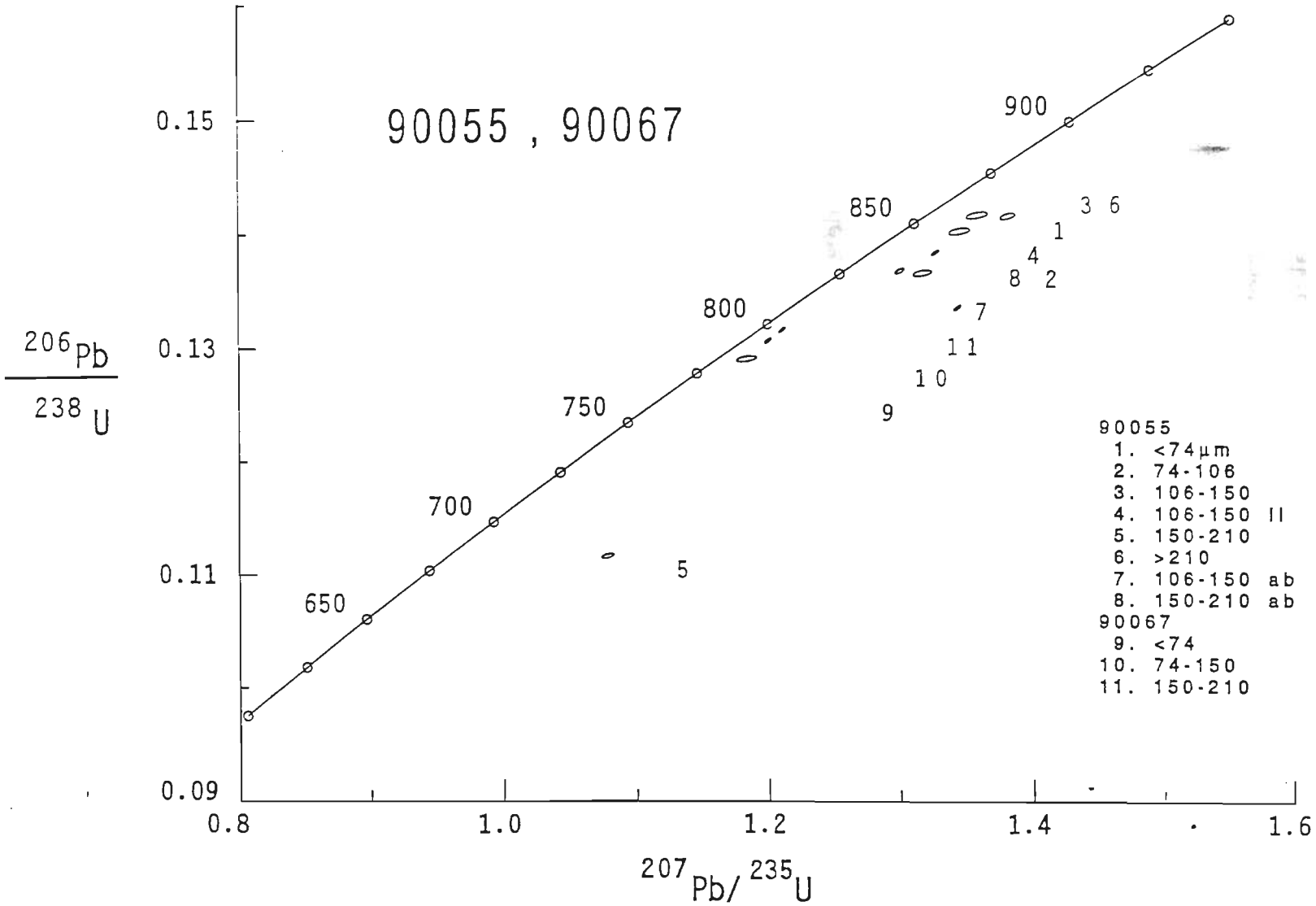

Figure 6.14 : U-Pb concordia diagram for the Chor granitoid body from the Chor Mountain.

TABLE 6.7 : Analytical Rb-Sr data for whole rock samples from the HHC and the Jutogh Nappe, Himachal Pradesh

Sample	Type	Rb[a] ppm	Sr[a] ppm	Rb/Sr[b]	$^{87}Rb/^{86}Sr$[c]	$^{87}Sr/^{86}Sr$[d]	Model age	$(^{87}Sr/^{86}Sr)_i$
90054	Wangtu granitoid	253	147	1.713	5.025	0.849070±10	1866 Ma	0.7163497±10
90055	Chor granitoid	263	161	1.630	4.743	0.767681±08	912 Ma	0.7062572±08
90067	Chor granitoid	226	767	0.2948	0.8540	0.719233±10	859 Ma	0.7081703±10

(a) XRF, approximate content

(b) XRF, estimated precision ± 0.6-0.8%

(c) XRF and Mass-Spectometer

(d) Mass-Spectometer, errors given as two standard errors of the mean.

three samples RR 7/6 (90054), CH 1/1 (90055) and CH 4/11 (90067) range from 0.7062 to 0.7163, and are indicative of crustal provenance (Table 6.7).

CHAPTER 7: DISCUSSION AND CONCLUSION

7.1 INTRODUCTION

The geodynamics of the Himalaya has been conceptualised in terms of northward movement and subduction of the Indian Plate beneath the Eurasian Plate along major suture zones like the Indus Suture Zone during the Late Mesozoic. This has possibly caused the closure of the Tethys Ocean by the ocean-continent subduction progressing into continent-continent collision. The latter phenomenon is associated with intracontinental crustal shortening and deformation either along southerly migrating major thrusts viz., the Main Central Thrust (MCT), the Main Boundary Thrust (MBT) or large-scale strike-slip faults in Tibet (Dewey and Bird, 1970; Dewey and Burke, 1973; Narain, 1973; Le Fort, 1975; Molnar and Tapponnier, 1975; Valdiya, 1980; Mattauer, 1986; Sharma, 1991; Thakur, 1993). As a consequence of intense crustal shortening during the Collision Tectonics, the Higher Himalayan rocks have been deformed and metamorphosed during the Cenozoic (Le Fort, 1975, 1986; Bouchez and Pecher, 1981; Honeggar et al., 1982; Searle and Rex, 1989; Jain and Anand, 1988).

The present work is an attempt to understand the Collision Tectonics in parts of Himachal Pradesh incorporating deformation, metamorphism, igneous geochemistry and geochronology in a segment of the metamorphic terrain, essentially made up of Proterozoic remobilised basement.

7.2 SUMMARY OF PRESENT WORK

7.2.1 Geological and tectonic framework

Detailed geological mapping in parts of Sutlej valley and Chor Mountains has revealed major tectonostratigraphic units of the Lesser Himalayan Proterozoic sedimentary foreland, exposed in the Kulu-Rampur Window and numerous other small windows. These include the Shali Formation and Rampur Group of limestone, dolomite, slate, phyllite and a thick orthoquartzite-volcanic association. The para-autochthon of the window sequence is thrust over by the southward migrating Bajura/Kulu Nappe of the Middle Proterozoic mylonitised augen gneiss, which truncates and probably overrides the frontal Chail Nappe. In the north, the Higher Himalayan Crystalline (HHC) belt between Jakhri and Wangtu, and the Jutogh Nappe in parts of the Chor Mountain and Luhri-Dalash region contain essentially metapelite sequence, having occasional quartzite, marble and amphibolite. These are prolifically emplaced by various types of granitoids. Numerous metamorphic nappes are distinctly demarcated by major tectonic boundaries like the Main Central Thrust (MCT), the Kulu Thrust (KT) and the Chaura Thrust between basal Jeori Formation of the HHC and the Wangtu Gneissic Complex; the Jutogh Thrust (JT) and the Chor Thrust between the Chor granitoid and the Jutogh metamorphics.

7.2.2 Deformation and metamorphism

The HHC belt along the Sutlej valley between Jakhri and Wangtu is thrust over the Rampur Group along the antiformally folded MCT and characterised by four distinct deformation phases. Of these, the second phase D_2 is marked by

prominent axial-plane foliation S_2 of reclined F_2 folds, which plunge N to NNE. A coaxial stretching/mineral lineation L_2 to these folds is very prominently seen throughout the HHC. These structures are developed during southwesterly-verging ductile shearing during the Himalayan Orogeny. The trend of regional foliation and orientation of strain ellipsoid in parts of porphyroclastic Wangtu gneiss indicate that this zone probably incorporates at least three subsidiary ductile shear zones with bulk strain field of flattening-type throughout the progressive deformation. It is also evident that the contact between the Wangtu granite gneiss and garnetiferous mica schist of the Jeori Formation is characterised by numerous structures of ductile deformation regime in a shear zone.

In contrast, the Chor Mountain region exhibits three distinct deformational phases, of which the most prominent is the first D_{C1} phase, producing a distinct nearly horizontal E or W plunging folds and a coaxial lineation. The D_{C1} deformational phase corresponds to the D_2 deformation of the the HHC and inner parts of the Jutogh Nappe along the Sutlej valley, where this nappe is thrust over the Shali para-autochthon and represents the souhwestern limb of a large-scale synform.

Mutual structural relationships in this part of the Himalayan metamorphic belt indicate that main displacement along the MCT and Jutogh Thrust *sensu stricto* post-date the orogen-parallel fabric of the D_3 deformational event, and transported the ductily-deformed metamorphic pile.

The Himalayan metamorphic belt of the HHC and the Jutogh Nappe has undergone polyphase Barrovian-type metamorphism. The Lesser Himalayan units of the Kulu-Rampur Window are essentially metamorphosed within greenschist facies, while the metamorphism in the hanging wall of the MCT and Jutogh thrust varies from upper greenschist to amphibolite facies condition.

In the HHC, earliest recognisable first deformation D_1 is associated with metamorphism M_1 and is absent in frontal part of the Jutogh Nappe in Chor Mountain region. This metamorphism M_1 is weak, probably having quartz-sericite-chlorite-biotite-feldspar-opaque assemblage of the greenschist facies.

During the most pervasive main D_2/D_{C1} deformation in the HHC and the frontal part of the Jutogh Nappe respectively, most of the metamorphic minerals like mica, garnet, staurolite, kyanite, chloritoid and amphibole have grown syntectonically both along S- and C- shear planar fabric. Growth of these minerals produces concordant S_i S_e relationship during main metamorphism (M_2/M_{C1}). Garnet has grown in at least two distinguishable metamorphic episodes, which are documented by inclusion-rich syntectonic core, overgrown by inclusion-free post-tectonic rim. Staurolite is found only in a few sample, whereas kyanite is noticed in staurolite-kyanite grade rocks of the Sutlej valley. Chloritoid is present with staurolite in a few samples of garnet and staurolite-kyanite grade transitional zone in both the areas.

Metamorphism during D_3/D_{C2} deformation is weak and manifested by synkinematic crystallisation of low grade minerals like quartz, muscovite and greenish biotite along axial plane foliation of F_3/F_{C2} folds as well as post-tectonic cross-mica growth. Retrogression during late D_3/D_{C2} deformation develops chlorite at the expense of garnet and biotite, and sericite from feldspar.

Mineralogical and P-T data indicate that metamorphism remains in garnet to staurolite-kyanite grade conditions. The base of the HHC on northeastern parts of the Kulu-Rampur Window, and parts of the Jutogh metamorphics in the Chor Mountains mark the transition zone between garnet and staurolite-kyanite grades, as is evident from the presence of chloritoid, staurolite and chlorite in the assemblage. In the Jutogh Nappe, P-T estimation on syntectonic garnet

core during M_{C1} metamorphism indicate a variation of about 130° C from 520° C to 650° C, while post-tectonic garnet rim reveals a cooling path of the metamorphic pile with temperature falling between 480° C and 550° C at 5.4 to 7.8 kbar from its base towards higher topographic and structural levels in the section. This variation seems to be real rather than apparent, hence is indicative of the metamorphic inversion in the Jutogh Nappe. In addition, the HHC also reveals a temperature estimation of 520° C near its base during the M_2 metamorphism and attains a maximum of 650° C towards higher structural level. This section also provides evidences of possible metamorphic inversion in the HHC.

7.2.3 Magmatism

The HHC and Jutogh Nappe contain numerous Proterozoic granitoid bodies, now deformed into gneisses, probably due to the Himalayan Orogeny. Although various bodies were emplaced at least during three Proterozoic episodes, these granitoids have identical crustal protoliths, and their geographical distribution seems to be controlled by distinct tectonostratigraphic units within the Proterozoic basement. Basal parts of the HHC for many kilometers lack any Tertiary leucogranites and in contrast to the higher reaches, where the Akpa and Rakhcham leucogranites frequent the HHC.

The granitoids from the Sutlej valley and the Chor Mountain, contain quartz, K-feldspar, plagioclase, biotite and muscovite in varying proportions with accessories such as zircon, apatite and opaques. The modal plot of these granites indicate that grey granite is mostly tonalitic, whereas other granites are of granite to quartz-monzodiorite in composition. However, the normative plots indicate that grey granite, Wangtu and porpyroclastic granitoids are more of granite to quartz-monzonite in composition, and the Chor granitoid is

more of quartz-mozonite to monzonite in composition.

All these granitoids from the HHC and Jutogh Nappe are similar in their geochemical characters and also bear resemblance to the pre-collision granites. When trace elements of these granites are compared with the A-type and S-type granites, these bodies appear to be more like S-type granite, except the grey granite, which has more affinity towards A-type granite. Rb vs SiO_2 variation plot and Rb vs (Y + Nb) discrimination plot indicates that all these granitoids are distinctly anorogenic Within Plate Granite (WPG) and unrelated to collisional Tertiary granites. The ORG-normalised plot suggest that these granites intruded into the continental crust of normal or attenuated thickness.

The U-Pb zircon ages from these granitoid bodies indicate the crystallisation around 2.0 Ga, 1.8 Ga and 0.9 Ga within the remobilised basement of the Himalayan metamorphic belt. High $^{87}Sr/^{86}Sr$ initial ratio from these granitoid, and incorporation of restites and xenoliths of numerous metamorphics within these bodies like the Wangtu granitoid indicate extensive crustal contamination during their upward migration.

7.3 COLLISION TECTONICS : PRESENT MODEL

7.3.1 Proterozoic evolution

Numerous age determinations from various parts of the Lesser Himalayan para-autochthon, exposed in many windows as well as the metamorphic allochthons in the NW-Himalaya distinctly cluster around 1.8-2.0 Ga, 1.2-1.4 Ga and 0.50 Ga (Chapter 1; Table 1.1; also Sorkhabi and Stump, 1993), thus revealing

extensive involvement of the Middle Proterozoic basins and basement rocks in the Cenozoic Himalayan collision zone. An extensive orthoquartzite-volcanic association in the Lesser Himalayan para-autochthon window zone from Kishtwar, Kulu-Rampur and inner Lesser Himalayan sedimantatary belt of Garhwal-Kumaon Himalaya is of great interest to trace the Proterozoic evolutionary trends (Fuchs, 1975; Sharma, 1977; Valdiya, 1980; Bhat and Le Fort, 1992).

These Proterozoic interstratified mafic-volcanic magmatic bodies associated with orthoquartzite-limestone, indicate a typical platform setup. Geochemically these volcanics are typically characterised by transitional tholeiitic to alkalic composition and having relatively enriched incompatible trace elements, similar to the basalt erupted in a so-called "plume" setting (Bhat, 1984, 1987; Bhat and Ahmad, 1985). Bhat and Le Fort (1992) have recently obtained a very good Sm-Nd whole-rock isochron from these volcanics of the Kulu-Rampur Window. These represent an intense rift-related volcanism at 2509 ± 94 Ma, thus constraining the Proterozoic rift basin around Archean-Proterozoic boundary. Some of these orthoquartzite-volcanic platform sequences are intruded by 1.8 Ga granitoids of which the Kishtwar and Bandal bodies reveal Rb-Sr whole-rock isochrons of 1861 ± 32 Ma and 1840 ± 70 Ma respectively (Frank et al., 1977; Miller and Frank, 1992). The former also reveals a Within Plate environment (Miller and Frank, 1992).

In addition, geochronological data are now available from many metamorphic allochthons of the HHC and Lesser Himalaya and reveal almost coeval ages of this extremely important phase of plutonism in the Lesser and Higher Himalayan region. Of these, two U-Pb zircon primary crystallisation ages of granitoids from the HHC in immediate vicinity of the Kulu-Rampur Window are most significant and indicate 1.8-2.0 Ga anorogenic Within Plate Granitoids (WPG) like the Kaghan valley granitoid in Pakistan (Spencer, 1992; pers. com. 1993), or younger Champawat granitoids (Singh et al., 1993).

On the basis of Rb-Sr whole-rock isochrons and U-Pb zircon ages from various formations of the Lesser and Higher Himalayan units, three major magmatic phases have been demarcated from the Sutlej valley. These phases are 2.5 Ga Rampur Volcanics (Sm-Nd whole-rock age; Bhat and Le Fort, 1992), 2.0 Ga grey granitoid from basal part of the HHC (U-Pb isotope dilution zircon age; present work) and the 1.8 Ga Wangtu granitoid also from the HHC (U-Pb isotope dilution zircon age; present work). The oldest phase appears to be basic volcanics interstratified with orthoquartzite-limestone association of the Kulu-Rampur Window zone and affected by the 1.8 Ga Bandal-Kishtwar granitoids. However, in the HHC, 1.8 to 2.0 Ga granitoids represent the earliest magmatic phase intruding the still older fine grained pelities and banded biotite gneiss. As no deformation episodes is associated with this anorogenic magmatic event, it appears that biotite gneiss and thinly banded pelitic sequences of the HHC represent original geoclinal facies of shale and thin sandstone intercalations, probably coeval to the 2.5 Ga orthoquartzite-volcanic platformal association of foreland, deposited on a still older unknown basement. This setting appears to be similar to the basinal setting of the Aravalli's, Dharwars and other Proterozoic basins of the Peninsular India.

This compels us to visualise an Early Proterozoic extensive ensialic basin in the Himalayan region with its shoulder, located southward in the Lesser Himalaya and represented by 2.5 Ga sedimentation of volcanic-orthoquartzite platform association and geoclinal pelites of the Higher Himalaya (Fig. 7.1). Mafic volcanism was more likely to be asociated with adiabatic rise of mantle plume in an extremely attenuated lithosphere rather than ocean floor spreading due to horizontal movement of continental plates by convection roll (Bhat, 1987).

Geochemical signatures of the 1.8-2.0 Ga granitoids from the Kishtwar Window and the HHC reveal anorogenic WPG emplacement and possibly represent rise of the Early Protrozoic mantle plume diapirs within extended crust, both in the

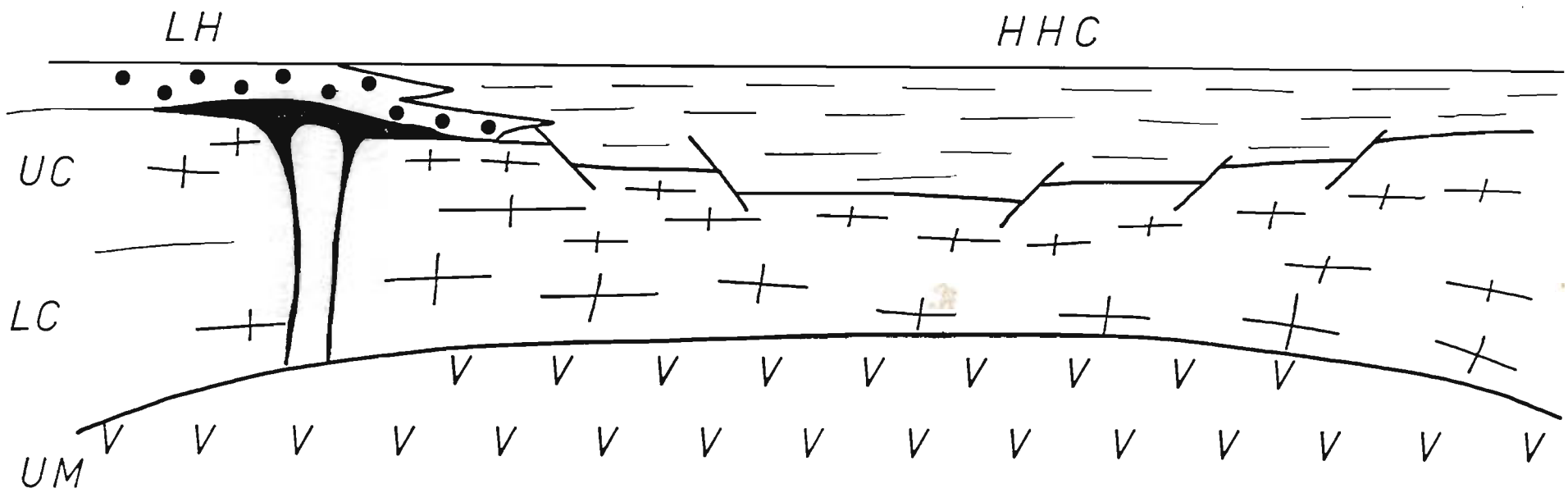

Figure 7.1 : Diagmatic sketch of postulated model of 2.5 Ga ensialic basin in the Himalaya. UM - upper mantle, LC - lower crust, UC - upper crust, LH - Lesser Himalayan volcanic-orthogneiss platform association and HHC - Higher Himalayan Crystalline (geoclinal pelites, now exposed as biotite-rich paragneiss).

Lesser and Higher Himalayan domains. Heat source from such plumes has possibly partially melted lower and middle continental crust to generate granitoids (Fig. 7.2). It is also evident from the high $^{87}Sr/^{86}Sr$ initial ratio between 0.70 to 0.74 from these bodies. Rise of these small granitoids plutons like Bandal, Kishtwar and Wangtu incorporated numerous deformed metamorphosed restites and xenoliths. Such accretionary processes appear to be repeated during the later part of Proterozoic around 1.2-1.4, 1.0-0.9 and in the Early Paleozoic around 0.5 Ma, when the Nirath-Baragaon mylonitised augen gneiss (Bajura/Kulu Nappe) Chor plutons and Mandi plutons were emplaced. However, repeated mantle diapiric acitivity needs further and clearer explanations as to how such diapirs have been generated episodically throughout the Proterozoic and Early Paleozoic.

7.3.2 Himalayan Collision

Geochemical and geochronological data, now available from the present work, provide better constraints on the Proterozoic evolutionary trends in the Himalaya, where "within plate" magmatic activities repeatedly affected an Archean-Early Proterozoic ensialic basin. This has subsequently been involved in the Cenozoic Himalayan collision tectonics, which caused its deformation, metamorphism and subsequent imbrication.

a. <u>Deformation</u>: Deformation during the Himalayan orogeny is characterised by numerous structures of ductile deformation regime in a shear zone, related to main deformational phase. This has produced a consistent down-the-dip lineation on prominent axial-plane foliation S_2 of reclined F_2 folds, and plunging N to NNE.

Orientation of mineral elongation in Nirath-Baragaon mylonitised augen gneiss of the Bajura/Kulu Nappe and the mineral stretching lineation of the HHC

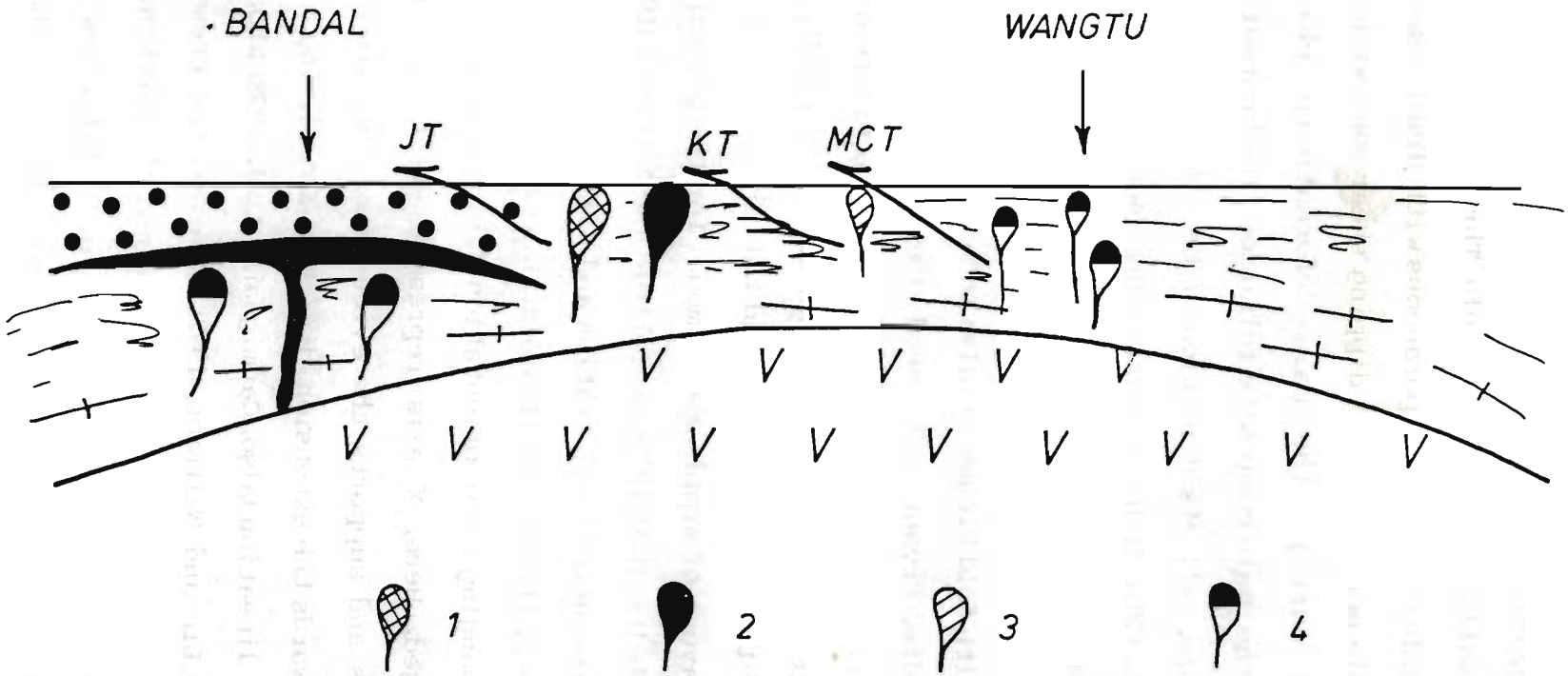

Figure 7.2 : Postulated evolutionary model of ensialic Himalayan crust since Proterozoic, showing emplacement of variuos granitoids of different ages since 2.0 Ga, with partially melted lower and middle continental crust. Disosition of various thrust is only skematic. 1 - 0.5 Ga granitoids, 2 - 0.9 to 1.0 Ga granitoids, 3 - 1.2 to 1.4 Ga granitoids and 4 - 1.8 to 2.0 Ga granitoids. JT - Jutogh Thrust, KT - Kulu Thrust, MCT - Main Central Thrust.

and the Lesser Himalayan Proterozoic foreland window rock is parallel to each other without any deflection within the MCT and Kulu Thrust zones. This indicates that stretching linear fabric was contemporaneous with displacement of the nappes in a broad low-angle northeasterly dipping shear zone with an overthrust sense of movement during the main deformational phase. Mineral/stretching lineation on the main composite foliation trend normal to the Himalayan belt and, therefore, reflects direction of tectonic transport (Mattauer, 1975, 1986; Bordet et al., 1981; Andrieux et al., 1981; Coward et al., 1982; Brunel, 1986; Jain and Anand, 1988; Lin and Williams, 1992).

Parallelism of linear fabric with fold hinges has also been observed by many workers in different folded belts. Bryant and Reed (1969) suggested that penetrative lineation, parallel to minor folds, is formed due to tightening, flattening and rotation of earlier passive open folds, which were initially at right angles to the direction of translation. Escher and Watterson (1974) have given convincing arguments in favour of simple shear model for the principal deformation mechanism in mobile belts. Bell (1978) and Cobbold and Quinquis (1980) have observed that XY-plane representing the foliation and linear elements in L-S tectonite, parallels the X axis of the strain ellipsoid. This model postulates that X and Z strain axis keep changing their orientation during deformation, while Y axis remain unchanged. Here, X axis represent stretching and translation direction of nappes and supports the evidence of the passive rotation of early fold hinges towards the extension direction X resulting into parallelism with the stretching lineation (also, Carmignani et al., 1978; Rhodes and Gayer, 1977; Williams, 1978; Lin and Williams, 1992). However, the present investigations do not support rotation of early fold hinges into the stretching direction. On the other hand, it appears that main foliation is contemporaneously developed during the main ductile deformation in a shear zone, whose transport direction is indicated by down-the-dip plunging stretching lineation (Fig. 7.3 a).

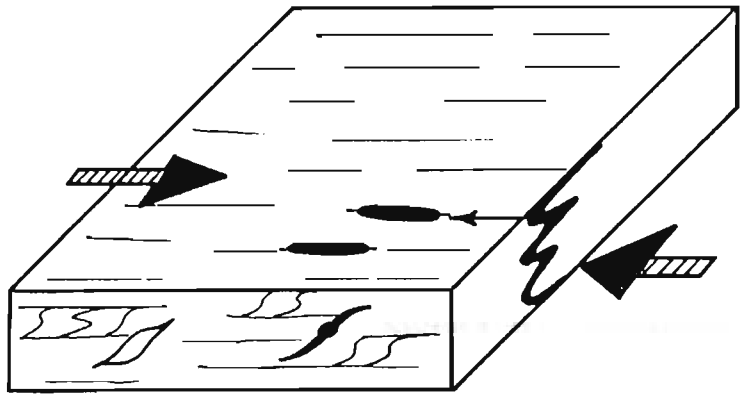

(a)

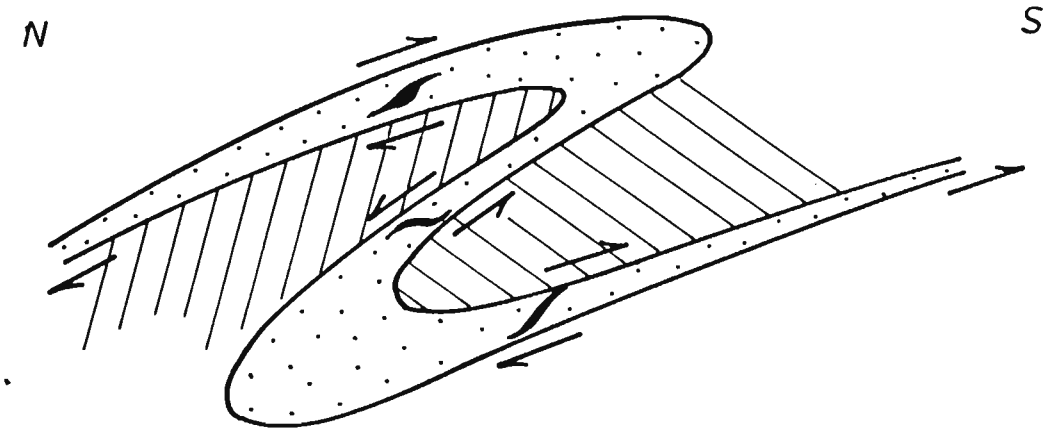

(b)

Figure 7.3 : Model showing shear indicators in different tectonic regimes. (a) Intracontinental ductile shear of overthrust-type showing development of main foliation, lineation and folds. (b) Large-scale overturned fold with reversal of vergence on limbs of antiform and synform.

Within the Kulu-Rampur Window, the Manikaran quartzite is intensely imbricated with the Rampur Volcanics due to presence of small-scale thrusts (Fig. 2.1). Such an imbrication is likely to be associated over the ramp within the window zone and producing tectonic lenses within volcanic-quartzite association. Ramping appears to post date the main Himalayan deformation event.

On the regional scale, the Bajura/Kulu Nappe is mainly developed within the inner parts of the Lesser Himalaya at the base of the HHC and the Jutogh Nappe. The Chail Nappe appears to be absent in inner parts, but is mainly developed in frontal parts. This leads us to believe localised development of the latter, and presence of a zone between the frontal and inner parts, where the Bajura/Kulu Nappe transgresses over the Chail Nappe. In addition, one deformational phase is missing in frontal parts of the Jutogh Nappe. This needs further detailed geological and structural mapping in parts of the Jutogh Nappe.

Further, the Chor granitoid is thrust over the Jutogh metamorphics and now rests over the Jutogh metamorphics. This granitoid body is an allochthon and are not formed *in situ*. It also does not constitutes part of core of the large-scale recumbent fold as described by earlier workers (Pilgrim and West, 1928). All the shear indicators within the granitoid and the Jutogh metamorphics indicate top-to-SW movement direction, unlike the shear criteria one would expect in the fold model (Fig. 7.3 b).

b.Inverted metamorphism: Many models have been proposed to explain classic inversion of metamorphic isograds in the Himalaya. These models include (i) recumbent folding of isograds, (ii) imbrication and juxtaposition due to thrusts, (iii) frictional heating along the MCT, (iv) hot-over-cold model, (v) diverging isograd model and (vi) ductile shearing due to S-and C- shear fabric. Suitability of these models in the present area is briefly discussed below.

(i) Recumbent folding: Some of the typical cross-sections through the Himalaya in Simla Hills, Kulu valley, and Zanskar have postulated recumbent folds to explain large-scale structures of various tectonic units (Pilgrim and West, 1928; Naha and Ray, 1970; Frank et al., 1977; Searle and Rex, 1989). Therefore, existence of inverted metamorphic isograds in lower parts of the sequence and normal disposition in the upper parts have been explained due to post-metamorphic recumbent folding (Pilgrim and West, 1928; Searle et al., 1992). However, structures likely to be asociated in such a model and indicating shear sense would reveal alternating southerly vergence on normal limb and northerly vergence on inverted limb of such large folds in the Himalaya (Fig. 7.3 b). Such a model is inconsistent with many observations across the metamorphic belt, where only southerly top-to-SW shear vergence has been observed.

(ii) Thrust imbrication: Another likely model to cause inversion of metamorphic isograds is due to imbrication and juxtaposition due to post-metamorphic thrusting e.g., Scandinavian Caledonides (Gee, 1974; Andreasson, 1980; Andreasson and Gorbatschev, 1980). Further, Treloar et al. (1989) and Mohan et al. (1989) noticed such a phenomenon in Pakistan and Darjeeling Hills respectively, where each mapped metamorphic isograds are bounded by thrusts. However, thrust-bound metamorphic isograds have not been reported in many other parts of the Himalaya like this area.

(iii) Frictional heating: Models, based on frictional heating along large-scale intracontinental thrusts like the MCT causing the inversion of metamorphism, have also been proposed from Nepal (Le Fort, 1975). Such models postulate increasing isotherm frictional (shear) heating during thrusting along the MCT. However, shear heating can only cause localised thermal increase in restricted narrow zones for short duration and may not develop inverted metamorphism far away from the MCT as is evident in the area. Apart from this, localised shear heating requires high slip velocity of about 30 cm/yr (Bird, 1978), high stresses

and a long time span (Mohan et al., 1989).

(iv) Hot-over-cold model: Metamorphic inversion has also been explained by emplacement of hot granitic bodies or an overriding hot crustal stack of the Higher Himalayan belt (St-Onge, 1981; Jaupart and Provost, 1985). Le Fort (1986) postulated generation of MCT-related Miocene leucogranite and its emplacement near the top of the High Himalayan slab, thus providing the heat source for high grade metamorphic rocks in upper reaches. Thermal effects of such small bodies would have been restricted to localised zones and may not have possibly produced metamorphic inversion in large areas.

(v) Diverging isograd model: Thakur (1976) proposed a model for decreasing of metamorphic grades upward as well as downward in succession from sillimanite zone in Himachal, Kumaon and Nepal. This model designated decrease in metamorphism outward in opposite direction from the high grade areas of sillimanite zone as divergent isograds

(vi) Ductile shearing due to S-and C- shear fabric: This model postulates that noncoaxial ductile shearing has caused the development of S-C fabric at depth during the main Himalayan D_2 deformation because of continuous variation in orientation of the strain ellipsoid (Jain and Manickavasagam, 1993). Millimetre-spaced C-surfaces sigmoidally bent the S-foliation on a small- scale towards the direction of ductile tectonic transport. It also suggests that metamorphic isograd boundaries also underwent small-scale displacement along the C-shear surfaces in the ductile shear zone, which has caused the inverted metamorphism in the Zanskar region (Jain and Manickavasagam, 1993).

In the area under consideration, many evidences have been elaborated in Chapters 3 and 4, wherein numerous shear criteria consistently reveal a southwestward vergence of the metamorphic nappes. Of these, S- and C- shear

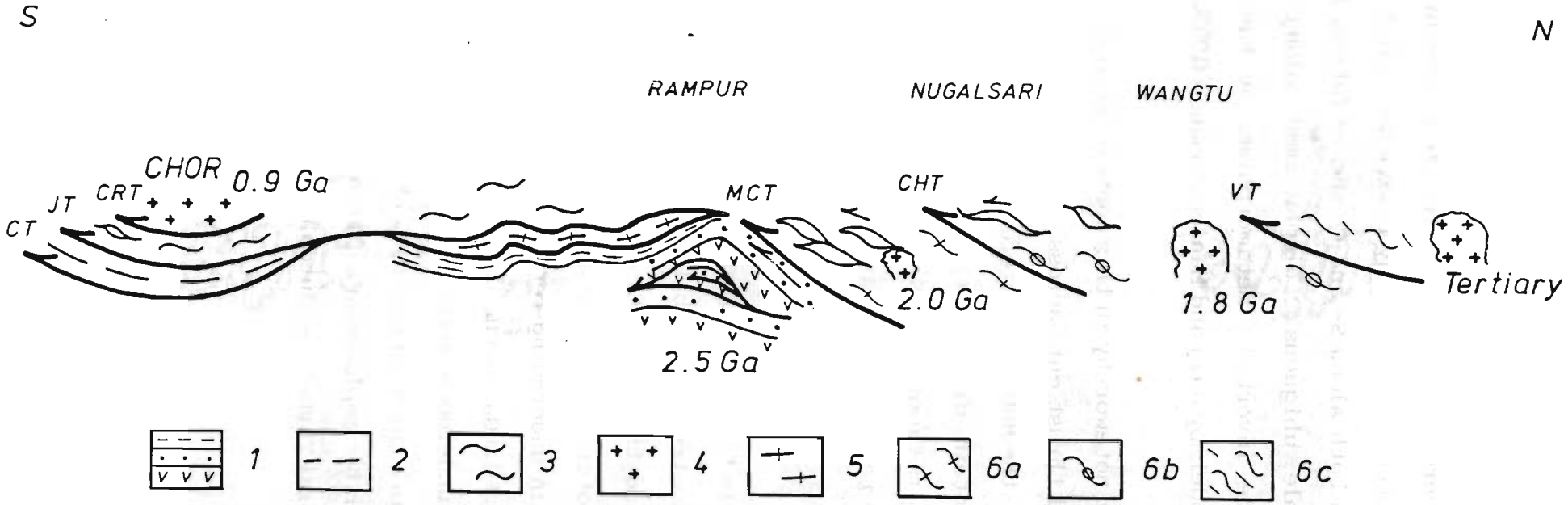

Figure 7.4 : Schematic cross-section through the NW-Himalayan in Himachal Pradesh showing disposition of various metamorphic nappes, thrusts and magmatic bodies. 1 : Lesser Himalayan Proterozoic foreland showing imbricated quartzite-volcanics. 2 : Chail Nappe. 3 : Jutogh Nappe. 4 : Chor granitoid. 5 : Bajura/Kulu Nappe. 6 : Higher Himalayan Crystalline - (a) Jeori Formation, (b) Wangtu granite Complex and (c) Vakrita Group. CT - Chail Thrust, JT - Jutogh Thrust, CRT - Chor Thrust, KT - Kulu Thrust, MCT - Main Central Thrust, CHT - Chaura Thrust and VT - Vaikrita Thrust. Each unit is characterised by volcanics and granitoid bodies, emplaced during 2.5 Ga, 2.0 Ga, 1.8 Ga, 0.9 Ga and Late Cenozoic.

fabric is more significant, where small-scale shear displacement are ubiquitously observed. It is also noteworthy that many index mineral have been syntectonically rotated and grown both along S- and C- shear fabric. It is, therefore, likely that small-scale ubiquous displacement along such penetrative fabric may cause the inverted metamorphism, as has been postulated in a newly-presented model by Jain and Manickavasagam (1993).

Certain observation are further noteworthy in this context from Himachal Pradesh. Megascopically, many small thrust cut across crenulation foliation, developed during D_3 deformation in the HHC and, therefore, post-date the peak M_2 metamorphism. In the Chor Mountain, discrete mylonite fabric related to thrust event also post-dates the M_{C1} metamorphism. Moreover, no P-T estimation from the HHC and the Jutogh Nappe reveal an increase in temperature in the thrust zone of the MCT and JT.

To conclude it, therefore, appears that the collision tectonics in parts of the NW-Himalaya has intensely imbricated the remobilised Proterozoic basement in various metamorphic nappes and the Lesser Himalayan foreland (Fig 7.4). Evolutionary trends within the Proterozoic regime are indicated probably by the presence of 2.5 Ga ensialic basin undergoing repeated anorogenic within plate magmatism around 1.8-2.0 Ga, 0.9-1.0 Ga and 0.5 Ga in the Lesser and Higher Himalayas. These nappes have undergone main Himalayan metamorphism, synchronous with ductile shearing in a thick intracontinental shear zone, which predates the brittle-ductile to brittle emplacement of these nappes along the various thrusts, like the Main Central Thrust and Jutogh Thrust etc. (Fig. 7.4).

REFERENCES

Allegre, C.J., Albarede, F., Grunenfelder, M. and Koppel,V., (1974) : $^{238}U/^{206}Pb$-$^{235}U/^{207}Pb$-$^{232}Th/^{208}Pb$ zircon geochronology in Alpine and non-Alpine environment. *Contrib. Mineral. Petrol.*, 43, 163-194.

Anand, A., (1986) : Deformation and strain patterns of the Central Himalayan metamorphics from Nortwestern Garhwal. *Unpublished Ph.D. thesis*, University of Roorkee, Roorkee, India.

Andreasson, P. G., (1980) : Metamorphic in the Tommeras area, Central Scandinavian Caledonides. *Geol. Foren. Stockl. Forh.*, 101, 273-290.

Andreasson, P. G., and Gorbatschev, R., (1980) : Metamorphism in extensive nappe terrain : a study of the Central Scandinavian Caledonides. *Geol. Foren. Stockl. Forh.*, 102, 335-357.

Auden, J.B., (1934) : The geology of the Krol belt. *Rec. Geol. Surv. India*, 67, 357-454

Auden, J.B., (1935) : Traverses in the Himalaya. *Rec. Geol. Surv. India*, 69, 357-454

Auden, J.B., (1937) : The structure of Himalaya in Garhwal. *Rec. Geol. Surv. India*, 71, 357-454

Bagati, T. N., (1990) : Lithostratigraphy and facies variation in the Spiti basin (Tethys). Himachal Pradesh, India. *Jour. Him. Geol.*, 1, 35-47.

Bell, T. H., (1978) : Progresive deformation and reorientation of fold axes in a ductile mylonite zone. The Woodroofe Thrust. *Tectonophysics*, 49, 285-320.

Berman, R.G., (1988) : Internally consistent thermodynamic data for minerals in the system Na_2O-K_2O-CaO-MgO-FeO-Fe_2O_3-Al_2O_3- SiO_2-TiO_2-H_2O-CO_2. *J. Petrol.*, 29, 445-522.

Berthe, D., Choukroune, P. and Jegouzo, P., (1979) : Orhthogenesis mylonite and non-coaxial deformation of granites: the example of the South American Shear Zone. *J. Struct. Geol.*, 1, 31.42.

Berthelsen, A., (1951) : A geological section through the Himalayan section. *Meddelsar fra Dansk Geologish Forening Bd. 12 Kobenbavn*, 102-104.

Bhalla, N.S. and Gupta, J.N., (1979) : U-Pb isotopic ages of Uranites from Kulu, Himachal Pradesh and Berinag, Uttar Pradesh. *Jour. Geol. Surv. India*, 20, 10, 481-488.

Bhanot, V.B., Gill, J.S., Arora, R.P. and Bhalla, J.K., (1974) : Radiometric dating of the Dalhousie granite. *Curr. Sci.*, 43, 208.

Bhanot, V.B., Goel, A.K., Singh, V.P. and Kwatra, S.K., (1975) : Rb-Sr radiometric studies in the Dalhousie and Rohtang area. *Curr. Sci.*, 44, 219.

Bhanot, V.B., Bhandari, A.K., Singh, V.P. and Kansal, A.K., (1976) : Precambrian (1220 my.) Rb-Sr whole rock isochron age for Bandal granite, Kulu Himalaya, Himachal Pradesh, *Abstr. Him. Geo. Sem., Delhi, Sep. 1976.*

Bhanot, V.B., Kwatra, S.K., Kansal, A.K., and Pandey, B.K., (1978) : Rb-Sr whole rock age for Chail Series of Northwestern Himalaya. *Jour. Geol. Soc. India*, 19, 224-227.

Bhanot, V.B., Bhandari, A.K., Singh, V.P. and Kansal, A.K., (1979) : Geochronological and geological studies of granites of Higher Himalaya, Northeast of Manikaran, H.P.. *Jour. Geol. Soc. India*, 20, 90-94.

Bhargava, O. N., Narain, K. and Dass, A.S., (1972) : A note on the Rampur window, district Mahasu, H.P.. *Jour. Geol. Soc. India*, 13, 277-280.

Bhargava, O. N., (1980) : Outline of stratigraphy of Eastern Himachal Pradesh, with special reference to the Jutogh Group. *In : Stratigraphy and Correlations of Lesser Himalayan Formations (edited by Valdiya, K.S., and Bhatia, S.B.,)*

Hindustan Publication Corp., New Delhi, India, pp. 117-125.

Bhargava, O. N., (1982) : The tectonic windows of the Lesser Himalayas. *Him. Geol.*, 10, 135-155.

Bhargava, O. N., (1990) : Holocene tectonics south of the Indus Suture, Lahaul-Ladakh Himalaya, India, A consequence of Indian Plate motion. *Tectonophysics*, 174, 315.

Bhargava, O. N., Bassi, U. K. and Sharma, R. K., (1991) : The Crystalline thrust sheets, age of metamorphism - Evolution and mineralization of the Himachal Himalaya. *Indian Minerals*, 45 (1 & 2), 1-18.

Bhat, M.I., (1984) : Abor Volcanics : further evidence for the birth of Tethys Ocean in the Himalayan segment. *Jour. Geol. Soc. London*, 141, 763-775.

Bhat, M.I., (1987) : Spasmodic rift reactivation and its role in the pre-orogenic evolution of the Himalaya region. *In : Deep Seated Processes in Collision Zones (edited by Gupta, H. K.), Tectonophysics*, 134, 103-127.

Bhat, M.I. and Ahmad, T., (1985) : Petrogenesis of the Abor Volcanics, Eastern Himalaya. *Abstr. Int. Volcanol. Congr. New Zealand.*

Bhat, M.I. and Le Fort, P., (1992) : Sm-Nd age and petrogenesis of Rampur metavolcanic rocks, NW-Himalaya : Late Archean relics in the Himalayan belt. *Precam. Res.*, 56, 191-210.

Bhattacharya, A.K., Bhatnagar, G.S., Narayan, Das, G.R., Gupta, J.N., Chabria, T. and Bhalla, N.S., (1981) : Rb-Sr dating and geological interpretation of sheared granite-gneiss of Brijranigad-Ingedinala, Bhilangana. *Abstr. Him. Geo. Sem.* 12, Dehradun.

Bird, P.J., (1978) : Initiation of intracontinental Subduction in the Himalaya. *Jour. Geophys. Res.*, 83, 4975-4987.

Steiger, R.H. and Jagger, E., (1977) : Convention on the use of decay constants in geo- and cosmochronology. *Earth Planet. Sci. Lett.*, 36, 359-362.

Stern, C. R., Kligfield, R., Schelling, D., Virdi, N.S., Futa, K., Peterman, Z. E. and Amini, H., (1989) : The Bhagirathi leucogranite of the High Himalaya (Garhwal, India); Age, petrogenesis and tectonic implications. *Geol. Soc. Am. Specl. Publ. 232*, 33-45.

Stoliczka, A., (1866) : Summary of the geological observations during a visit to the provinces Rupsu Karnag, south Ladakh, Zanskar, Sumdo, Dras and Western Tibet. *Mem. Geol. Surv. India*, 5, 337-354.

St-Onge, M. R., (1981) : "Normal" and "inverted" metamorphic isograds and their relation to syntectonic Proterozoic batholiths in the Wopmay Orogen, Northwest Territories, Canada. *Tectonophysics*, 76, 295-316.

Strachey, R., (1851) : On the geology of parts of the Himalayan mountain and Tibet. *Quart. Jour. Geol. Soc.*, 7, 292-310.

Streikeisen, A.L., (1976) : To each plutonic rock in proper name. *Earth Sci. Rev.*, 12, 1-33.

Sun, S.S. and Mcdonough (1989) : Chemical and isotopic systematics of Oceanic basalt : implication for mantle composition and processes. *In : Magmatism in the Ocean Basins (edited by Saunders, A.B. and Norry, M.J.), Geological Society Special Publication*, 42, 313-345.

Thakur, V.C. (1976) : Divergent isograds of metamorphism in some part of higher Himalaya Zone. *In : Himalaya, Science de la Terra, CNRS, Paris*, 268, 433-442.

Thakur, V.C. (1980) : Tectonics of the Central Crystallines of Western Himalaya. *Tectonophysics*, 62, 141-154.

Thakur, V.C. (1983) : Granites of Western Himalaya and Karakoram - structural framework, geochronology and tectonics. *In : Granites of Himalaya,*

REFERENCES

Allegre, C.J., Albarede, F., Grunenfelder, M. and Koppel,V., (1974) : $^{238}U/^{206}Pb$-$^{235}U/^{207}Pb$-$^{232}Th/^{208}Pb$ zircon geochronology in Alpine and non-Alpine environment. *Contrib. Mineral. Petrol.*, 43, 163-194.

Anand, A., (1986) : Deformation and strain patterns of the Central Himalayan metamorphics from Nortwestern Garhwal. *Unpublished Ph.D. thesis*, University of Roorkee, Roorkee, India.

Andreasson, P. G., (1980) : Metamorphic in the Tommeras area, Central Scandinavian Caledonides. *Geol. Foren. Stockl. Forh.*, 101, 273-290.

Andreasson, P. G., and Gorbatschev, R., (1980) : Metamorphism in extensive nappe terrain : a study of the Central Scandinavian Caledonides. *Geol. Foren. Stockl. Forh.*, 102, 335-357.

Auden, J.B., (1934) : The geology of the Krol belt. *Rec. Geol. Surv. India*, 67, 357-454

Auden, J.B., (1935) : Traverses in the Himalaya. *Rec. Geol. Surv. India*, 69, 357-454

Auden, J.B., (1937) : The structure of Himalaya in Garhwal. *Rec. Geol. Surv. India*, 71, 357-454

Bagati, T. N., (1990) : Lithostratigraphy and facies variation in the Spiti basin (Tethys). Himachal Pradesh, India. *Jour. Him. Geol.*, 1, 35-47.

Bell, T. H., (1978) : Progresive deformation and reorientation of fold axes in a ductile mylonite zone. The Woodroofe Thrust. *Tectonophysics*, 49, 285-320.

Berman, R.G., (1988) : Internally consistent thermodynamic data for minerals in the system Na_2O-K_2O-CaO-MgO-FeO-Fe_2O_3-Al_2O_3- SiO_2-TiO_2-H_2O-CO_2. *J. Petrol.*, 29, 445-522.

Berthe, D., Choukroune, P. and Jegouzo, P., (1979) : Orhthogenesis mylonite and non-coaxial deformation of granites: the example of the South American Shear Zone. *J. Struct. Geol.*, 1, 31.42.

Berthelsen, A., (1951) : A geological section through the Himalayan section. *Meddelsar fra Dansk Geologish Forening Bd. 12 Kobenbavn*, 102-104.

Bhalla, N.S. and Gupta, J.N., (1979) : U-Pb isotopic ages of Uranites from Kulu, Himachal Pradesh and Berinag, Uttar Pradesh. *Jour. Geol. Surv. India*, 20, 10, 481-488.

Bhanot, V.B., Gill, J.S., Arora, R.P. and Bhalla, J.K., (1974) : Radiometric dating of the Dalhousie granite. *Curr. Sci.*, 43, 208.

Bhanot, V.B., Goel, A.K., Singh, V.P. and Kwatra, S.K., (1975) : Rb-Sr radiometric studies in the Dalhousie and Rohtang area. *Curr. Sci.*, 44, 219.

Bhanot, V.B., Bhandari, A.K., Singh, V.P. and Kansal, A.K., (1976) : Precambrian (1220 my.) Rb-Sr whole rock isochron age for Bandal granite, Kulu Himalaya, Himachal Pradesh, *Abstr. Him. Geo. Sem., Delhi, Sep. 1976.*

Bhanot, V.B., Kwatra, S.K., Kansal, A.K., and Pandey, B.K., (1978) : Rb-Sr whole rock age for Chail Series of Northwestern Himalaya. *Jour. Geol. Soc. India*, 19, 224-227.

Bhanot, V.B., Bhandari, A.K., Singh, V.P. and Kansal, A.K., (1979) : Geochronological and geological studies of granites of Higher Himalaya, Northeast of Manikaran, H.P.. *Jour. Geol. Soc. India*, 20, 90-94.

Bhargava, O. N., Narain, K. and Dass, A.S., (1972) : A note on the Rampur window, district Mahasu, H.P.. *Jour. Geol. Soc. India*, 13, 277-280.

Bhargava, O. N., (1980) : Outline of stratigraphy of Eastern Himachal Pradesh, with special reference to the Jutogh Group. *In : Stratigraphy and Correlations of Lesser Himalayan Formations (edited by Valdiya, K.S., and Bhatia, S.B.,)*

Hindustan Publication Corp., New Delhi, India, pp. 117-125.

Bhargava, O. N., (1982) : The tectonic windows of the Lesser Himalayas. *Him. Geol.*, 10, 135-155.

Bhargava, O. N., (1990) : Holocene tectonics south of the Indus Suture, Lahaul-Ladakh Himalaya, India, A consequence of Indian Plate motion. *Tectonophysics*, 174, 315.

Bhargava, O. N., Bassi, U. K. and Sharma, R. K., (1991) : The Crystalline thrust sheets, age of metamorphism - Evolution and mineralization of the Himachal Himalaya. *Indian Minerals*, 45 (1 & 2), 1-18.

Bhat, M.I., (1984) : Abor Volcanics : further evidence for the birth of Tethys Ocean in the Himalayan segment. *Jour. Geol. Soc. London*, 141, 763-775.

Bhat, M.I., (1987) : Spasmodic rift reactivation and its role in the pre-orogenic evolution of the Himalaya region. *In : Deep Seated Processes in Collision Zones (edited by Gupta, H. K.), Tectonophysics*, 134, 103-127.

Bhat, M.I. and Ahmad, T., (1985) : Petrogenesis of the Abor Volcanics, Eastern Himalaya. *Abstr. Int. Volcanol. Congr. New Zealand.*

Bhat, M.I. and Le Fort, P., (1992) : Sm-Nd age and petrogenesis of Rampur metavolcanic rocks, NW-Himalaya : Late Archean relics in the Himalayan belt. *Precam. Res.*, 56, 191-210.

Bhattacharya, A.K., Bhatnagar, G.S., Narayan, Das, G.R., Gupta, J.N., Chabria, T. and Bhalla, N.S., (1981) : Rb-Sr dating and geological interpretation of sheared granite-gneiss of Brijranigad-Ingedinala, Bhilangana. *Abstr. Him. Geo. Sem.* 12, Dehradun.

Bird, P.J., (1978) : Initiation of intracontinental Subduction in the Himalaya. *Jour. Geophys. Res.*, 83, 4975-4987.

Bisaria, R.C. and Saxena, M.N., (1968) : On the olivine bearing dolerite and gabbros of the Chor area. *Publication of the Centre of Advanced study in Geology*, Panjab University, Chandigarh, 5, 65-73.

Bordet, P., (1973) : On the position of the Himalayan Main Central Thrust within Nepal Himalaya. *Proc. Semin. Geodynamics Himalayan Region, NGRI*, Hydrabad, 148-155.

Bordet, P., Colchen, M., Le Fort, P. and Pecher, A., (1981) : The geodynamics of the Himalaya. Ten years of research in Central Nepal Himalaya and some other regions. *In : Zagros-HinduKush-Himalaya Geodynamic Evolution, Am. Geophys. Union*, 3, 149-168.

Bouchez, J.L. and Pecher, A., (1981) : The Himalayan Main Central Thrust pile and its quartz rich tectonites in Central Nepal. *Tectonophysics*, 78, 23-50.

Brookfields, M.E. and Reynold, P.H., (1981) : Late Cretaceous emplacement of the Indus Suture Zone ophiolitic melanges and an Eocene-Oligocene magamatic arc on the northern edge of the Indian Plate. *Earth Planet. Sci. Lett.*, 55, 157-162.

Brun, J.P., Burg, J.P. and Chen, G.M., (1985) : Strain trejectories above the Main Central Thrust (Himalaya) in southern Tibet. *Nature*, 313, 388-390.

Brunel, M., (1986) : Ductile thrusting in the Himalaya: Shear sense criteria and stretching lineation. *Tectonics*, 5, 247-265.

Bryant, B. and Reed, J. C., (1969) : Significance of lineation and minor folds near major thrust faults in the Southern Applachians and the British and Norwegian Caledonides. *Geol. Mag.*, 106(5), 412-429.

Burchfeil, B.C. and Royden, L.H., (1985) : North-south extension within the convergent Himalayan region. *Geology* , 13 : 679 - 682.

Burg, J.P., Guirand, M., Chen, G.M. and Li, G.C., (1984) : Himalayan metamorphism and deformations in the Northern Himalayan Belt (Southern Tibet, China). *Earth Planet. Sci.Lett.*, 69, 391-400.

Butler, R.W.H. (1982) : The terminology of structures in thrust belts. *Jour. Struc. Geol.*, 4(3), 239-245.

Carmignani, L., Giglia, G. and Kligfield, R., (1978) : Structural evolution of Apalane Alps : an example of continental margin deformation, the Northern Appenniens, Italy. *Jour. Geol.*, 86, 487-504.

Chakrabarti, B.K., (1973) : Report on systematic geological mapping in parts of Simla, Kulu and Kinnaur district, Himachal Pradesh, *Unpublished report Geol. Surv. India.*

Chakrabarti, B.K., (1976) : Some observation on the rocks of Rampur Bushahr area, Himachal Pradesh. *Abstract, Symp. Geol. Surv. India*, Lucknow.

Chakrabarti, B.K., (1979) : Tholeiitic basic rocks of Rampur area, Simla Himalaya. *Q. Jour. Geol. Min. Met. Soc. India*, 51, 89-104.

Chappell, B. W. and White, A. J. R., (1974) : Two constrasting granite types. *Pac. Geol.*, 8, 173-174.

Cobbold, P. R. and Quinquis, H., (1980) : Development of sheath folds in shear regime. *Jour. Struc. Geol.*, 2, 119-126.

Copeland, P., Parrish, R. R. and Harrison, T. M., (1988) : Identification of inherited radiogenic Pb in monazite and its implications for U-Pb systematics. *Nature*, 333, 760-763.

Coward, M.P., Windley, B.F., Broughton, R., Luff, I., Petterson, M.G., Pudsey, C., Rex, D. and Khan, M.A., (1986) : Collision tectonics in the NW Himalayas. *In : Collision Tectonics (edited by Coward, M.P., and Ries, A.,). Spec. Publs. Geol. Soc.Lond.*, 19, 203-219.

Cuney, M., Le Fort, P. and Wang, Z. X., (1984) : Uranium and thorium geochemistry and minerology in the Manasalu leucogranite (Nepal, Himalaya). *In : Proc. Symp. Geology of granites and their Metallogenic Relations Nanjing Univ. 1982*, 853-873.

Das, B.K., (1987) : Petrology of Barrovian-Type regional metamorphism in pelitic schists of Kishtwar, Kashmir Himalaya, India. *Proc. Nat. Sem. Tert. Orogeny*, 153-187.

Debon, F., LeFort, P., Sonet, J., LIU Guohue, JIN Chengwei and XU Ronghua, (1981) : About the Lower Paleozoic age of Kangman granite (Lhagoi-Kangri plutonic belt, South Tibet, China). *Terra Cognita, Special issue*, I 14, 67-68.

Debon, F. and LeFort, P., (1982) : A chemical-mineralogical classification of common plutonic rocks and associations. *Trans. R. Soc. Edin. Earth Sci.*, 72, 135-149.

Debon, F., LeFort, P., Sheppard, S.M.F. and Sonet, J., (1986) : The four plutonic belts of the Transhimalaya-Himalaya : A chemical, minerological, isotopic and chronological synthesis along a Tibet-Nepal Section. *Jour. Petr.*, 27, 219-250.

Debon, F., LeFort, P., Dautel, D., Sonet, J., and Zimmerman, J.L., (1987) : Granites of western Karakoram and northern Kohistan (Pakistan) : a composite Mid-Cretaceous to Upper Cenozoic magmatism. *Lithos*, 20, 19-40.

Deniel, C., Vidal, Ph., Fernandez, A., Le Fort, P. and Peucat, J.J., (1987) : Isotopic study of the Manaslu granite (Himalaya, Nepal) : inference on the age and source of Himalayan Leucogranites. *Contr. Miner. Petr.*, 96, 78-92.

Dewey, J.F. and Bird, J.M., (1970) : Mountain belts and the new global tectonics. *Jour. Geophys. Res.*, 75, 2625-2647.

Dewey, J. F. and Burk, K. C. A., (1973) : Tibetan, Variscan and Precambrian basement reactivation : products of Continental Collision. *Jour. Geol.*, 81 (6), 683-692.

Dubey, A.K. and Bhat, M.I., (1991) : Structural evolution of the Simla area, NW Himalayas: implications for crustal thickening. *Jour. Southern Asia Earth Sci.*, 6(1), 41-53.

Dunnet, D., (1969) : A techique of finite strain analysis using elliptical particles. *Tectonophysics*, V.7, pp.117-136.

Escher, A. and Watterson, J., (1974) : Streching fabrics, folds and crustal shortening. *Tectonophysics*, V.22, pp. 223-231.

Essene, E., (1982) : Geologic thermometry and barometry. *In: Characterization of metamorphism through mineral equilibria* (edited by Ferry, J.M.), Reviews in Mineralogy, Mineral. Soc. Am., 10, 153-206.

Faiya, A.K., (1987) : Deformation and strain patterns of Luhri- Baragaon mylonite augen gneiss, H.P.. *Unpublished M.Sc. dissertation*, University of Roorkee, Roorkee, India, 60p.

Ferry, J.M., (1982) : A comparative geochemical study of pelitic schists and metamorphosed carbonate rocks from south-central Maine, U.S.A.. *Contri. Mineral. Petrol.*, 80, 59-72.

Ferry, J.M. and Spear, F.S., (1978) : Experimental calibration of the partitioningfo Fe and Mg between biotite and garnet. *Contri. Mineral. Petrol.*, 66, 113-117.

Florence, F.P. and Spear, F.S., (1991) : Effects of diffusional modification of garnet growth zoning on P-T path calculations. *Contri. Mineral. Petrol.*, 107, 487-500.

Frank, W., Hoinkes, G., Purtscheller, F., Richter, W. and Thoni, M., (1973) : Relation between metamorphic and orogeniy in a typical section of Himalaya. *Tscher. Min. Petr. Milt.*, 20, 303- 332.

Frank, W., Thoni, M. and Purtscheller, F., (1977) : Geology and Petrography of Kulu-South Lahoul area. *Colloq.Internat. Du, C.N.R.S., 268 Ecolo.Geol. de*

l'Himalaya, 147-166.

Fuchs, G., (1975) : Contribution to the geology of the North-Western Himalayas. *Abhanlunge der Geologischen Bundesanstalt*, Wien, 32.

Ganguly, J. and Saxena, S.K., (1984) : Mixing properties of alumino-silicate garnets: constraints from natural and experimental data, and application to geothermobarometry. *Am. Mineral.*, 69, 88-97.

Gapais, D., Bale, P., Choukroune, P., Cobbold, P.R., Mahjoub, Y. and Marquer, D., (1987) : Bulk kinematics from shear zone patterns some field examples. *Jour. Struct. Geol.*, 9 (5/6), 635 - 646.

Gebauer, D. and Grunenfelder, M., (1976) : U-Pb zircon and Rb-Sr whole rock dating of low grade metasediments. Example: Montage Noire (Southern France). *Contrib. Mieral. Petrol.*, 59, 13-32.

Gebauer, D. and Grunenfelder, M., (1979) : U-Th-Pb dating of Minerals. *Lecture in Isotope Geology (edited by Jager, E. and Hunziken, J.C.)* Springer-Verlag, 105-131.

Gee, D. G., (1974) : Comments on the metamorphic allochthon in northern Trondelag, Central Scandinavian Caledonides. *Norsk. geol. Tidsskr.*, 54, 435-440.

Ghent, E.D., (1976) : Plagioclase-garnet-Al2SiO5-quartz: a potential geobarometer-geothermometer. *Am. Mineral.*, 61, 710-714.

Ghent, E.D., Robbins, D.B. and Stout, M.Z., (1979) : Geothermometry, geobarometry and fluid composition of metamorphosed calc-silicates and pelites, Mica Creek, British Columbia. *Am. Mineral.*, 64, 874-885.

Ghent, E. D. and Stout, M. Z., (1981) : Geobarometry and geothermometry of plagioclase- biotite- garnet- muscovite assemblages. *Contri. Mineral. Petrol.*, 76, 92-97.

Goldich, S.S. and Mudrey, Jr., (1972) : Dilatancy model for discordent U-Pb zircon ages. *In : Contribution to recent geochmistry and analytical chemistry (Vinogradov Volume)*, Moscow, Nauka Publ. office, 415-418.

Goldman, D.S. and Albee, A.L., (1977) : Correlation of Mg/Fe partitioning between garnet and biotite with O^{18}/O^{16} partitioning between quartz and magnetite. *Am. Jour. Sci.*, 277, 750-761.

Govindraju, K., (1989) : Compilation of working values and sample description for 272 Geostandards. *Geostandard newsletter*, vol. XIII, page 15 of Appendix I.

Gururajan, N.S., (1985) : Structure and metamorphism of the Chail Formation in the area between Baragaon and Nirath (Himachal Pradesh) in Simla Himalaya with a special reference to the genesis of the associated mylonite gneiss. *Unpublished Ph.D. thesis*, Garhwal University, Garhwal, Srinagar.

Gururajan, N.S. and Virdi, N.S., (1982) : Petrographic studies of the mylonitic augen gneisses in the Chail Formation of Sutlej valley, Simla Himalaya, H. P.. *Him. Geol.*, 12, 206-211.

Gururajan, N.S. and Virdi, N.S., (1984) : Superposition of early Palaeozoic contact metamorphism by Tertiary regional metamorphism around Dalash, district Kulu, Himachal Pradesh, India. *Jour. Geol. Soc. India*, V.25, N.8, pp.522-527.

Gururajan, N.S., (1990) : Deformation microstructures and geochemistry of the mylonitic augen gneiss in the Chail Thrust Zone in Satluj valley of Himachal Pradesh. *Jour. Geol. Soc. India*, 36, 290-306.

Griesbach, C.L., (1893) : Notes on the Central Himalaya. *Rec. Geol. Surv. India*, 26(1), 19-25.

Hanson, G. N., (1980) : Rare earth elelments in petrogenetic studies of igneous rocks. *Ann. Rev. Earth Planet. Sci.*, 8, 371- 406.

Hayden, H.H., (1904) : The geology of Spiti with parts of Bushar and Rupshu. *Mem. Geol. Surv. India*, 36, 121p.

Helgeson, H.C., Delony, J.M., Nesbitt, H.W. and Bird, D.K., (1978) : Summary and critique of the thermodynamic properties of rock forming minerals. *Am. Jour. Sci.*, 278-A.

Heim, A. and Gansser, A., (1939) : The Central Himalayas: geological observations of the Swiss Expedition of 1936. *Mem. Soc. Helv. Sci. Nat.*, 73, 1-245.

Herren, E., (1987) : The Zanskar Shear Zone : Northeasth- southwest extension within the Higher Himalaya (Ladakh, India). *Geology*, 15, 409 - 413.

Hodges, K. V. and Crowley, P. D., (1985) : Error estimation and empirical geothermobarometry for pelitic system. *Am. Mineral.*, 70, 702-709.

Hodges, K.V. and Spear, F.S., (1982) : Geothermometry, geobarometry and the Al2SiO5 triple point at Mt. Moosilauke, New Hampshire. *Am. Mineral.*, 67, 1118-1134.

Honegger, K., Dietrich, V., Frank, W., Gansser, A., Thoni, M. and Trommsdorff, V., (1982) : Magmatism and metamorphism in the Ladakh Himalaya (The Indus-Tsangpo Suture Zone). *Earth Panet. Sci. Lett.*, 60, 253-292.

Hoschek, G., (1969) : The stability of staurolite- and chloritoid and their significance in metamorphism of pelitic rocks. *Contr. Mineral. Petrol.*, 22, 208-232.

Hubber, M., Ramsay, J.G. and Simpson, C., (1980) : Deformation in the Maggia and Antigorio nappes, lepontine Alps. *Ecolo. Geol. Helv.*, 7312, 593-606.

Indares, A. and Martignole, J., (1985) : Biotite-garnet geothermometry in granulite facies: the influence of Ti and Al in biotite. *Am. Mineral.*, 70, 272-278.

Jager, E., Bhandari, A.K. and Bhanot, V.B., (1971) : Rb-Sr age determinations on biotites and whole rock samples from the Mandi and Chor granites, Himachal

Pradesh, India. *Ecologae Geol. Helv.*, V.64, N.3, pp.521-527.

Jain, A.K. and Anand, A., (1988) : Deformational and strain patterns of an intracontinental collision ductile shear zone - an example from the Higher Garhwal Himalaya. *Jour. Struct. Geol.*, 10 (7), 717-734.

Jain, A.K., Singh, S., Patel, R.C. and Gee, D.G., (1991) : Extensional tectonics in orogenic belts: Comparative structures from the Himalaya and Scandinavian Caledonides. *Terra Nova Abstract Suppliment 4. (Tac 91)*, 20.

Jain, A. K. and Manickavasagam, RM., (1993) : Inverted metamorphism in the intracontinental ductile shear zone during Himalayan Collision tectonics. *Geology*, 21, 407-410.

Jaupart, C. and Provost, A., (1985) : Heat focussing, granite gneiss and inverted metamorphic gradients in Continental Collision Zone. *Earth Planet. Sci. Lett.*, 73, 385-397.

Jhingran, A.G., Kohli, G. and Shukla, B. N., (1950) : Geological notes on the traverses to the Spiti valley (Punjab) jointly with the third Danish expedition to Central Asia. *Unpublished report, Geol. Surv. India*, 1-9.

Jiang, J. and Lasaga, A.C., (1990) : The effect of post-growth thermal events on growth- zoned garnet: implications for metamorphic P-T history calculations. *Contri. Mineral. Petrol.*, 105, 454-459.

Kai, K., (1981) : Rb-Sr ages of biotite and muscovite of the Himalayas, eastern Nepal; its implication in the uplift history. *Geochem. Jour.*, 15, 63-68.

Kanwar, R.C. and Singh, I., (1979) : Structural history of the Jutogh metasediments, SW of Chor mountain, Sirmur district, Himachal Pradesh. *Structural Geology of the Himalaya (edited by Saklani, P.S.)*, 183-200.

Kishor, N. and Kanwar, R.C., (1984) : Structural history of the granitic rocks of the Nauhra-Haripurdhar area of Chor pluton. *Bull. Ind. Geol. Assoc.*, 17(2), 195-205.

Kishor, N. and Kanwar, R.C., (1986) : Source and place of origin of Chor granitoids of Simla hills of Himachal Pradesh, *India. Bull. Ind. Geol. Assoc.*, 19(2), 103-107.

Koziol, A.M. and Newton, R.C., (1988) : Redetermination of the anorthite breakdown reaction and improvement of the plagioclase-garnet-Al_2SiO_5-quartz geobarometer. *Am. Mineral.*, 73, 216-223.

Krogh, T.E.(1973) : A low contamination method for hydrothermal decomposition of zircon and extraction of U and Pb for isotopic age determination. *Geochim. Cosmochim. Acta*, 37, 485-494.

Krogh, T.E. and Davis, G.L.(1975) : Alteration in zircon and differantial dissolution of altered and metamict zircon. *Canegie Inst. Wasington Yearb.*, 74, 619-623.

Kumar, A. (1992) : Calibration of fission track dating system and its applications in geothermochronometry of a part of NW-Himalaya in Zanskar and Himachal Pradesh. *Unpublished Ph.D. thesis*, Kurukshetra University, Kurukshetra, India.

Kundig, R., (1989) : Domal structures and high-grade metamorphism in the Higher Himalayan Crystalline, Zanskar region, north-west Himalaya, India. *Jour. Meta. Geol.*, 7, 43 - 55.

Kwatra, S.K., Bhanot, V.B., Kakar, R.K. and Kansal, A.K., (1986) : Rb-Sr radiometric ages of the Wangtu Gneissic Complex, Kinnaur district, Higher Himachal Himalaya. *Bull. Ind. Geol. Asso.*, 19 (2), 127-130.

Le Fort, P., (1975) : Himalaya: the collided range. Present knowledge of the continental arc. *Am. Jour. Sci.*, 275, 7-44.

Le Fort, P., (1986) : Metamorphism and magmatism during the Himalayan Collision. *In : Collision Tectonics (edited by Coward, M.P. and Ries, A.) Spec. Publs. Geol. Soc. London*, 19, 159- 172.

Le Fort, P., (1988) : Granites in the tectonic evolution of the Himalaya, Karakoram and Southern Tibet. *Phil. Trans. R. Soc. Lond.*, A 326, 281-299.

Le Fort, P., Debon, F. and Sonet, J., (1983 a) : The lower Paleozoic "Lesser Himalayan" granitic belt : emphesis on the Simchar pluton of Central Nepal. *In : Granites of Himalaya, Karakoram and Hindukush (edited by Shams, F.A.)*, 235-255.

Le Fort, P., Michard, A., Sonet, J. and Zimmermann, J.L., (1983 b) : Petrography, geochemistry and geochronology of some samples from the Karakoram axial Batholith (Northern Pakistan). *In : Granites of Himalaya, Karakoram and Hindukush (edited by Shams, F.A.)*, 377-387.

Le Fort, P., Debon, F., Pecher, A., Sonet, J. and Vidal, P., (1986) : The 500 Ma magmatic event in alpine southern Asia, a thermal episode at Gondwana Scale. *Sciences de la Terre, Memoire* 47, 191-209.

Le Fort, P., Cunney, M., Deniel, C., France-Lanord, C., Sheppard, S. M. F., Upreti, B. N. and Vidal, P., (1987) : Crustal generation of the Himalayan leucogranites. *Tectonophysics*, 134, 39-57.

Lin, S. and Williams, P. F., (1992) : The geometrical relationship between the stretching lineation and movement direction of shear zones. *Jour. Struc. Geol.*, 14, 491-497.

Lisle, R.J., (1977) : Estimation of tectonic strain ratio from the mean shape of deformed elliptical markers. *Geologie Mijnb.*, 56, 140-144.

Lisle, R.J., (1985) : *Geological strain analysis : A Manual for the Rf/ϕ Method.* Pergamon Press, Oxford.

Lister, L.S. and Snoke, A.W., (1984) : S-C mylonites. *Jour. Struc. Geol.*, 6: 617-638.

Loomis, T.P., (1983) : Compositional zoning of crystals. A record of growth and reaction history. *In: Kinetics and equilibrium in mineral reactions. (edited*

by Saxena, S.K.), 1-60, Springer-Verlag, New York.

Ludwig, K.R., (1980) : Calculation of uncertainties of U-Pb isotope data. *Earth Planet. Sci. Lett.*, 46, 212-220.

Manhes, G., Minster, J. F. and Allegre, C. J., (1978): Comparative Uranium-Thorium-Lead and Rubidium-Strontium study of the Saint Severin Amphoterite: consequence for early solar system chronology. *Earth Plan. Sci. Lett.*, 39, 14-24.

Maluski, H., Matte, Ph., Brunel, M. and Xiao, X., (1988) : $^{39}Ar/^{40}Ar$ dating of metamorphic and plutonic events in the north and High Himalaya Belt (southern Tibet-China). *Tectonics*, 7, 299- 326.

Mattauer, M., (1986) : Intracontinental Subduction, crust-mantle decollement and crustal stacking wedge in the Himalaya and other collision belt. *In : Collision Tectonics (edited by Coward, M.P. and Ries, A.) Spec. Publs. Geol. Soc. London*, 19, 37-50.

McDonald, R., Davies, G.R., Bliss, C.M., Leat, P.T., Bailey, D.K. and Smith, R.L., (1987) : Geochemistry of High-silica Peralkaline Rhyolite, Naivasle, Kenya Rift Valley. *Jour. Petr.*, 28 (6), 979- 1008.

McMahon, C.A., (1877) : The Blaini group and the `Central Gneiss' in the Simla Himalaya. *Rec. Geol. Surv. India*, 10, 204-222.

McMahon, C.A., (1884) : Microscopic structures of some Himalayan granites and gneissose granites. *Rec. Geol. Surv. India*, 17, 53- 73.

McMahon, C.A., (1886) : On the microscopic characters of some eruptive rocks from the Central Himalaya. *Rec. Geol. Surv. India*, 19, 115-119.

McMahon, C.A., (1887) : Some notes on the dolerites of the Chor. *Rec. Geol. Surv. India*, 20, 112-117.

Medlicott, H.B. (1864) : On the geological structure and relationship of the southern portion of the Himalayan ranges between the rivers Ganges and Ravee. *Mem. Geol. Surv. India*, 3, 1-212.

Mehta, P.K., (1976) : Structural and metamorphic history of the crystalline rocks of Kulu valley, Himachal Pradesh, in relation to the tectonics of the northwestern Himalya. In : Geotetton. Delle zone orogeniche del Kashmir Himalaya, Karakoram-Hindukush- Pamir. *Coll. inte. Acad. Nazio. Linoci.*, Roma, 215-244.

Mehta, P.K., (1977) : Rb-Sr geochronology of the Kulu-Mandi belt: Its implication for the Himalayan tectonogenesis. *Geol. Rdsch.*, 66, 156-288.

Mehta, P.K., (1980) : Tectonic significance of the young mineral dates and the rate of cooling and uplift of the Himalaya. *Tectonophysics*, 62, 205-217.

Mehta, P.K., and Rex, D.C., (1977) : K-Ar geochemistry of the Kulu-Mandi belt, NW Himalaya, India. Naves. *Jahrb. Min., Monatsh*, 343-355.

Miller, Ch. and Frank, W., (1992) : Geochemistry and isotope geology of Proterozoic and Early Paleozoic granitoids in the NW Himalaya. *Abstr. 7th Himalaya-Karakoram-Tibet workshop, Oxford*, 58.

Mohan, A., Windley, B. F. and Searle, M. P., (1989) : Geothermobarometry and development of inverted metamorphism in the Darjeeling-Sikkim region of the eastern Himalaya. *Jour. Meta. Geol.*, 7 (1), 95-100.

Molnar, P. and Taponier, P., (1975) : Cenozoic tectonics of Asia: effects of Continental collision. *Science*, 189, 419-426.

Naha, K. and Ray, S., (1970) : Metamorphic history of the Jutogh Series in the Simla Klippe, Lower Himalaya. *Contr. Min. Petr.*, 28, 147-164.

Naha, K. and Ray, S., (1971) : Evidence of overthrusting in the metamorphic terrain

of the Simla Himalaya. *Am. Jour. Sci.*, 270, 30-42.

Naha, K. and Ray, S., (1972) : Structural evolution of the Simla Klippe in the Lower Himalaya. *Geol. Rund.*, 61, 1050-1086.

Narain, H., (1973) : Crustal-structure of Indian Subcontinent. *Tectonophysics*, 20, 249-250.

Newton, R.C. and Haselton, H.T., (1981) : Thermodynamics of the Garnet-Plagioclase-Al_2SiO_5-Quartz geobarometer. *In: Thermodynamics of minerals and melts (edited by R.C. Newton et al.)*, 131-147, Springer-Verlag, New York.

Nicolayson, L.O., (1957) : Solid diffusion in radioactive minerals and the measurement of the absolute age. *Geochim.Cosmochim.Acta*, 11, 41-59.

Oldham, R.D., (1883) : Note on a traverse between Almora and Mussoorie made in October 1882. *Rec. Geol. Surv. India*, 16, 162- 164.

Oldham, R.D., (1887) : Prelimnary sketch of the geology of Simla and Jutogh. Rec. *Geol. Surv. India*, 20, 143-152.

Pande I.C. and Virdi, N.S., (1970) : On the Chareota window structure, district Mahasu, Himachal Pradesh. *Jour. Geol. Soc. India*, 11(3), 275-278.

Pandey, B.K., Singh, V.P., Bhanot, V.B. and Mehta, P.K., (1981) : Rb-Sr geochronological studies of the gneissic rocks of the Ranikhet and Masi area of Almora Crystallines, Lesser Himalaya, Kumaun, U.P. *Abstr. Him. Geo. Sem. 12th*, 70

Pareek, H.S., (1973) : Geological setting, petrography and petro- chemistry of the Dark Trap and its comparitive study with Mandi and Panjal Traps. *Jour. Geol. Soc. India*, 19(4), 335-368.

Parrish, R., (1990) : U-Pb dating of monazite and its application to geological problems. *Cand. Jour. Earth Sci.*, 27, 1431-1450.

Patel, R.C., Singh, S., Asokan, A., Manickavasagam, RM. and Jain, A.K., (1993) : Extensional tectonics in the Collisional Zanskar Himalayan belt. *In : Himalayan Tectonics (edited by Treloar, P. J. and Searle, M. P.), Jour. Geol. Soc., London, Special Publication No. 74.*

Patwardhan, A.M. and Bhandari, A., (1974): Petrogenesis of spilites occurring in the Mandi, H.P., India. *In : Spilite and Spilitic rocks (edited by Amstutz),* Springer-Verlag, 175-189.

Pearce, J. A., Harris, N. B. W. and Tindle, A. G., (1984) : Trace element discrimination diagram for the tectonic interpretation of granitic rocks. *Jour. Petro.,* 25, 956-983.

Pecher, A., (1989) : The metamorphism in the Central Himalaya. *Jour. Metamor. Geol.,* 7, 31-41.

Pecher, A. and Le Fort, P., (1986) : The metamorphism in central Himalaya, its relation with te thrust tectonics. *Mem. Sci. Terr. (ed Fond. Sci. Geo. et de ses appl.) Nancy,* 47, 285pp.

Pilgrim, G.E. and West, W.D., (1928) : The structure and correlation of the Simla rocks. *Mem. Geol. Surv. India,* 53, 1-140.

Pitcher, W. S., (1983) : Granite : typology, geological environment and melting relationships. *In : Migmatites, melting and metamorphism (edited by Atherton, M. P. and Gribble, C. D.),* Shiva Publisher Ltd., Cheshire, U.K., 277-285.

Platt, J.P. and Vissers, R.L.M., (1980) : Extensional structures in anisotropic rocks. *Jour. Struct. Geol.,* 2, 397 - 410.

Pognante, G., Castelli, D., Benna, P., Genovese, G., Oberli, F., Mercier, M., and Tonarini, R., (1990) : The crystalline units of the High Himalayas in the Lahaul-Zanskar region (north west India) : metamorphic-tectonic history and geochronology of the collided and imbricated Indian Plate. *Geol. Mag.,* 127 (2), 101- 116.

Potts, P.J., (1987) : *A handbook of silicate rock analysis.* Blackie, London.

Raju, B.N.V., Chabria, T., Prasad, R.N., Mahadevan, T.M. and Bhalla, N.S., (1982) : Early Proterozoic Rb-Sr isochron age for Central Crystalline, Bhilangana valley, Garhwal Himalaya. *Him. Geol.*, 12, 196-205.

Ramsay, J.G., (1967) : *Folding and Fracturing of Rocks.* McGraw- Hill, New York.

Ramsay, J.G. and Graham, R.H., (1970) : Strain variation in shear belts. *Canad. Jour. Earth Sci.*, 7, 786-813.

Ramsay, J.G., (1980) : Shear zone geometry: a review. *Jour. Struc. Geol.*, 2, 83-89.

Ramsay, J.G. and Huber, M.I., (1983) : *The Techniques of Modern Structural Geology. Volume I : Strain Analysis.* Academic Press, London, 307 pp.

Rex, A. J., Searle, M. P., Tirrul, R., Crawford, Prior, D. J., Rex, D. C. and Barnicoat, A., (1988) : The geochemical and tectonic evolution of the central Karakoram, North Pakistan. *Phil. Trans. R. Soc. London*, A 326, 220-255.

Rhodes, S. and Gayer, R. A., (1977) : Non-cylinderical folds, linear structures in the X direction and mylonite development during translation of the Caledonian Kalak Nappe Complex of Finnmark. *Geol. Mag.*, 114, 322-408.

Richardson, S.W., (1968) : Staurolite stability in a part of the system Fe-Al-Si-O-H. *Jour. Petrol.*, 9, 467-488.

Robie, R.A., Bethki, P.M., Touimin, M.S. and Edwards, J.L., (1966) : X-ray crystallographic data, densities and molar volumes of minerals. *In: Handbook of physical constants (edited by Clark, S.P.Jr.), Geol. Soc. Am. Memo.*, 97, 27-74.

Robie, R.A., Hemingway, B.S. and Fisher, J.R., (1978) : Thermodynamic properties of minerals and related substances at 298.15°K and 1bar (105 Pascals) pressure and at higher temperature. *U.S. Geol. Surv. Bull.*, 1452, 456pp.

Roy, M. K. and Mukherjee, A. (1976) : Time-relationship between the metamorphic and the movement episode in the Jutogh Series west of the Chor granite near Rajgarh, Himachal Pradesh. *Him. Geol.*, 6, 240–246.

Sandhu, C.S., (1985) : Deformation and Barrovian metamorphism of Kishtwar area- an example from Lower Himalayan terrain, India. *In: Geology of western Himalaya (edited by Gupta, V.J.), Contri. Him. Geol.*, 3, 121–149.

Sah, S.C.D., Maithy, P.K. and Bhargava, O.N., (1977) : Some significant polynomorphs from B member of the Jutogh Formation of Simla Hills. *Jour. Geol. Soc. India*, 18(3), 139–145.

Scharer, U., Xu, R.H. and Allegre, C.J., (1984) : U-Pb geochronology of Gandase (Transhimalya) plutonism in the Lahasa- Xigaze region, Tibet. *Earth Planet. Sci. Lett.*, 69, 311–320.

Scharer, U., Xu, R.H. and Allegre, C.J., (1986) : U-(Th)-Pb systematics and ages of Himalayan Leucogranites, south Tibet. *Earth Planet. Sci. Lett.*, 77, 35–48.

Searle, M.P., (1986) : Structural evolution and sequence of thrusting in the High Himalayan, Tibetan-Tethys and Indus Suture Zones in Zanskar and Ladakh, Western Himalaya. *Jour. Struct. Geol.*, 8, 923–936.

Searle, M.P., (1991) : *Geology and Tectonics of the Karakoram Mountains*. John Wiley & Sons, Chichester, 358 p.

Searle, M.P., Windley, B.F., Coward, M.P., Cooper, D.J.W, Rex, A.J., Rex, D.C., Li Tingdong, Xiao Xuchang, Jan, M.Q., Thakur, V.C. and Kumar, S., (1987) : The closing of Tethys and the tectonics of the Himalaya. *Geol. Soc. Am. Bull.*, 98, 678–701.

Searle, M. P. and Rex, A. J., (1989) : Thermal model for the Zanskar Himalaya. *Jour. Meta. Geol.*, 7 (1), 127–134.

Searle, M.P., Waters, D.J., Rex, D.C. and Wilson R.N., (1992) : Pressure, temperature and time constraints on Himalayan metamorphism from eastern Kashmir and

western Zanskar. *Jour. Geol. Soc. London*, 149, 753-773.

Shams, F. A., (1969) : The geology of the Mansera-Amb State area, northern West Pakistan. *Geol. Bull. Punjab Univ. Lahor*, 8, 1-31.

Sharma, K.K. (1976) : A contribution to the Geolgy of the Sutlej Valley, Kinnaur, H.P., India. *In : Himalaya, Science de la Terra, CNRS, Paris*, 268, 369-378.

Sharma, K. K. (1983) : Granitoid belts of the Himalayas. *In : Granites of Himalaya, Karakoram and Hindukush (edited by Sham, F.A.)*, Peshawar University, Pakistan, 11-37.

Sharma, K.K., (1991) : *Geology and Geodynamic evolution of the Himalayan Collision Zone. Physics and Geochemistry of the Earth*, 18 (I-II), Pergmon Press, 446 p.

Sharma, V.P. (1977) : The Stratigraphy and structure of parts of the Simla Himalaya. *Mem. Geol. Surv. India*, 106, 488.

Simpson, C. and Schmid, S.M., (1983) : An evaluation of criteria to deduce the sense of movement in sheared rocks. *Geol. Soc. Am. Bull.*, 94: 1281 - 1288.

Singh, S., (1987) : Deformation and strain pattern in the Higher Himalayan metamorphics along the Sutlej valley, Himachal Pradesh. *Unpublished M. Tech. dissertation thesis*, University of Roorkee, Roorkee, India.

Singh, V.P., Bhanot, V.B. and Singh, R.P., (1985) : Geochronology of the granitic and gneissic rocks from Munsiari, Namik and Tawaghat areas of the Central Crystalline Zone, Kumaun Himalaya, U.P.. *Preprint presented at the 3rd National Symposium on Mass Spectrometry (Hydrabad Sep. 22-24, 1985).*

Singh, R.P., Singh, V.P., Bhanot, V.B. and Mehta, P.K., (1986) : Rb-Sr ages of the gneissic rocks of Rihee-Gangi Bhatwari, Hnumanchatti and Naitwar areas of the Central Crystalline Zone of Kumaun Himalaya (U.P.). *Indian Jour. Earth Sci.*, 13, 197-208.

Roy, M. K. and Mukherjee, A. (1976) : Time-relationship between the metamorphic and the movement episode in the Jutogh Series west of the Chor granite near Rajgarh, Himachal Pradesh. *Him. Geol.*, 6, 240-246.

Sandhu, C.S., (1985) : Deformation and Barrovian metamorphism of Kishtwar area- an example from Lower Himalayan terrain, India. *In: Geology of western Himalaya (edited by Gupta, V.J.), Contri. Him. Geol.*, 3, 121-149.

Sah, S.C.D., Maithy, P.K. and Bhargava, O.N., (1977) : Some significant polynomorphs from B member of the Jutogh Formation of Simla Hills. *Jour. Geol. Soc. India*, 18(3), 139-145.

Scharer, U., Xu, R.H. and Allegre, C.J., (1984) : U-Pb geochronology of Gandase (Transhimalya) plutonism in the Lahasa- Xigaze region, Tibet. *Earth Planet. Sci. Lett.*, 69, 311-320.

Scharer, U., Xu, R.H. and Allegre, C.J., (1986) : U-(Th)-Pb systematics and ages of Himalayan Leucogranites, south Tibet. *Earth Planet. Sci. Lett.*, 77, 35-48.

Searle, M.P., (1986) : Structural evolution and sequence of thrusting in the High Himalayan, Tibetan-Tethys and Indus Suture Zones in Zanskar and Ladakh, Western Himalaya. *Jour. Struct. Geol.*, 8, 923-936.

Searle, M.P., (1991) : *Geology and Tectonics of the Karakoram Mountains*. John Wiley & Sons, Chichester, 358 p.

Searle, M.P., Windley, B.F., Coward, M.P., Cooper, D.J.W, Rex, A.J., Rex, D.C., Li Tingdong, Xiao Xuchang, Jan, M.Q., Thakur, V.C. and Kumar, S., (1987) : The closing of Tethys and the tectonics of the Himalaya. *Geol. Soc. Am. Bull.*, 98, 678-701.

Searle, M. P. and Rex, A. J., (1989) : Thermal model for the Zanskar Himalaya. *Jour. Meta. Geol.*, 7 (1), 127-134.

Searle, M.P., Waters, D.J., Rex, D.c. and Wilson R.N., (1992) : Pressure, temperature and time constraints on Himalayan metamorphism from eastern Kashmir and

western Zanskar. *Jour. Geol. Soc. London*, 149, 753-773.

Shams, F. A., (1969) : The geology of the Mansera-Amb State area, northern West Pakistan. *Geol. Bull. Punjab Univ. Lahor*, 8, 1-31.

Sharma, K.K. (1976) : A contribution to the Geolgy of the Sutlej Valley, Kinnaur, H.P., India. *In : Himalaya, Science de la Terra, CNRS, Paris*, 268, 369-378.

Sharma, K. K. (1983) : Granitoid belts of the Himalayas. *In : Granites of Himalaya, Karakoram and Hindukush (edited by Sham, F.A.)*, Peshawar University, Pakistan, 11-37.

Sharma, K.K., (1991) : *Geology and Geodynamic evolution of the Himalayan Collision Zone. Physics and Geochemistry of the Earth*, 18 (I-II), Pergmon Press, 446 p.

Sharma, V.P. (1977) : The Stratigraphy and structure of parts of the Simla Himalaya. *Mem. Geol. Surv. India*, 106, 488.

Simpson, C. and Schmid, S.M., (1983) : An evaluation of criteria to deduce the sense of movement in sheared rocks. *Geol. Soc. Am. Bull.*, 94: 1281 - 1288.

Singh, S., (1987) : Deformation and strain pattern in the Higher Himalayan metamorphics along the Sutlej valley, Himachal Pradesh. *Unpublished M. Tech. dissertation thesis*, University of Roorkee, Roorkee, India.

Singh, V.P., Bhanot, V.B. and Singh, R.P., (1985) : Geochronology of the granitic and gneissic rocks from Munsiari, Namik and Tawaghat areas of the Central Crystalline Zone, Kumaun Himalaya, U.P.. *Preprint presented at the 3rd National Symposium on Mass Spectrometry (Hydrabad Sep. 22-24, 1985).*

Singh, R.P., Singh, V.P., Bhanot, V.B. and Mehta, P.K., (1986) : Rb-Sr ages of the gneissic rocks of Rihee-Gangi Bhatwari, Hnumanchatti and Naitwar areas of the Central Crystalline Zone of Kumaun Himalaya (U.P.). *Indian Jour. Earth Sci.*, 13, 197-208.

Singh, B. N., Goel, O. P., Joshi, M. and Sheraton, J. W., (1993) : Geochemistry and petrogenesis of the Champawat granitoid occuring around Dhunaghat, district Pithoragarh, Uttar Pradesh, India. *Jour. Geol. Soc. India*, 42, 289-302.

Sorkhabi, R. B. and Stump, E., (1993) : Rise of the Himalaya : A geochronological approach. *GSA Today*, 3 (4), 85 & 88-92.

Spear, F.S., (1988) : Metamorphic fractional crystallization and internal metasomatism by diffusional homogenization of zoned garnets. *Contri. Mineral. Petrol.*, 99, 507-517.

Spear, F.S. and Selverstone, J., (1983) : Quantitative P-T paths from zoned minerals. Theory and tectonic applications. *Contri. Mineral. Petrol.*, 83, 348-357.

Spencer, D. A., (1992) : Geochemistry of the peraluminous Higher Himalayan Crystalline granite basement, Upper Kaghan, Pakistan. *Abstr. 7th Himalay-Karakoram-Tibet workshop, Oxford*, 126.

Srikantia, S.V., (1976) : Sedimentary cycles in the Himalaya and their significance on the orogenic evolution of the mountain belt. *In : Himalaya, Science de la Terra, CNRS, Paris*, 268, 395- 407.

Srikantia, S.V. and Sharma, R.P., (1971) : Simla Group - a reclassification of the Chail Series, Jaunsar Series and Simla slates in the Simla Himalaya. *Jour. Geol. Surv. India*, 12, 234- 240.

Srikantia, S.V. and Bhargava, O.N. (1974) : The Salkhalas and the Jutogh relationship in the Kashmir and Himachal. A reappraisal. Him. Geol., V.4, pp.394-413.

Srikantia, S.V. and Sharma, R.P., (1977) : Geology of the Shali belt and adjoining areas. *Mem. Geol. Surv. India*, 106 (1), 31-166.

Staubli, A., (1989) : Polyphase metamorphism and the development of the Main Central Thrust. *Jour. Meta. Geol.*, 7: 73-93.

Steiger, R.H. and Jagger, E., (1977) : Convention on the use of decay constants in geo- and cosmochronology. *Earth Planet. Sci. Lett.*, 36, 359-362.

Stern, C. R., Kligfield, R., Schelling, D., Virdi, N.S., Futa, K., Peterman, Z. E. and Amini, H., (1989) : The Bhagirathi leucogranite of the High Himalaya (Garhwal, India); Age, petrogenesis and tectonic implications. *Geol. Soc. Am. Specl. Publ. 232*, 33-45.

Stoliczka, A., (1866) : Summary of the geological observations during a visit to the provinces Rupsu Karnag, south Ladakh, Zanskar, Sumdo, Dras and Western Tibet. *Mem. Geol. Surv. India*, 5, 337-354.

St-Onge, M. R., (1981) : "Normal" and "inverted" metamorphic isograds and their relation to syntectonic Proterozoic batholiths in the Wopmay Orogen, Northwest Territories, Canada. *Tectonophysics*, 76, 295-316.

Strachey, R., (1851) : On the geology of parts of the Himalayan mountain and Tibet. *Quart. Jour. Geol. Soc.*, 7, 292-310.

Streikeisen, A.L., (1976) : To each plutonic rock in proper name. *Earth Sci. Rev.*, 12, 1-33.

Sun, S.S. and Mcdonough (1989) : Chemical and isotopic systematics of Oceanic basalt : implication for mantle composition and processes. *In : Magmatism in the Ocean Basins (edited by Saunders, A.B. and Norry, M.J.), Geological Society Special Publication*, 42, 313-345.

Thakur, V.C. (1976) : Divergent isograds of metamorphism in some part of higher Himalaya Zone. *In : Himalaya, Science de la Terra, CNRS, Paris*, 268, 433-442.

Thakur, V.C. (1980) : Tectonics of the Central Crystallines of Western Himalaya. *Tectonophysics*, 62, 141-154.

Thakur, V.C. (1983) : Granites of Western Himalaya and Karakoram - structural framework, geochronology and tectonics. *In : Granites of Himalaya,*

Karakoram and Hindukush (edited by Sham, F.A.), Peshawar University, Pakistan, 327-339.

Thakur, V.C. (1987) : Development of major structures across the northwestern Himalaya, India. *Tectonophysics*, 135, 1-13.

Thakur, V.C. (1993) : *Geology of the Western Himalaya*. Pergmon Press, Oxford and New York, 355 p.

Thompson, A.B., (1976) : Mineral reactions in pelitic rocks (I) Prediction of P-T-X (Fe-Mg) phase relation (II) Calculation of some P-T-X (Fe-Mg) phase relation. *Am. Jour. Sci.*, 276, 401-454.

Thompson, A.B. and England, P.C., (1984) : Pressure-Temperature- Time paths of regional metamorphism II. Their inference and interpretation using mineral assemblages in metamorphic rocks. *Jour. Petrol.*, 25 (4), 929-955.

Tilton, G.R., Patterson, C., Brown, H., Inghram, M., Hayden, R., Hess, D. and Larson, E., (1955) : Isotopic composition and distribution of lead,uranium and thorium in a Precambrian granite. *Geol. Soc. Am. Bull.*, 66, 1131-1148.

Tilton, G.R., (1960) : Volume diffusion as a mechanism for discordent lead ages. *Jour. Geophys. Res.*, 65, 2933-2945.

Tracy, R.J., (1982) : Compositional zoning and inclusions in metamorphic minerals. *In: Characterization of metamorphism through mineral equilibria (edited by J.M. Ferry), Mineral. Soc. Am., Rev. Mineral.*, 10, 355-397.

Treloar, P.J., Rex, D.C., Guise, P.G., Coward, M.P., Searle, M.P., Windley, B.F., Petterson, M.G., Jan, M.Q. and Luff, I.W., (1989) : K-Ar and Ar-Ar geochronology of the Himalayan Collision in NW-Pakistan : constraints on the timing of suturing, deformation, metamorphism and uplift. *Tectonics*, 8 (4), 881-909.

Trivedi, J.R., Gopalan, K. and Valdia, K.S., (1984) : Rb-Sr ages of granitic rocks within the Lesser Himalayan nappes, Kumaun, India. *Jour. Geol. Soc. India*,

25, 641-653.

Turner, F.J., (1981) : *Metamorphic petrology - mineralogy, field and tectonic aspects.* 2nd edn., McGraw-Hill, New York.

Turner, F.J. and Weiss, L.F. (1963) : *Structural analysis of metamorphic tectonites.* McGraw-Hill Pub., London, 345p.

Valdiya, K.S., (1962) : A study of the Champawat Granodiorite and associated metamorphics of the Lohaghat sub. division, district Almora, U.P. *Indian Minerologists*, 3, 6-37.

Valdiya, K.S., (1973) : Lithological subdivision and tectonics of the "Central Crystalline Zone" of Kumaun Himalaya. *In : Proceedings of a Symp. on Geodynamics of the Himalayan region. Hyderabad, India, NGRI*, 204-205.

Valdiya, K.S., (1976) : Structural set-up of the Kumaun Lesser Himalaya. *In : Himalaya, Scie. de le Terra, CNRS, Paris*, 268, 449-462.

Valdiya, K.S., (1980) : *Geology of the Kumaun Lesser Himalaya.* Wadia Inst. Him. Geol., Dehradun, 291p.

Valdiya, K.S., (1989) : Trans-Himadri intracrustal fault and basement upwarps south of Indus-Tsangpo Suture Zone. *Geol. Soc. Am., Spl. pub., 232*, 153-168.

Vidal, Ph., (1978) : Rb-Sr systematics in granites from Central Nepal (Manaslu) : significance of the Oligocene age and high $^{87}Sr/^{86}Sr$ ratio in Himalayan Orogeny: comment. *Geology*, 6(4), 196.

Vidal, Ph., Cocherie, A. and Le Fort, P., (1982) : Geochemical investigations of the origin of the Manaslu leucogranite (Himalaya, Nepal). *Geochem. et. Cosmo. Acta.*, 64, 2274-2292.

Vidal, Ph., Bernard-Griffiths, J., Cocherie, A., Le Fort, P., Peucat, J. J. and Shepard, S. M. F., (1984) : Geochemical comparision between Himalayan and Hercynian leucogranites. *Phys. Earth and Plant. Inter., Spec. issue, 35*, 179-190.

Virdi, N.S. (1971) : Geology of the Narkanda area with special reference to its metamorphic and tectonic history. *Unpublished Ph.D. Thesis*, Panjab University, Chandigarh, India.

Virdi, N.S., (1976) : Stratigraphy and structure of the area around Nirath, district Simla , Himachal Pradesh. *Him. Geol.*, 6, 163-175.

Virdi, N.S., (1980) : Problem of the root zone of nappes in the western Himalaya : A critical review. *Him. Geol.*, 10, 55-77.

Virdi, N.S., (1981) : Chail metamorphism of the Himachal Lesser Himalaya. *In : Himalayan Thrust and Associated Rocks (edited by P.S. Saklani)*, Today and Tommorrows Printers and Publishers, New Delhi, 10, 89-100.

Virdi, N.S., (1988) : Pre-Tertiary geotectonic events in the Himalaya. *Z. geol. wiss. Berlin*, 16, 571-585.

Wadia, D.N., (1928) : The geology of the Poonch State (Kashmir) and adjacent parts of the Panjab. *Mem. Geol. Surv. India*, 51, 233p..

Wadia, D.N., (1957) : *Geology of the India*. McMillan & Co., London, 536p.

Wahlen, J. B., Currie, K. L. andd Chapple, B. W., (1987) : A-type granites : geochemical characteristics, discrimination and petrogenesis. *Contrib. Miner. Petrol.*, 95, 407-419.

Walsh, J. N., Buckley, F. and Barker, J., (1981) : The simultaneous dtermination of the rare earth elements in rocks using ICP source spectrometry. *Chem. Geol.*, 33, 141-153.

Wasserburg, G.J., (1963) : Diffusion processes in lead uranium system. *Jour. Geophys. Res.*, 68, 4823-4846.

West, W.D. (1935) : Some recent advances in Indian geology. *Curr. Sci.*, 3, 231-232 and 286-289.

West, W.D. (1939) : The structure of the Shali `window' near Simla. *Rec. Geol. Surv. India*, 74 (1), 133-163.

Wetherill, G.S., (1956 a) : An interpretation of the Rhodesia and Withwatersrand age patterns. *Geochim. Cosmochim. Acta.*, 9, 290-292.

Wetherill, G.S., (1956 b) : Discordent uranium-lead ages,I. *Trans. Am. Geophys. Union*, 37, 320-326.

Wetherill, G.S., (1963) : Discordent uranium lead age,II. Discordent ages resulting from diffusion of lead and uranium. *Jour. Geophys. Res.*, 68, 2957-2965.

White, A. J. R., (1979 a) : Source of granite magmas. Abstr. with programs. *Geol. Soc. Am. An. Gen. Meet.*, 539p.

White, S.H., (1979 b) : Large strain deformation. Report on a tectonic studies group discussion metting held at Imperial College., London. *Jour. Struct. Goel.*, 1, 333 - 339.

White, A. J. R. and Chappel, B. W., (1977) : Ultrametamorphism and granitoid gneiss. *Tectonophysics*, 43, 7-22.

Wiliams, G. D., (1978) : Rotation of contemporary folds into the X direction during overthrust processes in Laksefjord, Finmark. *Tectonophysics*, 48, 29-40.

Windley, B.F., (1988) : Tectonic framework of the Himalaya, Karokoram and Tibet and problems of their evolution. *Phil. Trans. R. Soc. London*, A 326, 3 - 16.

Winkler, H.G.F., (1979) : *Petrogenesis of metamorphic rocks.* Springer-Verlag, New York Inc., 5th edn., 348 p.

Woldai, G., (1987) : Structural, deformation and metamorphic pattern of the Chail metamorphics, Anni-Dalash Area, Lesser Himalaya, H.P.. *Unpublished M.Sc. dissertation*, University of Roorkee, Roorkee, India, 67p.

Wolde, G.G., (1987) : Deformation and strain patterns in Dalash granite gneiss of the Chail metamorphics, Lesser Himalaya, Himachal Pradesh. *Unpublished M.Sc. dissertation*, University of Roorkee, Roorkee, India, 60p.

Wood, D.A., (1979) : A variable veined suboceanic upper mantle - Genetic significance for mid-ocean ridge basalts for geochemical evidence. *Geology*, 7, 499-503.

Zietler, P.K., Johnson, N.M., Naseer, C.W. and Tahirkheli, R.A.K., (1982) : Fission Track evidence for Quaternary uplift of Nangaparbat region, Pakistan. *Nature*, London, 298, 255-257.

Zietler, P.K., Sutter, J.F., Williams, I.S., Zartman, R and Tahirkheli, R.A.K., (1989) : Geochronology and temperature history of the Nanga Parbat-Haramosh Massif, Pakistan. *Geol. Soc. Am., Spl. pub., 232*, 1-22.